REGULATION OF DEVELOPMENTAL TIMING IN DROSOPHILA MELANOGASTER: GENETICS VERSUS ENVIRONMENT

A DISSERTATION
SUBMITTED TO THE FACULTY OF THE GRADUATE SCHOOL
OF THE UNIVERSITY OF MINNESOTA
BY

XUEYANG PAN

IN PARTIAL FULFILLMENT OF THE REQUIREMENTS
FOR THE DEGREE OF
DOCTOR OF PHILOSOPHY

MICHAEL B. O'CONNOR, ADVISOR

JULY 2019

ACKNOLEDGEMENTS

Firstly, I would like to acknowledge Dr. Michael O'Connor, my advisor, for providing me this valuable opportunity to work on my thesis project in his lab and for his continuous support and wise advises on my research. I would like to thank all the members of the O'Connor lab, particularly MaryJane O'Connor, Naoki Yamanaka, Aidan Petersen and Ambuj Upadhyay, for their assistance and discussion on my thesis work. Thanks are also given to members of the Thomas Neufeld Lab for their help on my work. I'm also grateful to my committee members, Dr. Thomas Neufeld, Dr. David Greenstein, Dr. Sean Conner, Dr. Timothy Starr and Dr. Do-Hyung Kim, for their advises and guidance during my graduate study. Finally, I would like to give my gratitude to my family and my friends for their support and help in my out-of-campus life.

ABSTRACT

Development of animals involves both an intrinsic program determined by genetics and an adaptive system reacting to environmental variants. In fruit fly *Drosophila melanogaster,* the juvenile-to-adult transition is largely governed by a neuroendocrine axis in which the PTTH-producing PG neurons and the larval endocrine organ prothoracic gland (PG) play the central role. However, the mechanism underlying the regulation of this neuroendocrine axis is not fully understood. In this thesis two discoveries are made on both the genetic control of the neuroendocrine axis and its response to nutritional stress.

Firstly, the author demonstrates that autophagy acts as a nutritionally-regulated gating mechanism which helps ensure productive metamorphosis in *Drosophila*. Autophagy in the PG is specifically stimulated by nutrient restriction at the early, but not the late third instar larva stage, which inhibits precocious metamorphosis during nutrient restriction in undersized larvae. Induction of autophagy disrupts production of the steroid hormone ecdysone at the time of pupariation not by destruction of hormone biosynthetic capacity, but rather by limiting the availability of the steroid hormone precursor cholesterol in the endocrine cells via a lipophagy mechanism. These findings demonstrate an autophagy mechanism in PG cells that helps shape the nutritional checkpoints and guarantee a successful juvenile-to-adult transition in animals confronting nutritional stress.

Secondly, the author shows that Jeb/Alk and Pvf/Pvr pathways function jointly with PTTH/Torso pathway in the PG neuron-PG neuroendocrine axis to control developmental timing in *Drosophila*. In the two pathways, Jeb and Pvf ligands are expressed in the PG neurons, which activate the Alk and Pvr receptors respectively in the PG. Suppression of the Jeb/Alk or Pvf/Pvr pathway causes developmental timing delay in the larva, which is exacerbated when combined with mutation of *ptth*. Activation of the pathways rescues the developmental delay caused by *ptth* mutation, indicating a compensatory effect. These data demonstrate that the Jeb/Alk and Pvf/Pvr pathways are among the previously

proposed additional signals from the PG neuron-PG axis which function jointly with the PTTH/Torso pathway to control developmental timing.

Six movies, Movie 1-6, showing the movements of autophagy structures in the PG cells (related to Figure 28 and 29 in Chapter 2) are included as supplementary files in the thesis. The details of the movies are described in the related texts.

TABLE OF CONTENTS

LIST OF TABLES

CHAPTER 3

LIST OF FIGURES

CHAPTER 1

CHAPTER 2

CHAPTER 3

CHAPTER 1

Introduction

In multicellular organisms, successful development involves both precise intrinsic controls on the developmental procedures, such as cell growth, differentiation, tissue patterning and body organization, but also a flexible system that regulates the developmental processes in response to environmental variants. Understanding how animals orchestrate the “solid” developmental program determined by the genetics and the “fluctuating” environmental conditions will provide us not only an insight on the “designing” strategy of animal development by evolution but also a reference to the understand of human development disorders.

A good example in animal development reflecting the orchestration between genetics and environment is the juvenile-to-adult transition, which marks a milestone during development of an individual - the attainment of sexual maturity. In metazoan, the transition can be achieved by developmental processes of stark differences, such as metamorphosis in insects and puberty in mammals. However, the determination of the transition is achieved by quite comparable mechanism across species, which involves both internal developmental signals and a system responding to environmental changes. For example, in both fruit fly *Drosophila melanogaster* and human being, the hormone that directly triggers the transition is produced from steroid, while the hormone production is regulated by both neuroendocrine circuit and environmental factors such as the nutritional status of the animal (Navarro & Tena-Sempere, 2011; Nijhout et al., 2014). Rested on these similarities, studies on the juvenile-to-adult transition in model system such as *Drosophila* may shed light on the understand of human disorders on puberty control, such as puberty retardation and precocious puberty caused by either neurologic disorders or overnutrition.

In my thesis work, I follow the idea above to study the genetic and environmental control of the timing of juvenile-to-adult transition in *Drosophila*. As a well-developed model organism, *Drosophila* has abundant tools and resources to carry out both genetic manipulation and biochemical and cell biological tests. The life cycle of *Drosophila* also makes it amenable to precise tracking of

development in several days. Especially, the progress of the juvenile-to-adult transition in *Drosophila*, the metamorphosis process, has been well characterized and the onset of the transition can be easily recognized by the event of puparium formation (Yamanaka, Rewitz & O'Connor, 2013). All these advantages make *Drosophila* an excellent model for the study of juvenile-to-adult transition and its regulation.

In this chapter, I introduce an overview of what is known about the juvenile-to-adult transition in *Drosophila* and the mechanism underlying the timing of the transition by both intrinsic and environmental factors.

1.1 Overview of hormonal control of development in *Drosophila melanogaster*

1.1.1 Life cycle and developmental timing of *Drosophila*

Similar to most metazoan species, the life cycle of *Drosophila melanogaster* starts from a fertilized egg and completes as a fertile adult fly. Upon egg laying, embryonic development occurs within the egg chamber, which develops into a 1st instar (L1) larva. After hatched from the egg, the L1 larva keep foraging and growing, during which it undergoes two molting activities to develop into 2nd (L2) and 3rd instar (L3) larva. At the end of L3 stage, the larva experiences a wandering stage, in which it leaves the food source and crawl around to search for an appropriate site to undergo metamorphosis. At the beginning of the metamorphic transition, a larva firstly undergoes puparium formation (pupariation), during which the cuticle of the L3 larva turns into the puparium case. At this stage, the developing fly is named prepupa. Afterward, one more molting event (larva-pupa apolysis) takes place to form a pupa, and metamorphosis continue to progress within the puparium and pupa cases (Fraenkel & Bhaskaran, 1973). At the end of the pupa stage, the adult fly ecloses from the pupa case and becomes sexually mature shortly (~8 hrs) after eclosion.

Under a favorable situation, the timing of development of *Drosophila* is also precisely programmed by its genetics (Figure 1). Under a favorable living

temperature (25°C), each of the embryonic development, the L1 and L2 stages takes around 24 hours to complete, while the L3 stage takes around 2 days. Following a wandering stage at the end of L3 stage, the larva pupariates and undergoes metamorphosis in another 3.5-4.5 days. Upon completion of metamorphosis, the eclosion activity of *Drosophila* is largely affected by diurnal cycle (Bakker & Nelissen, 1963). Thus, the full life cycle of *Drosophila* takes 8.5-9.5 days, depending on the time in the day at which metamorphosis is completed.

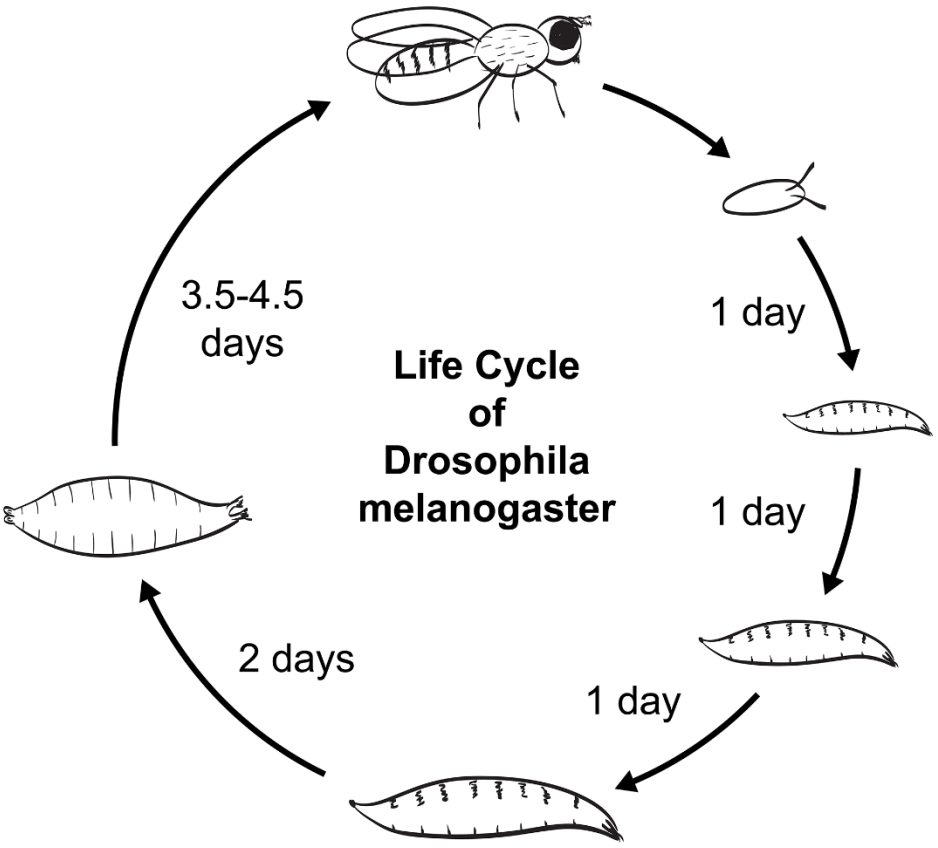

Figure 1. Life cycle of *Drosophila melanogaster*.

The schematic picture shows the developmental stages and the time spent in each stage during the life cycle of *Drosophila melanogaster*. The timing scheme represents a typical development progress under favorable condition (25°C with sufficient food supply).

1.1.2 Hormonal control of developmental timing in *Drosophila*

In species in Insecta, the timing of developmental transitions including larval moltings and metamorphosis is predominantly controlled by the coordination of activities of two hormones, ecdysone and juvenile hormone (JH). In some holometabolous orders such as Lepidoptera and Coleoptera, the pulses of ecdysoneinduce molting activities, while JH determines the nature of the molting (either larva-larva or larva-pupa apolysis). At the last instar stage of these species, the synthesis of JH is suppressed, which allows larvae to undergo larva-pupa molting thus starting metamorphosis (C. K. Mirth & Riddiford, 2007; Nijhout & Williams, 1974a). Addition of JH at the last larva stage causes repetition of larva-larva molting in the animal (Riddiford, 1994), while experimental removal of JH results in precocious larva-pupa molting and metamorphosis (Minakuchi, Namiki, Yoshiyama & Shinoda, 2008; Tan, Tanaka, Tamura & Shiotsuki, 2005). In *Drosophila*, however, JH does not function in the same way as in the other holometabolous species mentioned above. The removal of JH producing organ, the corpus allatum (CA), causes change on growth rate but not on determination of the fate of molting (C. K. Mirth et al., 2014; Riddiford, Truman, Mirth & Shen, 2010). Therefore, the focus of the following text is only put on E, the master regulator of developmental timing in *Drosophila*.

Unlike JH, the biology of ecdysone in *Drosophila* is quite comparable to other holometabolous insects. As a steroid hormone, ecdysone is synthesized from cholesterol or other relevant steroid precursors following a series of enzymatic steps (Niwa & Niwa, 2014). Most of these steps are completed in one of the major endocrine organs in *Drosophila* larva, the prothoracic gland (PG), which comprises of a large part of the ring gland (Yamanaka, Rewitz, et al., 2013). Ahead of each molting activity, a pulse of ecdysone is produced in the PG cells and released into hemolymph through a vesicle-mediated pathway (Figure 2) (Yamanaka, Marques & O'Connor, 2015). Upon releasing, ecdysone is taken up by targeting tissues where it is converted into 20-hydroxyecdysone (20E) by a specific P450 enzyme Shade (Petryk et al., 2003). 20E works as the functional

ecdysone which binds to ecdysone receptor (EcR) and its functioning co-receptor Ultraspiracle (Usp) and subsequently leads to a downstream gene expression cascade that directs the metamorphosis process (Riddiford, Cherbas & Truman, 2001). At the same time, 20E also stimulates expression of *Cyp18a1*, a 20E inactivating P450 enzyme, which leads to a negative feedback lowering the 20E level in the targeting cells when the surge of ecdysone production ceases (Rewitz, Yamanaka & O'Connor, 2010).

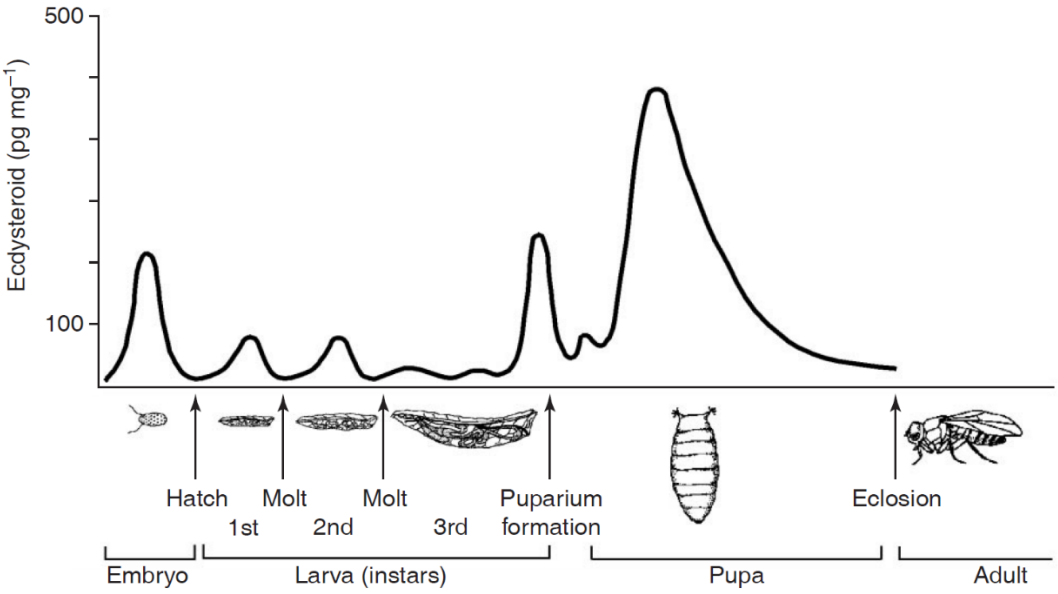

Figure 2. Ecdysone titer profile during *Drosophila* development.

The schematic picture shows the ecdysone titers during *Drosophila* development that trigger developmental transitions. Figure adapted from (Kozlova & Thummel, 2000).

1.1.3 Ecdysone biosynthetic pathway

As mentioned above, ecdysone is synthesized by a series of enzymatic steps from cholesterol. Like most insects, *Drosophila* is a strict auxotroph of cholesterol whose steroid hormone synthesis thoroughly relies on dietary sterols (Clayton, 1964). Upon food uptake, sterols are transported via hemolymph and stored in lipid droplets in various tissues including the PG (Talamillo et al., 2013). Mutant flies with defects on lipid transportation in the hemolymph or cholesterol trafficking within cells often present severe developmental defects. For example, mutants of apolipoprotein genes, such as *apolipophorin* (*apolpp*) and apolipoprotein lipid transfer particle (*Apoltp*), are embryonic or L1 larval lethal (Palm et al., 2012). Similarly, mutation of cholesterol trafficking proteins such Niemann-Pick type C-1a (*Npc1a*) and Niemann-Pick type C-2a/2b (*Npc2a/2b*) causes L1 larval and L3 larval/pupal lethality respectively (Huang, Suyama, Buchanan, Zhu & Scott, 2005).

In the ecdysone synthesis pathway, cholesterol is firstly converted into 7-dehydrocholesterol (7dC) by Neverland (Nvd), a Rieske protein functioning as a 7,8-dehydrogenase (Yoshiyama-Yanagawa et al., 2011; Yoshiyama, Namiki, Mita, Kataoka & Niwa, 2006) (Figure 3). Subsequently, 7dC is converted into 5β-ketodiol in multiple steps. So far, the intermediates in these steps have not been successfully elucidated, possibly due to the unstable nature of the reaction intermediates. Therefore, these not-fully-characterized steps are collectively referred to as the “Black Box” in the pathway (Niwa & Niwa, 2014) (Figure 3). In the “Black Box” several candidate intermediates has been identified, such as cholesta-5,7-diene-3-one (3-oxo-7dC), cholesta-4,7-diene-3,6-dione-14α-ol (Δ^4-diketol), and 5β[H]cholesta-7-ene-3,6-dione-14α-ol (diketol) (Blais et al., 1996; Saito, Kimura, Kaieda, Nishida & Ono, 2016; Warren, O'Connor & Gilbert, 2009). Additionally, several genes are also found involved in the catalytic steps in the “Black Box”, including *shroud* (*sro*), *Cyp6t3*, *spook* (*spo*) and *spookier* (*spok*) (Namiki et al., 2005; Niwa et al., 2010; Ono et al., 2006; Ou, Magico & King-Jones, 2011). Despite of these findings, the clear positioning of these enzymes and steroid intermediates in the “Black Box” has not been resolved. Downstream of

the “Black Box”, the enzymatic processes from 5β-ketodiol, the immediate product out of the “Black Box”, to the functional hormone product 20E has been clearly delineated. Sequential hydroxylation are carried out on the 25’, 22’, 2’ and finally the 20’ position carbon by four cytochrome-P450 monooxygenases Phantom (Phm), Disembodied (Dib), Shadow (Sad) and Shade (Shd) respectively (Chavez et al., 2000; Niwa et al., 2004; Petryk et al., 2003; Warren et al., 2002; Warren et al., 2004) (Figure 3). Mutants of all the ecdysone synthetic genes are embryonic/early-stage larval lethal, which reflects the strict requirement of ecdysone in development. To be noted, the phenotype of many of the mutants, such as those of *phm*, *dib*, *sad*, *shd* and *spo*, were firstly documented in the screening for larval cuticle patterning defects carried out by Christiane Nüsslein-Volhard and Eric Wieschaus (Jurgens, Wieschaus, Nussleinvolhard & Kluding, 1984; Nussleinvolhard, Wieschaus & Kluding, 1984; Wieschaus, Nussleinvolhard & Jurgens, 1984). The genes were given ghost-relevant names due to the naked cuticle phenotype of the mutants. And following this idea, the ecdysone synthetic genes discovered afterward were also named under this criterion and the whole class of genes are collectively called Halloween genes.

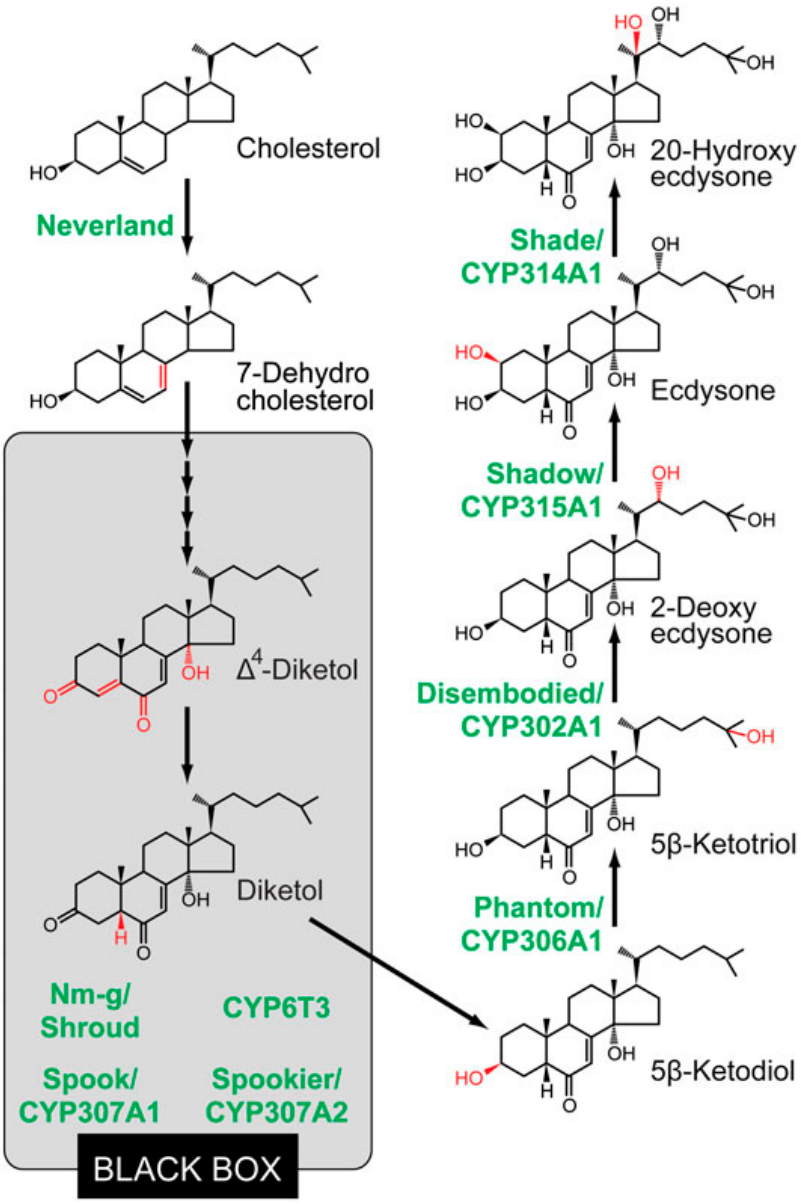

Figure 3. Ecdysone biosynthetic pathway in *Drosophila*.

The figure shows the ecdysone biosynthetic pathway that is known so far. The biosynthetic intermediates and ecdysteroidogenic enzymes involved are also noted. Figure cited from (Niwa & Niwa, 2014).

1.1.4 Biological actions in response to ecdysone

Upon releasing from the PG, the surge of ecdysone triggers a complex cascade of gene transcription activities in targeting cells. After converted into its active form in the targeting cells, ecdysone (the active form 20E) binds with its receptor, a heterodimer of EcR and Usp (Yao et al., 1993; Yao, Segraves, Oro, Mckeown & Evans, 1992). The EcR/Usp receptor complex recognizes specific consensus DNA sequence defined as ecdysone response element (EcRE), which frequently locates in the promoter region of ecdysone responsive genes, and induces complex changes on gene transcription activities in response to ligand binding.

As a transcription factor, the EcR/Usp complex is able to interact with various cofactors in ligand dependent or independent fashion, which largely determines its activity. For instance, the ligand-independent interaction between the EcR/Usp complex and corepressor SMRTER mediates transcription repression of target genes (Tsai, Kao, Yao, McKeown & Evans, 1999). However, the interaction between EcR/Usp and another corepressor, dMi-2 in the nucleosome remodeling and deacetylation (NuRD) complex, is facilitated by ecdysone binding (Kreher et al., 2017). On the other hand, coactivators such as the nucleosome remodeling factor (NURF) complex (Ables & Drummond-Barbosa, 2010; Badenhorst et al., 2005), the Brahma (SWI/SNF) complex (Zraly & Dingwall, 2012; Zraly, Middleton & Dingwall, 2006) and Taiman (Bai, Uehara & Montell, 2000; Zhang et al., 2015) bind with the receptor all in ecdysone dependent way, triggering receptor mediated gene activation. Besides direct binding partners, a series of histone modifier, such as histone acetyltransferase CREB binding protein (CBP) (Kirilly et al., 2011), lysine methyltransferase TRR (Carbonell, Mazo, Serras & Corominas, 2013; Sedkov et al., 2003) and arginine methyltransferase DART1 (Kimura et al., 2008), are also functionally relevant to the action of the receptor. With the regulation from these cofactors, the ecdysone receptor can exert precise control on the targeting genes expression, especially in response to the ecdysone titers during developmental transitions.

The sophisticated activity of ecdysone receptor and its cofactors unsurprisingly leads to a complicated, but well organized, downstream gene expression cascade. The biological actions in response to ecdysone were firstly studied in *Drosophila* by Ashburner and colleagues. The pioneering studies tested the ecdysone induced puffing pattern in larval salivary gland polytene chromosomes, following which a model was proposed to explain the temporal regulation of puffing activities following ecdysone stimulation in 1974 (Ashburner, Chihara, Meltzer & Richards, 1974). In this model, ecdysone stimulates gene expression temporally during development (Figure 4). The ligand bound receptor firstly activates expression of the “early” puff genes and subsequently the “early” gene products suppress the promoter region of the “early” genes themselves and simultaneously activate “late” puff genes. The “late” puff genes can be further classified into “early-late” and “late-late” genes. The “early-late” genes are activated comparatively earlier, which requires existence of ecdysone for their activation. By contrast, the “late-late” genes are induced later when ecdysone level decreases and remain activated in the absence of E. The activation cascade of different groups of genes occurs in parallel with the ecdysone titer during development, thus achieving a precise coordination between hormone level and transcription factor activities in targeting tissues (Thummel, 1996).

Among the ecdysone responsive genes, many of the well-characterized “early” genes are transcriptional factors, such as E74, E75 and the Broad Complex (Br-C) (Burtis, Thummel, Jones, Karim & Hogness, 1990; DiBello, Withers, Bayer, Fristrom & Guild, 1991; Segraves & Hogness, 1990; Thummel, Burtis & Hogness, 1990). Structural genes are also recognized in “early” puffs, such as E63-1 which encodes a calcium binding protein that regulates salivary gland glue secretion at the time of pupariation (Andres & Thummel, 1995; Biyasheva, Do, Lu, Vaskova & Andres, 2001; Vaskova et al., 2000). Compared with “early” genes, the “late” genes are regulated by more factors (including the “early” genes) and show higher diversity in both functionality and tissue specificity. Thus, a clear landscape of “late” gene activity in the ecdysone induced cascade has not been well drawn by case

studies. However, as genome-wide approaches are introduced in recent years, new tools are employed in the study of ecdysone responsive network (Ables, Hwang, Finger, Hinnant & Drummond-Barbosa, 2016; Davis & Li, 2013; T. R. Li & White, 2003; Shlyueva et al., 2014; Stoiber, Celniker, Cherbas, Brown & Cherbas, 2016), which leads to a more and more clear answer to the longstanding question.

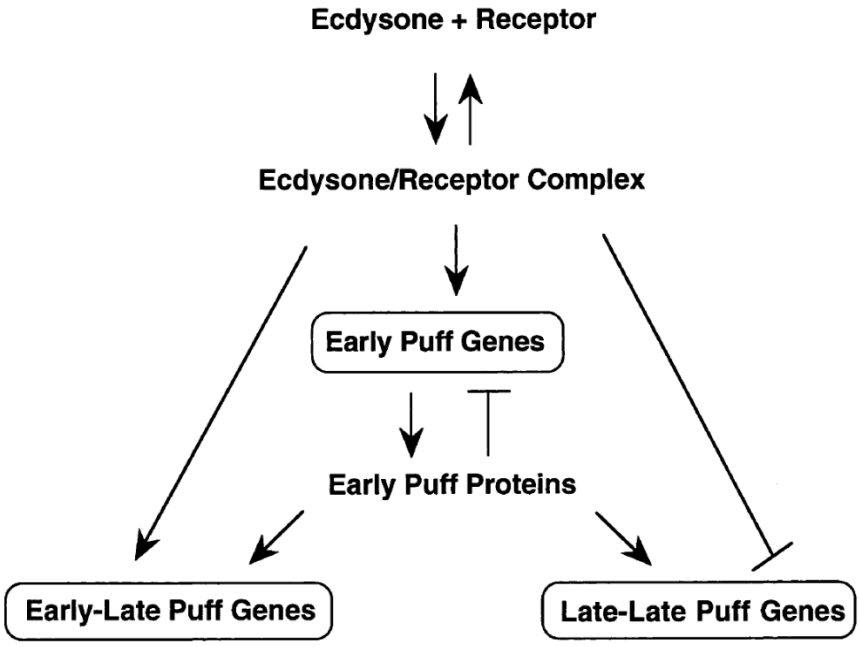

Figure 4. The Ashburner model of ecdysone induced cascade in *Drosophila*. The schematic picture shows the Ashburner model that was proposed by Ashburner and colleagues in 1974 (Ashburner et al., 1974). The additional concepts of “early-late” and “late-late” genes defined in the following studies are also included (Ashburner & Richards, 1976). Picture cited from (Thummel, 2002).

1.2 Upstream signals controlling developmental timing of *Drosophila melanogaster*

As the ecdysone producing organ, the PG is considered the organization center of that determines the timing of ecdysone production and thereby the onset of molting activities and metamorphosis. To achieve the decision-making role in this process, the PG cells orchestrate signals from multiple resources which reflects the physiological conditions of the animal as well as the influences from environment. In this session I introduce the upstream signals that contribute to the control of hormone synthesis in the PG.

1.2.1 Prothoracicotropic Hormone and Torso pathway

Considered as the predominant upstream controller of PG function for decades, prothoracicotropic hormone (PTTH) is a neuropeptide hormone that directly triggers the ecdysteroidogenic activity of the PG. From the first prediction as an unknown brain-derived factor in 1920s (Kopeć, 1922), PTTH has been studied in depth in multiple insect species (review, see (W. Smith & Rybczynski, 2012)). Due to these intensive studies, the PTTH-producing neurons (commonly named PG neurons after their innervating target) has been considered the controlling center of developmental timing, which integrates upstream (mostly neuronal) signals and interprets them into a single output toward the PG. More recently, however, studies begin to show that a series of other factors can affect PG function through PTTH-independent, endocrine-based pathways (introduced in sections below). These observations suggest that the PG, instead of the PG neurons, might be considered the *bona fide* decision-maker in the determination of developmental transitions. Even though, the activity of PTTH is still one of the most important upstream factors signaling to the PG.

In *Drosophila*, PTTH was firstly purified in 1997 (A. J. Kim, Cha, Kim, Gilbert & Lee, 1997) and the *ptth* gene was identified in 2007 (McBrayer et al., 2007). PTTH is produced in two pairs of lateral neuroendocrine neurons in the larval brain lobe, whose axons send direct projection to the PG. The expression of PTTH in the PG neurons exhibits a cyclic pattern, while at the end of L3 stage a surge of

expression occurs which precedes the subsequent ecdysone titer produced by the PG (McBrayer et al., 2007). In consistence with the function of PTTH, ablation of the PG neurons causes severe developmental delay (~5 days) (McBrayer et al., 2007). However, a follow-up study tested *ptth* mutants and observed much shorter developmental delay (~1 day) in the mutant animals compared with the neuron ablation model (Shimell et al., 2018). The difference on the developmental timing phenotype indicates that some alternative signal may exist in the tropic signals emanating from the PG neurons.

Functionally, the PG neurons receive multiple upstream neuronal signals and integrate them into a precise signaling output to the PG. The pigment dispersing factor (PDF) expressing neurons, which response to the diurnal cycle, send projections to the PG neurons and contribute to the rhythmic expression of PTTH in the PG neurons (McBrayer et al., 2007; Vafopoulou & Steel, 1996). Another class of neurons expressing leucine-rich repeat-containing G protein-coupled receptor 3 (Lgr3) are also found to project to the PG neurons to suppress PTTH expression (Colombani et al., 2015; Garelli et al., 2015). Lgr3 is the receptor of Dilp8, an insulin-like peptide which responses to tissue injury during larva stage (Colombani, Andersen & Leopold, 2012; Garelli, Gontijo, Miguela, Caparros & Dominguez, 2012). Upon the occurrence of tissue damage, Dilp8 is secreted from the injured tissue which suppresses pupariation activity through the Dilp8-Lgr3 neuron-PG neuron-PG signaling axis and arrests development temporarily to allow regenerative tissue repair. Recently, one more upstream signal is discovered from a screening for defects of PTTH production in the PG neurons. Two pairs of Allatostatin-A (AstA) expressing neurons are found to signal to the PG neurons through the AstA receptor (AstAR) expressed on the PG neurons (Deveci, Martin, Leopold & Romero, 2019). Unlike the Lgr3-expressing neurons which functions to sensing stress, the activity of AstA neurons is required for the intrinsic control developmental timing (Deveci et al., 2019). More interestingly, AstA and AstAR are homologous to human kisspeptin (Kiss) and its receptor GPR54 (Felix et al., 2015), two key factors in the hypothalamic-pituitary-gonadal

(HPG) axis that controls timing of puberty in human (Clarkson, Han, Liu, Lee & Herbison, 2010), suggesting a conserved molecular mechanism in the juvenile-to-adult transition of insects and human (Figure 5).

Despite of the long history of studies on PTTH, the identity of the receptor of PTTH remains elusive until not long ago (compared with the decades-long research on PTTH). PTTH has long been predicted to signal through a G-protein coupled receptor (GPCR). The prediction stems from the facts that calcium (Ca^{2+}) signaling and cAMP signaling are involved in the PTTH triggered ecdysone production pathway (W. A. Smith, Gilbert & Bollenbacher, 1984; W. A. Smith, Varghese, Healy & Lou, 1996; Venkatesh & Hasan, 1997). In 2009, however, Rewitz, et al. demonstrated that the receptor tyrosine kinase (RTK) Torso functions as the *bona fide* receptor of PTTH in *Drosophila* (Rewitz, Yamanaka, Gilbert & O'Connor, 2009). Activation of Torso receptor leads to downstream Ras-Raf-Erk signaling cascade (Rewitz et al., 2009), which is consistent with previous findings that the Ras-Raf-Erk pathway is required for ecdysone synthesis (Caldwell, Walkiewicz & Stern, 2005; Rybczynski, Bell & Gilbert, 2001; Rybczynski & Gilbert, 2003). However, how the Ca^{2+} and cAMP signaling is activated by PTTH signal remains unclear.

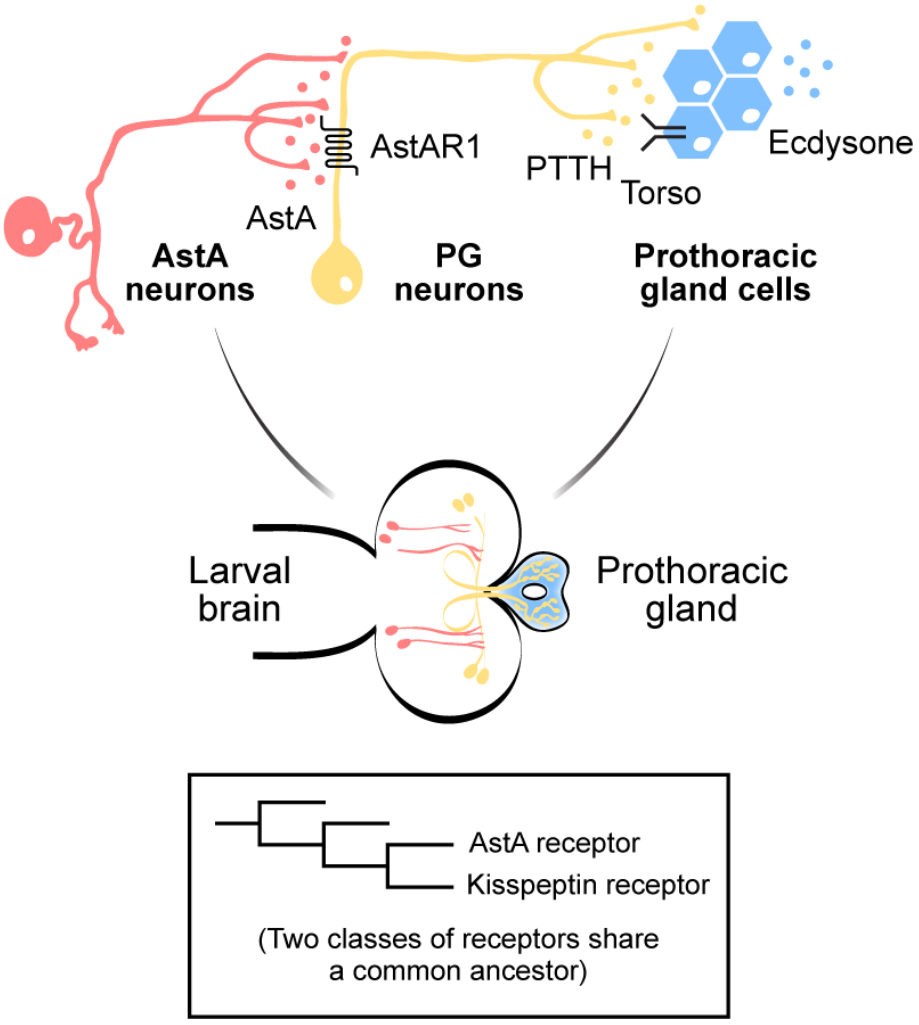

Figure 5. Neuroendocrine signaling pathways regulating developmental timing in *Drosophila*.

The diagram shows the signaling axis between AstA-producing neurons, PTTH-producing PG neurons and the prothoracic gland (PG) which regulates the onset of metamorphosis in Drosophila. Two pairs of AstA neurons directly project to the dendritic region of the PG neurons. At the end of the third instar stage, AstA (red dots) is strongly expressed and released from AstA neurons, binds to its receptor AstAR1 on the PG neuron membrane and activates the neurons to release PTTH (yellow dots), which subsequently stimulates synthesis and secretion of ecdysone (blue dots) from PG cells through activation of its receptor Torso. The AstA

receptor shares a common ancestor with the Kisspeptin receptor in mammals, indicating a conserved molecular mechanism controlling juvenile-to-adult transition across species. Figure adapted from (Pan & O'Connor, 2019).

1.2.2 Insulin/Insulin-like Signaling pathway

Insulin/insulin-like peptides have been identified in a large number of animals, from flies to human beings. In *Drosophila*, eight insulin-like peptides (ILPs), namely Dilp1-8, have been detected in its genome, whose spatial and temporal expression patterns differs dramatically from each other. Among the eight DILPs, the loci of 5 DILP genes (*dilp1-5*) form a cluster of four continuous genes (*dilp1-4*) with *dilp5* separated by one other gene from *dilp4*. In parallel to the adjacency of the gene loci, four out of the five DILPs (Dilp1-3, 5) are expressed in a groups of neurosecretory cells (named insulin producing cells, IPCs) in larval brain lobe and three out of five (Dilp2, 3, 5) in adult IPCs (Brogiolo et al., 2001; Ikeya, Galic, Belawat, Nairz & Hafen, 2002). The activity of IPC-derived DILPs is dynamically regulated by nutrient condition in the animals (Ikeya et al., 2002), and ablation of the IPCs causes severe growth defects, developmental timing delay and diabetic phenotypes (Rulifson, Kim & Nusse, 2002). Since the IPC-derived DILPs are the only DILPs that are expressed throughout the larval stages and function systemically, they are proposed to be the major source of DILP ligands that regulates PG function.

Except for Dilp8 which binds with a GPCR family receptor Lgr3 (Colombani et al., 2015; Garelli et al., 2015), all other DILPs are proposed to function through a single receptor, the *Drosophila* insulin receptor (InR) (Brogiolo et al., 2001; Fernandez, Tabarini, Azpiazu, Frasch & Schlessinger, 1995). Following ligand binding, InR and its signaling adaptor protein Chico (homolog to human insulin receptor substrate 1-4) initiates the downstream signaling cascade from activation of phosphatidylinositide 3-kinase (Pi3K92E), which turns phosphatidylinositol 4,5-bisphosphate (PIP2) to phosphatidylinositol 3,4,5-trisphosphate (PIP3) (Bohni et al., 1999; Leevers, Weinkove, MacDougall, Hafen & Waterfield, 1996; Weinkove, Neufeld, Twardzik, Waterfield & Leevers, 1999). Pten, a phosphatase that mediates the reverse reaction, functions as a negative regulator of the signaling pathway (Goberdhan, Paricio, Goodman, Mlodzik & Wilson, 1999). Subsequently, PIP3 recruits phosphoinositide-dependent kinase 1 (Pdk1) to the cytosolic side of

cell membrane, which phosphorylates and activates Akt1 (Cho et al., 2001; Verdu, Buratovich, Wilder & Birnbaum, 1999). Upon activation, Akt1 phosphorylates multiple downstream effectors that mediate metabolic control of the cell, such as transcription factor forkhead box protein O (Foxo) (Junger et al., 2003) and tumor sclerosis complex 1 and 2 (Tsc1 and Gigas in *Drosophila* respectively), the key regulator of target of rapamycin (TOR) pathway (Ito & Rubin, 1999; Tapon, Ito, Dickson, Treisman & Hariharan, 2001).

It has been shown that insulin/insulin-like signaling (IIS) pathway plays crucial role in developmental timing control in *Drosophila*. In studies involving systemic suppression of the IIS pathway, both ablation of IPCs and mutations in *InR* result in severe delay of the onset of metamorphosis (7 and 10 days respectively) (Brogiolo et al., 2001; Rulifson et al., 2002). In the following studies, tissue specific manipulation of the IIS pathway further corroborates this finding. In three independent studies, suppression of the IIS pathway by overexpressing either Pten or dominant negative form of Pi3K92E causes obvious developmental delay at the onset of metamorphosis (Caldwell et al., 2005; Colombani et al., 2005; C. Mirth, Truman & Riddiford, 2005), proving that the timing phenotype observed in *InR* mutant and the IPC ablation model attributes to the loss of IIS in the PG cells. Despite of the delayed timing phenotype, activation of the IIS by overexpressing Pi3K92E in the PG does not cause acceleration of development (Colombani et al., 2005), indicating that the IIS pathway itself is not sufficient to induce the ecdysone synthesis pathway in the PG.

1.2.3 Target of Rapamycin (TOR) pathway

Similar to the IIS pathway, the Target of Rapamycin (TOR) pathway is also a highly conserved pathway that responds to nutritional signals and regulates tissue growth (for review, see (Wullschleger, Loewith & Hall, 2006)). The TOR pathway is centered by the *Tor* gene, which encodes a serine/threonine kinase TOR. The TOR protein can form into two types of multiprotein complexes, TOR complex 1 (TORC1) and TOR complex 2 (TORC2). TORC1 promotes cell and tissue growth by directly regulating two downstream effectors, ribosomal protein S6 kinase (S6K)

and eukaryotic translation initiation factor 4E-binding protein (4E-BP, or Thor in *Drosophila*). Under favorable condition, phosphorylated S6K becomes activated and facilitates protein translation (Montagne et al., 1999). Phosphorylation of 4E-BP causes the dissociation between 4E-BP and translation initiation factor 4E (eIF4E), thus allowing eIF4E to function in translation process (Sonenberg & Hinnebusch, 2009). In addition, TORC1 also regulates cell growth by inhibiting autophagy. Autophagy function as a catalytic process which encloses cytosolic contents such as proteins, lipids, nucleic acids, et al. and delivers them to lysosomes for degradation (Chang & Neufeld, 2010). TORC1 suppresses autophagy by phosphorylating and thereby inhibiting the function of Atg1 and Atg13, two key components of the initiation complex of autophagy (Jung, Ro, Cao, Otto & Kim, 2010). Under nutrient deficient condition, TORC1 activity is suppressed and thus autophagy is activated, which mediates degradation of cellular contents to provide cells with essential nutrients. In contrast to TORC1, TORC2 does not have as intimate relevance as TORC1 to cell growth regulation. TORC2 is well known as a regulator of actin dynamics and cytoskeleton organization (Cybulski & Hall, 2009). However, TORC2 also phosphorylates Akt1 and thus enhances the activity of TORC1 (Hietakangas & Cohen, 2007), which establishes a link between TORC2 and cell growth regulation (Figure 6).

It has been known that TORC1 responds to multiple lines of upstream signals. Tuberous sclerosis complex (TSC), which consists of TSC1 and TSC2 (Gigas in *Drosophila*), functions as a central negative regulator of TORC1 (Gao & Pan, 2001; Potter, Huang & Xu, 2001). Nutrient and energy sensitive signals such as PI3K/Akt (Inoki, Li, Zhu, Wu & Guan, 2002; Manning, Tee, Logsdon, Blenis & Cantley, 2002; Potter, Pedraza & Xu, 2002), mitogen-activated protein kinases (MAPK) (Ma, Chen, Erdjument-Bromage, Tempst & Pandolfi, 2005; Tee, Anjum & Blenis, 2003) and AMP-activated protein kinase (AMPK) pathways (Inoki, Zhu & Guan, 2003) converge on TSC, inactivating TSC by phosphorylating TSC2. TSC functions as a GTPase activating protein (GAP) of Ras homolog enriched in brain (Rheb). Thus inactivation of TSC allows formation of GTP-bound active form of Rheb, which

subsequently activates TORC1 (Tee, Manning, Roux, Cantley & Blenis, 2003). Besides TSC and the upstream signaling pathways above, TORC1 is also directly affected by amino acid level in the cell. In mammalian cells, the cellular leucine and arginine levels are specifically detected by sensors such as sestrins (Lee, Cho & Karin, 2016), cytosolic arginine sensor for mTORC1 (CASTOR) (Chantranupong et al., 2016; Saxton, Chantranupong, Knockenhauer, Schwartz & Sabatini, 2016) and SLC38A9 amino acid transporter (Rebsamen et al., 2015; Wang et al., 2015). The sensors signal to mTORC1 depending on a machinery comprised of Rag GTPases, Ragulator complex and v-ATPase on the surface of lysosomes (Figure 6) (for review, see (Gonzalez & Hall, 2017; Saxton & Sabatini, 2017)). In *Drosophila*, homologs of most components in this amino acid sensing pathway, such as sestrin, Rag GTPases, and v-ATPase components are identified (Gleixner et al., 2014; E. Kim, Goraksha-Hicks, Li, Neufeld & Guan, 2008; Lee et al., 2010; Sancak et al., 2010) (Figure 6). In addition, a *Drosophila* amino acid transporter Slimfast is found as an amino acid sensor that regulates TOR activity, resembling the function of SLC38A9 in mammals (Colombani et al., 2003).

As a key factor that controls cellular growth, the TOR pathway links nutrient condition to the timing of *Drosophila* development. The activity of TOR pathway in PG cells responds to the systemic nutritional condition and regulates Halloween gene expression accordingly. Suppression of TOR pathway in the PG causes attenuated PG cell growth, compromised ecdysone synthesis and consequently severe developmental delay (Layalle, Arquier & Leopold, 2008). In addition to the regulation of developmental timing, TOR pathway also works as a determining factor of the nutritional checkpoints during development, which is discussed in section 1.3.1 of the Introduction session. Despite of the important role in developmental timing control, activation of TOR pathway in the PG does not cause faster development (Layalle et al., 2008) or rescue the developmental delay in *ptth* mutant (unpublished data from O'Connor lab), indicating that TOR pathway works as a STOP signal under unfavorable conditions but not a GO signal that directly stimulates ecdysone synthesis.

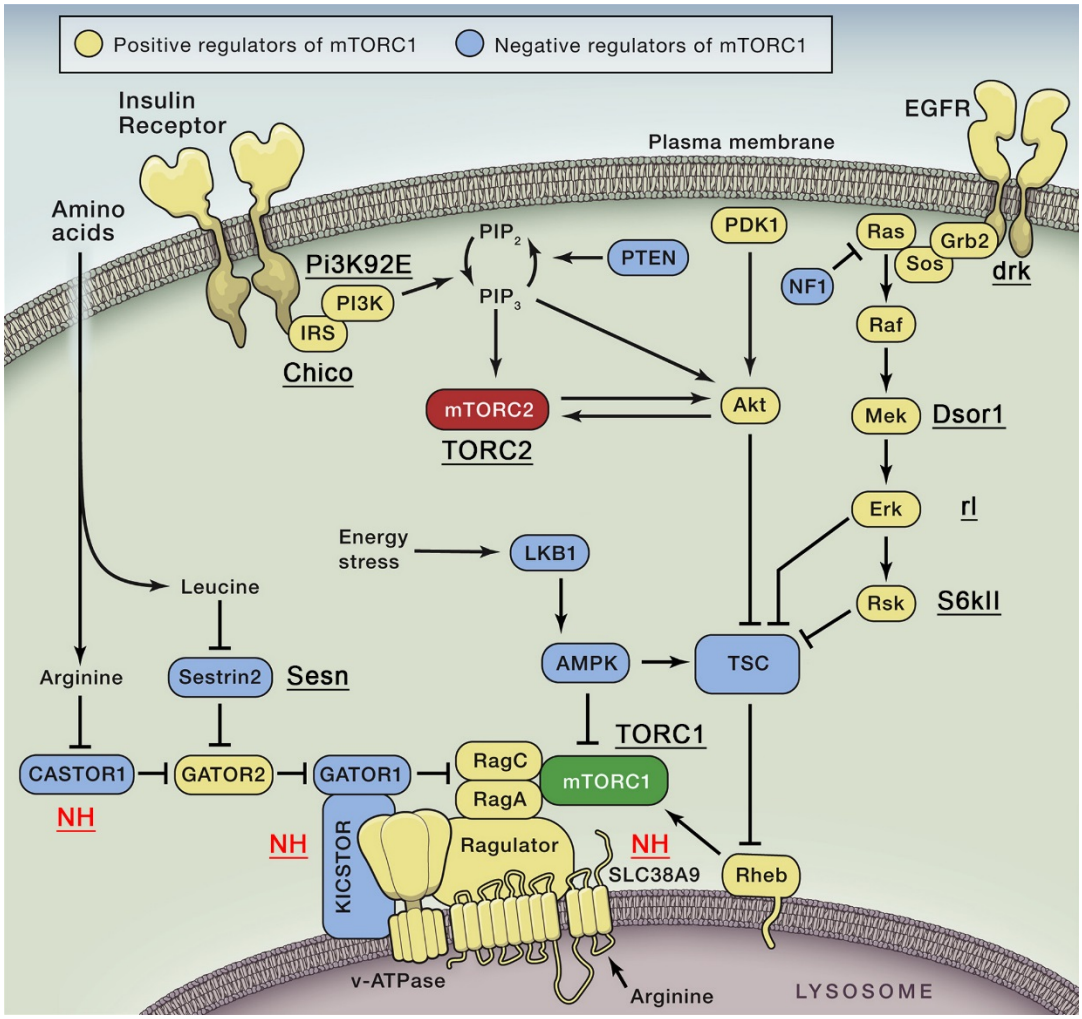

Figure 6. Target of Rapamycin pathway in mammals and *Drosophila*.
The diagram shows the upstream signaling that controls activity of TOR pathway in mammals and *Drosophila*. Most of the signaling components in mammals have recognized homologs in *Drosophila* (unmarked or marked by underscored gene symbols). “NH” in red shows the signaling components that do not have known *Drosophila* homolog. Figure adapted and simplified from (Saxton & Sabatini, 2017).

1.2.4 Transforming Growth Factor β (TGF-β) pathway

TGF-β signaling pathway is well known as a key regulator of development playing versatile roles in morphogenesis, tissue patterning, cell proliferation, cell differentiation, etc. in multiple developmental stages (for review, see (Upadhyay, Moss-Taylor, Kim, Ghosh & O'Connor, 2017)). In *Drosophila*, the TGF-β superfamily ligands can be divided into two branches, the Activin branch and the Bone Morphogenetic Protein (BMP) branch. Despite of the distinct functions, both branches of ligands signal through heterodimeric receptors comprised of type I and type II subunits, and the downstream signaling pathways also exhibit high level of similarity. In the Activin branch, three ligands Activin-β (Actβ), Dawdle (Daw) and Myoglianin (Myo) signal through type I receptor Baboon (Babo) and one of two type II receptors, either Punt or Wishful thinking (Wit). In the BMP branch, ligands including Decapentaplegic (Dpp), Glass-bottom boat (Gbb) and Screw (Scw) are recognized by type I receptor Thickveins (Tkv) or Saxophone (Sax) together with type II receptor Punt or Wit. Following activation by ligand binding, the receptors phosphorylate a Smad substrate (dSmad2 in the Activin branch or Mad in the BMP branch) which subsequently forms a complex with a co-Smad protein Medea and translocates into nucleus playing its role as a transcription factor (Figure 7) (Upadhyay et al., 2017).

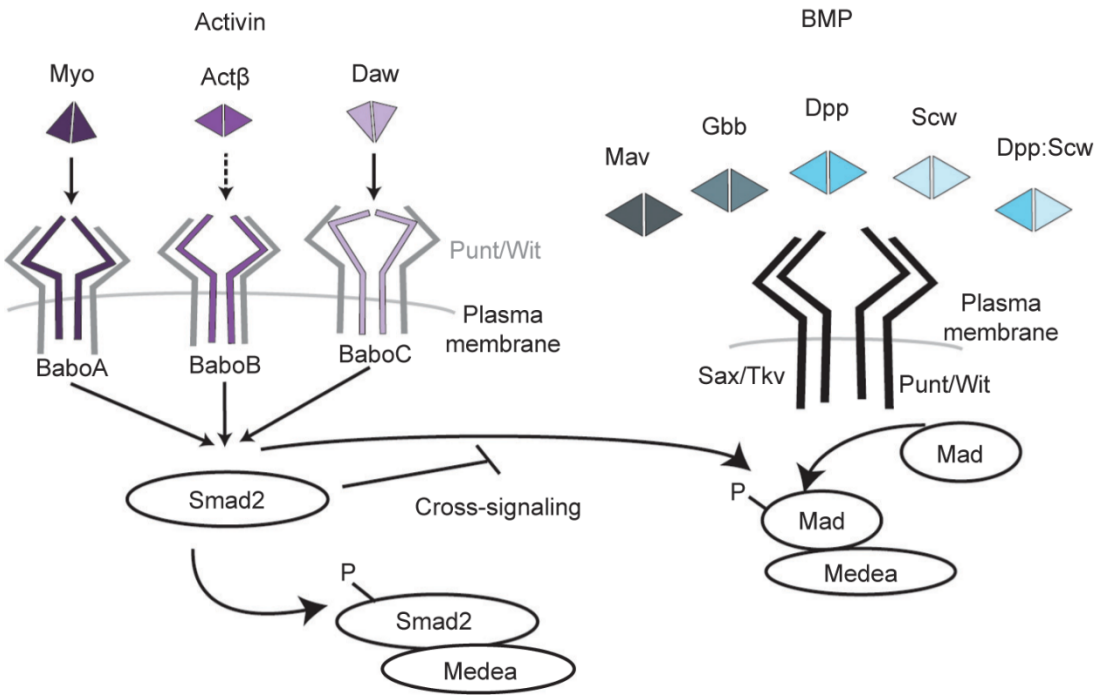

Figure 7. TGF-β signaling pathway in *Drosophila*.

The diagram shows the core signaling components of the TGF-β signaling pathway in *Drosophila*. Figure cited from (Upadhyay et al., 2017).

Both branches of the TGF-β signaling has been linked to the developmental timing control in *Drosophila*. Actβ signaling is proved critical for the ecdysteroidogenesis in PG cells. Suppression of the Actβ pathway causes strong developmental delay or developmental arrest by downregulating expression of both Torso and InR, suggesting that Actβ pathway works as a competence signal that enables the PG to respond to PTTH and insulin signals (Gibbens, Warren, Gilbert & O'Connor, 2011). In contrast to the Activin pathway, the BMP signaling is shown recently to suppress the function of PG cells. In early L3 stage the BMP family ligand Dpp is released from wing discs, which binds with receptors on PG cells. As time progressed into late L3 stage, the circulating Dpp level decreases and the suppressive effect from Dpp signaling disappears. Constitutive activation of the Dpp signaling causes dysfunction of PG cells and developmental arrest. Suppression of Dpp signaling in the PG does not cause faster development but disrupts the larval response to starvation during early stage development (Setiawan, Pan, Woods, O'Connor & Hariharan, 2018). It is intriguing that the two branches of TGF-β signaling play opposite roles in developmental timing control, especially considering the shared components such as the type II receptors and the co-Smad Medea and the crosstalk between the two pathways (Peterson & O'Connor, 2013). More details on how the pathways modulate developmental timing scheme and whether they have crosstalk in this process awaits future studies.

1.3 Environmental factors affecting developmental timing of *Drosophila melanogaster*

Although the developmental program is by large coded by the genetic constitution of a species, environment factors also pose considerable influences on the developmental progress. In *Drosophila*, a series of mechanisms have been evolved to adapt to various environmental changes during development, which are discussed below in this session.

1.3.1 Nutrient signals and nutritional checkpoints involved in developmental transition commitment

Unlike embryonic development which consumes nutrient and energy from either maternal deposits in eggs or direct support from parent, the post-embryonic development of animals largely depends on external food resources. In *Drosophila*, post-embryonic developmental stage is isolated into a high-rate foraging larval stage, which starts from larva hatching toward pupa formation (Figure 1). Beyond pupa formation, no nutrient intake and no net body mass gain occur during metamorphosis, although a very complicated developmental transition is achieved in this stage. Determined by this developmental strategy, the adult body size of *Drosophila* is mostly determined at the end of larval stage. Since the larva keeps foraging most all the time, its growth rate is largely dependent on the nutrient abundance in food. However, it is intensively difficult, if not impossible, for *Drosophila* larva to migrate to a remote food source during development when the current environment is not nutritionally favorable. To overcome the potential occurrence of poor nutrient supply, the animal evolves a mechanism to regulate its timing of development, which provides the animal an opportunity to accumulate sufficient body mass under low growth rate to support a successful development during metamorphosis.

To study the larval response to variation of nutrient condition, people designed an assay to starve the animals at different body weight and observe their response to starvation. The larval response to starvation in this assay lead to the definition of two nutritional checkpoint, minimal viable weight (MVW) and critical weight (CW). MVW is defined as the minimal body weight that enables a larva to commit to pupariate during starvation, while surpassing the CW checkpoint further makes a larva pupariate without delay under starvation (C. K. Mirth & Riddiford, 2007). Starvation before the checkpoints are reached causes developmental arrest of the animal. Under this condition, refeeding the larva results in a normal sized animal which experiences a longer period of larva stage. By contrast, starvation of a larva that has reached the CW checkpoint does not lead to any developmental

delay. In this case, the animal develops into a smaller-sized but healthy adult (Beadle, Tatum & Clancy, 1938) (Figure 8). The MVW and CW checkpoint were originally defined in other insect model systems such as tobacco hornworm *Manduca sexta*, in which MVW is reached earlier than CW (Nijhout, 1975; Nijhout & Williams, 1974a, 1974b). However, in *Drosophila* the two checkpoints coincide to be reached at the same weight (thus referred to as nutrient restriction checkpoints in Chapter 2), although they can be separated under some certain circumstances (Shimell et al., 2018; Stieper, Kupershtok, Driscoll & Shingleton, 2008). The checkpoints enable larvae to evaluate the nutrient and energy accumulation in their body when nutrient shortage takes place, thus providing the animals a better chance to successfully metamorphose into a healthy adult under this challenging situation.

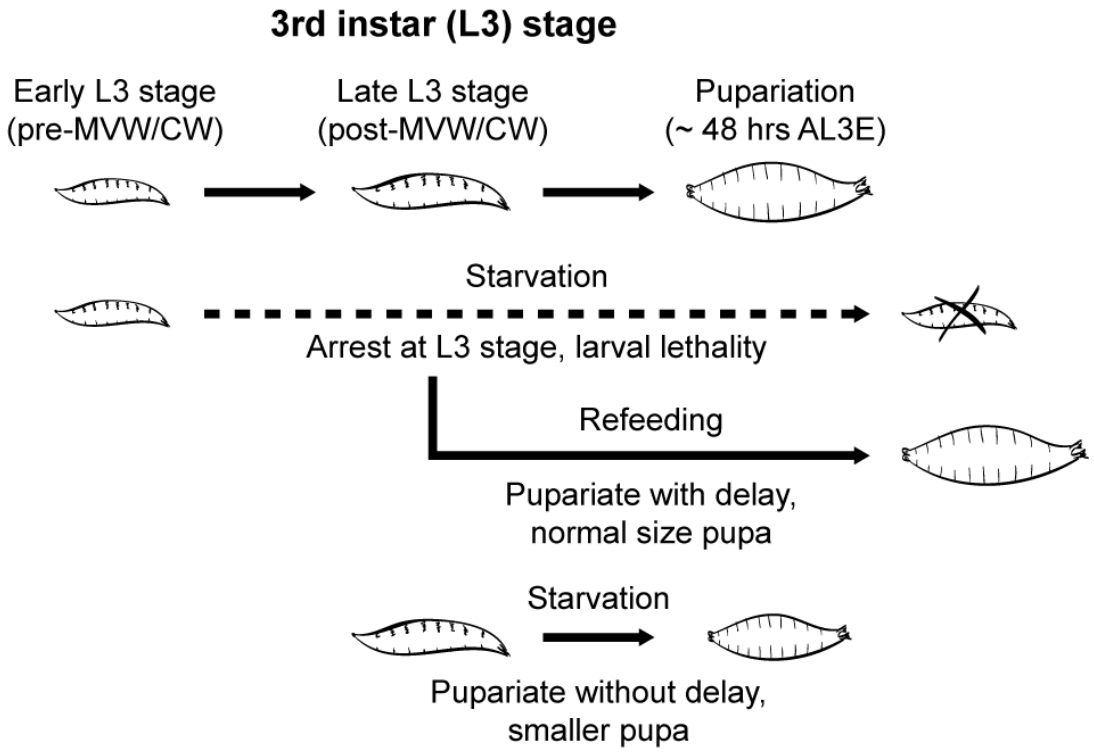

Figure 8. Developmental timing response of *Drosophila* larva to nutrient restriction.

The diagram shows how *Drosophila* larva responds to starvation treatment before and after reaching the nutritional checkpoints (MVW and CW).

Although the nutritional checkpoints have been studied for decades, the underlying mechanism that determines the checkpoints is not fully understood. Like in the timing regulation in fed condition, PG is also considered the central determining organ of the nutritional checkpoints. Studies have found that signaling pathways that respond to nutritional signals also play roles in the shaping of the checkpoints. Activation of either IIS pathway (C. Mirth et al., 2005) or TOR pathway (results in Chapter 2) in the PG causes larvae to neglection the nutritional checkpoints under starvation regardless of their body weight. As a transcription factor regulated by the IIS pathway, FoxO suppresses ecdysone synthesis by silencing Halloween gene expression in a complex with Usp during starvation. The silencing effect from FoxO/Usp complex retracts gradually as larva returns to foraging stage from the short non-foraging L2/L3 molting activity, which leads to the emergence of a small ecdysone titer in early L3 stage that coincides with the attainment of the checkpoints (Koyama, Rodrigues, Athanasiadis, Shingleton & Mirth, 2014). Feeding ecdysone at early developmental stage causes precocious pupariation of undersized larvae during starvation, suggesting that the early L3 ecdysone pulse helps determine the nutritional checkpoints (Koyama et al., 2014). Another factor that may participate in the shaping of the checkpoints is the endoreplication in PG cells which lifts the copy number of the chromosomes and thus grants cells a higher capacity of gene expression and hormone production. The endocycle keeps progress in the PG cells as larva grows during L3 stage, which achieves two rounds of replication making the chromatin value shifting from 16C to 64C. Unfavorable nutrient condition halts the endocycle progression, mediated by TORC1 inhibition. The attainment of a certain chromatin value is found required for efficient ecdysone synthesis, which marks the achievement of the nutritional checkpoints (Ohhara, Kobayashi & Yamanaka, 2017). In the Chapter 2 of this thesis, I find that autophagy, another process controlled by TOR pathway, participates in the shaping of the nutritional checkpoints. Autophagy is induced by starvation specifically in early-L3, but not late-L3 stage, which correlates with the larval pupariation response to starvation. Unlike FoxO

signaling or endoreplication of the PG cells, autophagy regulates ecdysone synthesis by disrupting cholesterol trafficking pathway, exemplifying a way to regulate pupariation activity without influencing expression of the hormone producing enzymes (Pan, Neufeld & O'Connor, 2019).

1.3.2 Temperature and photoperiod signals

It's known for long that temperature regulates the rate of growth and differentiation, and thus the timing of development and the final body size of ectothermic animals. Under most circumstances, lower temperature results in larger final body size, although the two key parameters, growth rate and duration of growth, are not always influenced in the same way (Angilletta & Dunham, 2003; Angilletta, Steury & Sears, 2004; van der Have & de Jong, 1996; Walters & Hassall, 2006; Zuo, Moses, West, Hou & Brown, 2012). The development of *Drosophila*, like other ectodermic species, is also largely influenced by the living temperature. In both wild and laboratory conditions, lower temperature causes lower growth rate, longer duration of development and cumulatively larger body size (French, Feast & Partridge, 1998; Partridge, Barrie, Fowler & French, 1994; Santos, Fowler & Partridge, 1994). Although temperature can affect growth rate directly by altering the rate of general chemical reactions, it is also found that the ambient temperature can be sensed by specific neurons in *Drosophila* which signal to the IPCs and thereby regulate body growth (Q. Li & Gong, 2015). On the other hand, temperature change also alters developmental timing by shifting the critical weight nutritional checkpoint. Under low temperature, the critical size required for non-delayed pupariation increases while the growth rate turns lower, which jointly cause a significant delay of the developmental transition (De Moed, Kruitwagen, De Jong & Scharloo, 1999; Ghosh, Testa & Shingleton, 2013).

Another important aspect of animal adaptation to the environment is their responses to light. For *Drosophila* larva, light itself does not directly impact animal development like the nutrient condition. However, it indicates other environmental information such as temperature, humidity and even chance of exposure to predators. To maximize the chance of successful metamorphic transition,

Drosophila evolves to adjust its developmental timing in response to light. In larval brain, the pigment dispersing factor (PDF) producing neurons, which play key roles in the coordination between the behavioral rhythm of animal and photoperiod (Taghert & Shafer, 2006), send direct projection to the PG neurons, which leads to rhythmic expression of PTTH in the PG neurons (McBrayer et al., 2007). Interestingly, PTTH plays dual roles at the time of larva-to-pupa transition, as a neuroendocrine factor that activates PG function and a circulating factor that induces light avoidance behavior. At the time PTTH stimulates PG function and the pupariation activity, it also signals to the Bolwig's organ and the peripheral class IV dendritic arborization neurons to induce light avoidance, which prompts the larva to initiate immobilized metamorphic stage at a dark environment (Yamanaka, Romero, et al., 2013). This mechanism also explains the observation that the timing of larval wandering behavior is well paralleled with the scotophase of photoperiod (Roberts, Henrich & Gilbert, 1987) and demonstrates the mechanism underlying the coordination between the endocrine and environmental control of developmental timing.

1.3.3 Tissue growth signals

Besides adverse environmental changes, tissue damages also cause change, frequently a delay, of developmental timing which spares animals time for regenerative repair of the injured tissues. Since the polyploidy larval tissues such as gut and fat body are digested during metamorphosis, studies on tissue damage and its influence on developmental timing are largely focused on the imaginal tissues. Using imaginal disc as a model organ, people find that damage of the discs, by either genetic manipulation or irradiation treatment, results in significant delay of development (Hackney, Zolali-Meybodi & Cherbas, 2012; Poodry & Woods, 1990; Simpson, Berreur & Berreur-Bonnenfant, 1980; Stieper et al., 2008). The tissue damage signal can further affects critical weight checkpoint, establishing a coordination between the tissue growth and nutritional signals on developmental timing control (Stieper et al., 2008). Interestingly, tissue damage causes developmental delay prior to but not after a certain time point in mid-late

L3 stage, suggesting that the developmental response to tissue damage is also developmental stage dependent (Hackney et al., 2012).

When studying the mechanism underlying the tissue growth signaling, multiple pathways have been found to play roles, such as retinoid synthesis pathway which regulates PTTH expression in the PG neurons (Halme, Cheng & Hariharan, 2010) and Dilp8 signaling which is sensed by specific neurons that innervates the PG neurons (see section 1.2.1) (Colombani et al., 2015; Colombani et al., 2012; Garelli et al., 2012; Garelli et al., 2015). In addition, BMP signaling also works as an indicator of incomplete tissue growth, which suppresses early stage ecdysteroidogenesis in PG cells and thus prevents precocious developmental transition (see section 1.2.4) (Setiawan et al., 2018). Among the signals, both Dilp8 and BMP signals emit from the imaginal discs, which explains the fact that full loss of imaginal discs does not cause developmental delay (Simpson et al., 1980). On the other hand, overgrowth of imaginal tissues also causes developmental delay while damage of the overgrown tissue rescues this defects (Sehnal & Bryant, 1993), indicating that the tissue growth signaling is not only a simple damage-response signal but a comprehensive sensing machinery that assess tissue growth and coordinate it with the overall developmental program.

In my thesis work, I uncover two more players in the developmental timing regulation and its response to environment in *Drosophila* larva. In Chapter 2, I show that autophagy functions as a temporal-specific mechanism that determines the MVW/CW nutritional checkpoints in response to starvation. I Chapter 3, I demonstrate that two additional RTK signalings, Jelly Belly (Jeb)/Anaplastic lymphoma kinase (Alk) and PDGF- and VEGF-related factor (Pvf)/ PDGF- and VEGF-receptor related (Pvr), affect developmental timing through the PG neuron-to-PG signaling axis.

CHAPTER 2

A tissue and temporal-specific autophagic switch controls pre-metamorphic nutritional checkpoints in *Drosophila melanogaster*.

2.1 Introduction

During the juvenile stage, Drosophila larvae monitor internal and external cues to properly time the onset of metamorphosis. For example, among external cues, avoidance of light at the time of pupation allows pupae to elude predation and diminish dehydration during this immobile phase of development (Yamanaka, Romero, et al., 2013). Likewise, the monitoring of internal organ health and the ability to slow larval development in response to tissue insult is advantageous since it provides an opportunity to repair tissue damage before committing to irreversible differentiation during metamorphosis (Boone, Colombani, Andersen & Leopold, 2016; Colombani et al., 2015; Colombani et al., 2012; Garelli et al., 2012; Garelli et al., 2015). Together these monitoring systems help ensure a high probability of healthy adult eclosion.

Nutrition is another key factor that requires continuous assessment during the larval stages to ensure that sufficient nutrient stores are acquired before the cessation of feeding at the onset of metamorphosis. In Lepidoptera, two distinct pre-metamorphosis nutritional checkpoints have been identified: critical weight and minimal viable weight. Critical weight is defined as the weight at which nutrient restriction (NR) no longer delays the onset of pupariation, while minimal viable weight is the minimal larval mass that is required for metamorphosis to occur (C. K. Mirth & Riddiford, 2007). In Drosophila, these two checkpoints occur at the same weight (C. K. Mirth & Riddiford, 2007), but can be separated at a certain circumstance (Shimell et al., 2018; Stieper et al., 2008). In this work, we refer to the two checkpoints collectively as the nutrient restriction checkpoints (NRCs), only distinguishing them from each other as required for additional clarity. By inhibiting pupariation of underweight larvae the nutritional checkpoints help prevent a precocious transition that would otherwise lead to pupal lethality due to storage of insufficient energy reserves. After surpassing the checkpoints, Drosophila third instar (L3) larva actually slightly accelerate development when starved and pupariate earlier than larva that do not experience NR (C. K. Mirth & Riddiford, 2007) (Figure 8), perhaps providing an adaptive advantage when food

sources become limiting.

Induction of macroautophagy (hereafter referred to as autophagy) is a common response in many tissues to NR which leads to degradation of various cellular organelles and macromolecules into their constituent components, thereby helping satisfy nutrient and energy demands during NR (Russell, Yuan & Guan, 2014). This aspect of autophagy likely plays important roles during development. For example, in some insects, autophagy aids in mobilization of nutrient stores to fuel the metamorphic remodeling process during the non-feeding pupal stage (McPhee & Baehrecke, 2009). Given that determination of the NRCs involves starvation, the mechanistic output triggered by the checkpoints could involve weight- or temporally-regulated autophagy in the prothoracic gland (PG), the major steroid hormone-producing organ in larvae. In this model, we hypothesize that induction of autophagy prior to, but not after, the NRCs could limit hormone production and thereby slow development, allowing larvae more time to search for the additional nutrients needed to pass through the NRCs.

Here we confirm this model and show that autophagy is induced by NR in Drosophila PG cells. The induction of autophagy in PG cells occurs specifically in the early, but not the late L3 stage, and suppresses ecdysone synthesis to prevent precocious pupariation during the pre-NRC stage. Furthermore, induction of autophagy disrupts ecdysone production by limiting the availability of the steroid hormone precursor cholesterol through interactions with endo/lysosome system. We also find that there are several non-conventional morphological features of the autophagy process in PG cells. These observations suggest that there may be a specialized autophagic machinery in steroidogenic cells that is specifically devoted to regulating cholesterol trafficking in response to nutritional stress. Given that several studies have suggested a role for autophagy in altering hormone synthesis in mammalian endocrine organs, our findings may be applicable in other animals as a means of controlling hormone production in response to nutritional stress.

2.2 Results

2.2.1 Autophagy in the PG is temporally regulated during the L3 stage.

To test our hypothesis concerning temporally regulated autophagy induction, we monitored the formation of mCherry (mCh)-Atg8a labeled autophagosomes and autolysosomes in the PG in response to starvation at various time points pre- and post-NRC. In the fed condition, a small number of Atg8a-positive vesicles were observed at all time points during the L3 stage, suggesting that there is an ongoing basal level of autophagy in the PG throughout the L3 stage (Figure 9A). Upon starvation both the number and total area of Atg8a-positive vesicles in the PG increased significantly in early L3 (6 hrs after L3 ecdysis, AL3E) larvae (Figure 9A-9C). However, this effect of starvation on Atg8a-positive vesicle number and area was significantly reduced at 12 hrs AL3E and was further diminished as larvae grew into the mid-L3 stage (24 hrs AL3E) (Figure 9A-9C).

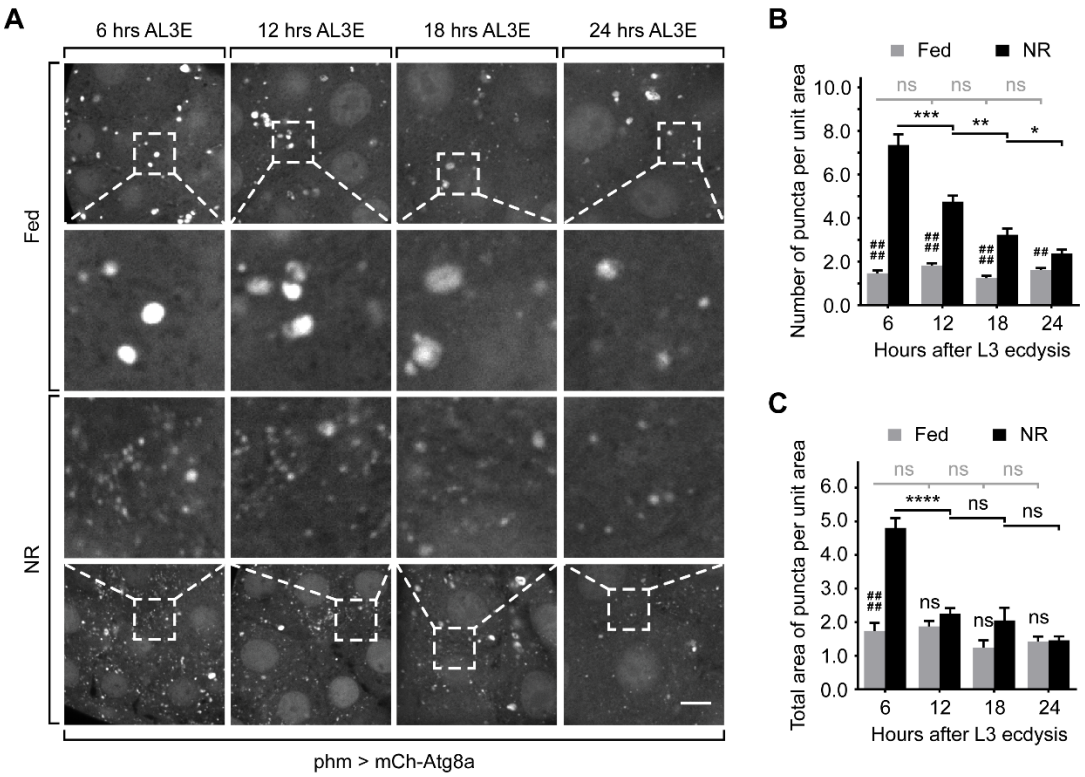

Figure 9. Autophagy in the PG is temporally regulated during the L3 stage. (A) Autophagy was visualized by mCh-Atg8a marker in PG cells. For fed groups, larvae were dissected and imaged at the indicated time points. For NR groups, larvae were starved for 4 hrs starting at the indicated time points before dissection. 4x magnified images of the indicated area are also shown. Scale bar, 10 μm. (B and C) Quantification of the number (B) and the total area (C) of Atg8a-positive puncta per unit cell area (100 μm2) in the PGs of fed and starved larvae. Mean ± SEM; p values by unpaired t-test (n=8; ns, not significant, *p<0.05, **p<0.01, ***p<0.001, ****p<0.0001, ##p<0.01, ####p<0.0001).

To test whether the increased number and area of Atg8a-positive vesicles result from autophagy induction or instead by blockage of downstream autophagic flux, we expressed GFP tagged Ref(2)P to test autophagy mediated degradation (DeVorkin & Gorski, 2014). Ref(2)P-positive protein aggregates were observed in fed larvae, which partially colocalized with Atg8a-positive autophagosomes (Figure 10A). Upon starvation, the number of Ref(2)P-positive structures did not change significantly, but the size of these structures became markedly smaller (Figure 10A-10C). These results show that protein degradation occurs normally during starvation treatment, suggesting that the changes in number and area of Atg8a-positive vesicles in PG cells represents an increased level of autophagy induction upon starvation rather than blocked degradation.

The timing of the loss of autophagy induction to starvation correlates with the NRCs, i.e. starvation pre-NRCs strongly induces autophagy while starvation post-NRCs has a much weaker effect (C. K. Mirth & Riddiford, 2007). This observation is consistent with our hypothesis that a temporally-regulated autophagy switch in PG cells contributes to suppressing the ability of larvae to pupariate before sufficient nutrient reserves are accumulated to ensure successful metamorphosis.

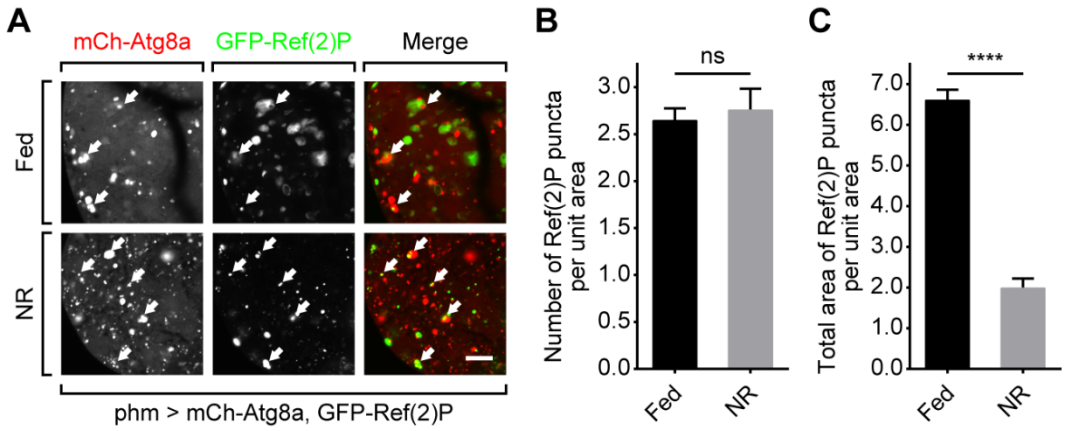

Figure 10. Autophagy induction clears Ref(2)P-positive protein aggregates in the PG.

(A) Protein aggregates and autophagosomes visualized by GFP-Ref(2)P and mCh-Atg8a respectively in fed and starved pre-MVW/CW (4 hrs AL3E) larvae. Arrows indicate the colocalization between Ref(2)P- and Atg8a-positive structures. (B and C) Quantification of the number (B) and the total area (C) of Ref(2)P-positive structures per unit cell area (100 μm^2) in the PGs of fed and starved larvae. Mean ± SEM; p values by unpaired t-test (n=6 in fed group and n=8 in NR group; ns, not significant, ****p<0.0001).

2.2.2 Autophagy induction prior to the NR checkpoints requires canonical ATG pathway components.

To determine whether autophagy induction in the PG requires known components of the autophagosome formation complex, we knocked down expression of various Atg genes in the PG using available RNAi reagents (Figure 11A-11E). We found that autophagy induction was significantly reduced by knocking down components of the autophagy initiation complex (*Atg1*, *Atg17* and *Atg101*), the membrane expansion complex (*Pi3K59F*) and the membrane recycling system (*Atg2*, *Atg9* and *Atg18*) (Feng, He, Yao & Klionsky, 2014) (Figure 11A, 11B, 11E and 11G). We also found that activation of the Target of Rapamycin (TOR) pathway in the PG through overexpression of Rheb (*phm>Rheb*) also effectively inhibited autophagy (Figure 11F and 11G). These findings indicate that the autophagy in the PG employs similar machinery and upstream control mechanisms as found during induction of canonical autophagy in other tissues (Diaz-Troya, Perez-Perez, Florencio & Crespo, 2008; Galluzzi, Pietrocola, Levine & Kroemer, 2014).

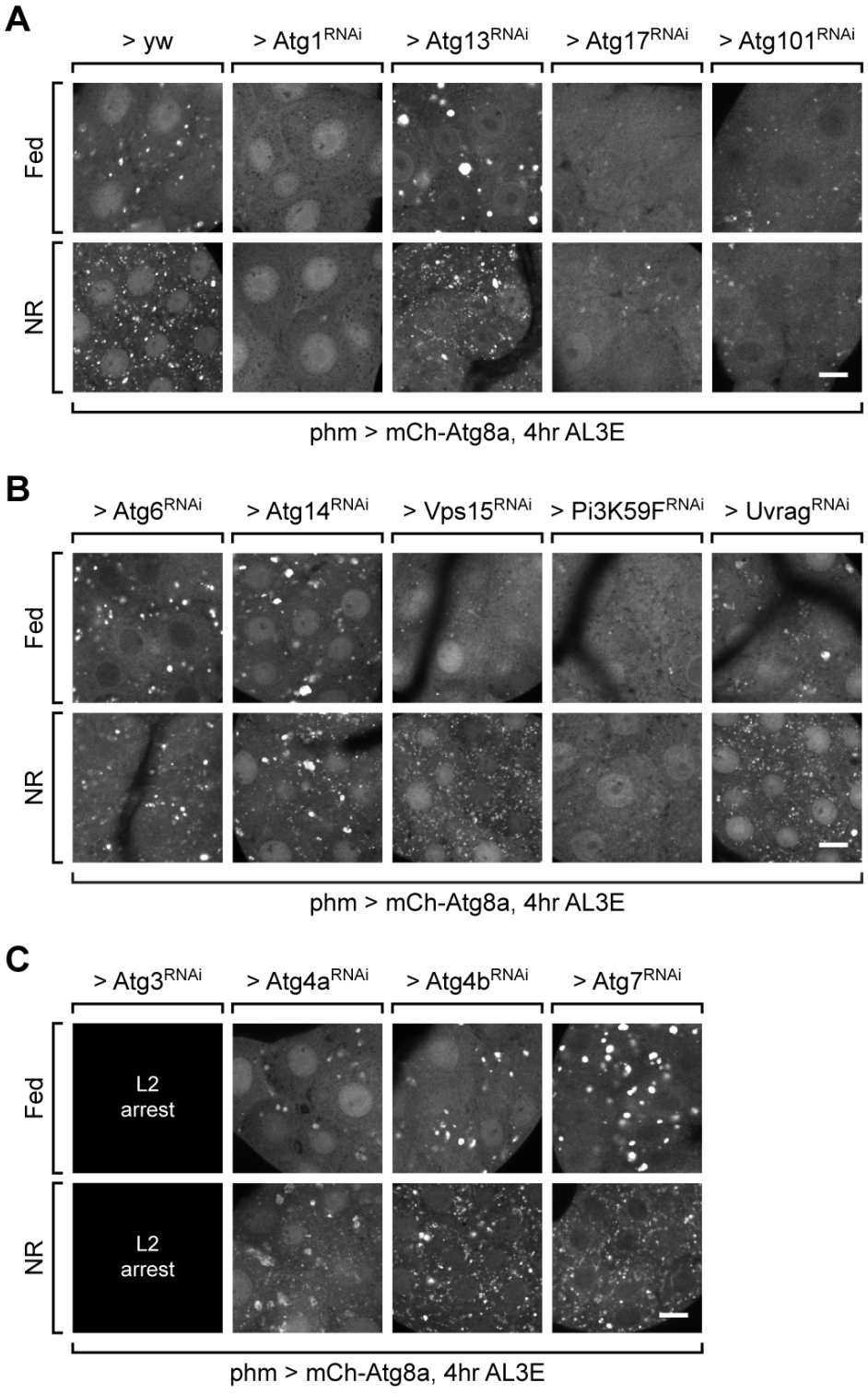

(continued in the next page)

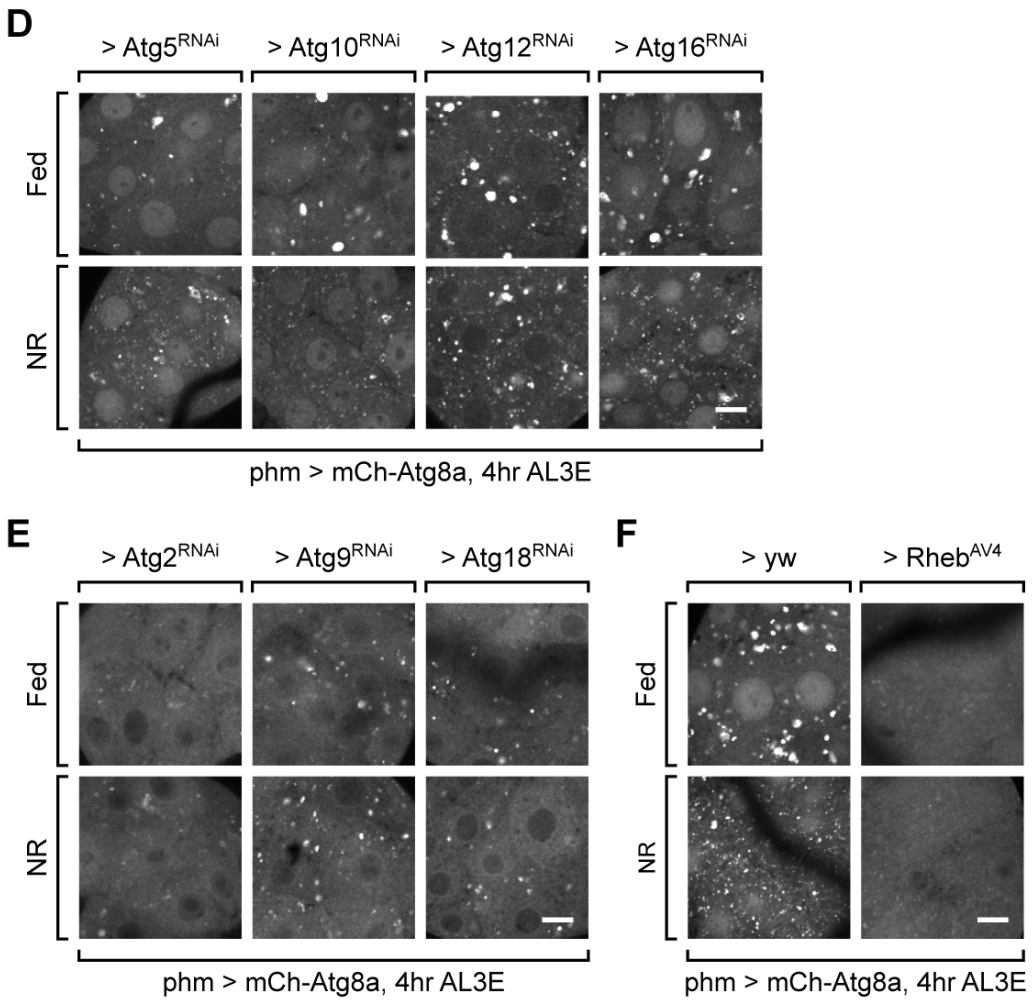
D
> Atg5RNAi
> Atg10RNAi
> Atg12RNAi
> Atg16RNAi
Fed
NR
phm > mCh-Atg8a, 4hr AL3E
E
> Atg2RNAi
> Atg9RNAi
> Atg18RNAi
Fed
NR
phm > mCh-Atg8a, 4hr AL3E
F
> yw
> RhebAV4
Fed
NR
phm > mCh-Atg8a, 4hr AL3E
G
Control
RhebAV4
Atg1
Atg13
Atg17
Atg101
Atg6
Atg14
Vps15
Pi3K59F
Uvrag
Atg4a
Atg4b
Atg7
Atg5
Atg10
Atg12
Atg16
Atg2
Atg9
Atg18
Fed
NR
0.0
2.0
4.0
6.0
8.0
Number of puncta per unit area

Figure 11. Autophagy in the PG is controlled by a subset of Atg genes and the upstream TOR pathway.

(A-E) Autophagy induction visualized by mCh-Atg8a in pre-NRC (4hr AL3E) larval PG tissues after single Atg gene knockdown. The majority of known Drosophila Atg genes were tested in five groups: the initiation complex that responds to TOR signaling (*Atg1*, *Atg13*, *Atg17* and *Atg101*) (A), the lipid kinase complex that mediates autophagosome formation (*Atg6*, *Atg14*, *Vps15*, *Pi3K59F* and *Uvrag*) (B), two ubiquitin-like conjugation systems for Atg5-Atg12-Atg16 complex (*Atg5*, *Atg10*, *Atg12* and *Atg16*) and Atg8-PE formation (*Atg3*, *Atg4a*, *Atg4b* and *Atg7*) (C and D) and the Atg9 centered system whose function is not fully understood (*Atg2*, *Atg9* and *Atg18*) (E). (F) Autophagy induction visualized by mCh-Atg8a in pre-NRC (4 hrs AL3E) *phm>yw* and *phm>Rheb*^{AV4} larval PG tissues. (G) Quantification of number of Atg8a-positive vesicle per unit cell area (100 μm2) in the Atg gene knockdown and Rheb overexpression PGs. Mean ± SEM. (n=3-5).

2.2.3 Autophagy inhibition in PG cells suppresses the NR checkpoints.

To determine whether autophagy induction is responsible for delayed pupariation upon starvation of pre-NRC larvae, we first tested pupariation activity of larvae when autophagy was suppressed in the PG. In fed animals, suppression of autophagy by expressing *phm>Atg1^{RNAi}*, *phm>Atg9^{RNAi}* or *phm>Rheb* did not significantly affect developmental timing nor larval growth rate. (Figure 12A and 12B). Early L3 starvation (2-8 hrs AL3E, pre-NRC stage) caused delayed pupariation and decreased the pupariation rate in control larvae (Figure 13A-13D, 14A and 14B), which is consistent with previous reports (Beadle et al., 1938; C. Mirth et al., 2005). However, *phm>Atg1^{RNAi}* and *phm>Atg9^{RNAi}* larvae showed higher rates of pupariation (although delayed) when starved during the early L3 stage (Figure 13E, 13F and 14A), indicating a shift of the minimal viable weight checkpoint in these larvae. Similarly, the majority of *phm>Rheb* larvae pupariated without delay regardless of the starting point of starvation (Figure 13G and 14A), showing that both the minimal viable weight and the critical weight checkpoints are altered. In contrast to pupariation, the eclosion rate under starvation was not affected by autophagy suppression (Figure 14C and 14D). Taken together, these data demonstrate that autophagy induction blocks pupariation activity of larvae during early stage NR. Upon autophagy suppression many more larvae formed pupa, but these pupae did not produce viable adults (Figure 14C). By preventing pupation before sufficient nutrient reserves have accumulated to produce viable adults, this mechanism likely improves the chance of survival during NR stress by enabling larva to search for new food sources instead of initiating an ill-fated attempt at metamorphosis.

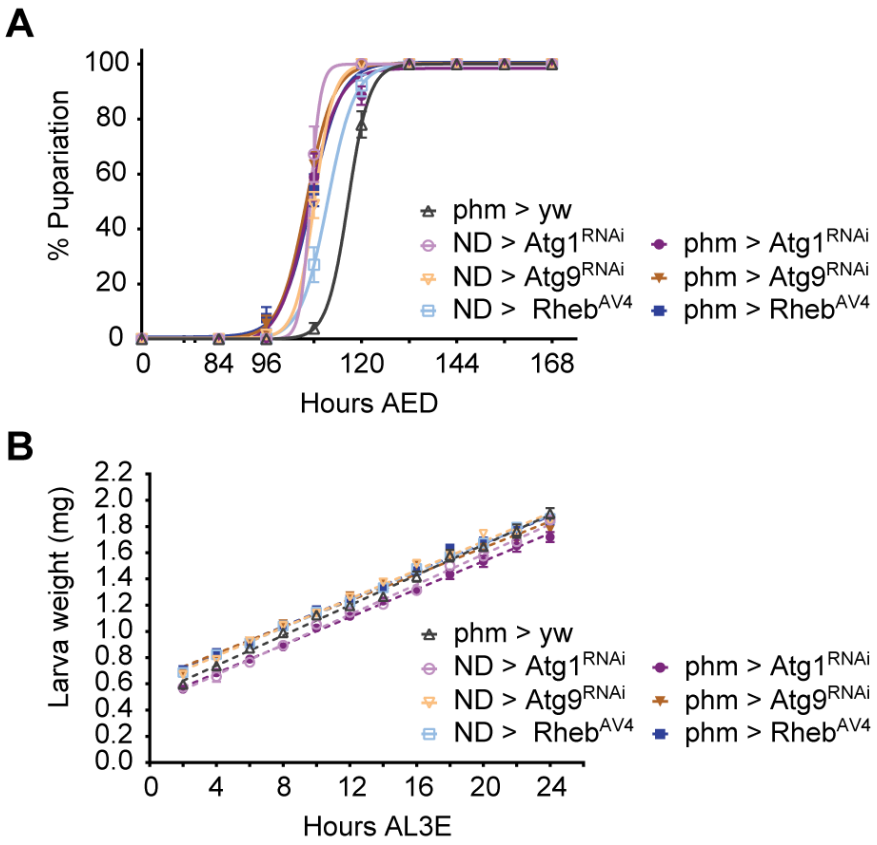

Figure 12. Autophagy suppression does not significantly affect developmental timing and growth rate under fed condition.

(A and B) Pupariation timing curve (A) and growth rate (B) of control (*phm-Gal4* and no driver (ND) control) and autophagy suppression larvae.

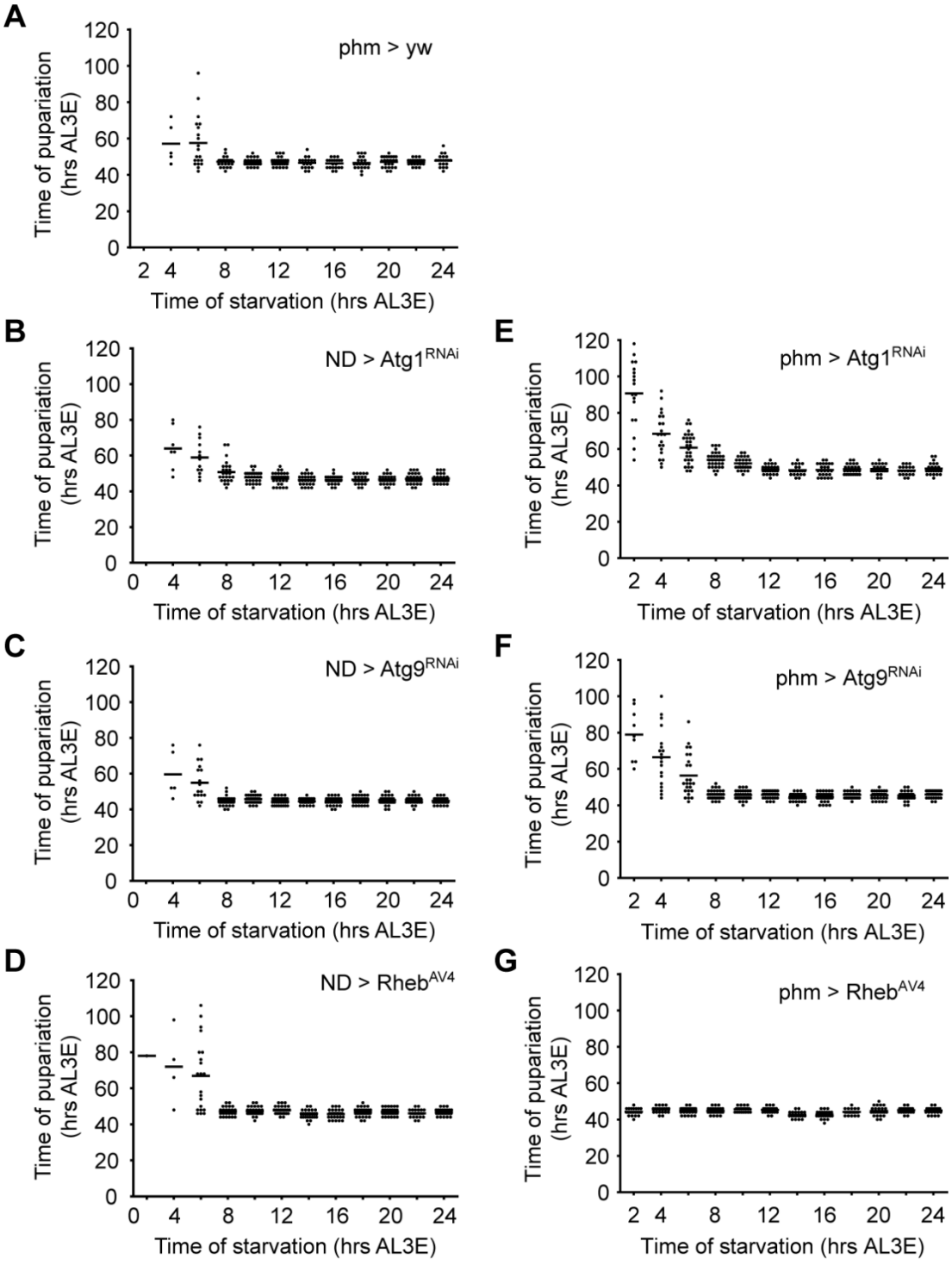
A
phm > yw
B
ND > Atg1RNAi
C
ND > Atg9RNAi
D
ND > RhebAV4
E
phm > Atg1RNAi
F
phm > Atg9RNAi
G
phm > RhebAV4
Time of pupariation (hrs AL3E)
Time of starvation (hrs AL3E)

Figure 13. Autophagy suppression in the PG during early stage NR stimulates inappropriate pupariation.

(A-G) Relationship between start time of starvation treatment and the time from the L2/L3 molting to pupariation for *phm>yw* (A), *ND>Atg1^{RNAi}* (B), *ND>Atg9^{RNAi}* (C) and *ND>Rheb^{AV4}* (D), *phm>Atg1^{RNAi}* (E), *phm>Atg9^{RNAi}* (F) and *phm>Rheb^{AV4}* (G) larvae (n > 30 for each time point).

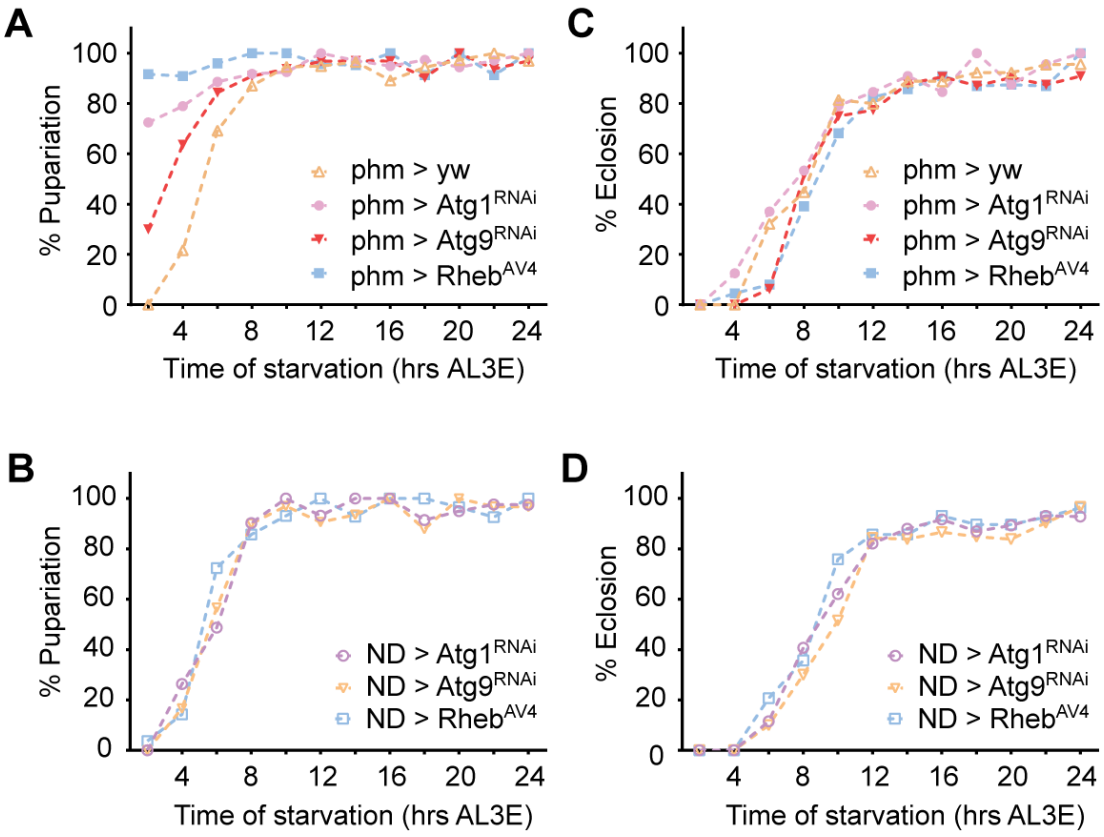

Figure 14. Autophagy suppression in the PG during early stage NR stimulates inappropriate pupariation (continued).

(A and B) Percentage of larvae that manage to pupariate after starvation treatment starting from different time points AL3E. (C and D) Percentage of larvae that end up eclosing from pupa after starvation treatment starting from different time points AL3E.

2.3.4 Forced autophagy induction in the PG causes developmental delay/arrest in fed larvae.

To further corroborate our finding that autophagy controls pupariation, we next examined whether ectopically activating autophagy is sufficient to block larval pupariation in the absence of NR stress. Constant autophagy induction in the PG (*phm>Atg1* or *phm>TSC1/2*) caused L1/L2 developmental arrest (data not shown). Therefore, we employed *phm^{GeneSwitch} (phm^{GS})-Gal4*, a driver induced by RU486 (Figure 15A and 15B), to activate autophagy specifically after L2/L3 molting (Roman, Endo, Zong & Davis, 2001). Without RU486 addition, neither *phm^{GS}>Atg1* nor *phm^{GS}>TSC1/2* stimulated autophagy induction or changed developmental timing (Figure 16A and 17A). However, RU486 administration markedly stimulated autophagy (Figure 17A) and caused developmental delay/arrest in *phm^{GS}>Atg1* and *phm^{GS}>TSC1/2* larvae (Figure 17C and 17D). Since autophagy induction by Atg1 overexpression may cause cell apoptosis (Scott, Juhasz & Neufeld, 2007), we sought to rule out this possibility by staining for apoptotic PG cells using an antibody targeting cleaved caspase-3 (Fan & Bergmann, 2010). In RU486 treated *phm^{GS}>Atg1* and *phm^{GS}>TSC1/2* larvae, we did not observe any of cleaved caspase-3 positive cells, showing that autophagy induction in PG cells does not causes apoptosis (Figure 17B). Thereby, we conclude that RU486 feeding likely causes developmental defects by inducing inappropriate levels of autophagy in the PG.

Intriguingly, the extent of the autophagy-induced developmental defects correlated with the length and the strength of autophagy induction. Stimulation of autophagy either at pre-NRC (4 hrs AL3E) or post-NRC (12 hrs AL3E) time points (Figure 16B) caused developmental delay and reduced pupariation rates. However, early induction (4 hrs AL3E) resulted in a longer delay and a higher rate of developmental arrest than late (12 hrs AL3E) induction. Similarly, feeding higher concentrations of RU486 also resulted in stronger developmental delays and lower pupariation rates (Figure 17C and 17D). These data demonstrate that strong induction of autophagy in the PG is capable of blocking pupariation

regardless of larva body weight and nutritional status and functions in a “dose” dependent manner. We propose that as wildtype larvae grow and surpass the NR checkpoints, NR is no longer able to induce autophagy to the threshold level required to block pupariation, thereby enabling larvae to initiate metamorphosis even when nutrient access is limited.

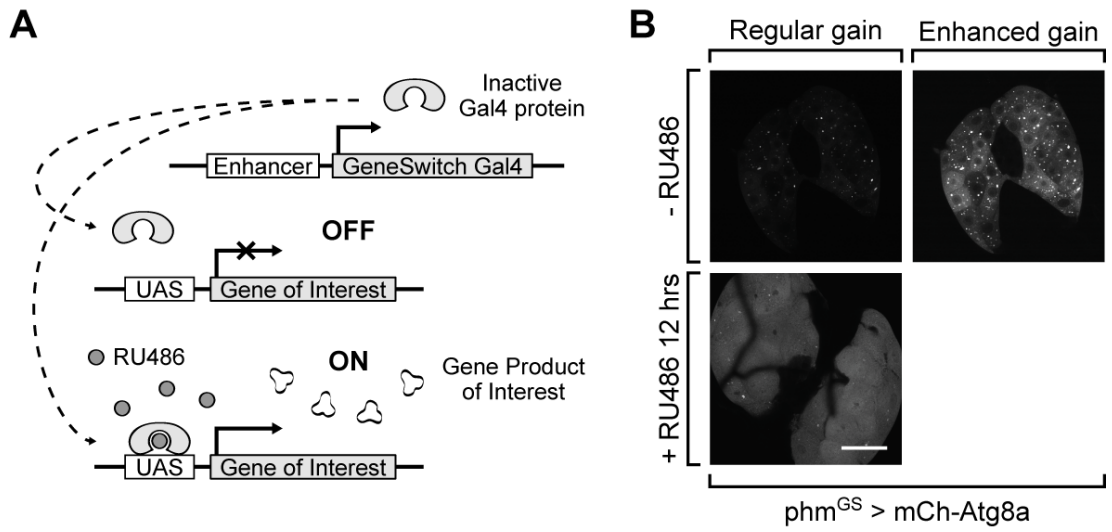

Figure 15. The chemical induced GeneSwitch system.

(A) Schematic diagram showing the RU486-induced GeneSwitch system. (B) Expression of mCh-Atg8a in *phm^{GS}>mCh-Atg8a* PGs before and after RU486 treatment. The treatment started at 12 hrs AL3E and lasted for 12 hrs. Both groups were imaged first under the same parameter (regular gain) to compare the level of target gene (here mCh-Atg8a) expression before and after RU486 treatment. Then the -RU486 images, in which the fluorescence signal was almost indiscernible under regular gain, were retaken with enhanced gain to show the tissue outline. Scale bar, 50 μm.

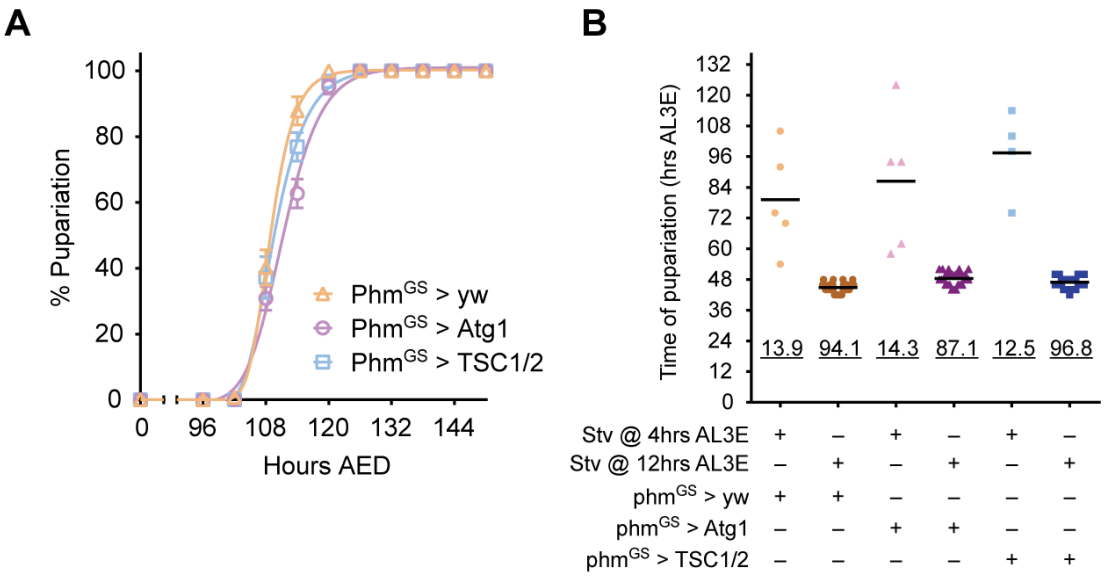

Figure 16. Uninduced GeneSwitch transgenes do not cause changes on developmental timing and nutritional checkpoint determination.

(A) Pupariation timing curves of *phm^{GS}>yw*, *phm^{GS}>Atg1* and *phm^{GS}>TSC1/2* larvae without RU486 feeding. (B) Pupariation of larvae after starvation treatment starting at early-L3 (4 hrs AL3E) or mid-L3 (12 hrs AL3E) stage. The result confirmed that the MVW/CW for all the tested groups were achieved between 4 hrs and 12 hrs AL3E. The scattered dots indicate the time of pupariation of each individual larva. The underscored numbers indicate the rate of pupariation. For each group n > 30.

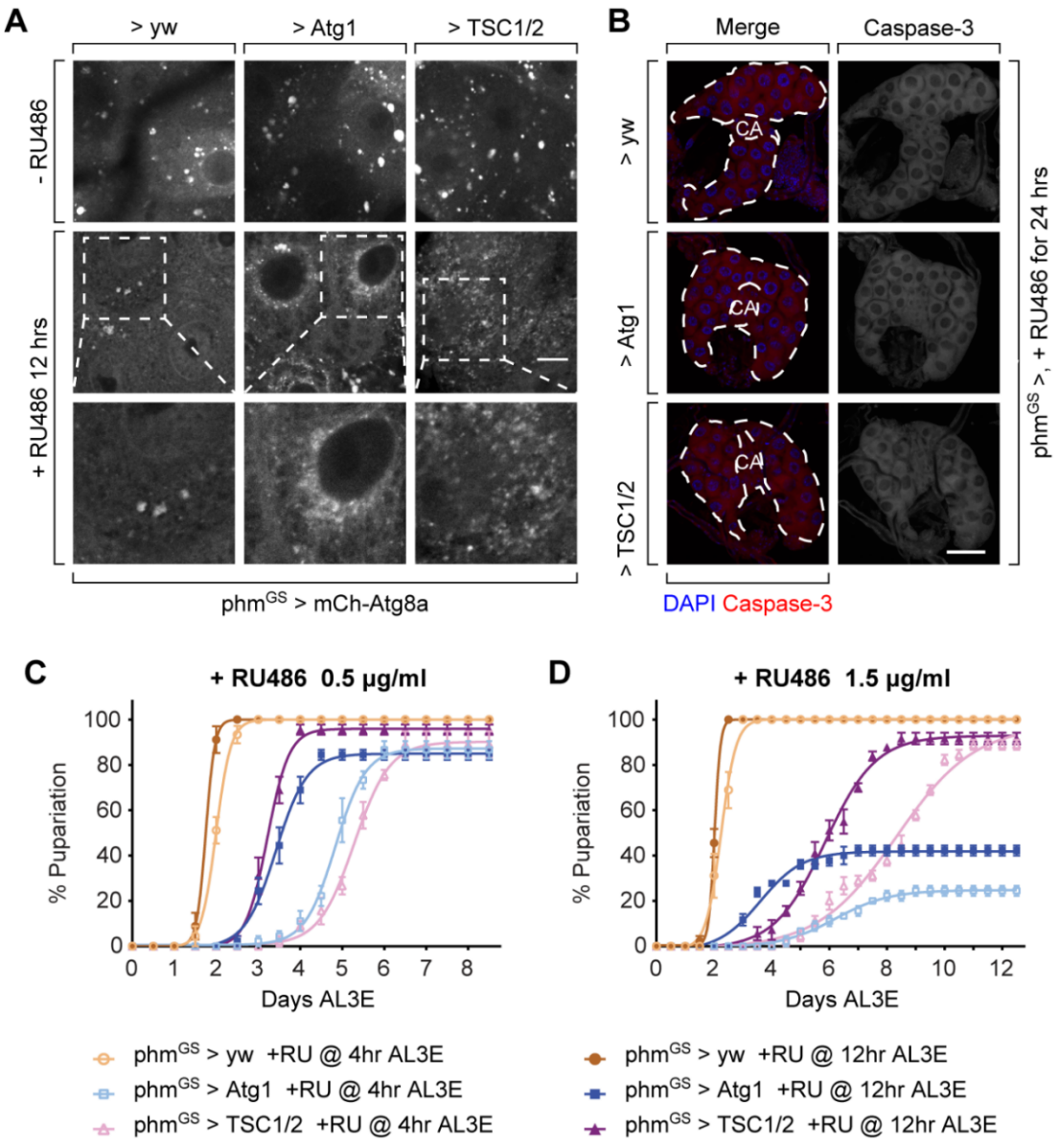

Figure 17. Forced autophagy induction in the PG causes developmental delay/arrest in fed larvae.

(A) Autophagy induction in the PG before and after RU486 induction in *phm^{GS}>yw*, *phm^{GS}>Atg1* and *phm^{GS}>TSC1/2* larvae at 12 hrs AL3E. In RU486 fed *phm^{GS}>Atg1* larvae the autophagic vesicles located at perinucleus region, which is consistent with previous study (Chang & Neufeld, 2009), while in *phm^{GS}>TSC1/2* larvae these vesicles showed similar distribution as NR-induced

autophagy. Scale bar, 10 μm. (B) Immunofluorescence images of PGs in RU486 treated *phm^{GS}>yw*, *phm^{GS}>Atg1* and *phm^{GS}>TSC1/2* larvae. Larvae were fed with RU486 for 24 hrs, starting at 12 hrs AL3E, before dissection. PG tissues were immunostained with antibody targeting cleaved caspase-3. Dash lines indicate the outline of PGs. Corpora allata (CA), whose cells were not affected by autophagy induction, were marked as internal control. Scale bar, 50 μm. (C and D) Pupariation timing curves of *phm^{GS}>yw*, *phm^{GS}>Atg1* and *phm^{GS}>TSC1/2* larvae fed with 0.5 μg/ml (C) or 1.5 μg/ml (D) RU486 at 4 hrs (pre-NRC) or 12 hrs AL3E (post-NRC) time points. Mean ± SEM, n=3.

2.3.5 Autophagy blocks ecdysone synthesis by limiting cholesterol availability in PG cells.

After confirming that induction of autophagy disrupts larva pupariation, we wished to determine how autophagy disrupts developmental timing and pupariation control. Since pupariation activity is directly regulated by ecdysone (Yamanaka, Rewitz, et al., 2013), we first measured the level of the larval wandering stage ecdysone pulse that triggers pupariation. In autophagy suppressed larvae, the ecdysone peak at larval wandering stage was comparable to the control without starvation. However, pre-NRC (4 hrs AL3E) starvation prevented the rise of in the ecdysone titer at the end of L3 stage in control, but not *phm>Rheb* larvae (Figure 18A), which is consistent with the increased pupariation of *phm>Rheb* larvae (Figure 13G and 14A). *phm>Atg1*^{RNAi} larvae showed a modest but insignificant increase in the ecdysone titer under pre-NRC starvation (Figure 18A), which may be attributed to the delayed and unsynchronized pupariation these larvae exhibit when starved (Figure 13E). In a complementary experiment where we induced autophagy post-NRC (12 hrs AL3E) in *phm*^{GS}*>Atg1* or *phm*^{GS}*>TSC1/2* larvae, we saw very limited ecdysone production at larval wandering stage compared to the control (Figure 18B). Thus, we conclude that autophagy blocks larva pupariation by disrupting ecdysone production in PG cells at the time of pupariation.

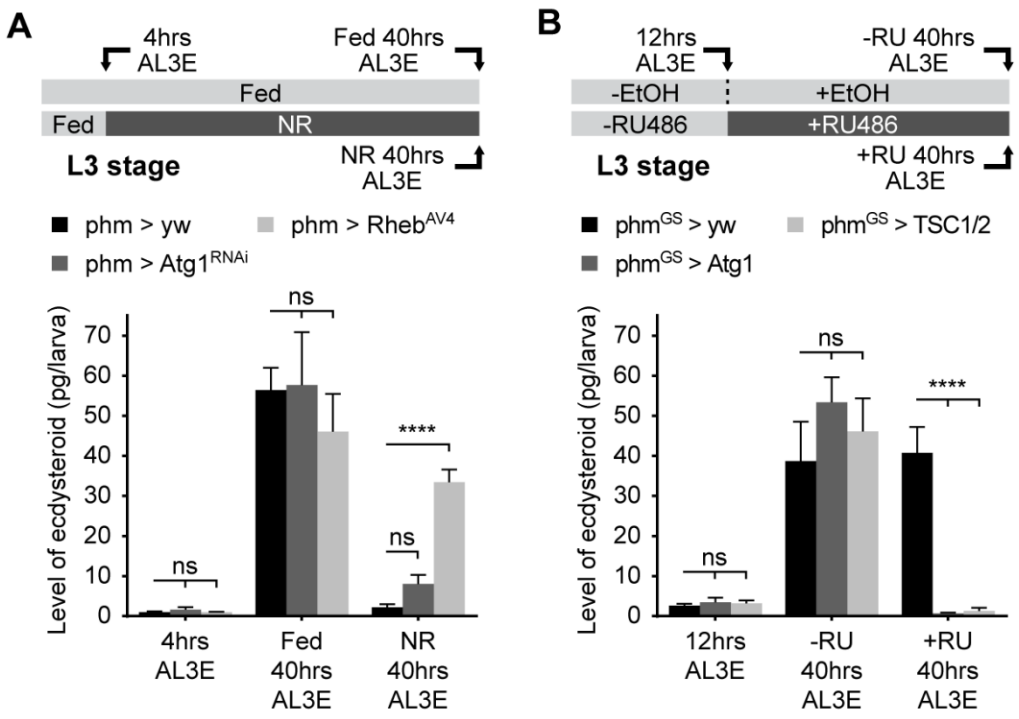

Figure 18. Autophagy blocks developmental transition by disrupting ecdysone synthesis.

(A) Quantification of ecdysone/20-hydroxyecdysone titers in whole L3 larvae at different timing stages and nutritional conditions in *phm>yw*, *phm>Atg1^{RNAi}* and *phm>Rheb^{AV4}* larvae. (B) Quantification of ecdysone/20-hydroxyecdysone levels in whole L3 larvae at different stages with or without 1.5 µg/ml RU486 feeding in *phm^{GS}>yw*, *phm^{GS}>Atg1* and *phm^{GS}>TSC1/2* larvae. (A and B) Mean ± SEM; p values by unpaired t-test (n=4; ns, not significant, ****p<0.0001).

Ecdysone is synthesized from cholesterol by a series of oxidation and reduction steps that involve a number of enzymes collectively encoded by the “Halloween” genes (Gilbert, 2004). Considering that autophagy commonly exerts degradative functions, we sought to determine if degradation of Halloween enzymes might be responsible for the low level of ecdysoneproduction when autophagy is induced. Examination of Phantom (Phm), Disembodied (Dib) and Spookier (Spok) protein levels in the PG using immunohistochemical (IHC) method indicates that autophagy induction does not substantially deplete any of these enzymes (Figure 19A-19C), suggesting that autophagy likely does not function through ecdysone biosynthetic protein degradation.

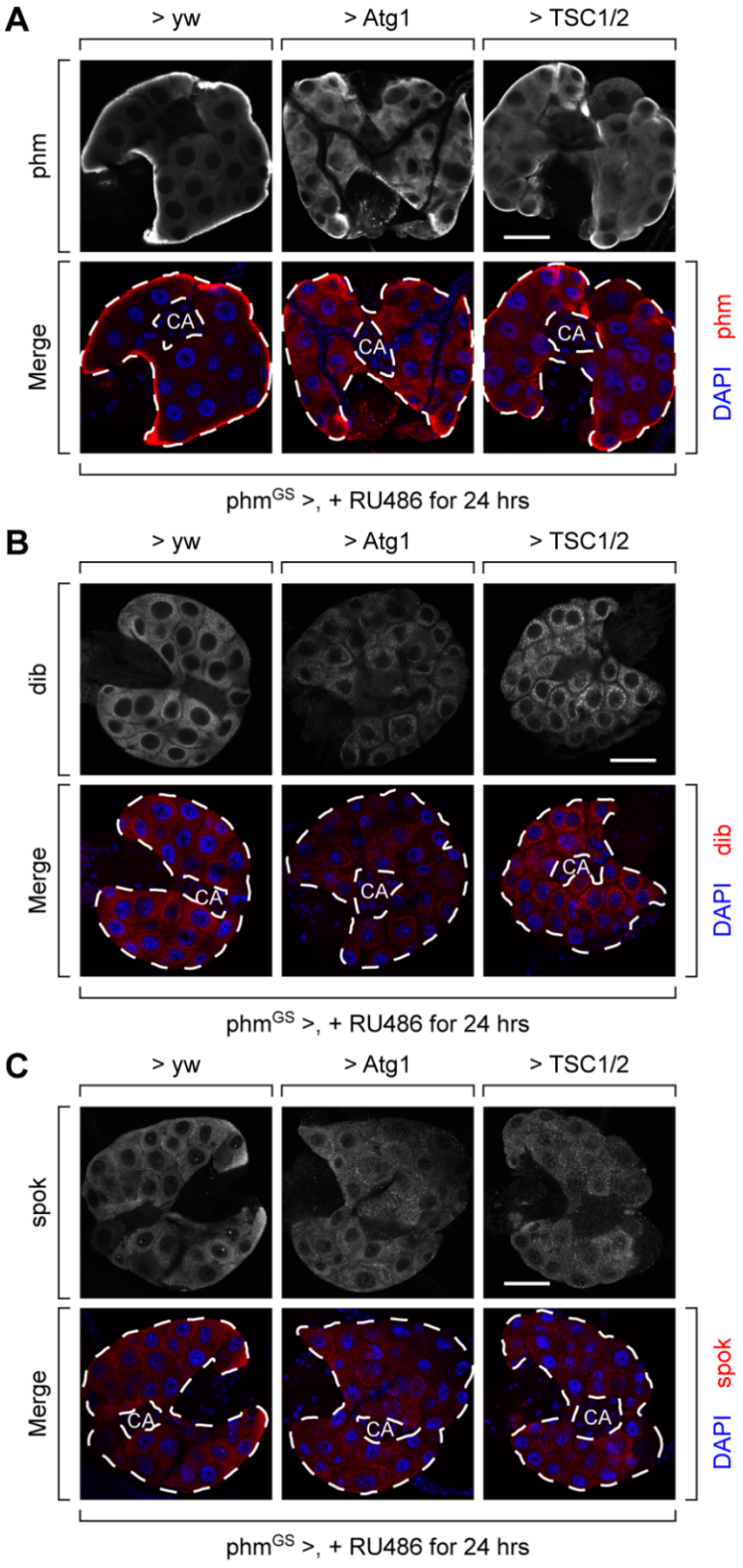
A
> yw
> Atg1
> TSC1/2
phm
Merge
CA
DAPI phm
phmGS >, + RU486 for 24 hrs
B
> yw
> Atg1
> TSC1/2
dib
Merge
CA
DAPI dib
phmGS >, + RU486 for 24 hrs
C
> yw
> Atg1
> TSC1/2
spok
Merge
CA
DAPI spok
phmGS >, + RU486 for 24 hrs

Figure 19. Autophagy does not deplete ecdysonesynthesizing enzymes in the PG.

(A-C) Immunofluorescence images of PGs in *phm^{GS}>yw*, *phm^{GS}>Atg1* and *phm^{GS}>TSC1/2* larvae. Larvae were treated with RU486 starting at 12 hrs AL3E and samples were dissected at 36 hrs AL3E. PG tissues were immunostained with anti-Phm (A), anti-Dib (B) and anti-Spok (C) antibodies. Dash lines indicate the outline of PGs. Corpora allata (CA), which do not express any Halloween gene, are also outlined and indicated in the images. Scale bar, 50 μm.

Since previous studies have demonstrated that autophagy can mediate cholesterol transportation in both mammals and flies (Danielsen et al., 2016; Ouimet et al., 2011), we next examined whether autophagy affects cholesterol homeostasis in the PG. As a steroid hormone producing organ, the PG maintains a pool of cholesterol storage in lipid droplets. We observed a number of lipid droplets in PG cells of pre-NRC fed larvae, consistent with previous findings (Danielsen et al., 2016; Talamillo et al., 2013), while the number of lipid droplets significantly decreased after NR treatment. In contrast, we observed an increased number of lipid droplets in *phm>Atg1*^{RNAi} and *phm>Rheb* larvae compared with *phm>yw* control, while the number did not significantly change during NR (Figure 20A and 20B). Additionally, autophagy induction in RU486 treated *phm*^{GS}*>Atg1* or *phm*^{GS}*>TSC1/2* larvae also caused a decrease in lipid droplet number in PG cells (Figure 20C and 20D). These data indicate that autophagy induces clearance of lipid droplets in PG cells.

To test the interaction between autophagy and cholesterol trafficking, we first cultured PG tissue *ex vivo* with NBD-cholesterol. Many Atg8a-positive vesicles overlapped with the NBD signal, suggesting that these autophagic vesicles contain cholesterol (Figure 20E). mCh-Atg8a also showed colocalization with EYFP-NPC1a (Figure 20F), a key transmembrane protein mediating cholesterol trafficking (Huang et al., 2005), consistent with the notion that autophagy functions to transport cholesterol. We then sought to visualize the ultrastructure of autophagy in PG cells using transmission electron microscopy (TEM). In the PG of starved pre-NRC animals, we observed double-membrane bound vesicles containing homogenous content of light density (Figure 21A), typical of structures found in cells undergoing lipid-processing autophagy (lipophagy) (Singh et al., 2009). In addition, we also observed lipophagy related structures which exhibited a cluster of small, single or double membrane bound vesicles that contain similar light-density content (Figure 21B) as well as double membrane bound autophagic vesicles containing non-lipid cargoes (Figure 21C). These structures were seldomly found in *phm>Atg1*^{RNAi} or *phm>Rheb* PG cells, confirming their

autophagic nature (Figure 21D-21G). Together, the data from both fluorescence and electron microscopy confirm that autophagy participates in cholesterol trafficking in PG cells.

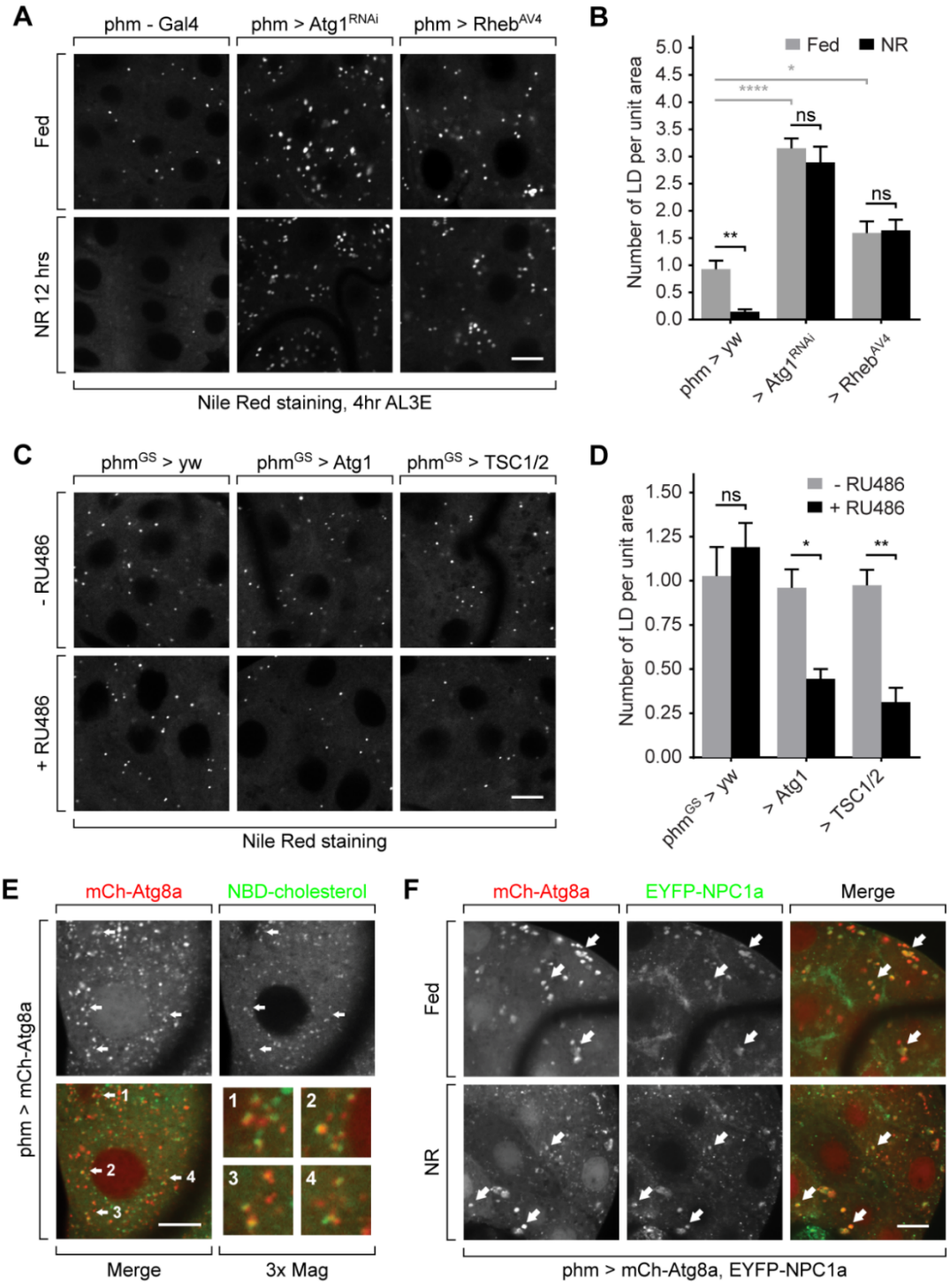
A
phm - Gal4
phm > Atg1RNAi
phm > RhebAV4
Fed
NR 12 hrs
Nile Red staining, 4hr AL3E
B
Fed
NR
Number of LD per unit area
5.0
4.5
4.0
3.5
3.0
2.5
2.0
1.5
1.0
0.5
0.0
*
****
ns
ns
**
phm > yw
> Atg1RNAi
> RhebAV4
C
phmGS > yw
phmGS > Atg1
phmGS > TSC1/2
- RU486
+ RU486
Nile Red staining
D
- RU486
+ RU486
Number of LD per unit area
1.50
1.25
1.00
0.75
0.50
0.25
0.00
ns
*
**
phmGS > yw
> Atg1
> TSC1/2
E
mCh-Atg8a
NBD-cholesterol
phm > mCh-Atg8a
1
2
3
4
Merge
3x Mag
F
mCh-Atg8a
EYFP-NPC1a
Merge
Fed
NR
phm > mCh-Atg8a, EYFP-NPC1a

Figure 20. Autophagy constrains cholesterol availability in the PG by interacting with cholesterol trafficking pathway.

(A) Lipid droplets visualized by Nile Red staining in *phm>yw*, *phm>Atg1^{RNAi}* and *phm>Rheb^{AV4}* PG cells before and after NR. Scale bar, 10 μm. (B) Quantification of number of lipid droplet per unit area (100 μm^2) in *phm>yw*, *phm>Atg1^{RNAi}* and *phm>Rheb^{AV4}* PG cells. Mean ± SEM; p values by unpaired t-test (n=5; ns, not significant, *p<0.05, **p<0.01, ****p<0.0001). (C) Lipid droplets visualized by Nile Red staining in *phm^{GS}>yw*, *phm^{GS}>Atg1* and *phm^{GS}>TSC1/2* larvae with or without RU486 feeding. Scale bar, 10 μm. (D) Quantification of number of lipid droplet per unit area (100 μm^2) in *phm^{GS}>yw*, *phm^{GS}>Atg1* and *phm^{GS}>TSC1/2* larvae. Mean ± SEM; p values by unpaired t-test (n=5; ns, not significant, *p<0.05, **p<0.01). (E) *phm>mCh-Atg8a* PGs were incubated *ex vivo* in culture medium containing 22-NBD-cholesterol (green) and then imaged by fluorescence microscopy. Arrows indicate the overlap of two signals and the numbered images show zoomed-in views of the corresponding areas indicated by the arrows. Scale bar, 10 μm. (F) Fluorescence microscopy images of PG tissues expressing mCh-Atg8a and EYFP-NPC1a. Arrows indicate colocalization of vesicles positive of both mCherry-Atg8a and NBD signals. Scale bar, 10 μm.

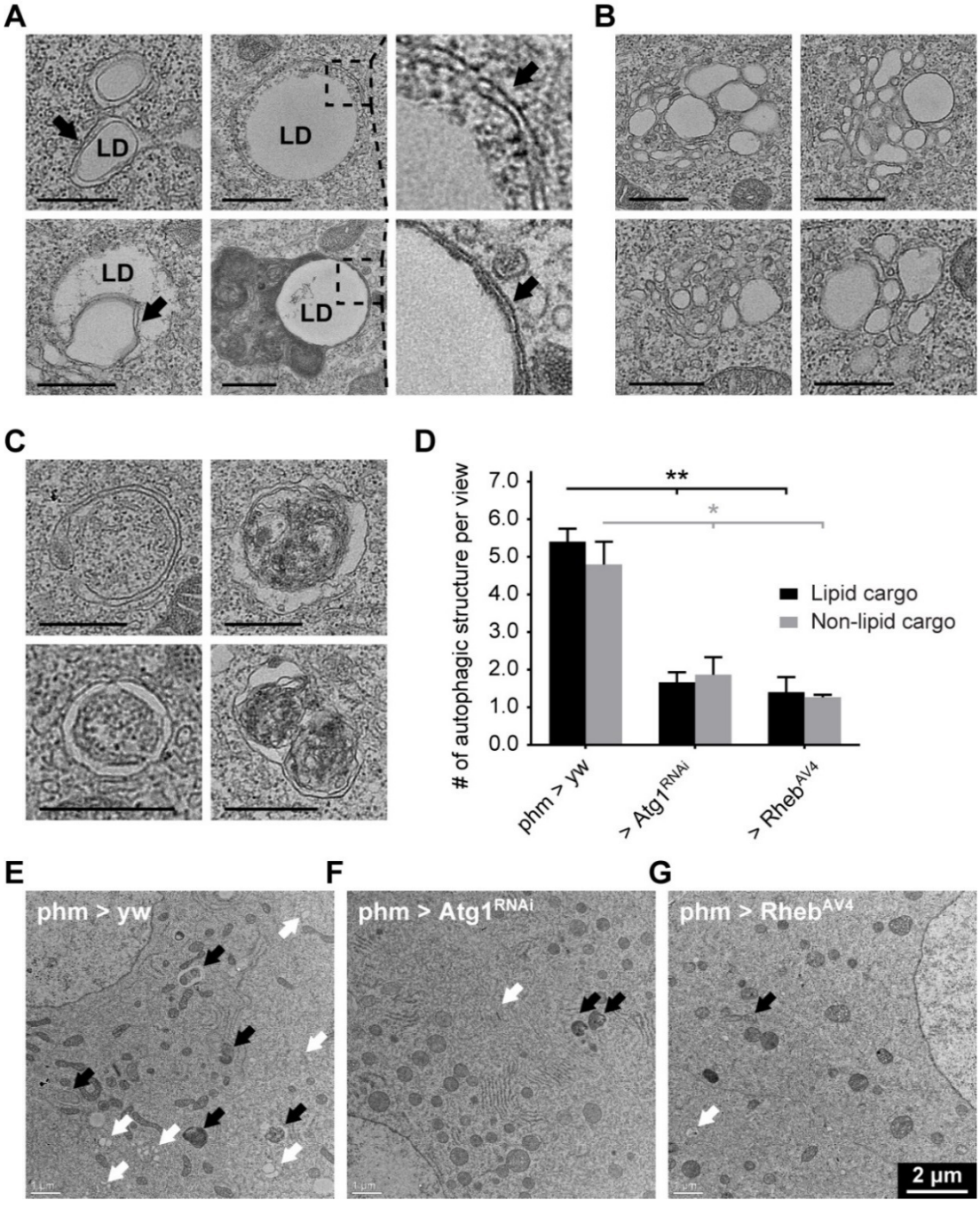
A
LD
LD
LD
LD
B
C
D
# of autophagic structure per view
7.0
6.0
5.0
4.0
3.0
2.0
1.0
0.0
**
*
Lipid cargo
Non-lipid cargo
phm > yw
> Atg1RNAi
> RhebAV4
E
phm > yw
F
phm > Atg1RNAi
G
phm > RhebAV4
2 µm

Figure 21. Autophagic and lipophagic structures in the PG visualized under TEM.

(A) Images of lipophagy structures in PG cells. Pre-NRC (4 hrs AL3E) larvae were starved for 6 hrs before sample preparation. Upper left, a typical double-membrane bound lipophagic vesicle; lower left, a lipophagic vesicle that occupies part of a lipid droplet; upper middle and right, an early stage, autophagic isolation membrane that is wrapping up a lipid droplet; lower middle and right, a lipid droplet processed by a late-stage autolysosome. Black arrows indicate double membrane structures. Scale bars, 0.5 μm. (B) Images of lipophagy related structures which contain a cluster of small membrane bound vesicles with light-density contents. Scale bars, 0.5 μm. (C) Images of autophagic structures that contain non-lipid cargoes. Upper left, an early stage isolation membrane; lower left, a typical double membrane bound autophagic vesicle; upper and lower right, late-stage structures with condensed cytoplasmic material. Scale bar, 0.5 μm. (D) Quantification of the number of autophagic structures in a single view under low magnification TEM (4700x). For each biological sample, 5 random images were taken and the autophagic structures were identified and counted manually. Mean ± SEM; p values by unpaired t-test (n=3; *p<0.05, **p<0.01). (E-G) Low magnification (4700x) images of PG cells of (E) starved *phm>yw*, (F) fed *phm>Atg1*^{RNAi} and (G) fed *phm>Rheb*^{AV4} larvae. Autophagic structures that contain lipid and non-lipid contents are annotated by white and black arrows respectively.

To examine whether reduction in cholesterol availability to the biosynthetic enzymes is responsible for the autophagy-induced developmental defects, we fed cholesterol to RU486 treated *phm^{GS}>Atg1* and *phm^{GS}>TSC1/2* larvae. Cholesterol feeding fully rescued the developmental delay/arrest in these larvae (Figure 22A-22C), demonstrating that cholesterol insufficiency, rather than induction of PG cell death or disruption of the hormone biosynthetic capacity, is the likely underlying cause of the autophagy-induced ecdysone deficiency and developmental defects.

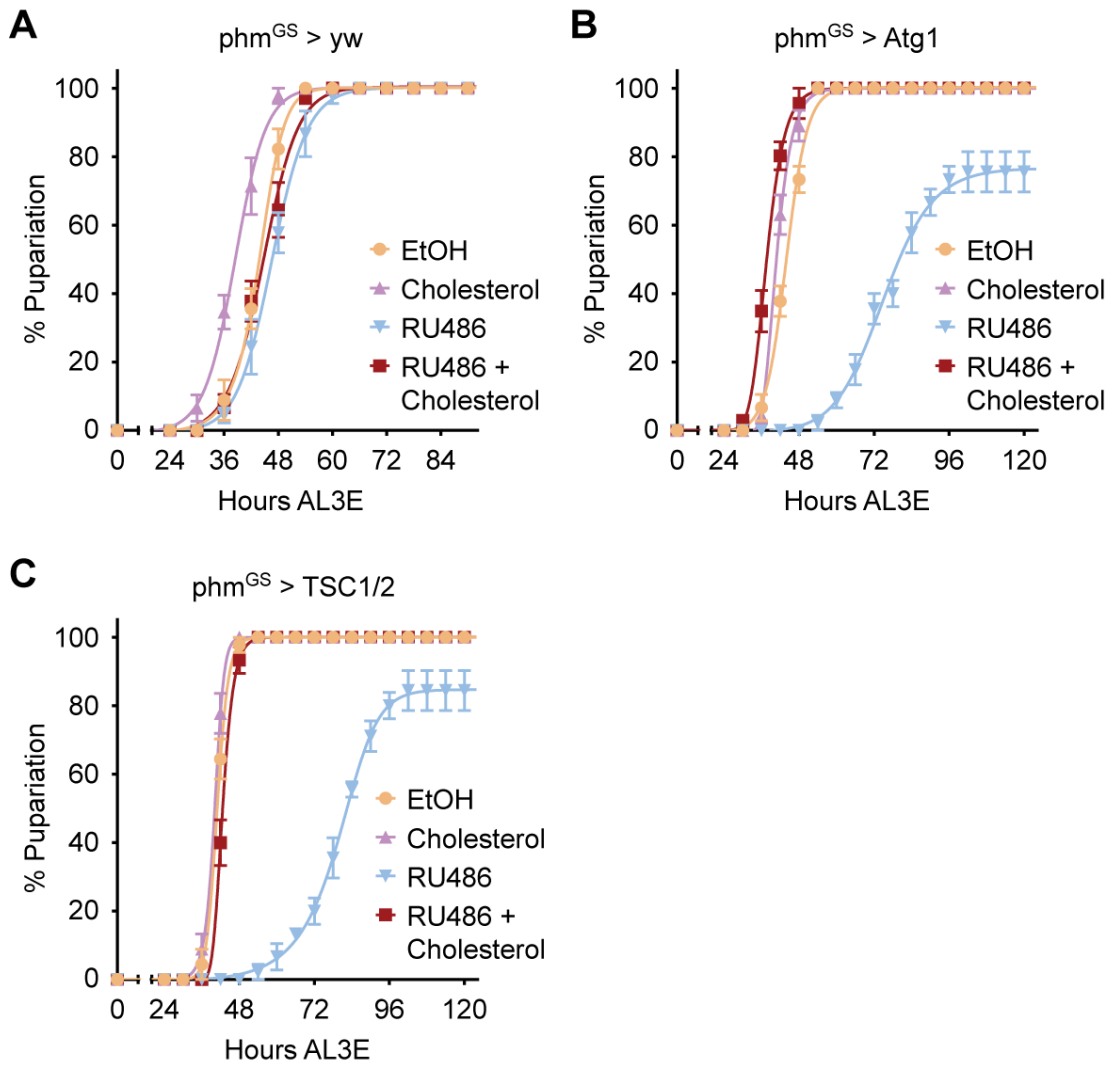

Figure 22. Cholesterol feeding rescues the developmental defects caused by autophagy induction.

(A-C) Pupariation timing curve of *phm^{GS}>yw* (A), *phm^{GS}>Atg1* (B) and *phm^{GS}>TSC1/2* (C) larvae with treatment indicated. Animals were fed with ethanol (EtOH), 40 μg/ml cholesterol (Chol), 0.5 μg/ml RU486 (RU486) or both (RU486+Chol) starting at 12 hrs AL3E.

2.3.6 Autophagy affects cholesterol trafficking by interacting with late endosome/lysosomes.

We then sought to determine how autophagy participates in the cholesterol trafficking pathway in PG cells. Previous studies have shown that autophagy delivers cholesterol esters to late endosomes and lysosomes for hydrolysis (Ouimet et al., 2011). Thus we examined whether similar autophagic flux occurs in the PG by testing the interaction between autophagosomes and late endosomes/lysosomes using specific vesicle markers. First, we examined the GFP-Vamp7 marker, which targets both late endosomes and lysosomes (Advani et al., 1999; Jean, Cox, Nassari & Kiger, 2015). We observed a high level of colocalization (revealed by Mander's Colocalization Coefficient, MCC) between mCh-Atg8a and GFP-Vamp7 (Figure 23A and 23E), indicating an interaction between autophagy and the endolysosome system in PG cells. However, we saw a different colocalization profile when labeling late endosomes and lysosomes separately. Frequent colocalization was observed between mCh-Atg8a and EYFP-Rab7 (M_{Red} =0.562±0.018 and M_{Green} = 0.484±0.028, under NR conditions) (Figure 23B and 23F), a late endosome marker, while the colocalization level was much lower with lysosome marker GFP-Lamp1 (M_{Red} = 0.168±0.009 and M_{Green} = 0.175±0.018, under NR conditions) (Figure 23C and 23G). These data are inconsistent with what we and others observed in fat body tissues (Figure 24), in which mCh-Atg8a overlaps frequently with GFP-Lamp1 during NR (Mauvezin, Nagy, Juhasz & Neufeld, 2015). A caveat for using the GFP-Lamp1 marker is that its GFP tag faces the intra-vesicular space and thus may be quenched by the acidity of the vesicle. To overcome this limitation, we examined overlap between mCh-Atg8a and Spinster (Spin) tagged with cytoplasm-facing GFP (Dermaut et al., 2005). In canonical autophagy this marker largely overlaps with Lamp1 in lysosomes (Rong et al., 2011; Sweeney & Davis, 2002). Similar to GFP-Lamp1, we still observed a comparatively low level of mCh-Atg8a colocalization with GFP-Spin under NR condition (M_{Red} = 0.264±0.011 and M_{Green} = 0.176±0.018) (Figure 23D and 23H). These results suggest that the autophagosome-endolysosome

interaction in PG cells does not occur in a way fully consistent with that of routine autophagic flux observed in other tissues such as fat body. The autophagosomes either interact more frequently with late endosomes than lysosomes, or persist in autophago-endosome stage for a longer time before transforming into auto-lysosome stage. Nevertheless, it is important to recognize that the endocytic pathway markers such as Rab7 and Lamp1 do not exclusively localize on the compartments they are proposed to label (Humphries, Szymanski & Payne, 2011). In tests with lysosome markers the M_{Green} value (percentage of green-positive pixels that are red-positive) increased upon starvation (Figure 23G and 23H), showing that a fraction of autophagosomes did fuse with lysosomes during NR. Under TEM we also observed autolysosome structures (Figure 21C), supporting the existence of autophago-lysosome communication. Taken together, we conclude that the autophagy in PG cells communicates with endolysosome system, but with an altered dynamics.

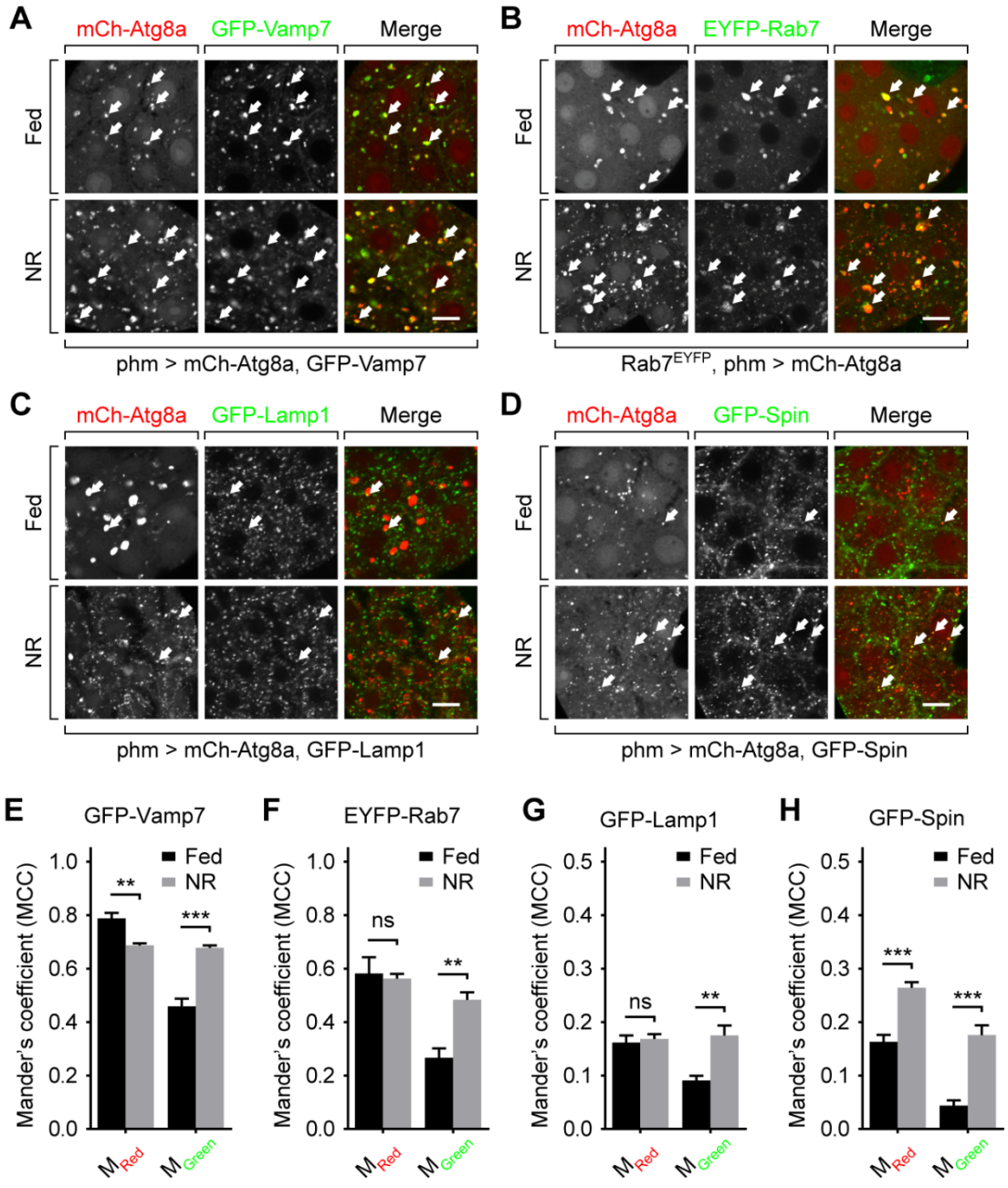

Figure 23. Autophagy interacts with late endosomes and lysosomes in PG cells.

(A-D) Fluorescence microscopy images of PGs expressing mCh-Atg8a and GFP-Vamp7 (A), EYFP-Rab7 (B), GFP-Lamp1 (C) or GFP-Spin (D). Arrows indicate colocalization of Atg8a and EYFP/GFP-positive puncta. Scale bar, 10 μm. (E-H)

Colocalization analysis of corresponding images in panel A-D. Mean ± SEM; p values by unpaired t-test (n=5-7; ns, not significant, **p<0.01, ***p<0.001).

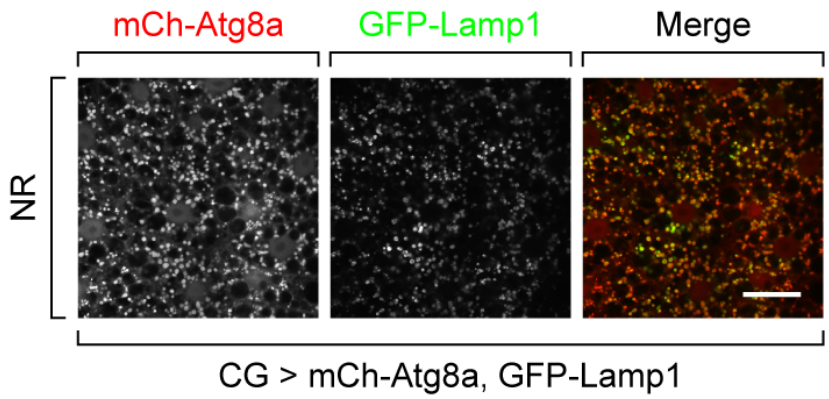

Figure 24. Autophagy interacts with lysosomes in fat body tissue.

Fluorescence microscopy images of fat body tissue expressing mCh-Atg8a and GFP-Lamp1. Scale bar, 50 μm.

We then examined whether the autophagy-endolysosome interaction is required for regulation of cholesterol trafficking by autophagy. In this test we introduced a tandem fluorescent-tagged GFP-mCh-Atg8a (tfAtg8a) marker to monitor vesicle acidification (Mauvezin, Ayala, Braden, Kim & Neufeld, 2014). When autophagosomes fuse with late endosome/lysosomes, the GFP in the marker is rapidly quenched by the acidity of the mature autolysosomes (Klionsky et al., 2016). In PG cells, the GFP of the majority of tfAtg8a marker in the autophagic vesicles was quenched (Figure 25A), indicating that most autophagic vesicles, even under fed conditions, are acidic. Depletion of v-ATPase subunits *Vha26* and *Vha55* effectively rescued the GFP signal of the tfAtg8a marker (Figure 26A and 26B), further verifying this finding (Mauvezin et al., 2015)

Three SNARE family proteins, *Syx17*, *Snap29* and *Vamp7*, are known to mediate vesicle fusion between the autophagosome and endolysosome systems (Itakura, Kishi-Itakura & Mizushima, 2012; Takats et al., 2013). Knockdown of Syx17 and Snap29, two autophagosome-associated components, caused an accumulation of small, cloudy looking Atg8a-positive structures during starvation (Figure 25B and 25C), consistent with findings in Drosophila fat body cells (Takats et al., 2013). Knockdown of Vamp7, the endolysosome relevant SNARE, resulted in accumulation of Atg8a vesicles of larger size in PG cells (Figure 25D-25F), similar to the effects of the vesicle fusion inhibitor Bafilomycin A1 in fat body cells (Mauvezin et al., 2015). These data indicate that depletion of the SNAREs disrupts autophagic flux in PG cells. All three groups of SNARE knockdown larvae pupariated precociously during pre-NRC starvation (Figure 25G), phenocopying the autophagy suppression larvae (Figure 13E-13G). These results show that the autophagosome-endolysosome interaction plays an essential role in the function of autophagy on pupariation control likely through alterations in cholesterol trafficking

Intriguingly, disruption of autophagic flux by depleting *Syx17*, *Snap29* or *Vamp7* did not rescue the GFP signal of tfAtg8a (Figure 25B-25D), in contrast to the requirement of these SNAREs for autophagosome acidification in other cell

types (Furuta, Fujita, Noda, Yoshimori & Amano, 2010; Takats et al., 2013). This data indicates that the acidification of autophagosomes in PG cells may not depend on fusion with endolysosomes, further suggesting that the mechanism of PG autophagic flux is not fully consistent with that in other well-studied cell/tissue types.

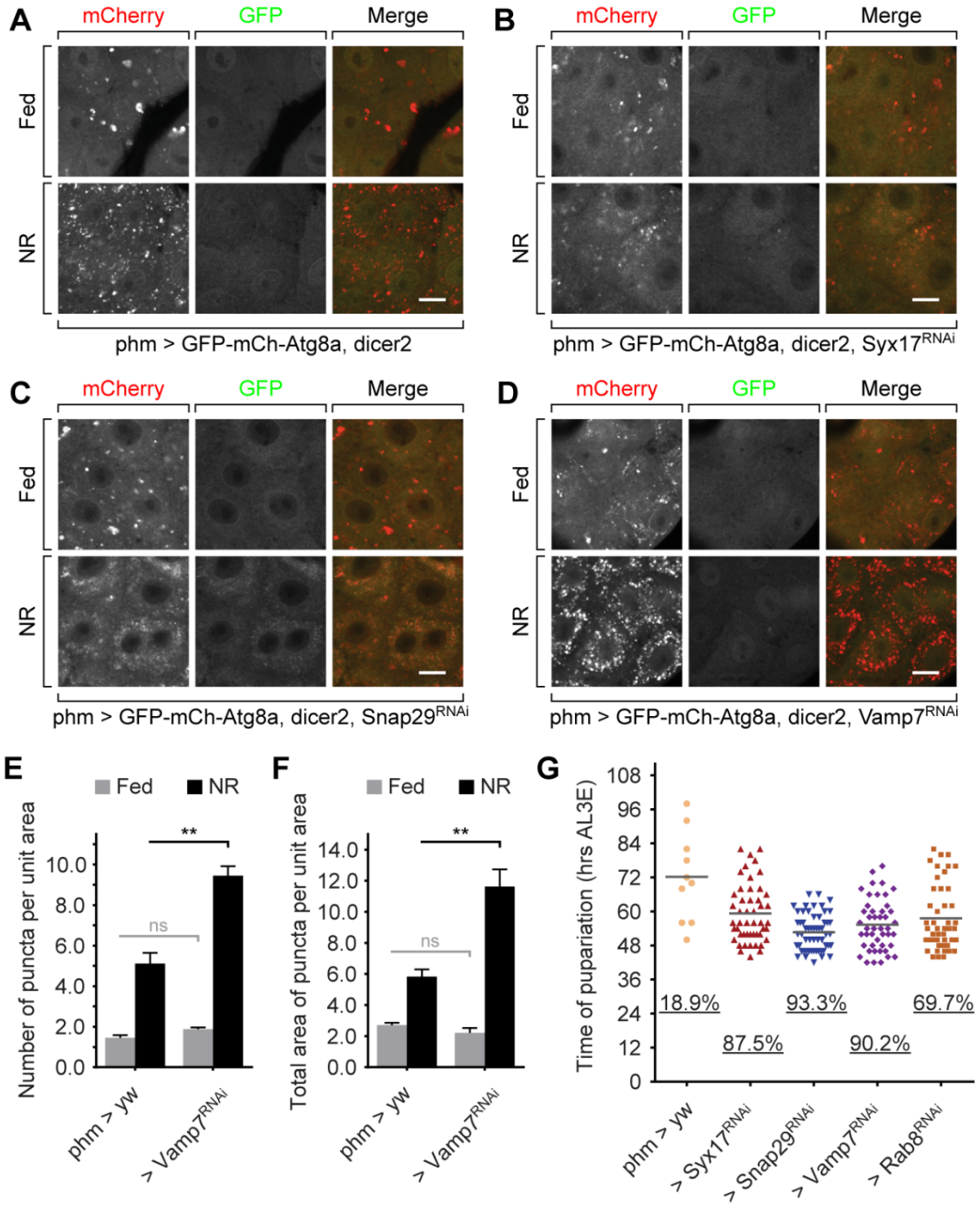

Figure 25. Autophagy affects cholesterol trafficking by interacting with endo/lysosomes.

(A-D) Autophagy visualized by tandem tagged Atg8a in control (A), *Syx17* RNAi (B), *Snap29* RNAi (C) and *Vamp7* RNAi (D) PGs. Scale bar, 10 μm. (E and F)

Quantification of number (E) and total area (F) of Atg8a positive puncta per unit cell area (100 μm^2) in control and *Vamp7* RNAi PGs. (G) Pupariation activity of larvae after starvation treatment from early L3 (4 hrs AL3E) stage. The scattered dots indicate the time of pupariation of each individual larva. The underscored numbers indicate the percentage rate of pupariation. For each group n > 50 larvae.

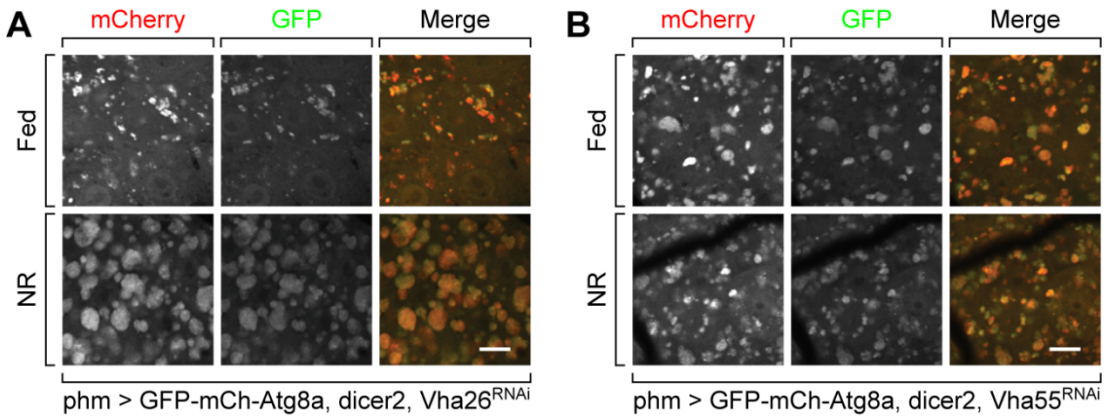

Figure 26. The autophagosomes in PG cells are acidified by v-ATPase.

(A and B) Autophagy visualized by tandem tagged Atg8a in *phm>Vha26^{RNAi}* (A) and *phm>Vha55^{RNAi}* (B) PGs. Scale bar, 10 μm.

2.3.7 PG autophagy is highly dynamic and exhibits additional non-conventional morphological features.

We were curious about the dynamics of PG autophagy activation upon NR. We first analyzed the size distribution of Atg8a-positive vesicles in addition to vesicle number. In early L3 (6 hrs AL3E) PG cells, the frequency of large-sized (> 1.0 μm^2) vesicles significantly decreased during NR, while that of the small-sized (< 1.0 μm^2) vesicles increased. In contrast, the effect of NR on vesicle size was reduced as larvae progressed to the mid-L3 stage (24 hrs AL3E) (Figure 27A and 27B). The simultaneous increase in vesicle number coupled with reduced vesicle size may be the result of a highly dynamic process, which has not been reported in NR-induced autophagy in other tissues such as that in the fat body (Scott, Schuldiner & Neufeld, 2004). To examine this possibility, we assessed the dynamics of Atg8a-positive structures in PG cells maintained in *ex vivo* culture using time-lapse live imaging. In fed early L3 larvae, the Atg8a-positive vesicles maintained their size and shape and exhibited limited mobility (Movie 1). Strikingly, after starvation in early, but not late L3 stage larvae, Atg8a vesicles showed highly dynamic movements (Movie 1) as well as many Atg8a-positive tubule-like structures that grew and retracted (Figure 28A-28C and Movie 2-4). We also observed that large vesicles shrank and fragmented into small ones (Figure 29A and Movie 5) and that ring-like structures budded out of existing large-size vesicles (Figure 29B, 29C and Movie 6). These observations can explain the changes on vesicle size distribution during NR and suggest that the autophagy process in the early PG is highly dynamic.

In addition to the active dynamics, we also noted that most of the tubular and ring-like structures were very sensitive to fixative since they were rarely seen in fixed tissues (Figure 30). Therefore, the apparent formation of small-size Atg8a-positive vesicles in fixed tissue likely represents fragmentation of the tubular network upon fixation. Another unusual property of all Atg8a-positive structures in the PG is their extreme sensitivity to detergents even after fixation. Addition of low concentrations of Triton X-100, Tween 20, or saponin, detergents commonly used

in most IHC staining procedures, destroyed most, if not all, of the Atg8a-positive structures (Figure 30). The detergent-sensitive property of these structures is in stark contrast to the behavior of NR-induced Atg8a-positive vesicles in the fat body which remain intact in the presence of detergents and are amenable to IHC procedures. Although not fully understood, the dynamics and the non-conventional morphological features of the autophagy in the PG is consistent with our finding that it performs a function (cholesterol depletion) that is distinct from canonical NR-induced autophagy.

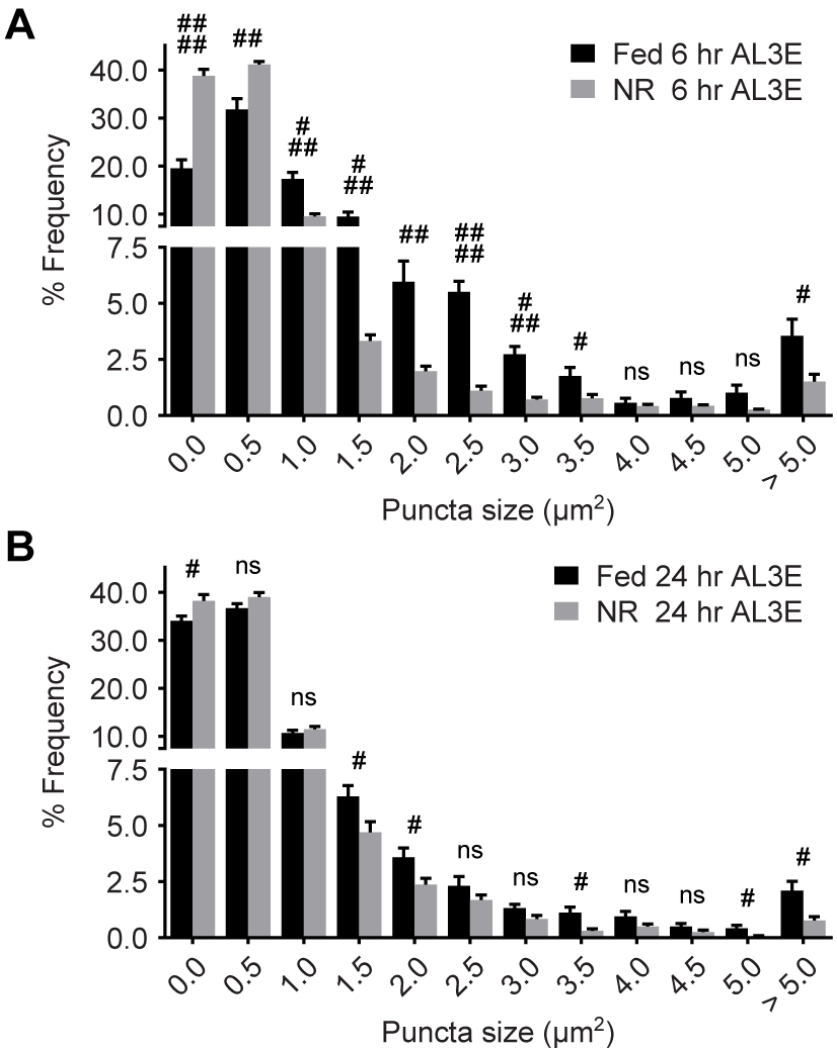

Figure 27. The size of autophagic vesicles decreases during autophagy induction.

(A and B) Frequency distribution of Atg8a-positive puncta size in 6 hrs (A) and 24 hrs AL3E (B) PGs. Mean ± SEM; p values by unpaired t-test (n=8; ns, not significant, #p<0.05, ##p<0.01, ###p<0.001, ####p<0.0001).

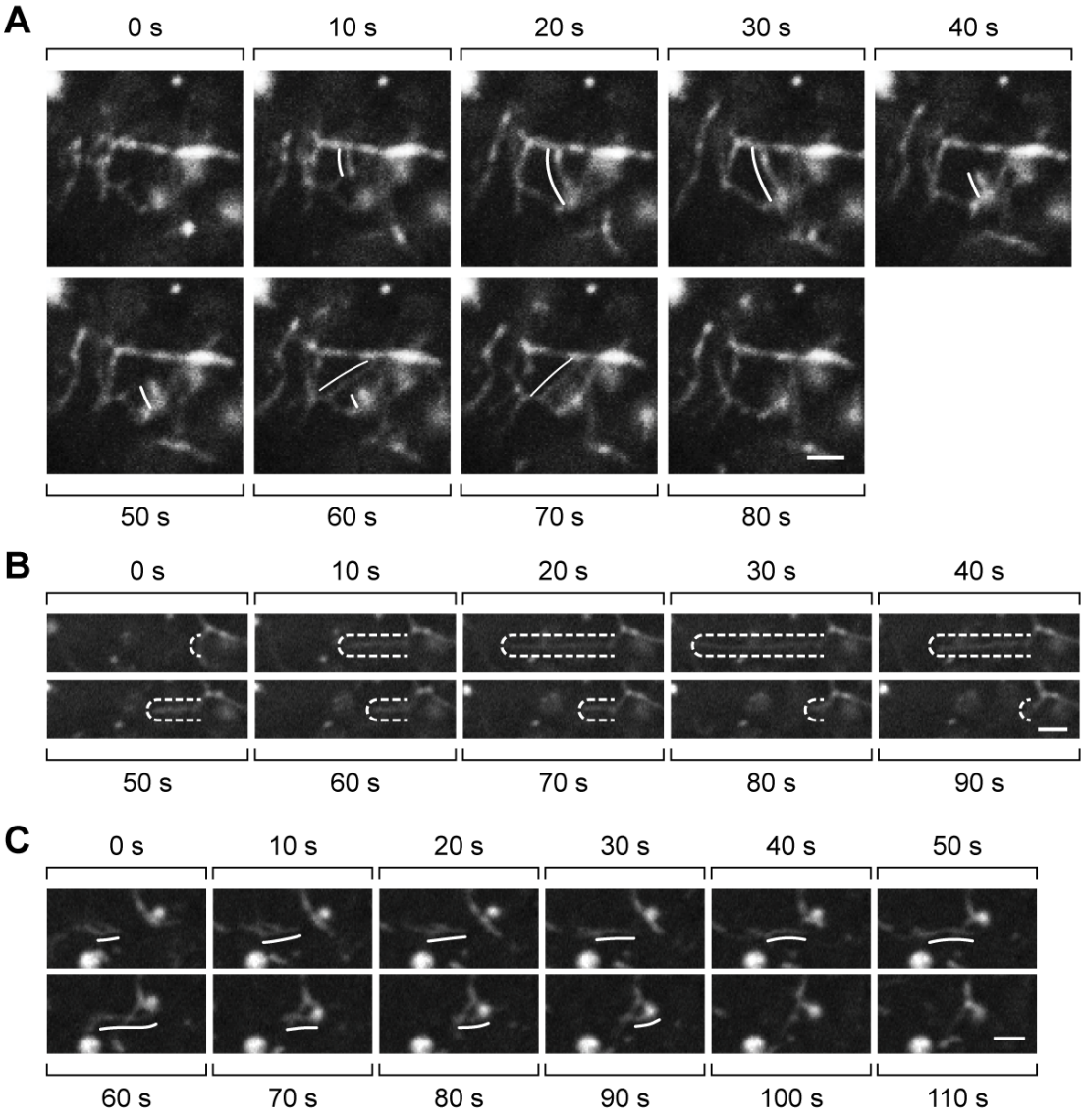

Figure 28. Tubular structures are formed during autophagy induction in PG cells.

(A) Time-lapse images showing an Atg8a-positive tubular network. A tubule formation event within the network is indicated by the solid lines. (B and C) Time-lapse images showing movement of Atg8a-positive tubular structures. A tubule protruding out from, and then retracting back to, a vesicle is outlined by the dash line (B). Another tubular structure moves toward and then fuses with a vesicle, indicated by the solid lines (C). (A-C) Scale bar, 2 μm.

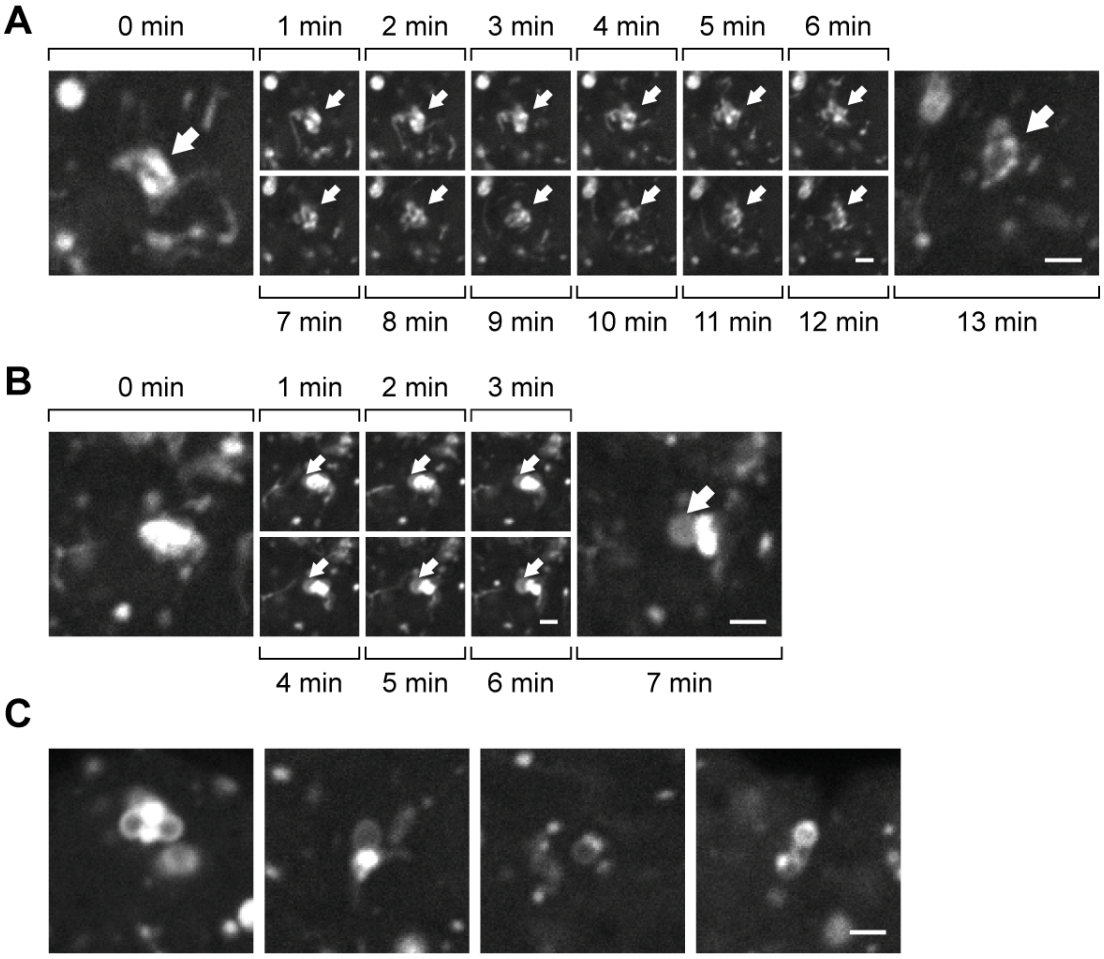

Figure 29. Vesicle fragmentation and ring-like structure formation during autophagy induction in PG cells.

(A) Time-lapse images showing fragmentation of a large Atg8a-positive vesicle. The morphological change is indicated by the arrows. (B) Time-lapse images showing formation of a ring-like structure (marked by arrows) beside an existing vesicle. (C) Additional examples of ring-like structures budded from existing vesicles. (A-C) Scale bar, 2 μm.

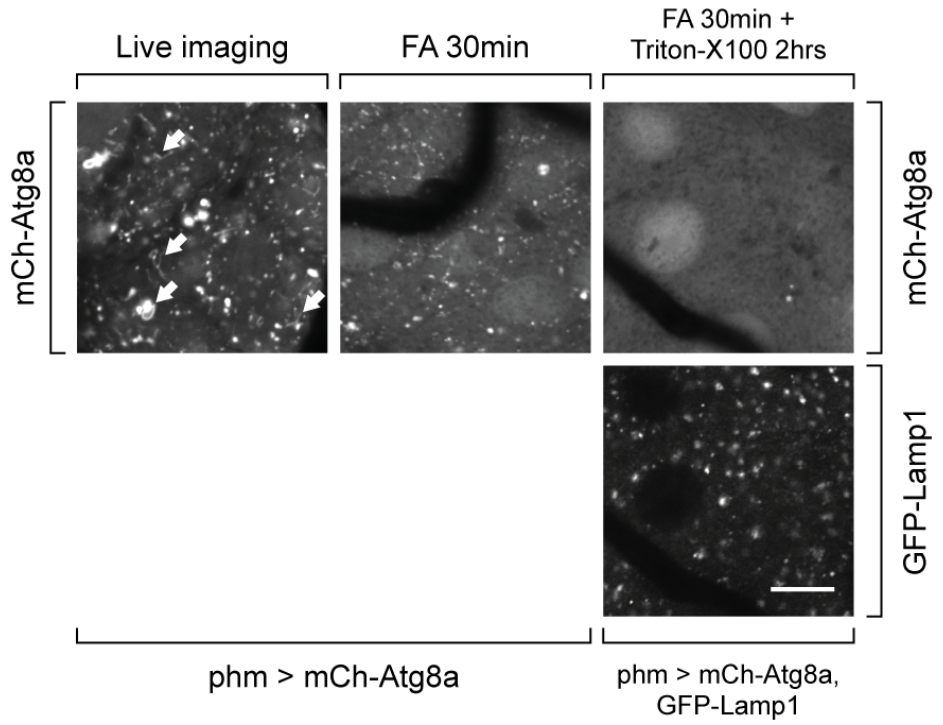

Figure 30. The autophagic structures in PG cells are sensitive to fixation and detergent treatment.

The autophagic structures in the PG were visualized by confocal microscope under live imaging and after treatment by fixative and detergent. FA 30 mins, tissues were treated by fixative (3.7% formaldehyde) for 30 mins. FA 30 mins + Triton X-100 2 hrs, tissues were treated by detergent (0.1% Triton X-100) following FA fixation. White arrows show the tubule- and ring-like structures under live imaging. GFP-Lamp1 shows that lysosome structures are not sensitive to detergent treatment. Scale bar, 10 μm.

2.3 Discussion

2.3.1 Temporally-regulated autophagy in the PG controls the NRCs.

The Drosophila NRCs are characterized by an abrupt switch in the response of larvae to starvation during the third instar stage of development, suggesting that the determinants of the checkpoints should be regulated (1) by nutritional conditions and (2) in a developmental stage dependent fashion. In this study, we identify autophagy as a NR induced, developmental time dependent mechanism that is the functional output of the checkpoints, i.e. it is the mechanism responsible for preventing larvae from undergoing pupariation before they have enough stored nutrients to give rise to viable adults.

In the PG, most characterized NR-responsive pathways, such as insulin/insulin-like signaling and TOR, are essential for development and are repressed under NR (Layalle et al., 2008; C. Mirth et al., 2005; Ohhara et al., 2017). In contrast, autophagy is induced by NR stress and suppression of autophagy did not disrupt development of well-fed larvae (Figure 12A), although a basal level of ATG8 positive vesicles are always present in PG cells (see below). We propose that autophagy has evolved as a specific stress responsive “STOP” pathway, which works together with essential “ON” pathways, to exert precise developmental timing control under nutritional stress.

Similar to other factors that influence the NRCs (Koyama et al., 2014; Ohhara et al., 2017), autophagy induction is temporally regulated. However, like most biological processes the regulation of autophagy inducibility is progressive (Figure 9B) and the number of Atg8 positive puncta does not exhibit an “all or none” switch that precisely correlates with the NRCs. However, when one considers the area of Atg8a puncta per unit area of gland cell (Figure 9C) which reflects the capacity of the autophagy in each cell, then there is a very strong correlation with the time of the NRCs. We found that autophagy suppresses pupariation in an “dose” dependent manner, in which stronger autophagy induction causes more severe developmental defects (Figure 17C and 17D). This is also consistent with the findings that strong TOR pathway suppression during the post-NRC stage delays

development (Figure 17C and 17D), while suppression using a weaker P0206-Gal4 driver does not (Layalle et al., 2008). We reason that the NRCs correlates with a certain threshold of autophagy induction, which can no longer be reached when the checkpoint is surpassed. On the other hand, autophagy is inducible through genetic manipulations during the post-NRC stage (Figure 17A), indicating that the normal silencing of autophagy in this stage is likely due to changes in upstream signaling. A compensatory pathway may function to antagonize the suppression of insulin/insulin-like and TOR pathway by NR, which resembles what happens during the organ sparing process reported in some imaginal tissues in post-NRC larvae (Cheng et al., 2011). It is also possible that some pathway that can regulate TOR activity, such as Hippo pathway (Texada et al., 2019), may function differently before and after the NRCs. In any case, the mechanism that controls the developmental stage dependent autophagy suppression requires further study.

2.3.2 Autophagy disrupts hormone synthesis by targeting cholesterol trafficking in PG cells.

In previous studies, most known pathways exert control of ecdysone synthesis by targeting hormone biosynthetic enzymes (Koyama et al., 2014; Layalle et al., 2008; C. Mirth et al., 2005; Shimell et al., 2018). However, we found that autophagy induction disrupts ecdysone synthesis likely by depleting cholesterol storage in the PG, which represents a new dimension of regulation of the ecdysone producing pathway. This mechanism is efficient from a design principle standpoint since it allows a more rapid means to ramp up hormone production when conditions turn favorable than does destruction of biosynthetic capacity which would require time for re-synthesis of ecdysone production components. Furthermore, insects are strict cholesterol auxotrophs and obtain sterols solely from their diet (Clayton, 1964), which potentially makes them particularly sensitive to this type of regulation. Nevertheless, some studies indicate that autophagy in mammalian endocrine organs can also affect hormone synthesis (Gawriluk, Ko, Hong, Christenson & Rucker, 2014; Yoshii et al., 2016),

indicating that this mechanism may be universally employed as a means of controlling hormone production in response to nutritional stress.

The regulation of cholesterol storage by autophagy in the PG is also corroborated at the cellular level by our observations that autophagy interacts dynamically with cholesterol containing structures and the endolysosome system. We observed cholesterol-containing autophagosomes under fluorescence microscopy (Figure 20E) and lipophagy related structures under TEM (Figure 21A), strongly suggesting that autophagy interacts with a cholesterol trafficking pathway. In addition, our findings on the interacting pattern between autophagy and the endolysosome system also provide support for this conclusion. The late endosome rather than the lysosome has been shown to be the key compartment that mediates cholesterol trafficking (Kobayashi et al., 1999). Cholesterol can egress from late endosomes to further destinations before reaching the lysosome (Mobius et al., 2003; Wojtanik & Liscum, 2003). NPC1 is a key cholesterol trafficking mediator and is primarily a late endosomal protein that only transiently associates with lysosomes (Higgins, Davies, Chen & Ioannou, 1999). We find that the Drosophila homolog, NPC1a, strongly localizes to autophagic vesicles in the PG (Figure 20F). We also find a stronger correlation of the autophagic marker mCh-Atg8a with late endosomes than with lysosomes (Figure 23A-23H), suggesting a more important role of the interaction between autophagosome and late endosome. Together these observations suggest that in the PG, the lysosome is not essential for removing or sequestering cholesterol from progressing into the ecdysone biosynthetic pathway.

How autophagy depletes cholesterol storage in the PG remains an unresolved question. Unlike proteins or triglycerides, cholesterol is typically not catabolized into small molecules. It is known that excessive cholesterol can be cleared from a cell via a specific recycling process involving cholesterol efflux (Ikonen, 2008). Autophagy facilitated cholesterol efflux has been reported in macrophages in mammalian system (Ouimet et al., 2011). It is possible that autophagy works in a similar way to facilitate cholesterol efflux in the PG. Interestingly Rab8 is required

for secretory autophagy (Dupont et al., 2011), and it has also been implicated in a cholesterol efflux pathway (Kanerva et al., 2013; Linder et al., 2009; Linder et al., 2007) and we find that knockdown of Rab8 in the PG leads to impairment of the NRCs similar to blocking the autophagosome endolysosome interaction (Figure 25G).

2.3.3 Non-conventional morphological features of the autophagy in PG cells.

Although the autophagy process in the PG requires most of the canonical autophagy machinery and is regulated by TOR signaling similar to what is found for the fat body (Figure 11A-11G), it exhibits some morphological features that are not commonly observed. We found dynamic Atg8a vesicle movements in PG cells from pre-NRC, starved animals, during which vesicle compartmentation, tubule formation and ring-like structure formation were observed (Figure 28 and 29). Autophagy-relevant tubular structures have been reported in previous studies (Johnson, Shu, Hauswirth, Tong & Davis, 2015; Yu et al., 2010). However, the tubular structure we observe are likely different. The tubule structures formed during lysosomal reformation (Yu et al., 2010) were visualized by the lysosome marker (Lamp1), which does not show clear colocalization with Atg8a in PG cells (Figure 23C and 23G). The tubular network found in muscle cells was detected by both Atg8a and Spinster marker (Johnson et al., 2015), but the two markers overlap well in muscles, unlike what we found in PG cells. Moreover, the formation of the muscle tubular network is not stimulated by starvation (Johnson et al., 2015), also suggesting that its function is distinct from that of the autophagy in PG cells.

Intriguingly, during cholesterol trafficking it has been shown that NPC1-positive vesicles can form tubular and ring-like structures (Ko, Gordon, Jin & Scott, 2001). In PG cells, NPC1a localizes on some autophagic vesicles (Figure 20F), thus the Atg8a-positive tubular and ring-like structures may be NPC1a-positive and represent the structures mediating cholesterol trafficking. In addition, the clustered lipophagy-like vesicles we observed under TEM (Figure 21B) may represent the autophagosomes undergoing fragmentation, which links the vesicle

fragmentation process with the cholesterol trafficking pathway. We hypothesize that the dynamic movement of Atg8a-positive structures facilitates cholesterol removal from the ecdysone biosynthetic enzymes either by an efflux mechanism or sequestering it to a novel membrane compartment. In either case, the removal of the cholesterol attenuates synthesis of hormone and thereby prevents nonproductive pupariation of larvae that do not have sufficient nutrient stores to survive the metamorphic remodeling of the body plan.

Lastly, it has recently been reported that autophagy is also required to produce ecdysone (Texada et al., 2019) which initially seems at odds with our findings. However, as we describe here there are always Atg8a positive vesicles present in the PG even under well fed conditions and these tend to be large. Starvation pre-NRC leads to induction of the highly dynamic tubular network and a reduction in the average Atg8a vesicle size. Post-NRC the tubule network formation is much and dynamics are reduced and the Atg8a-positive vesicles remain larger. We propose that there are two types of autophagic processes occurring in the PG; a constitutive level in well fed larva that is not so dynamic and is responsible for aiding flux of cholesterol into the biosynthetic pathway and a second highly inducible process that only occurs pre-NRC which is responsible for shunting cholesterol away from the biosynthetic pathway. Future studies aimed at elucidating the mechanism responsible for switching off the inducibility and the highly dynamic nature of the autophagic process post-NRC may aid in understanding how cholesterol flux can be directed into and away from the hormone biosynthetic pathway.

2.4 Materials and Methods

2.4.1 Flies

Unless noted, all flies were reared on standard agar-cornmeal food supplemented with yeast at 25 °C. Flies were cultured in 12:12 light-dark cycles: however, all experiments were carried out under constant light to avoid the potential impact of circadian cycle on developmental timing. *Phm-Gal4* (Ono et al., 2006) was used to drive gene expression specifically in PG cell. *Phm-GeneSwitch-Gal4* (Kaieda et al., 2017) was used to drive temporally specific gene expression under control of RU486 administration. *UAS-mCh-Atg8a* (Chang & Neufeld, 2009) and *UAS-GFP-mCh-Atg8a* (Nezis et al., 2010) were used to mark autophagosomes. *UAS-GFP-Ref(2)P* (Chang & Neufeld, 2009) were used to mark protein aggregates and to estimate level of protein degradation. *UAS-GFP-Lamp1* (Pulipparacharuvil et al., 2005), *UAS-GFP-Spinster* (Johnson et al., 2015), *UAS-GFP-Vamp7* (Jean et al., 2015) and endogenous-*YRab7* (Dunst et al., 2015) (Bloomington Stock Center (BDSC), 62545) were used to mark late endosome/lysosome. *UAS-Atg1*^{6B} (BDSC, 51655) and *UAS-TSC1/2* (Tapon et al., 2001) were used to induce autophagy. A collection of RNAi strains from Transgenic RNAi Project (TRiP) (Ni et al., 2011) were used to test their efficiency to suppress autophagy: *UAS-Atg1-RNAi* (BDSC, 26731), *UAS-Atg2-RNAi* (BDSC, 27706), *UAS-Atg3-RNAi* TRiP (BDSC, 34359), *UAS-Atg4a-RNAi* TRiP (BDSC, 35740), *UAS-Atg4b-RNAi* TRiP (BDSC, 56046), *UAS-Atg5-RNAi* TRiP (BDSC, 34899), *UAS-Atg6-RNAi* (BDSC, 28060), *UAS-Atg7-RNAi* (BDSC, 27707), *UAS-Atg9-RNAi* (BDSC, 28055), *UAS-Atg10-RNAi* (BDSC, 40859), *UAS-Atg12-RNAi* (BDSC, 27552), *UAS-Atg13-RNAi* (BDSC, 40861), *UAS-Atg14-RNAi* (BDSC, 55398), *UAS-Atg16-RNAi* (BDSC, 34358), *UAS-Atg17-RNAi* (BDSC, 36918), *UAS-Atg18-RNAi* (BDSC, 28061), *UAS-Atg101-RNAi* (BDSC, 34360), *UAS-Pi3K59F-RNAi* (BDSC, 64011), *UAS-Vps15-RNAi* (BDSC, 34092), and *UAS-Uvrag-RNAi* (BDSC, 34368). *UAS-Rheb*^{AV4} (BDSC, 9690) was also used to suppress autophagy. *UAS-Syx17-RNAi* TRiP (BDSC, 25896), *UAS-Snap29-RNAi* TRiP (BDSC, 25862) and *UAS-Vamp7-RNAi* TRiP (BDSC, 38300) were used to

block interaction between autophagosome and late endosome/lysosome. *UAS-Vha26-RNAi* (VDRC, 102378) and *UAS-Vha55-RNAi* (VDRC, 46553) were used to disrupt function of v-ATPase.

2.4.2 Developmental staging and starvation assay

Before egg collection, flies were transferred to constant light environment for at least 2 days and all subsequent treatments were carried out under constant light. Eggs were collected on apple juice plates with yeast paste and early L1 larvae were transferred to standard lab fly food with yeast paste after 24 hrs. Newly-molted L3 larvae were picked out every 2 hrs and transferred to fly food without yeast paste. For the starvation assay, L3 larvae were cultured for appropriate time and then transferred to 1% agar. Larvae were then monitored every 2 hrs until they pupariated or died.

2.4.3 Fluorescence microscopy

Larvae were dissected in PBS and fixed using 3.7% formalderhyde for 15 mins at room temperature. Tissues were then washed in PBS and mounted in 90% glycerol for imaging. All confocal images were captured using Zeiss LSM710 confocal microscope. To be noted, detergent was strictly avoided in all imaging process involving visualization of autophagy in the PG.

2.4.4 Time-lapse imaging

Larvae were dissected in M3 culture medium (Sigma) and the brain-ring gland complexes were transferred to a glass-bottom culture dish (MatTek). In the dish, ring glands were carefully dissected from the attached brains, after which a coverslip was positioned on top of the tissues to prevent sample movement. The samples were imaged with a Zeiss LSM 710 confocal microscope using the time-lapse configuration.

2.4.5 Immunohistochemistry

Larvae were dissected in PBS and fixed using 3.7% formalderhyde for 15 mins at room temperature. Tissues were washed in PBS containing 0.1% Triton X-100 (PBT) for 3 times and then permeablized and blocked simultaneously using PBT containing 5% normal goat serum (NGS) for 1 hour. Tissues were then

incubated with primary antibody (anti-Phm, 1:1000, anti-Dib, 1:1000, anti-Spok, 1:500, anti-cleaved caspase-3 (Cell Signaling Technology), 1:200) in PBT containing 10% NGS overnight at 4 degrees, followed by 5 washes and then post-secondary incubation for 2 hours at room temperature. DAPI staining occurred for 5 minutes at the pen-ultimate washing step after secondary antibody incubation. Finally, tissues were transferred to 70% glycerol/PBS mounting medium and then mounted on glass slide for imaging. Images were captured using a Zeiss LSM 710 confocal microscope.

2.4.6 Ecdysteroid titer measurement

The ecdysteroid titers of larvae were measured using the 20-hydroxyecdysone Enzyme Immunoassay (EIA) kit, (Cayman Chemicals) which detects both ecdysone and 20-hydroxyecdysone. Briefly, frozen larvae were homogenized in methanol and ecdysteroids were extracted as described previously (Warren et al., 2006). The extracts les were evaporated in a Speed Vac and the residue resuspended in EIA buffer (Cayman Chemical) and analyzed following the manufacturer's protocol. A standard curve was determined using a dilution series containing a known amount of purified 20-hydroxyecdysone solution provided by the kit. Absorbance at 415 nm was detected using a benchtop microplate reader (Bio-Rad).

2.4.7 *Ex vivo* incubation assay

The assay was adapted from previous studies (Enya et al., 2014; J. Kim & Neufeld, 2015). Briefly, wandering larvae were dissected in M3 culture medium and the brain-ring gland complexes were isolated. The tissues were then incubated in M3 medium containing 10% fetal bovine serum and 0.5% dilution of 10 μM NBD-cholesterol for 6 hours at room temperature. The samples were subsequently fixed in 3.7% formaldehyde for 15 mins and then imaged using a Zeiss LSM 710 confocal microscope.

2.4.8 Nile Red staining for lipid droplets

Larvae were dissected in PBS and fixed using 3.7% formalderhyde for 15 mins at room temperature. After washed in PBS, tissues were incubated in 1 μg/ml

Nile Red solution in PBS for 30 mins. Then samples were washed in PBS again and mounted in 90% glycerol for imaging. Images were captured using Zeiss LSM 710 confocal microscope.

2.4.9 Electron microscopy

Larvae were dissected in cacodylate buffer and fixed in 2% paraformaldehyde plus 2.5% glutaraldehyde in cacodylate buffer. Then samples were post-fixed in 1% osmium tetroxide, dehydrated progressively in acetone, and embedded in Epon 812 epoxy resin (Electron Microscopy Sciences). Resin blocks were then sectioned using Leica UC7 microtome. Finally, the section grids were post-stained by uranyl acetate and lead citrate and then imaged using FEI Tecnai G2 F30 transmission electron microscope.

2.4.10 Quantification of vesicles

The number and area of vesicles were quantified using imageJ software. Briefly, the vesicles were selected using the “threshold” function. Then the number and total area of the vesicles were calculated automatically using the “analyze particles” function in the software.

2.4.11 Quantification of colocalization

Colocalization analysis was carried out in ImageJ software using the JACoP plugin (Bolte & Cordelieres, 2006). Briefly, the particles in each channel were selected manually in the plugin in a similar way to the “threshold” function. Then Mander’s Colocalization Coefficient was automatically calculated by the plugin.

2.4.12 Statistics

GraphPad Prism software was used to carry out statistical analyses. Student’s t-test was used to determine statistical significance.

CHAPTER 3

Jeb/Alk and Pvf/Pvr pathways control developmental timing in *Drosophila melanogaster.*

3.1 Introduction

Body size is an important trait which largely determines the fitness of an animal. In holometabolous insects such as *Drosophila melanogaster*, the body size of an animal is mostly determined by its weight gain during the foraging larval stage. Under this evolutionary design, the timing of developmental transition from larva to pupa stage becomes a critical determinant of the final adult body size.

In *Drosophila*, the timing of metamorphic transition is largely determined by a neuroendocrine axis centered by the prothoracic gland (PG) and a group of tropic hormone producing neurons called PG neurons. As an endocrine organ, PG produces a steroid hormone ecdysone which functions as the direct trigger of metamorphosis during development. The ecdysteroidogenesis function of the PG is regulated by a series of signaling, among which the PG neuron-derived prothoracicotropic hormone (PTTH) signal plays a central role (review, see (Yamanaka, Rewitz, et al., 2013)). At late L3 stage, PTTH is highly expressed in the PG neurons. Simultaneously, the PG neurons are activated by upstream neuronal signals, which causes delivery of PTTH to the PG cell surface through direct axon innervation (McBrayer et al., 2007). PTTH binds with and activates the Torso receptor on the PG cells, which subsequently stimulates ecdysone synthesis activity via the Ras-Raf-Erk pathway (Rewitz et al., 2009).

As a critical controller of metamorphosis, PTTH was originally proposed as a brain-derived hormone in 1920s (Kopeć, 1922). In the following decades, the identity of PTTH was characterized and the biology of it was intensively studied in Lepidopteran insects such as *Bombyx mori* and *Manduca sexta* (review, see (Ishizaki & Suzuki, 1980)). Following these, *Drosophila* was introduced into the field which provides a powerful genetic tool and plays an increasingly important role. In 2007, the PTTH homolog in *Drosophila* was identified and the PTTH producing neurons (PG neurons) were successfully labelled using the Gal4-UAS system (McBrayer et al., 2007). Ablation of the PG neurons (*ptth>Grim*) caused a severe developmental delay (~ 5 days) of the animal, which confirms the vital function of PTTH in the metamorphic transition. The loss-of-PTTH phenotype was

further tested using *ptth* mutant flies in a following study. However, the *ptth* mutation caused a developmental delay of merely ~1 day, a much milder defect than the neuron ablation model (Shimell et al., 2018).

The discrepancy between the neuron ablation and the genetic model can be explained by the existence of additional, uncharacterized signal(s) transferred from PG neurons to the PG. This hypothesis was proved by a neuron activation assay, in which the PG neurons were activated in both wildtype and *ptth* mutant larvae. In animals of both genotypes, PG neuron activation resulted in acceleration of development, clearly showing that PTTH is not the only stimulatory signal derived from the PG neurons (Shimell et al., 2018). Despite, the identity of the additional signal(s) from PG neurons is still elusive.

In this study, we uncovered two receptor tyrosine kinases (RTKs), Anaplastic Lymphoma Kinase (Alk) and PDGF- and VEGF-receptor related (Pvr), function in the PG cells to regulate developmental timing. Suppression of either receptor causes developmental delay, which is exacerbated when suppression happens in *ptth* mutant background. Activation of either receptor causes acceleration of development and rescues the developmental delay in *ptth* mutants. We also find the ligand of both receptors, Jelly Belly (Jeb) and PDGF- and VEGF- related factor (Pvf), are expressed in the PG neurons, indicating that the upstream signals of the two pathways derive from these neurons. In all, our data uncover two novel signaling pathways in the PG that regulate developmental timing in *Drosophila* larva and provide a more comprehensive understand on the long-known but not-fully-characterized neuroendocrine axis that signals to the PG.

3.2 Results

3.2.1 Targeted screening for RTKs that affect developmental timing.

To identify the potential candidate signal(s) from PG neurons, we firstly carried out a targeted screening of RTKs in the PG cells. We performed this screening based on several preliminary evidences. Firstly, PTTH signals the PG through a RTK Torso (Rewitz et al., 2009); secondly, knocking down of components of Ras-Raf-Erk pathway results in more severe developmental defect than *ptth* mutants (Rewitz et al., 2009; Shimell et al., 2018); and thirdly, *Drosophila* genome has merely twenty identified RTKs and thus the screening is easy to perform using a strong and maturely developed phm-Gal4 driver (Danielsen et al., 2016). Instead of using RNAi fly lines constructed by Vienna Drosophila Resource Center (VDRC) which was tested in a genome-wide screening previously (Danielsen et al., 2016), we further screened the *Drosophila* RTKs using RNAi lines available from the Transgenic RNAi Project (TRiP) (Ni et al., 2011). By comparing data from the genome-wide screening and our more precise targeted screening, we sought to identify additional RTKs that affect developmental timing in the PG cells.

In the two screenings five RTKs were found to affect developmental timing in at least one of the tests (Table 1). Among the five, InR and Torso have been well known as regulators of PG function and developmental timing (C. Mirth et al., 2005; Rewitz et al., 2009), while EGFR was found to function in the PG in an autocrine-mediated pathway (unpublished data from personal communication). Therefore, we focused on the other two receptors, Alk and Pvr, in our following studies.

3.2.2 Alk and Pvr receptors are expressed in the PG.

We firstly sought to confirm the expression of Alk and Pvr in the PG cells. Using specific antibodies against the receptors, we stained the PG tissues from larvae of early- and mid-L3 stage. In mid-L3 stage (24 hrs after L2/L3 ecdysis), both receptors were successfully detected by antibody, showing clear signals on the PG cell membranes (Figure 31A and 31B). No membranous signal was detected in receptor knockdown samples, further verifying our findings (Figure

31A and 31B). Interestingly, we did not see any signal of either receptor in early L3 larvae (0-4 hrs after L2/L3 ecdysis), suggesting that the receptors are expressed in PG cells specifically after a certain time point in L3 stage (Figure 31A and 31B). In all, these data confirm the expression of Alk and Pvr receptors in the PG.

Symbol	Targeted Screening (Days @ 50% Pupariation)	p Value	Genome-wide Screening
Control	4.794 ± 0.059		
Alk	**5.253 ± 0.055**	**0.0013**	**NOP**
btl	4.727 ± 0.061	0.3281	NOP
Cad96Ca	4.704 ± 0.048	0.1703	NOP
CG10702	4.714 ± 0.060	0.2483	NOP
Ddr	4.817 ± 0.101	0.7998	NOP
dnt	4.741 ± 0.046	0.3779	NOP
drl	4.673 ± 0.046	0.0874	NOP
Drl-2	4.722 ± 0.033	0.2243	NOP
Egfr	**L3 arrest**		**NOP**
Eph	4.806 ± 0.032	0.8075	NOP
htl	4.488 ± 0.035	0.0061	NOP
InR	**> 5-day delay / L3 arrest**		**Major delay**
Nrk	4.528 ± 0.075	0.0186	NOP
otk	4.703 ± 0.080	0.2701	NOP
Pvr	**4.897 ± 0.068**	**0.1796**	**Major delay**
Ret	4.687 ± 0.055	0.1332	NOP
Ror	4.741 ± 0.050	0.387	NOP
sev	4.926 ± 0.048	0.0707	NOP
Tie	4.484 ± 0.080	0.0139	NOP
tor	**6.302 ± 0.126**	**0.0008**	**Delayed L3**

Table 1. Targeted screening of *Drosophila* RTKs for factors regulating developmental timing.

The targeted screening was carried out using phm-Gal4 driver and RNAi lines from TRiP project. *Phm>w1118* animals were used as control. The result for each group is shown as the time spent from egg laying to 50% pupariation. Comparisons were made between control and each knockdown group and p values were calculated using student t-test. $P<0.05$ was considered statistically significant. The results from a genome-wide screening using the same Gal4 driver but different batch of RNAi lines (Danielsen et al., 2016) are also included in the table. NOP, no obvious phenotype. The RTKs whose knockdown caused significant developmental delay in at least one screening are marked in bold.

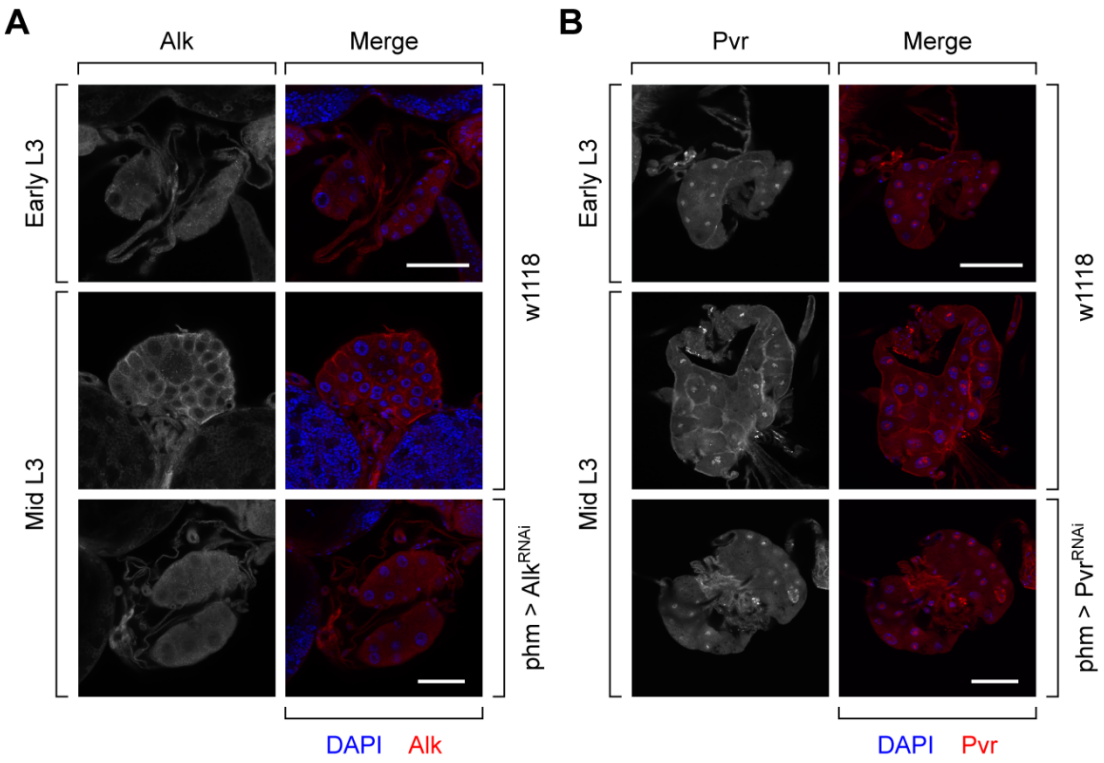

Figure 31. Alk and Pvr receptors are expressed in PG cells.

(A and B) Immunofluorescence images of PGs of early- and mid-L3 larvae. Larvae were fed until either early-L3 (0-4 hrs after L2/L3 ecdysis) or mid-L3 (24hrs after L2/L3 ecdysis) stage before dissection. PG tissues were immunostained with antibody against Alk (A) or Pvr (B). Mid-L3 stage *phm* > Alk^{RNAi} and *phm* > Pvr^{RNAi} larvae were also tested as negative control. Scale bar, 50 μm.

3.2.3 The Jeb and Pvf ligands that activate Alk and Pvr pathways in the PG are, at least partially, derived from the PG neurons.

We then tested whether the ligands that activate the Alk and Pvr receptors on the PG derive from the PG neurons. To achieve this, we employed a *Jeb-Gal4* line made by the Trojan recombination strategy (*Jeb^{Trojan}-Gal4*) (Diao et al., 2015) and a Gal4 line generated by the FlyLight project from Jenelia Farm (Jenett et al., 2012; Pfeiffer et al., 2008) in which the Gal4 sequence is fused with part of the non-coding region of *Pvf3*. Since *Pvf2* and *Pvf3* localize adjacently on the chromosome and *Pvf2* locates downstream to *Pvf3*, we propose that the Jenelia Farm Gal4 line exhibits expression pattern of either *Pvf2* or *Pvf3* and thus refer to it as *Pvf2,3-Gal4*. Using both Gal4 lines, we expressed GFP in the larvae and tried to observe the potential overlap between the GFP expressing neurons and the PG neurons labelled by PTTH antibody. In the *Jeb^{Trojan}>GFP* larvae GFP signals appeared in a large group of cells in both brain lobes and ventral ganglia (Figure 32A), while *Pvf2,3>GFP* marks numerous ventral ganglia cells but only two pairs of neurons in the brain lobes (Figure 32B). When immunostaining the GFP expressing brain tissues with PTTH antibody, we saw clear colocalization between the GFP and the PTTH signals, showing that both Jeb and Pvf ligands are expressed in the PG neurons (Figure 32C and 32D). Although we cannot tell so far whether these PG neuron derived Jeb and Pvf ligands are the only ligand source that activates their corresponding receptors in the PG, we conclude that the Alk and Pvr pathways in the PG are at least partially activated by the signals from the PG neurons.

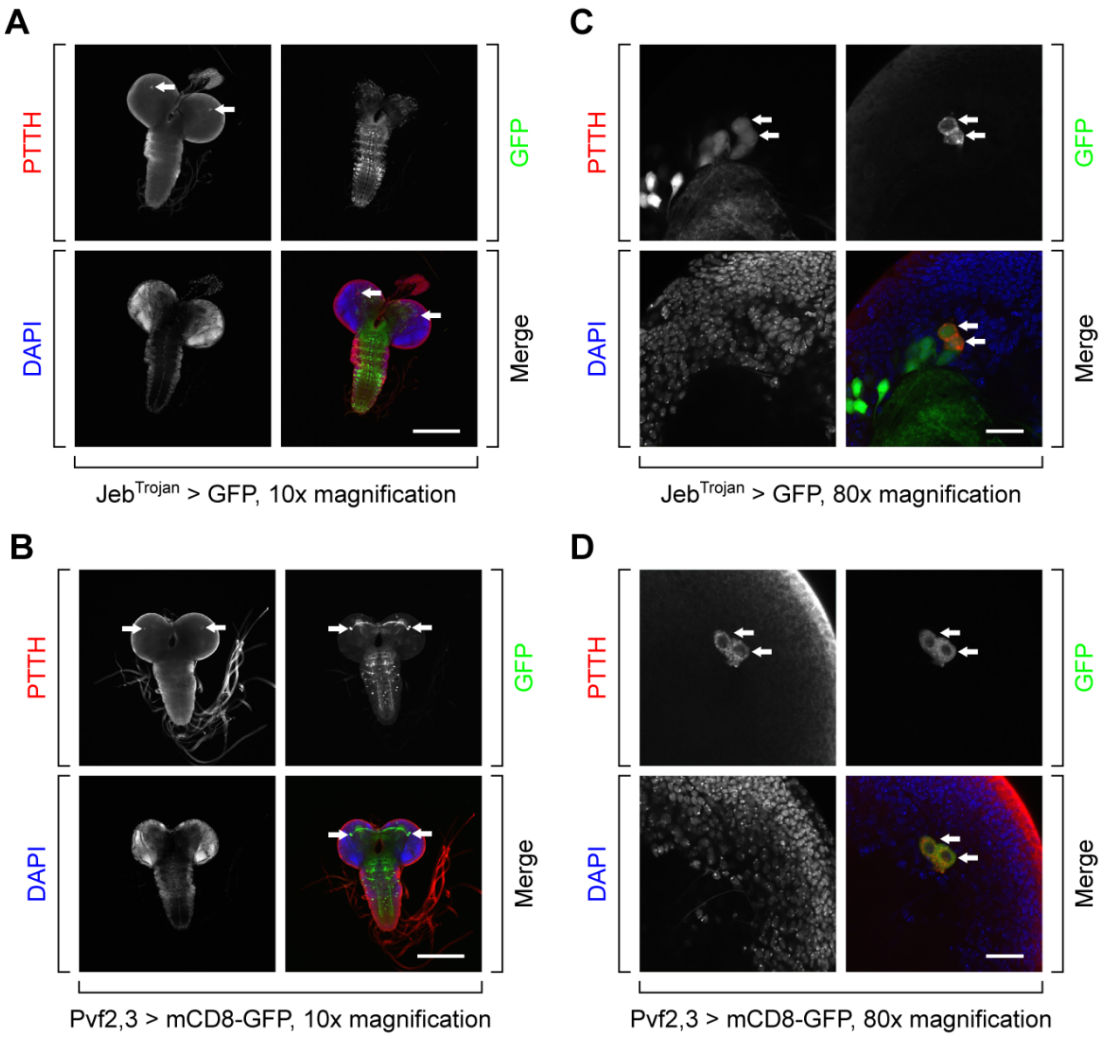

Figure 32. Jeb and Pvf ligands are expressed in the PG neurons.

(A and B) Immunofluorescence images of brains of *Jeb^{Trojan}>GFP* (A) and *Pvf2,3>mCD8-GFP* (B) larvae stained with antibody against PTTH. Arrows indicate the PG neurons in the brain lobes. Scale bar, 200 μm. (C and D) High magnification images of the brain lobe of *Jeb^{Trojan}>GFP* (C) and *Pvf2,3>mCD8-GFP* (D) larvae showing the overlap between GFP-positive and PTTH-positive neurons. Arrows indicate the two PG neurons that are positive of both signals. Scale bar, 20 μm.

3.2.4 Alk and Pvr pathways function jointly with PTTH/Torso pathway to control developmental timing.

Since Jeb and Pvf ligands are expressed in the PG neurons, we propose that the loss of these ligands accounts for the difference of phenotype between PG neuron ablation animals and *ptth* mutants. To verify this hypothesis, we tested whether the Jeb/Alk and Pvf/Pvr pathways have synergic effect with PTTH/Torso pathway.

We firstly confirmed the timing difference between wildtype control (*phm>w1118*) and Alk/Pvr suppression larvae. Knocking down of Alk using two RNAi constructs caused 10- and 18-hour developmental delay respectively (calculated by the time of 50% pupariation; *phm>w1118*, 116.16±2.19 hrs after egg deposit (AED); *phm>Alk$^{RNAi\ JF}$*, 126.08±1.32 hrs AED; *phm>Alk$^{RNAi\ KK}$*, 134.24±1.29 hrs AED) (Figure 33A). Expressing a dominant negative Alk receptor in the PG (*phm>Alk^{DN}*) caused developmental arrest at various larva stages, which may be due to some uncharacterized toxicity caused by the overexpressed proteins (Figure 33A). On the other hand, Pvr knockdown by one RNAi construct caused a 34-hour delay (*phm>Pvr$^{RNAi\ GD}$*, 150.43±2.44 hrs AED), but another RNAi construct resulted in L3 stage arrest. Expression of dominant negative Pvr receptor delayed pupariation by 36 hours (*phm>Pvr^{DN}*, 152.17±5.14 hrs AED), phenocopying the *phm>Pvr$^{RNAi\ GD}$* larvae (Figure 33B). These data confirm our findings in the targeted screening, showing that suppression of either Alk or Pvr receptor in the PG causes developmental defect.

Based on the results from the Alk/Pvr suppression animals, we chose *phm>Alk$^{RNAi\ JF}$* and *phm>Pvr^{DN}* models to examine the combining effects of multi-pathway suppression. Knocking down of Alk in the *ptth* mutants caused developmental arrest in 31% of the larvae and developmental delay longer than both *ptth* mutants and *phm>Alk$^{RNAi\ JF}$* animals in the pupariating larvae (Figure 33C). Further, the pupariated *ptth$^{120F2A;}$ phm>Alk$^{RNAi\ JF}$* animals were all pupal lethal and some of them showed incomplete spiracle protrusion. In addition, some arrested larvae had tanned cuticle without apolysis (Figure 33E). These

observations indicate that Alk pathway functions synergistically with PTTH/Torso pathway. When suppressing Pvr pathway in the absence of *ptth* (*ptth*$^{120F2A;}$ *phm>Pvr*^{DN}), we also observed a developmental delay longer than *ptth* mutants and *phm>Pvr*^{DN} animals, representing an additive effect of the two genetic changes (Figure 33D). Taken together, these data demonstrate that loss of PTTH/Torso signaling together with either the Alk or Pvr pathway leads to a stronger developmental defect than single pathway blockage, suggesting that the Alk and Pvr pathways are the proposed additional pathways that cause the stronger timing phenotype in the PG neuron ablation model.

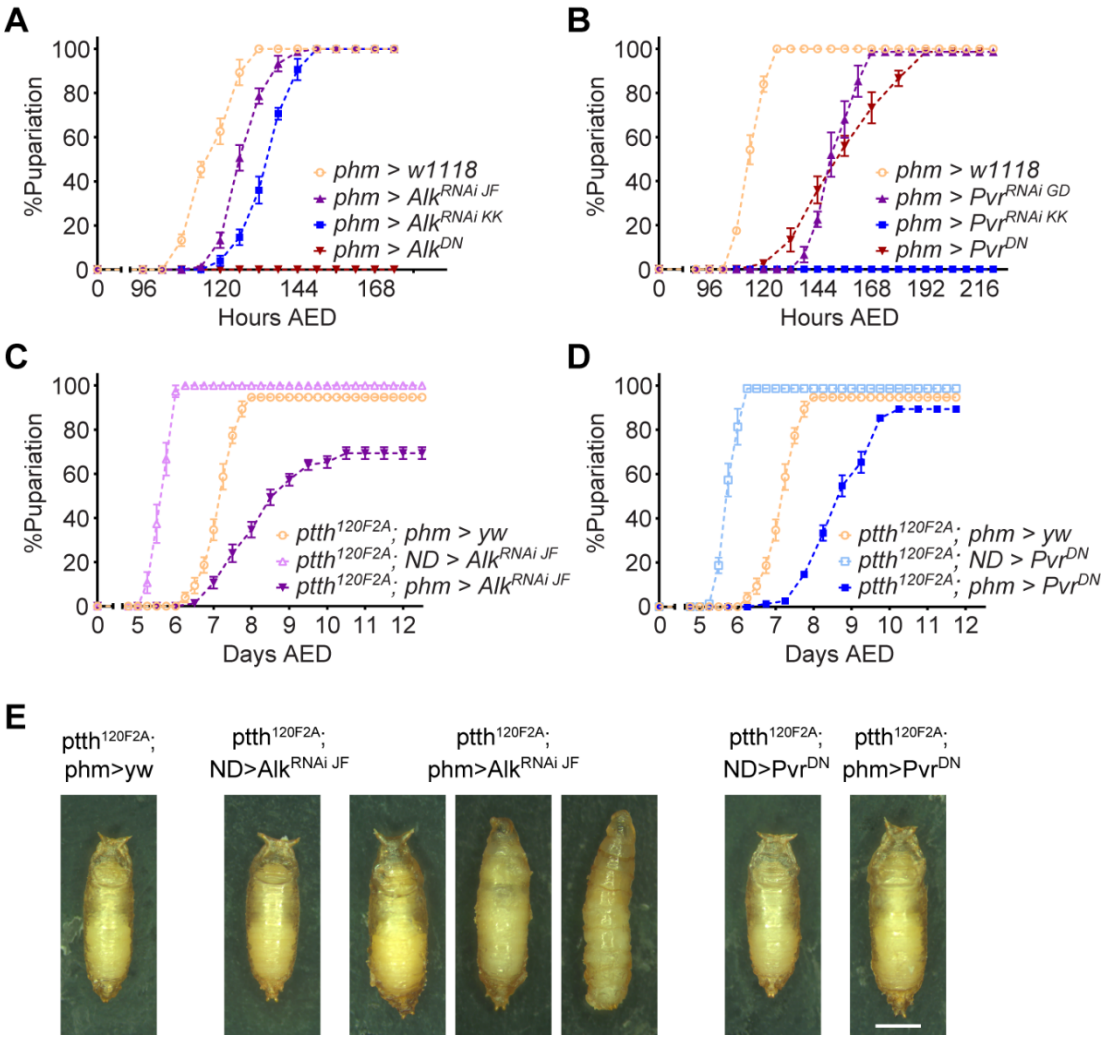

Figure 33. Alk and Pvr pathways function jointly with PTTH/Torso pathway to control developmental timing.

(A) Pupariation timing curve of *phm > w1118* control and Alk suppression larvae. Two RNAi lines, TRiP JF02668 (*phm>Alk$^{RNAi\ JF}$*) and VDRC KK107083 (*phm>Alk$^{RNAi\ KK}$*), were tested. *Phm > Alk^{DN}* larvae arrested at pre-L3 or L3 stage, which appears as a flat line in the figure. (B) Pupariation timing curve of control and Pvr suppression larvae. Two RNAi lines, VDRC GD43459 (*phm>Pvr$^{RNAi\ GD}$*) and VDRC KK105353 (*phm>Pvr$^{RNAi\ KK}$*), were tested. *Phm > Pvr$^{RNAi\ KK}$* larvae arrested at L3 stage, which is presented as a flat line. (C and D) Pupariation timing curve of Alk and Pvr suppression larvae in *ptth* mutant background. TRiP JF02668

Alk RNAi line and dominant negative Pvr were used to suppress the receptors respectively. (E) Images of pupae of *ptth* mutant animals with or without Alk or Pvr suppression. The *ptth*^{120F2A}*; phm>Alk*$^{RNAi\ JF}$ animals that experience normal pupariation (left), incomplete pupariation without spiracle protrusion (middle) and failed pupariation (right) are shown.

3.2.5 Activation of either Alk or Pvr pathway accelerates development.

Since suppression of Alk and Pvr pathway exacerbated the developmental defect caused by *ptth* mutation, we then sought to test whether activation of the two pathways rescued the developmental delay in *ptth* mutants. In wildtype background animals, activation of either Alk (*spok>Alk*^{CA}) or Pvr (*spok>Pvr*) pathway caused overgrowth of the PG (Figure 34A) and acceleration of development (Figure 34B). Interestingly, the early pupariation activities were only observed using *spok-Gal4*, a PG-specific driver that has much weaker activity than *phm-Gal4* driver. Both *phm>Alk*^{CA} and *phm>Pvr* arrested at L1/L2 stage, and expression of constitutively activated form of Pvr (Pvr^{CA}) using even the weak *spok-Gal4* driver caused pre-L3 arrest (Table 2). These findings indicate that constitutive overactivation of Alk and Pvr pathway has detrimental effect in the PG, which is consistent with the fact that the expression time window of the receptors is limited (Figure 31). In *ptth* mutants, activation of either Alk or Pvr receptor rescued the developmental delay (Figure 34C and 34D), indicating that the Alk and Pvr pathway function through the same signaling cascade as the PTTH/Torso pathway, e.g. the Ras-Raf-Erk pathway and that the two pathways may function to enhance the PTTH/Torso signal specifically in L3 stage.

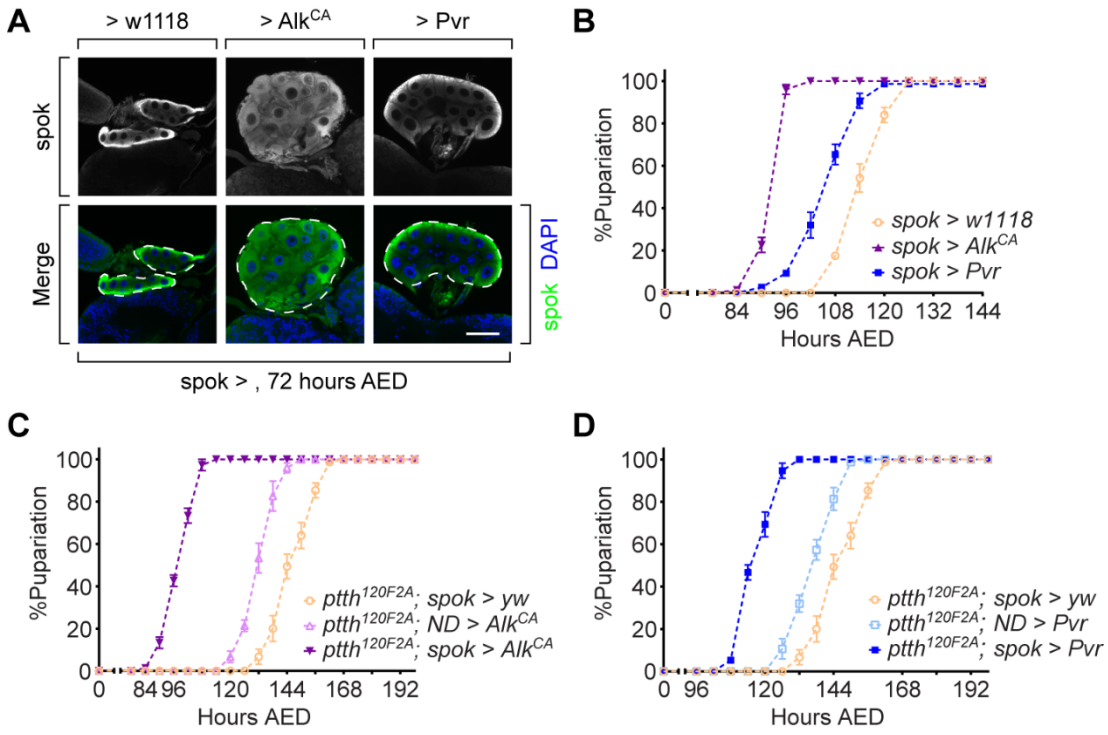

Figure 34. Activation of Alk and Pvr results in PG tissue overgrowth and acceleration of development.

(A) Immunofluorescence images of PGs of control (*spok>w1118*) and Alk (*spok>Alk^{CA}*) and Pvr (*spok>Pvr*) activation larvae which were stained with anti-Spok antibody to mark the PG tissue. The outlines of PG are indicated by the dash lines. Scale bar, 50 μm. (B) Pupariation timing curve of Alk and Pvr activation larvae in wildtype background. (C and D) Pupariation timing curve of Alk and Pvr activation larvae in *ptth* mutant background.

	> Alk^{CA}	> Pvr^{CA}	> Pvr
spok >	Advancement	Delay	Advancement
phm>	Pre-L3 arrest	Pre-L3 arrest	Pre-L3 arrest

Table 2. Developmental timing phenotypes of Alk and Pvr activation larvae. The table summarizes the developmental timing change caused by Alk and Pvr activation using either a weak (*spok-Gal4*) or a strong (*phm-Gal4*) PG-specific Gal4 driver. Advancement, larvae pupariated earlier than the Gal4 driver control (*spok* > *yw*) animals; delay, larvae pupariated later than the control animals; Pre-L3 arrest, animals failed to develop into L3 stage and die as L1/L2 larvae.

3.3 Discussion

The PG neuron-PG signaling axis plays a key role in the regulation of developmental timing in *Drosophila*. PTTH has long been regarded as the signaling molecule in this axis, however, data have accumulated recently suggesting that PTTH is not the only hormone produced by the PG neurons (Shimell et al., 2018). In this study, we screened RTKs for potential receptors in the PG that affect developmental timing and found two positive hits, Alk and Pvr (Table 1). We also observed that Jeb and Pvf, the ligands that activate the receptors are expressed in the PG neurons (Figure 32). These data uncover two novel signaling pathways that control developmental timing through the PG neuron-PG axis. Moreover, suppressing the Alk and Pvr receptors in *ptth* mutants resulted in more severe developmental defect than suppressing the receptors alone (Figure 33C-33E), indicating that the two receptors function jointly with the PTTH/Torso pathway. In addition, these data also provide an explanation to the discrepancy between the timing phenotype of the PG neuron ablation model and the *ptth* mutants (McBrayer et al., 2007; Shimell et al., 2018).

We also found that activation of the pathways caused overgrowth of the PG tissue and acceleration of development (Figure 34A and 34B). Compromised PG tissue growth were observed in both PG neuron ablation and *ptth* mutant animals (McBrayer et al., 2007; Shimell et al., 2018). Activation of the receptors in *ptth* mutants rescued the developmental delay caused by *ptth* mutation (Figure 34C), which may be due to the rescue of the reduced PG size. The PTTH/Torso pathway induces the Ras-Raf-Erk pathway which subsequently regulates both PG tissue growth and expression of hormone producing enzymes (Rewitz et al., 2009). It is reported that the Alk and Pvr pathways also activate the Ras-Raf-Erk in other tissues as well as cell culture models (Englund et al., 2003; Loren et al., 2001; Sansone et al., 2015; Sims, Duchek & Baum, 2009). Thus we propose that the two receptors function in the PG following the same signaling cascade, but the study on this hypothesis awaits future works.

Our data demonstrate a precise temporal control and coordination of multiple

signaling outputs from the PG neuron-PG axis. In the PTTH/Torso pathway, the strength of signal output is largely determined by PTTH expression level and the neuronal activity of the PG neurons. Torso receptor is constitutively expressed in the PG from embryonic stage (Rewitz et al., 2009). By contrast, the expression of PTTH shows a cyclic pattern which is determined by the upstream signal input from the PDF neurons and is highly upregulated at the time of pupariation (McBrayer et al., 2007). The activity of PG neurons is also activated at the end of L3 stage, stimulated by upstream AstA mediated neuronal signals (Deveci et al., 2019). On the contrary, it is likely that the Jeb/Alk and Pvf/Pvr pathways are regulated by the expression control of receptors in PG cells. In this study we demonstrated the expression of Jeb and Pvf in the PG neurons using Jeb- and Pvf-Gal4 drivers (Figure 32), which cannot detect the temporal expression pattern of the proteins. Whether the expression of Jeb and Pvf follows a similar rhythm to that of PTTH is not known yet. However, we found that Alk and Pvr receptors are expressed in the PG specifically from mid-L3 stage (Figure 31), indicating that the two pathways are not functional prior to this stage. Considering the temporal control of Alk and Pvr expression in the PG as well as the fact that constitutive overactivation of the two pathways causes severe developmental defect (Table 2), we propose that the Alk and Pvr pathways may work as “backup” or “supplementary” signals to the PTTH/Torso pathway in the L3 stage when a strong stimulatory signal is required to induce high level of ecdysone production in the PG (Yamanaka, Rewitz, et al., 2013). From a perspective of biological design, it is efficient to express both the timing signal and its “supplements” within the same source (e.g. the PG neurons). Further, the signals are controlled at different nodes in the axis, e.g. the major timing signal PTTH/Torso at the PG neurons while the “supplementary” signals at the PG, which allows the “supplementary” signals being temporally regulated independent on the PTTH/Torso signal.

3.4 Materials and Methods

3.4.1 Flies

Unless noted, all flies were reared on standard agar-cornmeal food supplemented with yeast at 25 °C. Flies were cultured in 12:12 light-dark cycles: however, all experiments were carried out under constant light to avoid the potential impact of circadian cycle on developmental timing. Phm-Gal4 (Ono et al., 2006) and spok-Gal4 were used to drive gene expression specifically in PG cell. A collection of RNAi strains from Transgenic RNAi Project (TRiP) (Ni et al., 2011) were used to carry out the targeted screening: UAS-Alk-RNAi JF02668 (Bloomington Stock Center (BDSC), 27518), UAS-btl-RNAi HMS02038 (BDSC, 40871), UAS-Cad96ca-RNAi HMC04150 (BDSC, 55877), UAS-CG10702-RNAi HMS02499 (BDSC, 42663), UAS-Ddr-RNAi HMC04190 (BDSC, 55906), UAS-dnt-RNAi HMC06353 (BDSC, 67251), UAS-drl-RNAi HMS01918 (BDSC, 39002), UAS-Drl-2-RNAi HMC04172 (BDSC, 55893), UAS-Egfr-RNAi JF01368 (BDSC, 25781), UAS-Eph-RNAi HMS01986 (BDSC, 39066), UAS-htl-RNAi HMS01437 (BDSC, 35024), UAS-InR-RNAi JF01183 (BDSC, 31594), UAS-Nrk-RNAi HMC04375 (BDSC, 56936), UAS-otk-RNAi HMC04139 (BDSC, 55869), UAS-Pvr-RNAi HMS01662 (BDSC, 37520), UAS-Ret-RNAi HMC04143 (BDSC, 55872), UAS-Ror-RNAi HMC05341 (BDSC, 62868), UAS-Tie-RNAi HMJ21428 (BDSC, 54005) and UAS-Torso-RNAi HMS00021 (BDSC, 33627). UAS-Alk-RNAi KK107083, UAS-Pvr-RNAi KK105353 and UAS-Pvr-RNAi GD43459 from VDRC are used to confirm the receptor knockdown phenotype in the screening. UAS-Pvr (BDSC, 58998), UAS-Pvr^{CA} (BDSC, 58496) and UAS-Pvr^{DN} (BDSC, 58431) are used to manipulate the activity of Pvr. UAS-Alk^{CA} (Zettervall et al., 2004) and UAS-Alk^{DN} (Bazigou et al., 2007) are used to manipulate the activity of Alk. Jeb^{Trojan}-Gal4 is constructed from MIMIC insertion line MI03124 (BDSC, 36200) (Venken, Schulze, et al., 2011) following the developer's instruction (Diao et al., 2015). Jeb^{Trojan}-Gal4, Pvf2,3-Gal4 (Jenelia Farm GMR77D12, BDSC 39966), UAS-GFP and UAS-mCD8-GFP are used to label cells expressing Jeb and Pvf ligands. *Ptth^{120F2A}* mutant and combination lines made from it are used to test the

synergistic effect between Alk/Pvr pathway and PTTH signaling on developmental timing.

2.4.2 Larva staging and developmental timing assay

Before egg collection, flies were transferred to constant light environment for at least 2 days and all subsequent treatments were carried out under constant light. Eggs were collected on apple juice plates with yeast paste. Early L1 larvae were transferred to standard lab fly food with yeast paste after 24 hrs. For developmental timing assay, larvae were cultured until wandering stage and then the pupariation activities of larvae were recorded every 6 hours. For more precise staging of L3 stage larvae, larvae were cultured until late L2 stage and newly-molted L3 larvae were picked out every 2 hrs and transferred to fly food without yeast paste. Then larvae were further cultured for a certain period and picked out for experiments.

2.4.3 Fluorescence microscopy

Larvae were dissected in PBS and fixed using 3.7% formalderhyde for 15 mins at room temperature. Tissues were then washed in PBS and mounted in 90% glycerol for imaging. All confocal images were captured using Zeiss LSM710 confocal microscope.

2.4.4 Immunohistochemistry

Larvae were dissected in PBS and fixed using 3.7% formalderhyde for 15 mins at room temperature. Tissues were washed in PBS containing 0.1% Triton X-100 (PBT) for 3 times and then permeablized and blocked simultaneously using PBT containing 5% normal goat serum (NGS) for 1 hour. Tissues were then incubated with primary antibody (anti-Alk, gift from Palmer Lab, 1:500; anti-Pvr, gift from Shilo Lab, 1:200; anti-PTTH, 1:500; anti-Spok, 1:500) in PBT containing 10% NGS overnight at 4 degrees, followed by 5 washes and then post-secondary incubation for 2 hours at room temperature. DAPI staining occurred for 5 minutes at the pen-ultimate washing step after secondary antibody incubation. Finally, tissues were transferred to 70% glycerol/PBS mounting medium and then mounted on glass slide for imaging. Images were captured using a Zeiss LSM 710 confocal

microscope.

2.4.5 Statistics

GraphPad Prism software was used to carry out statistical analyses. Student's t-test was used to determine statistical significance.

REFERENCES

Ables, E. T. & Drummond-Barbosa, D. (2010). The steroid hormone ecdysone functions with intrinsic chromatin remodeling factors to control female germline stem cells in Drosophila. *Cell Stem Cell, 7*(5), 581-592.

Ables, E. T., Hwang, G. H., Finger, D. S., Hinnant, T. D. & Drummond-Barbosa, D. (2016). A Genetic Mosaic Screen Reveals Ecdysone-Responsive Genes Regulating Drosophila Oogenesis. *G3 (Bethesda), 6*(8), 2629-2642.

Advani, R. J., Yang, B., Prekeris, R., Lee, K. C., Klumperman, J. & Scheller, R. H. (1999). VAMP-7 mediates vesicular transport from endosomes to lysosomes. *J Cell Biol, 146*(4), 765-776.

Andres, A. J. & Thummel, C. S. (1995). The Drosophila 63F early puff contains E63-1, an ecdysone-inducible gene that encodes a novel Ca(2+)-binding protein. *Development, 121*(8), 2667-2679.

Angilletta, M. J., Jr. & Dunham, A. E. (2003). The temperature-size rule in ectotherms: simple evolutionary explanations may not be general. *Am Nat, 162*(3), 332-342.

Angilletta, M. J., Jr., Steury, T. D. & Sears, M. W. (2004). Temperature, growth rate, and body size in ectotherms: fitting pieces of a life-history puzzle. *Integr Comp Biol, 44*(6), 498-509.

Ashburner, M., Chihara, C., Meltzer, P. & Richards, G. (1974). Temporal control of puffing activity in polytene chromosomes. *Cold Spring Harb Symp Quant Biol, 38*, 655-662.

Ashburner, M. & Richards, G. (1976). Sequential gene activation by ecdysone in polytene chromosomes of Drosophila melanogaster. III. Consequences of ecdysone withdrawal. *Dev Biol, 54*(2), 241-255.

Badenhorst, P., Xiao, H., Cherbas, L., Kwon, S. Y., Voas, M., Rebay, I., *et al.* (2005). The Drosophila nucleosome remodeling factor NURF is required for Ecdysteroid signaling and metamorphosis. *Genes Dev, 19*(21), 2540-2545.

Bai, J., Uehara, Y. & Montell, D. J. (2000). Regulation of invasive cell behavior by taiman, a Drosophila protein related to AIB1, a steroid receptor coactivator

amplified in breast cancer. *Cell, 103*(7), 1047-1058.

Bakker, K. & Nelissen, F. X. (1963). On the relations between the duration of the larval and pupal period, weight and diurnal rhythm in emergence in Drosophila melanogaster. *Entomol Exp Appl, 6*(1), 37-52.

Bazigou, E., Apitz, H., Johansson, J., Loren, C. E., Hirst, E. M., Chen, P. L.*, et al.* (2007). Anterograde Jelly belly and Alk receptor tyrosine kinase signaling mediates retinal axon targeting in Drosophila. *Cell, 128*(5), 961-975.

Beadle, G. W., Tatum, E. L. & Clancy, C. W. (1938). Food Level in Relation to Rate of Development and Eye Pigmentation in Drosophila Melanogaster. *Biol Bull, 75*(3), 447-462.

Biyasheva, A., Do, T. V., Lu, Y., Vaskova, M. & Andres, A. J. (2001). Glue secretion in the Drosophila salivary gland: a model for steroid-regulated exocytosis. *Dev Biol, 231*(1), 234-251.

Blais, C., DauphinVillemant, C., Kovganko, N., Girault, J. P., Descoins, C. & Lafont, R. (1996). Evidence for the involvement of 3-oxo-Delta(4) intermediates in ecdysteroid biosynthesis. *Biochem J, 320*, 413-419.

Bohni, R., Riesgo-Escovar, J., Oldham, S., Brogiolo, W., Stocker, H., Andruss, B. F.*, et al.* (1999). Autonomous control of cell and organ size by CHICO, a Drosophila homolog of vertebrate IRS1-4. *Cell, 97*(7), 865-875.

Bolte, S. & Cordelieres, F. P. (2006). A guided tour into subcellular colocalization analysis in light microscopy. *J Microsc, 224*(Pt 3), 213-232.

Boone, E., Colombani, J., Andersen, D. S. & Leopold, P. (2016). The Hippo signalling pathway coordinates organ growth and limits developmental variability by controlling dilp8 expression. *Nat Commun, 7*, 13505.

Brogiolo, W., Stocker, H., Ikeya, T., Rintelen, F., Fernandez, R. & Hafen, E. (2001). An evolutionarily conserved function of the Drosophila insulin receptor and insulin-like peptides in growth control. *Curr Biol, 11*(4), 213-221.

Burtis, K. C., Thummel, C. S., Jones, C. W., Karim, F. D. & Hogness, D. S. (1990). The Drosophila 74EF early puff contains E74, a complex ecdysone-inducible gene that encodes two ets-related proteins. *Cell, 61*(1), 85-99.

Caldwell, P. E., Walkiewicz, M. & Stern, M. (2005). Ras activity in the Drosophila

prothoracic gland regulates body size and developmental rate via ecdysone release. *Curr Biol, 15*(20), 1785-1795.

Carbonell, A., Mazo, A., Serras, F. & Corominas, M. (2013). Ash2 acts as an ecdysone receptor coactivator by stabilizing the histone methyltransferase Trr. *Mol Biol Cell, 24*(3), 361-372.

Chang, Y. Y. & Neufeld, T. P. (2009). An Atg1/Atg13 complex with multiple roles in TOR-mediated autophagy regulation. *Mol Biol Cell, 20*(7), 2004-2014.

Chang, Y. Y. & Neufeld, T. P. (2010). Autophagy takes flight in Drosophila. *FEBS Lett, 584*(7), 1342-1349.

Chantranupong, L., Scaria, S. M., Saxton, R. A., Gygi, M. P., Shen, K., Wyant, G. A.*, et al.* (2016). The CASTOR Proteins Are Arginine Sensors for the mTORC1 Pathway. *Cell, 165*(1), 153-164.

Chavez, V. M., Marques, G., Delbecque, J. P., Kobayashi, K., Hollingsworth, M., Burr, J.*, et al.* (2000). The Drosophila disembodied gene controls late embryonic morphogenesis and codes for a cytochrome P450 enzyme that regulates embryonic ecdysone levels. *Development, 127*(19), 4115-4126.

Cheng, L. Y., Bailey, A. P., Leevers, S. J., Ragan, T. J., Driscoll, P. C. & Gould, A. P. (2011). Anaplastic lymphoma kinase spares organ growth during nutrient restriction in Drosophila. *Cell, 146*(3), 435-447.

Cho, K. S., Lee, J. H., Kim, S., Kim, D., Koh, H., Lee, J.*, et al.* (2001). Drosophila phosphoinositide-dependent kinase-1 regulates apoptosis and growth via the phosphoinositide 3-kinase-dependent signaling pathway. *Proc Natl Acad Sci U S A, 98*(11), 6144-6149.

Clarkson, J., Han, S. K., Liu, X., Lee, K. & Herbison, A. E. (2010). Neurobiological mechanisms underlying kisspeptin activation of gonadotropin-releasing hormone (GnRH) neurons at puberty. *Mol Cell Endocrinol, 324*(1-2), 45-50.

Clayton, R. B. (1964). The Utilization of Sterols by Insects. *J Lipid Res, 5*, 3-19.

Colombani, J., Andersen, D. S., Boulan, L., Boone, E., Romero, N., Virolle, V.*, et al.* (2015). Drosophila Lgr3 Couples Organ Growth with Maturation and Ensures Developmental Stability. *Curr Biol, 25*(20), 2723-2729.

Colombani, J., Andersen, D. S. & Leopold, P. (2012). Secreted peptide Dilp8

coordinates Drosophila tissue growth with developmental timing. *Science, 336*(6081), 582-585.

Colombani, J., Bianchini, L., Layalle, S., Pondeville, E., Dauphin-Villemant, C., Antoniewski, C*., et al.* (2005). Antagonistic actions of ecdysone and insulins determine final size in Drosophila. *Science, 310*(5748), 667-670.

Colombani, J., Raisin, S., Pantalacci, S., Radimerski, T., Montagne, J. & Leopold, P. (2003). A nutrient sensor mechanism controls Drosophila growth. *Cell, 114*(6), 739-749.

Cybulski, N. & Hall, M. N. (2009). TOR complex 2: a signaling pathway of its own. *Trends Biochem Sci, 34*(12), 620-627.

Danielsen, E. T., Moeller, M. E., Yamanaka, N., Ou, Q., Laursen, J. M., Soenderholm, C*., et al.* (2016). A Drosophila Genome-Wide Screen Identifies Regulators of Steroid Hormone Production and Developmental Timing. *Dev Cell, 37*(6), 558-570.

Davis, M. B. & Li, T. (2013). Genomic analysis of the ecdysone steroid signal at metamorphosis onset using ecdysoneless and EcRnullDrosophila melanogaster mutants. *Genes Genomics, 35*(1), 21-46.

De Moed, G. H., Kruitwagen, C. L. J. J., De Jong, G. & Scharloo, W. (1999). Critical weight for the induction of pupariation in Drosophila melanogaster: genetic and environmental variation. *J Evol Biol, 12*(5), 852-858.

Dermaut, B., Norga, K. K., Kania, A., Verstreken, P., Pan, H., Zhou, Y*., et al.* (2005). Aberrant lysosomal carbohydrate storage accompanies endocytic defects and neurodegeneration in Drosophila benchwarmer. *J Cell Biol, 170*(1), 127-139.

Deveci, D., Martin, F. A., Leopold, P. & Romero, N. M. (2019). AstA Signaling Functions as an Evolutionary Conserved Mechanism Timing Juvenile to Adult Transition. *Curr Biol, 29*(5), 813-+.

DeVorkin, L. & Gorski, S. M. (2014). Monitoring autophagic flux using Ref(2)P, the Drosophila p62 ortholog. *Cold Spring Harb Protoc, 2014*(9), 959-966.

Diao, F., Ironfield, H., Luan, H., Diao, F., Shropshire, W. C., Ewer, J*., et al.* (2015). Plug-and-play genetic access to drosophila cell types using exchangeable exon cassettes. *Cell Rep, 10*(8), 1410-1421.

Diaz-Troya, S., Perez-Perez, M. E., Florencio, F. J. & Crespo, J. L. (2008). The role of TOR in autophagy regulation from yeast to plants and mammals. *Autophagy, 4*(7), 851-865.

DiBello, P. R., Withers, D. A., Bayer, C. A., Fristrom, J. W. & Guild, G. M. (1991). The Drosophila Broad-Complex encodes a family of related proteins containing zinc fingers. *Genetics, 129*(2), 385-397.

Dunst, S., Kazimiers, T., von Zadow, F., Jambor, H., Sagner, A., Brankatschk, B.*, et al.* (2015). Endogenously tagged rab proteins: a resource to study membrane trafficking in Drosophila. *Dev Cell, 33*(3), 351-365.

Dupont, N., Jiang, S., Pilli, M., Ornatowski, W., Bhattacharya, D. & Deretic, V. (2011). Autophagy-based unconventional secretory pathway for extracellular delivery of IL-1beta. *EMBO J, 30*(23), 4701-4711.

Englund, C., Loren, C. E., Grabbe, C., Varshney, G. K., Deleuil, F., Hallberg, B.*, et al.* (2003). Jeb signals through the Alk receptor tyrosine kinase to drive visceral muscle fusion. *Nature, 425*(6957), 512-516.

Enya, S., Ameku, T., Igarashi, F., Iga, M., Kataoka, H., Shinoda, T.*, et al.* (2014). A Halloween gene noppera-bo encodes a glutathione S-transferase essential for ecdysteroid biosynthesis via regulating the behaviour of cholesterol in Drosophila. *Sci Rep, 4*, 6586.

Fan, Y. & Bergmann, A. (2010). The cleaved-Caspase-3 antibody is a marker of Caspase-9-like DRONC activity in Drosophila. *Cell Death Differ, 17*(3), 534-539.

Felix, R. C., Trindade, M., Pires, I. R., Fonseca, V. G., Martins, R. S., Silveira, H.*, et al.* (2015). Unravelling the Evolution of the Allatostatin-Type A, KISS and Galanin Peptide-Receptor Gene Families in Bilaterians: Insights from Anopheles Mosquitoes. *PLoS One, 10*(7), e0130347.

Feng, Y., He, D., Yao, Z. & Klionsky, D. J. (2014). The machinery of macroautophagy. *Cell Res, 24*(1), 24-41.

Fernandez, R., Tabarini, D., Azpiazu, N., Frasch, M. & Schlessinger, J. (1995). The Drosophila insulin receptor homolog: a gene essential for embryonic development encodes two receptor isoforms with different signaling potential. *EMBO J, 14*(14), 3373-3384.

Fraenkel, G. & Bhaskaran, G. (1973). Pupariation and Pupation in Cyclorrhaphous Flies (Diptera) - Terminology and Interpretation. *Ann Entomol Soc Am, 66*(2), 418-422.

French, V., Feast, M. & Partridge, L. (1998). Body size and cell size in Drosophila: the developmental response to temperature. *J Insect Physiol, 44*(11), 1081-1089.

Furuta, N., Fujita, N., Noda, T., Yoshimori, T. & Amano, A. (2010). Combinational soluble N-ethylmaleimide-sensitive factor attachment protein receptor proteins VAMP8 and Vti1b mediate fusion of antimicrobial and canonical autophagosomes with lysosomes. *Mol Biol Cell, 21*(6), 1001-1010.

Galluzzi, L., Pietrocola, F., Levine, B. & Kroemer, G. (2014). Metabolic control of autophagy. *Cell, 159*(6), 1263-1276.

Gao, X. & Pan, D. (2001). TSC1 and TSC2 tumor suppressors antagonize insulin signaling in cell growth. *Genes Dev, 15*(11), 1383-1392.

Garelli, A., Gontijo, A. M., Miguela, V., Caparros, E. & Dominguez, M. (2012). Imaginal discs secrete insulin-like peptide 8 to mediate plasticity of growth and maturation. *Science, 336*(6081), 579-582.

Garelli, A., Heredia, F., Casimiro, A. P., Macedo, A., Nunes, C., Garcez, M.*, et al.* (2015). Dilp8 requires the neuronal relaxin receptor Lgr3 to couple growth to developmental timing. *Nat Commun, 6*, 8732.

Gawriluk, T. R., Ko, C., Hong, X., Christenson, L. K. & Rucker, E. B., 3rd. (2014). Beclin-1 deficiency in the murine ovary results in the reduction of progesterone production to promote preterm labor. *Proc Natl Acad Sci U S A, 111*(40), E4194-4203.

Ghosh, S. M., Testa, N. D. & Shingleton, A. W. (2013). Temperature-size rule is mediated by thermal plasticity of critical size in Drosophila melanogaster. *Proc Biol Sci, 280*(1760), 20130174.

Gibbens, Y. Y., Warren, J. T., Gilbert, L. I. & O'Connor, M. B. (2011). Neuroendocrine regulation of Drosophila metamorphosis requires TGFbeta/Activin signaling. *Development, 138*(13), 2693-2703.

Gilbert, L. I. (2004). Halloween genes encode P450 enzymes that mediate steroid hormone biosynthesis in Drosophila melanogaster. *Mol Cell Endocrinol,*

215(1-2), 1-10.

Gleixner, E. M., Canaud, G., Hermle, T., Guida, M. C., Kretz, O., Helmstadter, M., *et al.* (2014). V-ATPase/mTOR signaling regulates megalin-mediated apical endocytosis. *Cell Rep, 8*(1), 10-19.

Goberdhan, D. C., Paricio, N., Goodman, E. C., Mlodzik, M. & Wilson, C. (1999). Drosophila tumor suppressor PTEN controls cell size and number by antagonizing the Chico/PI3-kinase signaling pathway. *Genes Dev, 13*(24), 3244-3258.

Gonzalez, A. & Hall, M. N. (2017). Nutrient sensing and TOR signaling in yeast and mammals. *EMBO J, 36*(4), 397-408.

Hackney, J. F., Zolali-Meybodi, O. & Cherbas, P. (2012). Tissue damage disrupts developmental progression and ecdysteroid biosynthesis in Drosophila. *PLoS One, 7*(11), e49105.

Halme, A., Cheng, M. & Hariharan, I. K. (2010). Retinoids regulate a developmental checkpoint for tissue regeneration in Drosophila. *Curr Biol, 20*(5), 458-463.

Hietakangas, V. & Cohen, S. M. (2007). Re-evaluating AKT regulation: role of TOR complex 2 in tissue growth. *Genes Dev, 21*(6), 632-637.

Higgins, M. E., Davies, J. P., Chen, F. W. & Ioannou, Y. A. (1999). Niemann-Pick C1 is a late endosome-resident protein that transiently associates with lysosomes and the trans-Golgi network. *Mol Genet Metab, 68*(1), 1-13.

Huang, X., Suyama, K., Buchanan, J., Zhu, A. J. & Scott, M. P. (2005). A Drosophila model of the Niemann-Pick type C lysosome storage disease: dnpc1a is required for molting and sterol homeostasis. *Development, 132*(22), 5115-5124.

Humphries, W. H. t., Szymanski, C. J. & Payne, C. K. (2011). Endo-lysosomal vesicles positive for Rab7 and LAMP1 are terminal vesicles for the transport of dextran. *PLoS One, 6*(10), e26626.

Ikeya, T., Galic, M., Belawat, P., Nairz, K. & Hafen, E. (2002). Nutrient-dependent expression of insulin-like peptides from neuroendocrine cells in the CNS contributes to growth regulation in Drosophila. *Curr Biol, 12*(15), 1293-1300.

Ikonen, E. (2008). Cellular cholesterol trafficking and compartmentalization. *Nat Rev Mol Cell Biol, 9*(2), 125-138.

Inoki, K., Li, Y., Zhu, T., Wu, J. & Guan, K. L. (2002). TSC2 is phosphorylated and inhibited by Akt and suppresses mTOR signalling. *Nat Cell Biol, 4*(9), 648-657.

Inoki, K., Zhu, T. & Guan, K. L. (2003). TSC2 mediates cellular energy response to control cell growth and survival. *Cell, 115*(5), 577-590.

Ishizaki, H. & Suzuki, A. (1980). Prothoracicotropic Hormone. In T. A. Miller (Ed.), *Neurohormonal Techniques in Insects* (pp. 244-276). New York, NY: Springer New York.

Itakura, E., Kishi-Itakura, C. & Mizushima, N. (2012). The hairpin-type tail-anchored SNARE syntaxin 17 targets to autophagosomes for fusion with endosomes/lysosomes. *Cell, 151*(6), 1256-1269.

Ito, N. & Rubin, G. M. (1999). gigas, a Drosophila homolog of tuberous sclerosis gene product-2, regulates the cell cycle. *Cell, 96*(4), 529-539.

Jean, S., Cox, S., Nassari, S. & Kiger, A. A. (2015). Starvation-induced MTMR13 and RAB21 activity regulates VAMP8 to promote autophagosome-lysosome fusion. *EMBO Rep, 16*(3), 297-311.

Jenett, A., Rubin, G. M., Ngo, T. T., Shepherd, D., Murphy, C., Dionne, H.*, et al.* (2012). A GAL4-driver line resource for Drosophila neurobiology. *Cell Rep, 2*(4), 991-1001.

Johnson, A. E., Shu, H., Hauswirth, A. G., Tong, A. & Davis, G. W. (2015). VCP-dependent muscle degeneration is linked to defects in a dynamic tubular lysosomal network in vivo. *Elife, 4*.

Jung, C. H., Ro, S. H., Cao, J., Otto, N. M. & Kim, D. H. (2010). mTOR regulation of autophagy. *FEBS Lett, 584*(7), 1287-1295.

Junger, M. A., Rintelen, F., Stocker, H., Wasserman, J. D., Vegh, M., Radimerski, T.*, et al.* (2003). The Drosophila forkhead transcription factor FOXO mediates the reduction in cell number associated with reduced insulin signaling. *J Biol, 2*(3), 20.

Jurgens, G., Wieschaus, E., Nussleinvolhard, C. & Kluding, H. (1984). Mutations

Affecting the Pattern of the Larval Cuticle in Drosophila-Melanogaster .2. Zygotic Loci on the 3rd Chromosome. *Wilhelm Rouxs Archives of Developmental Biology, 193*(5), 283-295.

Kaieda, Y., Masuda, R., Nishida, R., Shimell, M., O'Connor, M. B. & Ono, H. (2017). Glue protein production can be triggered by steroid hormone signaling independent of the developmental program in Drosophila melanogaster. *Dev Biol, 430*(1), 166-176.

Kanerva, K., Uronen, R. L., Blom, T., Li, S., Bittman, R., Lappalainen, P.*, et al.* (2013). LDL cholesterol recycles to the plasma membrane via a Rab8a-Myosin5b-actin-dependent membrane transport route. *Dev Cell, 27*(3), 249-262.

Kim, A. J., Cha, G. H., Kim, K., Gilbert, L. I. & Lee, C. C. (1997). Purification and characterization of the prothoracicotropic hormone of Drosophila melanogaster. *Proc Natl Acad Sci U S A, 94*(4), 1130-1135.

Kim, E., Goraksha-Hicks, P., Li, L., Neufeld, T. P. & Guan, K. L. (2008). Regulation of TORC1 by Rag GTPases in nutrient response. *Nat Cell Biol, 10*(8), 935-945.

Kim, J. & Neufeld, T. P. (2015). Dietary sugar promotes systemic TOR activation in Drosophila through AKH-dependent selective secretion of Dilp3. *Nat Commun, 6*, 6846.

Kimura, S., Sawatsubashi, S., Ito, S., Kouzmenko, A., Suzuki, E., Zhao, Y.*, et al.* (2008). Drosophila arginine methyltransferase 1 (DART1) is an ecdysone receptor co-repressor. *Biochem Biophys Res Commun, 371*(4), 889-893.

Kirilly, D., Wong, J. J., Lim, E. K., Wang, Y., Zhang, H., Wang, C.*, et al.* (2011). Intrinsic epigenetic factors cooperate with the steroid hormone ecdysone to govern dendrite pruning in Drosophila. *Neuron, 72*(1), 86-100.

Klionsky, D. J., Abdelmohsen, K., Abe, A., Abedin, M. J., Abeliovich, H., Acevedo Arozena, A.*, et al.* (2016). Guidelines for the use and interpretation of assays for monitoring autophagy (3rd edition). *Autophagy, 12*(1), 1-222.

Ko, D. C., Gordon, M. D., Jin, J. Y. & Scott, M. P. (2001). Dynamic movements of organelles containing Niemann-Pick C1 protein: NPC1 involvement in late endocytic events. *Mol Biol Cell, 12*(3), 601-614.

Kobayashi, T., Beuchat, M. H., Lindsay, M., Frias, S., Palmiter, R. D., Sakuraba, H.*, et al.* (1999). Late endosomal membranes rich in lysobisphosphatidic acid regulate cholesterol transport. *Nat Cell Biol, 1*(2), 113-118.

Kopeć, S. (1922). Studies on the Necessity of the Brain for the Inception of Insect Metamorphosis. *Biol Bull, 42*(6), 323-342.

Koyama, T., Rodrigues, M. A., Athanasiadis, A., Shingleton, A. W. & Mirth, C. K. (2014). Nutritional control of body size through FoxO-Ultraspiracle mediated ecdysone biosynthesis. *Elife, 3*.

Kozlova, T. & Thummel, C. S. (2000). Steroid regulation of postembryonic development and reproduction in Drosophila (vol 11, pg 276, 2000). *Trends Endocrinol Metab, 11*(10), 436-436.

Kreher, J., Kovac, K., Bouazoune, K., Macinkovic, I., Ernst, A. L., Engelen, E.*, et al.* (2017). EcR recruits dMi-2 and increases efficiency of dMi-2-mediated remodelling to constrain transcription of hormone-regulated genes. *Nat Commun, 8*, 14806.

Layalle, S., Arquier, N. & Leopold, P. (2008). The TOR pathway couples nutrition and developmental timing in Drosophila. *Dev Cell, 15*(4), 568-577.

Lee, J. H., Budanov, A. V., Park, E. J., Birse, R., Kim, T. E., Perkins, G. A.*, et al.* (2010). Sestrin as a feedback inhibitor of TOR that prevents age-related pathologies. *Science, 327*(5970), 1223-1228.

Lee, J. H., Cho, U. S. & Karin, M. (2016). Sestrin regulation of TORC1: Is Sestrin a leucine sensor? *Sci Signal, 9*(431), re5.

Leevers, S. J., Weinkove, D., MacDougall, L. K., Hafen, E. & Waterfield, M. D. (1996). The Drosophila phosphoinositide 3-kinase Dp110 promotes cell growth. *EMBO J, 15*(23), 6584-6594.

Li, Q. & Gong, Z. (2015). Cold-sensing regulates Drosophila growth through insulin-producing cells. *Nat Commun, 6*, 10083.

Li, T. R. & White, K. P. (2003). Tissue-specific gene expression and ecdysone-regulated genomic networks in Drosophila. *Dev Cell, 5*(1), 59-72.

Linder, M. D., Mayranpaa, M. I., Peranen, J., Pietila, T. E., Pietiainen, V. M., Uronen, R. L.*, et al.* (2009). Rab8 regulates ABCA1 cell surface expression

and facilitates cholesterol efflux in primary human macrophages. *Arterioscler Thromb Vasc Biol, 29*(6), 883-888.

Linder, M. D., Uronen, R. L., Holtta-Vuori, M., van der Sluijs, P., Peranen, J. & Ikonen, E. (2007). Rab8-dependent recycling promotes endosomal cholesterol removal in normal and sphingolipidosis cells. *Mol Biol Cell, 18*(1), 47-56.

Loren, C. E., Scully, A., Grabbe, C., Edeen, P. T., Thomas, J., McKeown, M.*, et al.* (2001). Identification and characterization of DAlk: a novel Drosophila melanogaster RTK which drives ERK activation in vivo. *Genes Cells, 6*(6), 531-544.

Ma, L., Chen, Z., Erdjument-Bromage, H., Tempst, P. & Pandolfi, P. P. (2005). Phosphorylation and functional inactivation of TSC2 by Erk implications for tuberous sclerosis and cancer pathogenesis. *Cell, 121*(2), 179-193.

Manning, B. D., Tee, A. R., Logsdon, M. N., Blenis, J. & Cantley, L. C. (2002). Identification of the tuberous sclerosis complex-2 tumor suppressor gene product tuberin as a target of the phosphoinositide 3-kinase/akt pathway. *Mol Cell, 10*(1), 151-162.

Mauvezin, C., Ayala, C., Braden, C. R., Kim, J. & Neufeld, T. P. (2014). Assays to monitor autophagy in Drosophila. *Methods, 68*(1), 134-139.

Mauvezin, C., Nagy, P., Juhasz, G. & Neufeld, T. P. (2015). Autophagosome-lysosome fusion is independent of V-ATPase-mediated acidification. *Nat Commun, 6*, 7007.

McBrayer, Z., Ono, H., Shimell, M., Parvy, J. P., Beckstead, R. B., Warren, J. T.*, et al.* (2007). Prothoracicotropic hormone regulates developmental timing and body size in Drosophila. *Dev Cell, 13*(6), 857-871.

McPhee, C. K. & Baehrecke, E. H. (2009). Autophagy in Drosophila melanogaster. *Biochim Biophys Acta, 1793*(9), 1452-1460.

Minakuchi, C., Namiki, T., Yoshiyama, M. & Shinoda, T. (2008). RNAi-mediated knockdown of juvenile hormone acid O-methyltransferase gene causes precocious metamorphosis in the red flour beetle Tribolium castaneum. *FEBS J, 275*(11), 2919-2931.

Mirth, C., Truman, J. W. & Riddiford, L. M. (2005). The role of the prothoracic

gland in determining critical weight for metamorphosis in Drosophila melanogaster. *Curr Biol, 15*(20), 1796-1807.

Mirth, C. K. & Riddiford, L. M. (2007). Size assessment and growth control: how adult size is determined in insects. *Bioessays, 29*(4), 344-355.

Mirth, C. K., Tang, H. Y., Makohon-Moore, S. C., Salhadar, S., Gokhale, R. H., Warner, R. D.*, et al.* (2014). Juvenile hormone regulates body size and perturbs insulin signaling in Drosophila. *Proc Natl Acad Sci U S A, 111*(19), 7018-7023.

Mobius, W., van Donselaar, E., Ohno-Iwashita, Y., Shimada, Y., Heijnen, H. F., Slot, J. W.*, et al.* (2003). Recycling compartments and the internal vesicles of multivesicular bodies harbor most of the cholesterol found in the endocytic pathway. *Traffic, 4*(4), 222-231.

Montagne, J., Stewart, M. J., Stocker, H., Hafen, E., Kozma, S. C. & Thomas, G. (1999). Drosophila S6 kinase: a regulator of cell size. *Science, 285*(5436), 2126-2129.

Namiki, T., Niwa, R., Sakudoh, T., Shirai, K., Takeuchi, H. & Kataoka, H. (2005). Cytochrome P450 CYP307A1/Spook: a regulator for ecdysone synthesis in insects. *Biochem Biophys Res Commun, 337*(1), 367-374.

Navarro, V. M. & Tena-Sempere, M. (2011). Neuroendocrine control by kisspeptins: role in metabolic regulation of fertility. *Nat Rev Endocrinol, 8*(1), 40-53.

Nezis, I. P., Shravage, B. V., Sagona, A. P., Lamark, T., Bjorkoy, G., Johansen, T.*, et al.* (2010). Autophagic degradation of dBruce controls DNA fragmentation in nurse cells during late Drosophila melanogaster oogenesis. *J Cell Biol, 190*(4), 523-531.

Ni, J. Q., Zhou, R., Czech, B., Liu, L. P., Holderbaum, L., Yang-Zhou, D.*, et al.* (2011). A genome-scale shRNA resource for transgenic RNAi in Drosophila. *Nat Methods, 8*(5), 405-407.

Nijhout, H. F. (1975). A threshold size for metamorphosis in the tobacco hornworm, Manduca sexta (L.). *Biol Bull, 149*(1), 214-225.

Nijhout, H. F., Riddiford, L. M., Mirth, C., Shingleton, A. W., Suzuki, Y. & Callier, V. (2014). The developmental control of size in insects. *Wiley Interdiscip Rev*

Dev Biol, 3(1), 113-134.

Nijhout, H. F. & Williams, C. M. (1974a). Control of moulting and metamorphosis in the tobacco hornworm, Manduca sexta (L.): cessation of juvenile hormone secretion as a trigger for pupation. *J Exp Biol, 61*(2), 493-501.

Nijhout, H. F. & Williams, C. M. (1974b). Control of moulting and metamorphosis in the tobacco hornworm, Manduca sexta (L.): growth of the last-instar larva and the decision to pupate. *J Exp Biol, 61*(2), 481-491.

Niwa, R., Matsuda, T., Yoshiyama, T., Namiki, T., Mita, K., Fujimoto, Y.*, et al.* (2004). CYP306A1, a cytochrome P450 enzyme, is essential for ecdysteroid biosynthesis in the prothoracic glands of Bombyx and Drosophila. *J Biol Chem, 279*(34), 35942-35949.

Niwa, R., Namiki, T., Ito, K., Shimada-Niwa, Y., Kiuchi, M., Kawaoka, S.*, et al.* (2010). Non-molting glossy/shroud encodes a short-chain dehydrogenase/reductase that functions in the 'Black Box' of the ecdysteroid biosynthesis pathway. *Development, 137*(12), 1991-1999.

Niwa, R. & Niwa, Y. S. (2014). Enzymes for ecdysteroid biosynthesis: their biological functions in insects and beyond. *Bioscience Biotechnology and Biochemistry, 78*(8), 1283-1292.

Nussleinvolhard, C., Wieschaus, E. & Kluding, H. (1984). Mutations Affecting the Pattern of the Larval Cuticle in Drosophila-Melanogaster .1. Zygotic Loci on the 2nd Chromosome. *Wilhelm Rouxs Archives of Developmental Biology, 193*(5), 267-282.

Ohhara, Y., Kobayashi, S. & Yamanaka, N. (2017). Nutrient-Dependent Endocycling in Steroidogenic Tissue Dictates Timing of Metamorphosis in Drosophila melanogaster. *PLoS Genet, 13*(1), e1006583.

Ono, H., Rewitz, K. F., Shinoda, T., Itoyama, K., Petryk, A., Rybczynski, R.*, et al.* (2006). Spook and Spookier code for stage-specific components of the ecdysone biosynthetic pathway in Diptera. *Dev Biol, 298*(2), 555-570.

Ou, Q. X., Magico, A. & King-Jones, K. (2011). Nuclear Receptor DHR4 Controls the Timing of Steroid Hormone Pulses During Drosophila Development. *PLoS Biol, 9*(9).

Ouimet, M., Franklin, V., Mak, E., Liao, X., Tabas, I. & Marcel, Y. L. (2011).

Autophagy regulates cholesterol efflux from macrophage foam cells via lysosomal acid lipase. *Cell Metab, 13*(6), 655-667.

Palm, W., Sampaio, J. L., Brankatschk, M., Carvalho, M., Mahmoud, A., Shevchenko, A.*, et al.* (2012). Lipoproteins in Drosophila melanogaster--assembly, function, and influence on tissue lipid composition. *PLoS Genet, 8*(7), e1002828.

Pan, X. & O'Connor, M. B. (2019). Developmental Maturation: Drosophila AstA Signaling Provides a Kiss to Grow Up. *Curr Biol, 29*(5), R161-R164.

Pan, X., Neufeld, T. P. and O'Connor, M. B. (2019). A Tissue-Specific and Temporally-Regulated Autophagic Switch Controls a Drosophila Nutritional Checkpoint. Available at SSRN: https://ssrn.com/abstract=3348348

Partridge, L., Barrie, B., Fowler, K. & French, V. (1994). Evolution and Development of Body Size and Cell Size in Drosophila Melanogaster in Response to Temperature. *Evolution, 48*(4), 1269-1276.

Peterson, A. J. & O'Connor, M. B. (2013). Activin receptor inhibition by Smad2 regulates Drosophila wing disc patterning through BMP-response elements. *Development, 140*(3), 649-659.

Petryk, A., Warren, J. T., Marques, G., Jarcho, M. P., Gilbert, L. I., Kahler, J.*, et al.* (2003). Shade is the Drosophila P450 enzyme that mediates the hydroxylation of ecdysone to the steroid insect molting hormone 20-hydroxyecdysone. *Proc Natl Acad Sci U S A, 100*(24), 13773-13778.

Pfeiffer, B. D., Jenett, A., Hammonds, A. S., Ngo, T. T., Misra, S., Murphy, C.*, et al.* (2008). Tools for neuroanatomy and neurogenetics in Drosophila. *Proc Natl Acad Sci U S A, 105*(28), 9715-9720.

Poodry, C. A. & Woods, D. F. (1990). Control of the Developmental Timer for Drosophila Pupariation. *Rouxs Archives of Developmental Biology, 199*(4), 219-227.

Potter, C. J., Huang, H. & Xu, T. (2001). Drosophila Tsc1 functions with Tsc2 to antagonize insulin signaling in regulating cell growth, cell proliferation, and organ size. *Cell, 105*(3), 357-368.

Potter, C. J., Pedraza, L. G. & Xu, T. (2002). Akt regulates growth by directly phosphorylating Tsc2. *Nat Cell Biol, 4*(9), 658-665.

Pulipparacharuvil, S., Akbar, M. A., Ray, S., Sevrioukov, E. A., Haberman, A. S., Rohrer, J.*, et al.* (2005). Drosophila Vps16A is required for trafficking to lysosomes and biogenesis of pigment granules. *J Cell Sci, 118*(Pt 16), 3663-3673.

Rebsamen, M., Pochini, L., Stasyk, T., de Araujo, M. E., Galluccio, M., Kandasamy, R. K.*, et al.* (2015). SLC38A9 is a component of the lysosomal amino acid sensing machinery that controls mTORC1. *Nature, 519*(7544), 477-481.

Rewitz, K. F., Yamanaka, N., Gilbert, L. I. & O'Connor, M. B. (2009). The Insect Neuropeptide PTTH Activates Receptor Tyrosine Kinase Torso to Initiate Metamorphosis. *Science, 326*(5958), 1403-1405.

Rewitz, K. F., Yamanaka, N. & O'Connor, M. B. (2010). Steroid Hormone Inactivation Is Required during the Juvenile-Adult Transition in Drosophila. *Dev Cell, 19*(6), 895-902.

Riddiford, L. M. (1994). Cellular and Molecular Actions of Juvenile-Hormone .1. General-Considerations and Premetamorphic Actions. *Advances in Insect Physiology, Vol 24, 24*, 213-274.

Riddiford, L. M., Cherbas, P. & Truman, J. W. (2001). Ecdysone receptors and their biological actions. *Vitamins and Hormones - Advances in Research and Applications, Vol 60, 60*, 1-73.

Riddiford, L. M., Truman, J. W., Mirth, C. K. & Shen, Y. C. (2010). A role for juvenile hormone in the prepupal development of Drosophila melanogaster. *Development, 137*(7), 1117-1126.

Roberts, B., Henrich, V. & Gilbert, L. I. (1987). Effects of Photoperiod on the Timing of Larval Wandering in Drosophila-Melanogaster. *Physiol Entomol, 12*(2), 175-180.

Roman, G., Endo, K., Zong, L. & Davis, R. L. (2001). P[Switch], a system for spatial and temporal control of gene expression in Drosophila melanogaster. *Proc Natl Acad Sci U S A, 98*(22), 12602-12607.

Rong, Y., McPhee, C. K., Deng, S., Huang, L., Chen, L., Liu, M.*, et al.* (2011). Spinster is required for autophagic lysosome reformation and mTOR reactivation following starvation. *Proc Natl Acad Sci U S A, 108*(19), 7826-7831.

Rulifson, E. J., Kim, S. K. & Nusse, R. (2002). Ablation of insulin-producing neurons in flies: growth and diabetic phenotypes. *Science, 296*(5570), 1118-1120.

Russell, R. C., Yuan, H. X. & Guan, K. L. (2014). Autophagy regulation by nutrient signaling. *Cell Res, 24*(1), 42-57.

Rybczynski, R., Bell, S. C. & Gilbert, L. I. (2001). Activation of an extracellular signal-regulated kinase (ERK) by the insect prothoracicotropic hormone. *Mol Cell Endocrinol, 184*(1-2), 1-11.

Rybczynski, R. & Gilbert, L. I. (2003). Prothoracicotropic hormone stimulated extracellular signal-regulated kinase (ERK) activity: the changing roles of Ca2+- and cAMP-dependent mechanisms in the insect prothoracic glands during metamorphosis. *Mol Cell Endocrinol, 205*(1-2), 159-168.

Saito, J., Kimura, R., Kaieda, Y., Nishida, R. & Ono, H. (2016). Characterization of candidate intermediates in the Black Box of the ecdysone biosynthetic pathway in Drosophila melanogaster: Evaluation of molting activities on ecdysteroid-defective larvae. *J Insect Physiol, 93-94*, 94-104.

Sancak, Y., Bar-Peled, L., Zoncu, R., Markhard, A. L., Nada, S. & Sabatini, D. M. (2010). Ragulator-Rag complex targets mTORC1 to the lysosomal surface and is necessary for its activation by amino acids. *Cell, 141*(2), 290-303.

Sansone, C. L., Cohen, J., Yasunaga, A., Xu, J., Osborn, G., Subramanian, H.*, et al.* (2015). Microbiota-Dependent Priming of Antiviral Intestinal Immunity in Drosophila. *Cell Host Microbe, 18*(5), 571-581.

Santos, M., Fowler, K. & Partridge, L. (1994). Gene-environment interaction for body size and larval density in Drosophila melanogaster: an investigation of effects on development time, thorax length and adult sex ratio. *Heredity (Edinb), 72 (Pt 5)*, 515-521.

Saxton, R. A., Chantranupong, L., Knockenhauer, K. E., Schwartz, T. U. & Sabatini, D. M. (2016). Mechanism of arginine sensing by CASTOR1 upstream of mTORC1. *Nature, 536*(7615), 229-233.

Saxton, R. A. & Sabatini, D. M. (2017). mTOR Signaling in Growth, Metabolism, and Disease. *Cell, 169*(2), 361-371.

Scott, R. C., Juhasz, G. & Neufeld, T. P. (2007). Direct induction of autophagy by

Atg1 inhibits cell growth and induces apoptotic cell death. *Curr Biol, 17*(1), 1-11.

Scott, R. C., Schuldiner, O. & Neufeld, T. P. (2004). Role and regulation of starvation-induced autophagy in the Drosophila fat body. *Dev Cell, 7*(2), 167-178.

Sedkov, Y., Cho, E., Petruk, S., Cherbas, L., Smith, S. T., Jones, R. S.*, et al.* (2003). Methylation at lysine 4 of histone H3 in ecdysone-dependent development of Drosophila. *Nature, 426*(6962), 78-83.

Segraves, W. A. & Hogness, D. S. (1990). The E75 ecdysone-inducible gene responsible for the 75B early puff in Drosophila encodes two new members of the steroid receptor superfamily. *Genes Dev, 4*(2), 204-219.

Sehnal, F. & Bryant, P. J. (1993). Delayed Pupariation in Drosophila Imaginal Disc Overgrowth Mutants Is Associated with Reduced Ecdysteroid Titer. *J Insect Physiol, 39*(12), 1051-1059.

Setiawan, L., Pan, X., Woods, A. L., O'Connor, M. B. & Hariharan, I. K. (2018). The BMP2/4 ortholog Dpp can function as an inter-organ signal that regulates developmental timing. *Life Sci Alliance, 1*(6), e201800216.

Shimell, M., Pan, X., Martin, F. A., Ghosh, A. C., Leopold, P., O'Connor, M. B.*, et al.* (2018). Prothoracicotropic hormone modulates environmental adaptive plasticity through the control of developmental timing. *Development, 145*(6).

Shlyueva, D., Stelzer, C., Gerlach, D., Yanez-Cuna, J. O., Rath, M., Boryn, L. M.*, et al.* (2014). Hormone-responsive enhancer-activity maps reveal predictive motifs, indirect repression, and targeting of closed chromatin. *Mol Cell, 54*(1), 180-192.

Simpson, P., Berreur, P. & Berreur-Bonnenfant, J. (1980). The initiation of pupariation in Drosophila: dependence on growth of the imaginal discs. *J Embryol Exp Morphol, 57*, 155-165.

Sims, D., Duchek, P. & Baum, B. (2009). PDGF/VEGF signaling controls cell size in Drosophila. *Genome Biol, 10*(2), R20.

Singh, R., Kaushik, S., Wang, Y., Xiang, Y., Novak, I., Komatsu, M.*, et al.* (2009). Autophagy regulates lipid metabolism. *Nature, 458*(7242), 1131-1135.

Smith, W. & Rybczynski, R. (2012). 1 - Prothoracicotropic Hormone. In L. I. Gilbert (Ed.), *Insect Endocrinology* (pp. 1-62). San Diego: Academic Press.

Smith, W. A., Gilbert, L. I. & Bollenbacher, W. E. (1984). The Role of Cyclic-Amp in the Regulation of Ecdysone Synthesis. *Mol Cell Endocrinol, 37*(3), 285-294.

Smith, W. A., Varghese, A. H., Healy, M. S. & Lou, K. J. (1996). Cyclic AMP is a requisite messenger in the action of big PTTH in the prothoracic glands of pupal Manduca sexta. *Insect Biochem Mol Biol, 26*(2), 161-170.

Sonenberg, N. & Hinnebusch, A. G. (2009). Regulation of translation initiation in eukaryotes: mechanisms and biological targets. *Cell, 136*(4), 731-745.

Stieper, B. C., Kupershtok, M., Driscoll, M. V. & Shingleton, A. W. (2008). Imaginal discs regulate developmental timing in Drosophila melanogaster. *Dev Biol, 321*(1), 18-26.

Stoiber, M., Celniker, S., Cherbas, L., Brown, B. & Cherbas, P. (2016). Diverse Hormone Response Networks in 41 Independent Drosophila Cell Lines. *G3 (Bethesda), 6*(3), 683-694.

Sweeney, S. T. & Davis, G. W. (2002). Unrestricted synaptic growth in spinster-a late endosomal protein implicated in TGF-beta-mediated synaptic growth regulation. *Neuron, 36*(3), 403-416.

Taghert, P. H. & Shafer, O. T. (2006). Mechanisms of clock output in the Drosophila circadian pacemaker system. *J Biol Rhythms, 21*(6), 445-457.

Takats, S., Nagy, P., Varga, A., Pircs, K., Karpati, M., Varga, K.*, et al.* (2013). Autophagosomal Syntaxin17-dependent lysosomal degradation maintains neuronal function in Drosophila. *J Cell Biol, 201*(4), 531-539.

Talamillo, A., Herboso, L., Pirone, L., Perez, C., Gonzalez, M., Sanchez, J.*, et al.* (2013). Scavenger receptors mediate the role of SUMO and Ftz-f1 in Drosophila steroidogenesis. *PLoS Genet, 9*(4), e1003473.

Tan, A., Tanaka, H., Tamura, T. & Shiotsuki, T. (2005). Precocious metamorphosis in transgenic silkworms overexpressing juvenile hormone esterase. *Proc Natl Acad Sci U S A, 102*(33), 11751-11756.

Tapon, N., Ito, N., Dickson, B. J., Treisman, J. E. & Hariharan, I. K. (2001). The

Drosophila tuberous sclerosis complex gene homologs restrict cell growth and cell proliferation. *Cell, 105*(3), 345-355.

Tee, A. R., Anjum, R. & Blenis, J. (2003). Inactivation of the tuberous sclerosis complex-1 and -2 gene products occurs by phosphoinositide 3-kinase/Akt-dependent and -independent phosphorylation of tuberin. *J Biol Chem, 278*(39), 37288-37296.

Tee, A. R., Manning, B. D., Roux, P. P., Cantley, L. C. & Blenis, J. (2003). Tuberous sclerosis complex gene products, Tuberin and Hamartin, control mTOR signaling by acting as a GTPase-activating protein complex toward Rheb. *Curr Biol, 13*(15), 1259-1268.

Texada, M. J., Malita, A., Christensen, C. F., Dall, K. B., Faergeman, N. J., Nagy, S.*, et al.* (2019). Autophagy-Mediated Cholesterol Trafficking Controls Steroid Production. *Dev Cell, 48*(5), 659-671 e654.

Thummel, C. S. (1996). Flies on steroids--Drosophila metamorphosis and the mechanisms of steroid hormone action. *Trends Genet, 12*(8), 306-310.

Thummel, C. S. (2002). Ecdysone-regulated puff genes 2000. *Insect Biochem Mol Biol, 32*(2), 113-120.

Thummel, C. S., Burtis, K. C. & Hogness, D. S. (1990). Spatial and temporal patterns of E74 transcription during Drosophila development. *Cell, 61*(1), 101-111.

Tsai, C. C., Kao, H. Y., Yao, T. P., McKeown, M. & Evans, R. M. (1999). SMRTER, a Drosophila nuclear receptor coregulator, reveals that EcR-mediated repression is critical for development. *Mol Cell, 4*(2), 175-186.

Upadhyay, A., Moss-Taylor, L., Kim, M. J., Ghosh, A. C. & O'Connor, M. B. (2017). TGF-beta Family Signaling in Drosophila. *Cold Spring Harb Perspect Biol, 9*(9).

Vafopoulou, X. & Steel, C. G. (1996). The insect neuropeptide prothoracicotropic hormone is released with a daily rhythm: re-evaluation of its role in development. *Proc Natl Acad Sci U S A, 93*(8), 3368-3372.

van der Have, T. M. & de Jong, G. (1996). Adult size in ectotherms: Temperature effects on growth and differentiation. *J Theor Biol, 183*(3), 329-340.

Vaskova, M., Bentley, A. M., Marshall, S., Reid, P., Thummel, C. S. & Andres, A. J. (2000). Genetic analysis of the Drosophila 63F early puff. Characterization of mutations in E63-1 and maggie, a putative Tom22. *Genetics, 156*(1), 229-244.

Venkatesh, K. & Hasan, G. (1997). Disruption of the IP3 receptor gene of Drosophila affects larval metamorphosis and ecdysone release. *Curr Biol, 7*(7), 500-509.

Venken, K. J., Schulze, K. L., Haelterman, N. A., Pan, H., He, Y., Evans-Holm, M.*, et al.* (2011). MiMIC: a highly versatile transposon insertion resource for engineering Drosophila melanogaster genes. *Nat Methods, 8*(9), 737-743.

Venken, K. J., Simpson, J. H. & Bellen, H. J. (2011). Genetic manipulation of genes and cells in the nervous system of the fruit fly. *Neuron, 72*(2), 202-230.

Verdu, J., Buratovich, M. A., Wilder, E. L. & Birnbaum, M. J. (1999). Cell-autonomous regulation of cell and organ growth in Drosophila by Akt/PKB. *Nat Cell Biol, 1*(8), 500-506.

Walters, R. J. & Hassall, M. (2006). The temperature-size rule in ectotherms: may a general explanation exist after all? *Am Nat, 167*(4), 510-523.

Wang, S., Tsun, Z. Y., Wolfson, R. L., Shen, K., Wyant, G. A., Plovanich, M. E.*, et al.* (2015). Metabolism. Lysosomal amino acid transporter SLC38A9 signals arginine sufficiency to mTORC1. *Science, 347*(6218), 188-194.

Warren, J. T., O'Connor, M. B. & Gilbert, L. I. (2009). Studies on the black box: Incorporation of 3-oxo-7-dehydrocholesterol into ecdysteroids by Drosophila melanogaster and Manduca sexta. *Insect Biochem Mol Biol, 39*(10), 677-687.

Warren, J. T., Petryk, A., Marques, G., Jarcho, M., Parvy, J. P., Dauphin-Villemant, C.*, et al.* (2002). Molecular and biochemical characterization of two P450 enzymes in the ecdysteroidogenic pathway of Drosophila melanogaster. *Proc Natl Acad Sci U S A, 99*(17), 11043-11048.

Warren, J. T., Petryk, A., Marques, G., Parvy, J. P., Shinoda, T., Itoyama, K.*, et al.* (2004). Phantom encodes the 25-hydroxylase of Drosophila melanogaster and Bombyx mori: a P450 enzyme critical in ecdysone biosynthesis. *Insect Biochem Mol Biol, 34*(9), 991-1010.

Warren, J. T., Yerushalmi, Y., Shimell, M. J., O'Connor, M. B., Restifo, L. L. & Gilbert, L. I. (2006). Discrete pulses of molting hormone, 20-hydroxyecdysone, during late larval development of Drosophila melanogaster: correlations with changes in gene activity. *Dev Dyn, 235*(2), 315-326.

Weinkove, D., Neufeld, T. P., Twardzik, T., Waterfield, M. D. & Leevers, S. J. (1999). Regulation of imaginal disc cell size, cell number and organ size by Drosophila class I(A) phosphoinositide 3-kinase and its adaptor. *Curr Biol, 9*(18), 1019-1029.

Wieschaus, E., Nussleinvolhard, C. & Jurgens, G. (1984). Mutations Affecting the Pattern of the Larval Cuticle in Drosophila-Melanogaster .3. Zygotic Loci on the X-Chromosome and 4th Chromosome. *Wilhelm Rouxs Archives of Developmental Biology, 193*(5), 296-307.

Wojtanik, K. M. & Liscum, L. (2003). The transport of low density lipoprotein-derived cholesterol to the plasma membrane is defective in NPC1 cells. *J Biol Chem, 278*(17), 14850-14856.

Wullschleger, S., Loewith, R. & Hall, M. N. (2006). TOR signaling in growth and metabolism. *Cell, 124*(3), 471-484.

Yamanaka, N., Marques, G. & O'Connor, M. B. (2015). Vesicle-Mediated Steroid Hormone Secretion in Drosophila melanogaster. *Cell, 163*(4), 907-919.

Yamanaka, N., Rewitz, K. F. & O'Connor, M. B. (2013). Ecdysone control of developmental transitions: lessons from Drosophila research. *Annu Rev Entomol, 58*, 497-516.

Yamanaka, N., Romero, N. M., Martin, F. A., Rewitz, K. F., Sun, M., O'Connor, M. B.*, et al.* (2013). Neuroendocrine control of Drosophila larval light preference. *Science, 341*(6150), 1113-1116.

Yao, T. P., Forman, B. M., Jiang, Z. Y., Cherbas, L., Chen, J. D., Mckeown, M.*, et al.* (1993). Functional Ecdysone Receptor Is the Product of Ecr and Ultraspiracle Genes. *Nature, 366*(6454), 476-479.

Yao, T. P., Segraves, W. A., Oro, A. E., Mckeown, M. & Evans, R. M. (1992). Drosophila Ultraspiracle Modulates Ecdysone Receptor Function Via Heterodimer Formation. *Cell, 71*(1), 63-72.

Yoshii, S. R., Kuma, A., Akashi, T., Hara, T., Yamamoto, A., Kurikawa, Y.*, et al.* (2016). Systemic Analysis of Atg5-Null Mice Rescued from Neonatal Lethality by Transgenic ATG5 Expression in Neurons. *Dev Cell, 39*(1), 116-130.

Yoshiyama-Yanagawa, T., Enya, S., Shimada-Niwa, Y., Yaguchi, S., Haramoto, Y., Matsuya, T.*, et al.* (2011). The Conserved Rieske Oxygenase DAF-36/Neverland Is a Novel Cholesterol-metabolizing Enzyme. *J Biol Chem, 286*(29), 25756-25762.

Yoshiyama, T., Namiki, T., Mita, K., Kataoka, H. & Niwa, R. (2006). Neverland is an evolutionally conserved Rieske-domain protein that is essential for ecdysone synthesis and insect growth. *Development, 133*(13), 2565-2574.

Yu, L., McPhee, C. K., Zheng, L., Mardones, G. A., Rong, Y., Peng, J.*, et al.* (2010). Termination of autophagy and reformation of lysosomes regulated by mTOR. *Nature, 465*(7300), 942-946.

Zettervall, C. J., Anderl, I., Williams, M. J., Palmer, R., Kurucz, E., Ando, I.*, et al.* (2004). A directed screen for genes involved in Drosophila blood cell activation. *Proc Natl Acad Sci U S A, 101*(39), 14192-14197.

Zhang, C., Robinson, B. S., Xu, W., Yang, L., Yao, B., Zhao, H.*, et al.* (2015). The ecdysone receptor coactivator Taiman links Yorkie to transcriptional control of germline stem cell factors in somatic tissue. *Dev Cell, 34*(2), 168-180.

Zraly, C. B. & Dingwall, A. K. (2012). The chromatin remodeling and mRNA splicing functions of the Brahma (SWI/SNF) complex are mediated by the SNR1/SNF5 regulatory subunit. *Nucleic Acids Res, 40*(13), 5975-5987.

Zraly, C. B., Middleton, F. A. & Dingwall, A. K. (2006). Hormone-response genes are direct in vivo regulatory targets of Brahma (SWI/SNF) complex function. *J Biol Chem, 281*(46), 35305-35315.

Zuo, W., Moses, M. E., West, G. B., Hou, C. & Brown, J. H. (2012). A general model for effects of temperature on ectotherm ontogenetic growth and development. *Proc Biol Sci, 279*(1734), 1840-1846.

APPENDIX I. Verification of the existence of additional signals produced by the PG neurons.

MaryJane Shimell, **Xueyang Pan**, Francisco A. Martin, Arpan C. Ghosh, Pierre Leopold, Michael B. O'Connor and Nuria M. Romero. 2018. Prothoracicotropic hormone modulates environmental adaptive plasticity through the control of developmental timing. *Development*. 145, dev159699.

Prothoracicotropic hormone (PTTH) function as a crucial signal that stimulates the function of PG and thus the control of developmental transitions in insects including *Drosophila melanogaster* (review, see (Smith & Rybczynski, 2012)). In a recent work reported by Shimell et al. multiple *ptth* mutants were generated and studied to enhance the understand on the function of PTTH. The authors found that the *ptth* mutants exhibited a series of developmental defects including delayed development, increased body size, disrupted coordination between body and imaginal disc growth, increased critical weight under nutritional deprivation and compromised adaptation under nutritional insufficiency environment (Shimell et al., 2018). Besides the characterization of developmental defects, the authors also raised the possibility that some additional signal is produced by the PG neurons, which can explain the discrepancy on timing phenotype between PG neuron ablation model (McBrayer et al., 2007) and *ptth* mutants (Shimell et al., 2018).

In this study, I designed and carried out experiments to test the existence of additional signal in the PG neurons. I firstly expressed TRPA1 ion channel in the PG neurons and successfully activated the neurons by transferring the larvae into higher temperature (Venken, Simpson & Bellen, 2011). In wildtype larvae, temperature shift at early-L3 stage causes acceleration of development (Shimell et al., 2018, Figure 7C and 7E), which may be due to the precocious PG neuron activation and PTTH secretion. Using this model, I further found that PG neuron

activation in *ptth* mutants also caused advancement of development (Shimell et al., 2018, Figure 7D and 7F), showing that PTTH is not the only signal that PG neurons send to the PG. This finding leads to the follow up study which is shown in Chapter 3.

A reprint of the published article is included in Appendix I and the article can also be accessed by the link below.

https://dev.biologists.org/content/145/6/dev159699

© 2018. Published by The Company of Biologists Ltd | Development (2018) 145, dev159699. doi:10.1242/dev.159699

RESEARCH ARTICLE

Prothoracicotropic hormone modulates environmental adaptive plasticity through the control of developmental timing

MaryJane Shimell[1,*,‡], Xueyang Pan[1], Francisco A. Martin[2,3], Arpan C. Ghosh[1], Pierre Leopold[2], Michael B. O'Connor[1] and Nuria M. Romero[2,*,‡]

ABSTRACT

Adult size and fitness are controlled by a combination of genetics and environmental cues. In *Drosophila*, growth is confined to the larval phase and final body size is impacted by the duration of this phase, which is under neuroendocrine control. The neuropeptide prothoracicotropic hormone (PTTH) has been proposed to play a central role in controlling the length of the larval phase through regulation of ecdysone production, a steroid hormone that initiates larval molting and metamorphosis. Here, we test this by examining the consequences of null mutations in the *Ptth* gene for *Drosophila* development. Loss of *Ptth* causes several developmental defects, including a delay in developmental timing, increase in critical weight, loss of coordination between body and imaginal disc growth, and reduced adult survival in suboptimal environmental conditions such as nutritional deprivation or high population density. These defects are caused by a decrease in ecdysone production associated with altered transcription of ecdysone biosynthetic genes. Therefore, the PTTH signal contributes to coordination between environmental cues and the developmental program to ensure individual fitness and survival.

KEY WORDS: *Drosophila* development, Ecdysone, PTTH, Plasticity, Environmental cue

INTRODUCTION

During animal development, tissue growth and physiological integration of tissue function must be timed appropriately to maximize an organism's chances of survival and reproduction. In holometabolous insects, tissue growth is confined to the larval phases of development, which are punctuated by periodic shedding and resynthesis of cuticle (molts) to accommodate an increasing body size. In *Drosophila melanogaster*, embryonic development lasts ~24 h, as does each of the first and second larval instar stages. During the final, third larval instar, which lasts ~2-3 days, a great deal of growth occurs and body size becomes fixed in response to various neuroendocrine and hormonal signals that trigger metamorphosis, a process that transforms the larval body into that of the sexually mature adult fly (Mirth and Riddiford, 2007; Nijhout et al., 2014; Rewitz et al., 2013).

Both genetic and environmental factors influence larval growth rate and timing parameters (Danielsen et al., 2013; Di Cara and King-Jones, 2013; Rewitz et al., 2013). For instance, nutritional content of the food source and population density impact many life history traits resulting in numerous trade-offs that must be balanced for optimal survival (Barker and Podger, 1970; May et al., 2015; Miller and Thomas, 1958; Prout and Mcchesney, 1985). In its natural habitat, *D. melanogaster* utilizes rotting fruit, a short-lived food source, as its main dietary resource. As might be expected for such an ephemeral habitat, recent studies have shown that *Drosophila* larvae make nutritional choices that minimize developmental time. This choice impacts other life history traits such as body size, ovariole number (fecundity), viability and life span (Chippindale et al., 1993; Horvath and Kalinka, 2016; Kolss et al., 2009; Mendes and Mirth, 2016; Rodrigues et al., 2015). Despite the importance of balancing various life history traits for robust survival, the genetic mechanisms that adjust insect developmental time in response to various environmental factors are not well understood (Mirth and Shingleton, 2012; Tennessen and Thummel, 2011).

Both molting and metamorphosis require pulsed production and release of the steroid hormone ecdysone (E) from the larval prothoracic gland (PG), and classic ligature and transplantation experiments in Lepidoptera demonstrated that at least one brain-derived factor regulates E production in the PG (Kopec, 1922; Williams, 1952). Subsequent purification of the E-inducing substance from *Bombyx* heads identified prothoracicotropic hormone (PTTH) as a key ecdysteroidogenic inducer (Kawakami et al., 1990). PTTH is a secreted homodimer derived by processing of a precursor pro-protein and is a member of the cystine knot family of growth factors (Noguti et al., 1995). Genetic and biophysical studies have shown that it signals through the receptor tyrosine kinase Torso, which then activates a Ras/Raf/Erk MAP kinase signal transduction cascade (Jenni et al., 2015; Konogami et al., 2016; Rewitz et al., 2009). The targets of this signaling pathway are not fully identified, but are likely to include several of the E biosynthetic enzymes produced in the PG (Gibbens et al., 2011; Niwa et al., 2005).

In *Drosophila*, PTTH is produced by two bilateral neuroendocrine cells located in each brain hemisphere (termed PG neurons, in accordance with their innervation pattern) that project their axons contralaterally to terminate on the PG (McBrayer et al., 2007). These observations suggest that PTTH acts like a neurotransmitter for stimulating ecdysteroidogenesis rather than as a systemic hormone. However, *Drosophila* PTTH has a second role as a modulator of larval light sensitivity. This process involves the release of PTTH into circulation and its systemic delivery to larval light-sensing organs where it enhances larval light avoidance (Yamanaka et al., 2013b).

Genetic ablation or misspecification of the PG neurons revealed that these cells control developmental timing and body size (Ghosh et al., 2010; McBrayer et al., 2007). Loss of the PG neurons resulted

[1]Department of Genetics Cell Biology and Development, University of Minnesota, Minneapolis, MN 55455, USA. [2]University Côte d'Azur, CNRS, Inserm, Institute of Biology Valrose, Parc Valrose, 06108 Nice, France. [3]Cajal Institute, Av Doctor Arce 37, 28002 Madrid, Spain.
*These authors contributed equally to this work

[‡]Authors for correspondence (oconn033@umn.edu; nromero@unice.fr)

M.J.S., 0000-0003-1378-6017; N.M.R., 0000-0001-6235-1330

Received 20 September 2017; Accepted 12 February 2018

Development (2018) 145, dev159699. doi:10.1242/dev.159699

in substantially delayed pupariation (by 4-6 additional days) and the production of large flies. Delayed pupariation resulted from a belated surge in the 20-hydroxyecdysone (20E) titer during the wandering stage, and both the large body size and developmental delay could be rescued by feeding 20E to third instar larvae. Although these observations suggested that PTTH is likely to be important for proper timing of the normal metamorphic transition, its exact role could not be determined since ablation/misspecification of the PG neurons would eliminate other potential factors, in addition to PTTH, that might influence endocrine activity and the timing of developmental transitions.

To unambiguously determine the role of PTTH in modulating developmental timing in response to various environmental conditions, we produced *Ptth* null mutants using both TALEN and gene replacement technologies. We show that these mutants produce a variable developmental delay that is influenced by both nutrient availability and population density. Careful analysis reveals that mutant animals accumulate mass at wild-type rates and eventually produce larger adults due to a longer growth phase. We find that PTTH function is required throughout the third instar larval stage since the developmental delay extends both the time to reach critical weight – a crucial nutrition-dependent developmental checkpoint (reviewed by Mirth and Riddiford, 2007) – as well as the nutrition-independent terminal growth period (Shingleton et al., 2007). Our experiments also indicate that these phenotypes result from an alteration in the kinetics of E biosynthesis. Furthermore, we demonstrate that PTTH provides animals with better adaptability to challenging environmental conditions (crowding, nutritional limitation). Lastly, manipulation of PG neuron activity demonstrates that PTTH acts in conjunction with another, as yet unknown, factor(s) to properly time larval development. Taken together, our results indicate that PTTH is a central component of a mechanism that coordinates trade-offs in several life history traits in response to environmental inputs such as nutrition and population density.

RESULTS

PTTH controls the onset of metamorphosis, final body size and reproductive capacity

To genetically assess *Ptth* function, we generated three mutants: $Ptth^{Delta}$, $Ptth^{120F2A}$ and $Ptth^{8K1J}$ (Materials and Methods, Fig. 1A). The deletion mutant $Ptth^{Delta}$ removes the start codon and is a protein null, as shown by complete absence of immunostaining signal (Fig. S1A). By contrast, $Ptth^{120F2A}$ and $Ptth^{8K1J}$ are short deletions in the final exon (7 bp and 6 bp, respectively) and yield either a truncated protein or a mature protein that is shortened by two amino acids. The control strain for all $Ptth^{Delta}$ studies was w^{DAH}, while the control for $Ptth^{120F2A}$ and $Ptth^{8K1J}$ was w^{1118} (see Materials and Methods). We determined the ability of the three mutants to undergo metamorphosis by precisely timing the developmental profiles from L1 ecdysis to pupariation. As shown in Fig. 1B, larvae lacking PTTH undergo metamorphosis with a 1 day delay compared with their respective controls. $Ptth^{8K1J}$ exhibits the same 1 day delay as the other *Ptth* mutants, suggesting that all three alleles yield a PTTH product that is non-functional. Additionally, we consider the $Ptth^{120F2A}$ allele to be a genetic null since an identical 1 day delay is observed in transheterozygous ($Ptth^{120F2A}/Ptth^{Delta}$) animals (Fig. S1B). Since *Ptth* mutants show almost no effect on size and timing before third instar (data not shown), this 1 day delay occurs in the third instar larval stage. The developmental delay observed in *Ptth* mutants can be rescued by adding a genomic transgene containing wild-type *Ptth* into the $Ptth^{120F2A}$ background or by using *tub-Gal4* to ubiquitously express a *UAS-Ptth* transgene in the $Ptth^{Delta}$ background (Fig. 1C). These results imply a role for PTTH in precisely timing the transition from juvenile to adult.

Male and female *Ptth* mutant pupae are larger than their respective controls (Fig. 1D,D′), and *Ptth* mutant adults show significant weight increase (Fig. 1E) indicating that the extended larval growth period of these animals increases final adult size. Consistent with these results, *Ptth* mutant larvae gained weight at the same rate as control larvae (Fig. S2A). Accordingly, the size of brains, fat body nuclei and salivary gland nuclei at 24 h after the L2-to-L3 transition was comparable in $Ptth^{Delta}$ mutant and control animals (Fig. S2B-D). Overall, this indicates that PTTH determines final adult body size by controlling the duration of the larval growth period without affecting the bulk rate of mass accumulation in the third instar larva.

Since female body size correlates with ovary size in *Drosophila* (David, 1970; Bergland et al., 2008), we counted ovariole number in $Ptth^{Delta}$ and control females and observed a significant increase in ovariole number (by 8.5%) in the mutant compared with the control (Fig. 1F). This indicates that, by timing the end of the larval period and the onset of metamorphosis, PTTH also influences adult physiology, such as egg production and fecundity.

Ptth mutants exhibit a disrupted imaginal organ growth program

Given the role of E in controlling growth and differentiation of imaginal tissues (Gokhale et al., 2016; Hackney et al., 2012; Herboso et al., 2015; Jaszczak et al., 2016), we examined whether loss of *Ptth* could affect the rate of imaginal disc growth. We measured wing imaginal disc size at 15, 24 and 46 h after L3 ecdysis. As previously found in mutants with reduced E levels (Parker and Shingleton, 2011), $Ptth^{Delta}$ mutant discs grew significantly more slowly than controls (Fig. 2A). We did not observe any difference in cell size between the two genotypes, indicating that lack of PTTH leads to smaller discs with fewer cells (Fig. 2B). However, owing to an extended larval growth period, $Ptth^{Delta}$ wing discs are 14% larger at the onset of metamorphosis and give rise to larger adult wings (Fig. 2C,D). Thus, PTTH has a dual function in regulating both imaginal tissue growth rate and larval growth duration.

PTTH function is required throughout the third instar stage

Drosophila larvae pass through two developmental checkpoints during the final instar: the critical (CW) and the minimal viable weight (MVW) thresholds (Mirth and Riddiford, 2007). In third instar larvae, CW and MVW are reached concomitantly ~8 h (on rich food) after L2/L3 ecdysis at 0.84 mg/larva (Fig. 3A). It is noteworthy that our determination of CW for wild-type w^{1118} is nearly the same as that reported previously (McBrayer et al., 2007; Mirth et al., 2005) and virtually identical to that determined by Koyama et al. (2014) using the breakpoint method (Stieper et al., 2008). The CW for $Ptth^{120F2A}$ larvae increased to 1.9 mg/larva and occurred ~20 h after the L2/L3 transition (Fig. 3B). Interestingly, in these mutants, the MVW occurred slightly earlier than the CW and at a lighter weight (1.55-1.69 mg/larva; Fig. 3B). We also determined the length of the terminal growth period (TGP), defined as the time interval that transpires after attainment of CW to when 50% pupariation is achieved (Shingleton et al., 2007). This period was prolonged from 35 h for w^{1118} to 47 h for $Ptth^{120F2A}$ (Fig. 3C). Taken together, these results suggest that 12 h of the 24 h developmental delay in *Ptth* mutants occurs prior to achievement of CW and that the remainder occurs during the TGP.

Development (2018) 145, dev159699. doi:10.1242/dev.159699

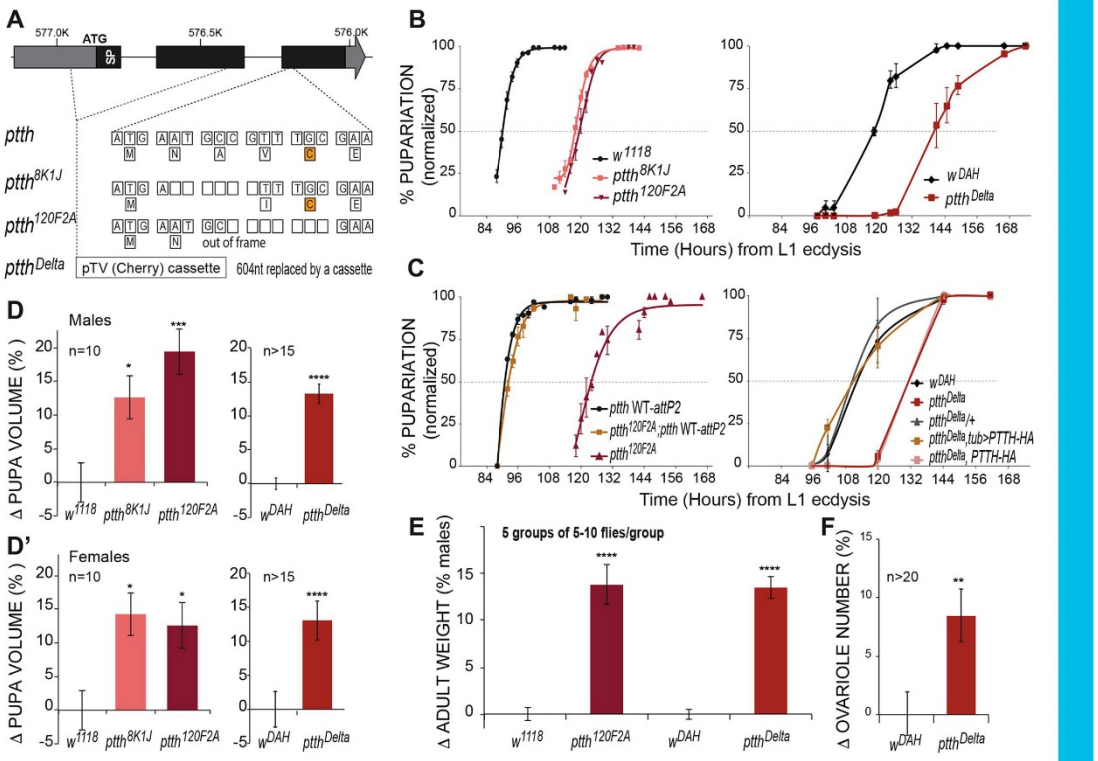

Fig. 1. PTTH controls the onset of metamorphosis, final body size and ovariole number. (A) The *Drosophila Ptth* gene showing nucleotide deletions and amino acid changes of $Ptth^{120F2A}$ and $Ptth^{8K1J}$, as well as the deleted region of $Ptth^{Delta}$. Orange-shaded Cs form part of the cystine knot. SP, signal peptide. (B) Developmental timing curves of w^{1118}, $Ptth^{8K1J}$, $Ptth^{120F2A}$, w^{DAH} and $Ptth^{Dolta}$ illustrate a 1 day pupariation delay in all mutant lines. (C) Developmental timing curves demonstrate complete rescue of the timing delay by the *Ptth* WT-*attP2* transgene or by *tub>PTTH-HA* ubiquitous expression as compared with controls. (D,D′) Pupal volumes of male (D) and female (D′) *Ptth* mutants are significantly larger than those of wild-type controls. (E) Adult male *Ptth* mutants are significantly heavier than wild-type controls. (F) The *Ptth* mutant possesses significantly more (8.5%) ovarioles than its wild-type counterpart. Dashed horizontal lines (B,C) denote 50% pupariation. (D-F) *$P \leq 0.05$, **$P \leq 0.01$, ***$P \leq 0.001$, ****$P \leq 0.0001$, unpaired *t*-test. Error bars indicate s.e.m.

Next, we examined the transcriptional timing of three E-responsive genes. Expression of the mid-L3 20E target gene *Sgs3* (Fig. S3A) (Warren et al., 2006) was first detected at 21 h in wild-type larvae and rose rapidly over the next 15 h. In $Ptth^{120F2A}$, *Sgs3* expression was first detected at 24 h (4 h after CW) at a very low level, increased gradually for 1 day (the mid-L3 stage), and then rose abruptly at 48 h. In both cases, white prepupae first appeared 6-8 h after peak *Sgs3* expression (36 h for w^{1118} and 59 h for $Ptth^{120F2A}$). We also examined the expression of *Atet* and *E23*, two putative E transporters that are late L3 20E targets (Hock et al., 2000; Yamanaka et al., 2015) and observed similar delays in their induction (Fig. S3B,C). Taken together, these results indicate that PTTH is likely to control E levels throughout the entire L3 stage.

Ptth mutants exhibit altered kinetics of E production

Since PTTH was originally described as a factor stimulating E production in the PG (Kataoka et al., 1991; Kawakami et al., 1990), we expected that the developmental delay observed in *Ptth* mutants would be the result of altered kinetics in E production. Consistent with this view, feeding 20E to *Ptth* mutant larvae rescued the developmental delay (Fig. S1C). To more directly address the timing of E production, we determined ecdysteroid titers in staged w^{1118} and $Ptth^{120F2A}$ L3 larvae (Fig. 3D). In control larvae, ecdysteroid titers rise to a first plateau of 6-8 pg at the time of CW (8-10 h after the L2-to-L3 transition), followed by a second jump at 18-20 h and then a steady rise to a peak at wandering stage. By contrast, $Ptth^{120F2A}$ mutants have lower basal ecdysteroid titers that reach a titer of ~6 pg/animal at 20 h after L2/L3 ecdysis, which correlates with the attainment of CW in these mutant larvae. The titer then rises at a slow rate, but eventually reaches a level similar to that of the control by the time of wandering (Fig. 3D). These results demonstrate that PTTH regulates the ecdysteroid production rate during the third instar larval stage to properly time metamorphosis.

We next analyzed the transcriptional timeline of seven E biosynthetic enzymes during the third instar stage of w^{1118} and $Ptth^{120F2A}$ (Fig. S4). The profiles of *nvd* and *spok* were similar, exhibiting a delayed rise in the mutant background, achieving only 50-65% of the w^{1118} peak level just prior to wandering (Fig. S4A,B). *shd* and *phm* displayed a similar slow rise in expression in the *Ptth* mutant background but reached approximately the same peak levels

Development (2018) 145, dev159699. doi:10.1242/dev.159699

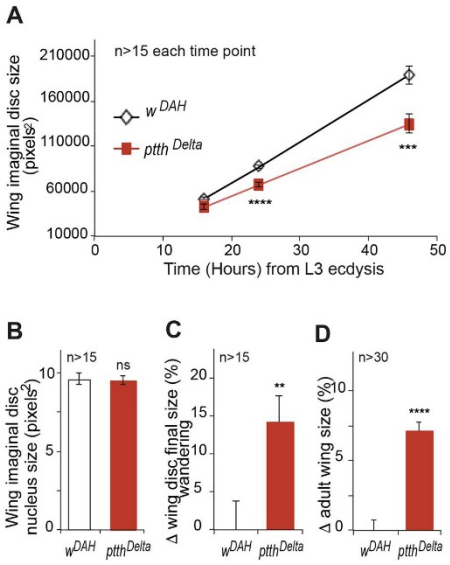

Fig. 2. *Ptth* null mutants exhibit slower imaginal disc growth rate but attain larger disc size. (A) The rate of wing imaginal disc growth of $Ptth^{Delta}$ (red) and w^{DAH} (black) during the third larval instar. (B) At 24 h after the L2/3 transition, there is no difference between wild-type (white) and *Ptth* mutant (red) wing disc nuclear size, suggesting a proliferative difference between wild type and the *Ptth* mutant. (C,D) By the wandering stage, wing imaginal discs of $Ptth^{Delta}$ (red) are larger than those of w^{DAH}, as is the final adult wing size. (A-D) ns, $P>0.05$; **$P\leq0.01$, ***$P\leq0.001$, ****$P\leq0.0001$, unpaired *t*-test. Error bars indicate s.e.m.

as the control (Fig. S4E,F). By contrast, although expression of *dib* also showed a slow rise, it was induced to less than 50% of wild-type levels (Fig. S4C).

sro and *Cyp6t3* revealed noticeably different transcription profiles compared with the control. In the *Ptth* mutant, *sro* expression peaked in mid-L3 at approximately twice the wild-type level and remained high during the entire extended developmental period before declining in early pupae (Fig. S4G). The expression profile of *Cyp6t3* was drastically reduced on normal food, but remained near normal levels on richer media (Fig. S4D; data not shown). Thus, expression of the E biosynthetic genes is not coordinately regulated in the *Ptth* mutant since transcripts are either upregulated, unchanged, downregulated or dependent on nutrition relative to wild type.

It has previously been suggested that the 'black box' step involving the enzymes Spo/Spok, Sro and Cyp6t3 might be rate-limiting during E biosynthesis (Lafont et al., 2005; Ou et al., 2011; Rewitz et al., 2009). To examine if alterations in the expression profiles of a single enzyme were responsible for the developmental delay, we individually overexpressed some of these genes (*spok*, *Cyp6t3*), as well as *dib* and *nvd* using a PG-specific driver (*p0206-Gal4*) in a *Ptth* mutant background, but observed no rescue of developmental delay induced by *Ptth* loss (Fig. S4H-K). Assuming that all of the UAS constructs provide high-level overexpression, these data suggest that no individual enzyme is rate-limiting as a result of *Ptth* loss. Rather, it is likely that the partial reduction in several enzymes, an as yet unidentified component, or another regulated step is responsible for the slower kinetics of E production and the developmental delay.

PTTH acts autonomously as a trophic factor for PG growth

We have previously suggested that PTTH-expressing neurons provide a growth signal to the PG, since hypomorphic mutations in the *giant* gene induce stochastic unilateral innervation of the PG resulting in an asymmetrically sized PG in which the innervated side is significantly larger than the non-innervated portion of the gland (Ghosh et al., 2010). To determine whether PTTH is the trophic signal, we examined PG nuclear size of innervated and non-innervated PG lobes derived from $Ptth^{120FA2}$, $giant^{E1}$ double-mutant larvae. Whereas the nuclei of innervated lobes were ~33% larger in $giant^{E1}$ PGs, the innervated lobes of $Ptth^{120FA2}$, $giant^{E1}$ double mutants displayed no difference in the size of nuclei compared with non-innervated lobes. Moreover, both innervated and non-innervated lobes of $Ptth^{120F2A}$, $giant^{E1}$ double mutants showed approximately the same nuclear size as the non-innervated PG lobe from $giant^{E1}$ mutants (Fig. 4A,A′). This indicates that loss of *Ptth* leads to the reduced size of the non-innervated PG lobe and demonstrates that PTTH is the trophic signal to the PG.

Next, we inspected glands from larvae in which *Ptth* expression is lost in only one hemisphere of the brain using a Gal4 driver with variegated expression in PG neurons (*NP0394-Gal4*) in combination with *UAS-Ptth-RNAi*. As shown in Fig. 4B, *Ptth* knockdown causes a reduction in lobe as well as nuclear size compared with the contralateral side that has activated PTTH signaling. This confirms that PTTH acts as a PG growth factor. Moreover, PTTH secretion onto one PG lobe cannot compensate for its loss in the other lobe, suggesting that PTTH acts in a local manner.

In most cases, we observed that each PG cell is in contact with at least one varicosity (Fig. S5A). Surprisingly, these varicosity structures co-express PTTH (Fig. 4C′) with synaptic markers such as NC82 (Bruchpilot) (Fig. 4C″, Fig. S5B), Csp (Fig. S5C) and Syb-GFP (Fig. 4C). When populations of PG cells with and without PTTH input are intercalated in the same lobe, the PG cells with PTTH input are larger and express a higher level of Dib than immediate adjacent cells that do not receive PTTH (Fig. 4D,D′). We next generated PG cell clones expressing RNAi targeting the PTTH receptor Torso and observed that PG cells depleted of Torso also contain smaller nuclei (Fig. 4E). These results reveal that synaptically released PTTH acts autonomously through its receptor Torso to control PG cell size.

PTTH is necessary for adaptive response to the environment

A common adaptive strategy that insects use in response to an adverse environment is to adjust the time of larval development at the expense of adult size (Rodrigues et al., 2015). To examine whether PTTH plays a role in adapting individual life history traits to changes in environmental conditions, we evaluated the ability of $Ptth^{Delta}$ larvae to undergo metamorphosis under three diets with different nutrient content depending on their levels of inactivated yeast extract: from 5% (poor) to 17% (normal) and 34% (rich) (see Materials and Methods). When grown on poor food, $Ptth^{Delta}$ larvae were delayed 1 additional day compared with controls (Fig. 5A), with a slight increase in mortality (from 6% to 15%, Fig. 5B). Therefore, concomitant reduction of nutrient signaling and PTTH pathways caused additive effects that could compromise the survival of the organism. We also investigated whether an artificial increase in PTTH levels generated using ubiquitous *tub-Gal4* to drive expression of *UAS-Ptth-HA* could rescue the additional delay caused by growing larvae in low nutrients. As shown in Fig. 5C, PTTH was unable to

Development (2018) 145, dev159699. doi:10.1242/dev.159699

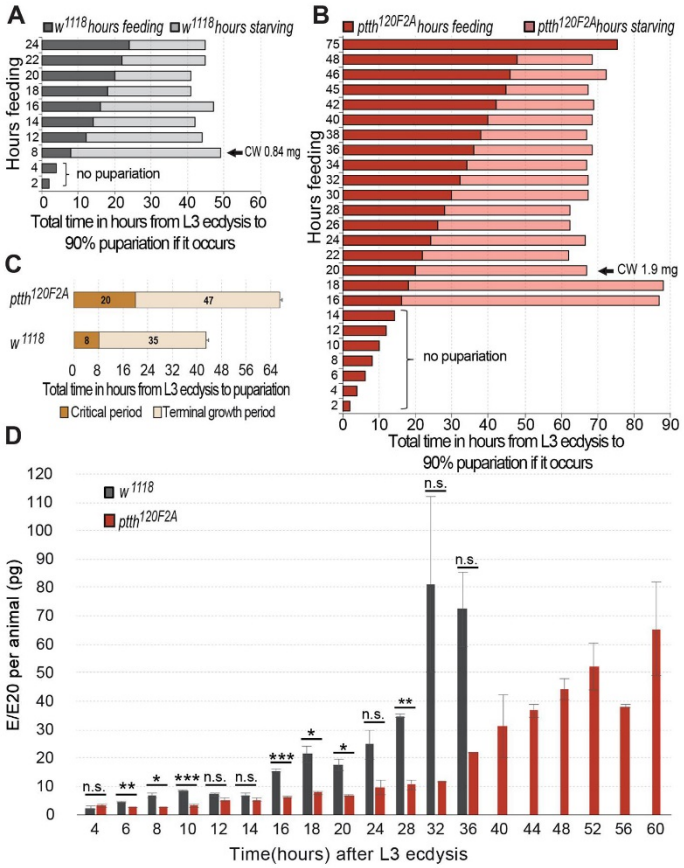

Fig. 3. PTTH sets the critical weight checkpoint and regulates the kinetics of ecdysone production. (A,B) The CW checkpoint of *Ptth*^{120F2A} is about twice that of *w*^{1118} and occurs 12 h later in the third instar stage. The darker bars denote the time spent feeding (value displayed on *y*-axis), while the lighter bars show the time between switching to starvation conditions and achieving 90% pupariation (n=10 feeding larvae per time point). (C) Graphical representation of the critical period and the terminal growth period (average post-CW values ±s.e.m.) along the developmental timeline of *Ptth* mutant and wild type in this trial. (D) Temporal quantitation of E/20E titers of whole third instar larvae. Biological replicates: n=8 for *w*^{1118}, n=2 for *Ptth*^{120F2A}. Shown are average values ±s.e.m. n.s., P>0.05; *P≤0.05, **P≤0.01, ***P≤0.001, unpaired *t*-test.

rescue the developmental delay caused by low nutritional input. Moreover, *Ptth*^{Delta} larvae grown on rich food were still delayed by at least 20 h (Fig. 5A). Thus, PTTH cannot compensate for a low nutritional input and vice versa. These results suggest that several ecdysteroidogenic signals, including PTTH, serotonin (Shimada-Niwa and Niwa, 2014) and nutrient response IIS/Target of Rapamycin (TOR) signaling (Caldwell et al., 2005; Lavalle et al., 2008; Mirth et al., 2005; Walkiewicz and Stern, 2009) are timing metamorphosis in a non-redundant manner and may have additive effects in controlling the adaptive response to the environment.

Next, we tested animal survival in response to a different environmental stress, larval crowding, which is frequently observed in natural populations of *Drosophila* (Bubli et al., 1998). Larval crowding is a multifactorial stressor that, in addition to nutrient restriction, results in inevitable exposure to high concentrations of larval products such as nitrogenous metabolic waste (Joshi et al., 1996a,b; Schering et al., 1984) and pheromones (Mast et al., 2014). Interestingly, a recent report found a strong negative correlation between development time and fitness at high density (Horvath and Kalinka, 2016), meaning that fast developers have higher fitness. To determine if PTTH plays an adaptive role in this condition, L1 larvae were collected and grown at increasing densities in tubes (L1/t) of normal food. As shown in Fig. 6A, *Ptth*^{Delta} mutant and *w*^{DAH} control animals equally survive until adulthood when grown at standard densities (40 L1/t and 150 L1/t). However, survival of *Ptth*^{Delta} animals was drastically reduced at high density (43% at 350 L1/t and 16% at 500 L1/t), compared with control animals (72% at 350 L1/t and 50% at 500 L1/t), with most animals dying at late larval stages (data not shown). This indicates that PTTH is required for optimal survival under crowded as well as nutrient restricted conditions, possibly by fine tuning the duration of larval development. Moreover, the *Ptth*^{Delta} mutant ecloses with a 3-4 day delay in the 500 L1/t condition (Fig. 6B). Therefore, without PTTH, animals cannot properly adapt larval development time and survival to an environmental stress, such as crowding or nutrient restriction.

Because we observed a drastic effect on larval survival in crowded conditions, we tested the effects of this stressor on adult size and ovariole number in *Ptth* mutants and controls. Whereas *w*^{DAH} flies showed strong size adaptation to crowding (73% size reduction in 500 L1/t conditions, see Fig. 6C), *Ptth*^{Delta} mutants were less plastic (52% reduction). This, and the additional delay observed in crowded conditions, mean that *Ptth*^{Delta} adult flies weighed more than 200% of controls at 500 L1/t density, whereas at 40 L1/t the weight difference between *Ptth* mutants and controls was

Development (2018) 145, dev159699. doi:10.1242/dev.159699

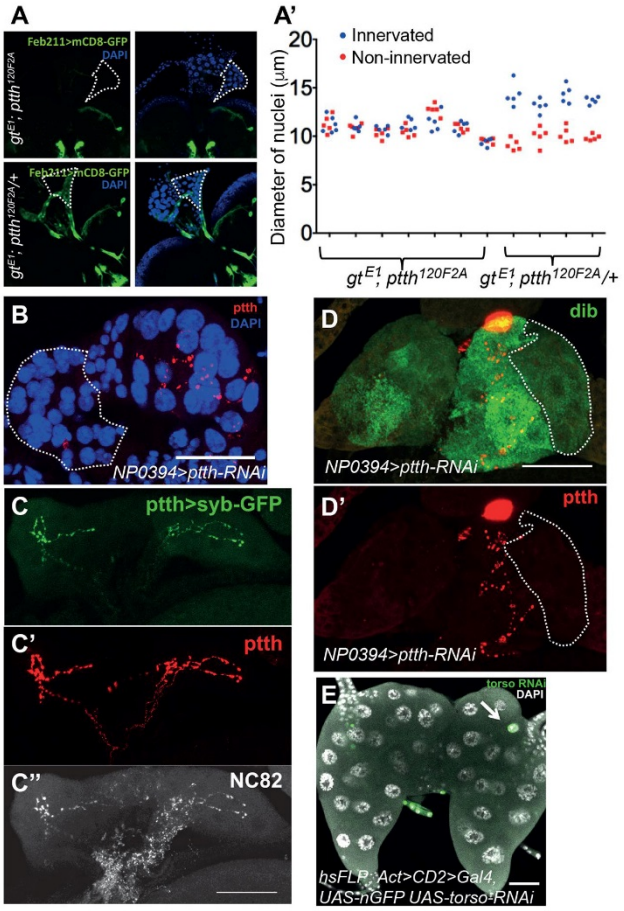

Fig. 4. PTTH acts autonomously as a trophic factor for PG growth. (A,A′) Immunohistochemistry using GFP to mark PG neurons (green) and DAPI staining (blue) to measure PG nuclear size in *Ptth*^{120F2A} (A, top row; A′, left) and wild-type (A, bottom row; A′, right) background illustrates that innervation of one PG lobe (indicated by green staining in the contralateral PG neuron) in the absence of PTTH cannot restore nuclear size to the wild-type level. Dotted line delineates non-innervated brain lobe. (B) Immunohistochemistry with anti-PTTH (red) shows that knockdown of *Ptth* locally in one lobe of the PG (outlined by dotted line; contralateral PG neuron cell bodies not shown) leads to smaller nuclei (blue). (C-C″) Immunohistochemistry showing co-expression of synaptic markers with PTTH in the PG (D,D′) Immunohistochemistry highlights that only PG cells that receive the PTTH signal (red, D′) express high levels of Dib (green, D), whereas neighboring non-innervated cells (outlined with dotted line) do not. (E) Immunohistochemistry shows that knockdown of *torso* in a single PG cell (arrow) marked with anti-GFP (green) leads to smaller nuclei. Scale bars: 50 µm (A-E).

only 20% (Fig. 6C). A similar reduced plasticity in ovariole number was found in *Ptth*^{Delta} females exposed to high population density (Fig. 6D). Overall, these results indicate that PTTH participates in a general mechanism of adaptation to environmental stress, allowing animals to adjust adult size and fecundity to maximize survival.

An additional ecdysteroidogenic signal is produced by PG neurons

The developmental delay that we observe with *Ptth* loss (1 day on rich food) is significantly less than that observed when PG neurons are ablated or misspecified (5-6 days on rich food; see also *Ptth>grim* in Fig. 7B) (Ghosh et al., 2010; McBrayer et al., 2007). In addition, the CW of the *Ptth* mutant (1.9 mg at 20 h after L3 ecdysis, Fig. 3B) is less than that of the PG neuron-ablated animals (2.6 mg at 72 h after L3 ecdysis, Fig. 7G). A simple explanation for these differences would be the existence of an additional ecdysteroidogenic signal(s) produced by the PG neurons. To assess this possibility, we manipulated neuronal activity of PTTH-producing neurons in control or *Ptth*^{120F2A} animals and measured the effect on developmental transitions. When control PG neurons were inactivated by selectively expressing either Kir2.1 (Hodge, 2009) or tetanus toxin (TetxLC) (Popoff and Poulain, 2010), we observed a 17-24 h developmental delay (Fig. 7A), similar to the delay produced by *Ptth* loss. However, inactivation of PG neurons in *Ptth*^{120F2A} larvae induced an additional delay of ~24 h (Fig. 7B).

In order to activate PG cells, we used the targeted expression of TrpA1 (Hamada et al., 2008) and activated the channel by a temperature shift at various times after the L2/3 transition. As shown in Fig. 7C,E, shifting before or near the time of CW results in the maximal developmental acceleration of ~17 h. Shifting after CW is still able to accelerate development, but in a graded manner. This is consistent with our data above describing a continuous requirement for PTTH signaling throughout the third instar period. Remarkably, we also see a developmental acceleration of 17 h when TrpA1 is activated in the PG neurons of *Ptth*^{120F2A} (Fig. 7D,F). This acceleration is able to rescue most of the delay caused by *Ptth* loss (Fig. 7F). These data indicate that at least one other factor may be released from the PG neurons to activate pupariation in the absence of PTTH. The existence of this additional signal could explain the

Development (2018) 145, dev159699. doi:10.1242/dev.159699

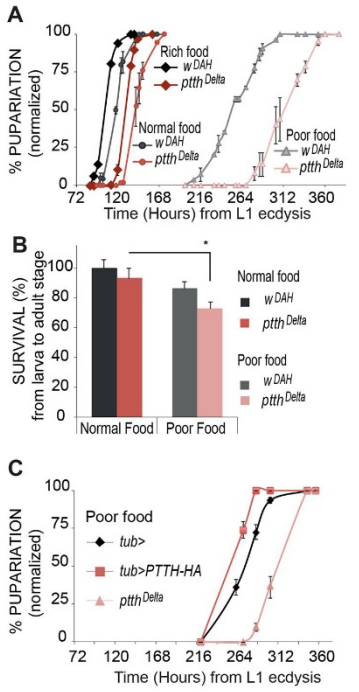

Fig. 5. Effects of nutrition on life history traits. (A,B) Comparison of developmental timing curves of w^{DAH} and $Ptth^{Delta}$ grown on rich, normal or poor food (A) illustrates that whereas $Ptth^{Delta}$ mutants are delayed 1 day when grown in rich or normal food, they are delayed an additional day under poor nutritional conditions and (B) have a slightly elevated rate of mortality. *$P \leq 0.05$, unpaired *t*-test. (C) Developmental timing curves in poor food demonstrate that even if levels of PTTH are elevated by ubiquitous expression using *tub-Gal4* in a wild-type background, timing remains delayed (compare with wild-type expression) from the low nutritional input. Loss-of-function in $Ptth^{Delta}$ on poor food displays the additional 2 day delay. Error bars indicate s.e.m.

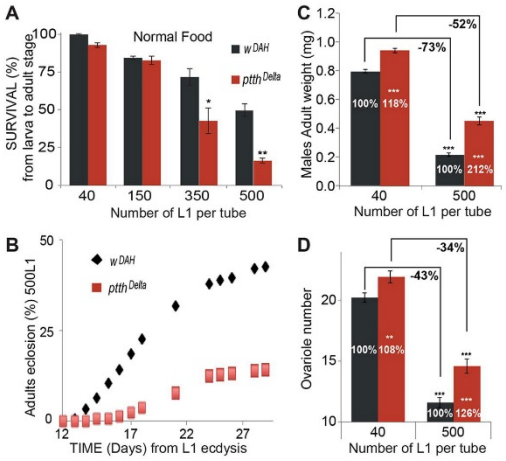

Fig. 6. PTTH plays an adaptive role under larval crowding conditions. (A) Survival graph of w^{DAH} and $Ptth^{Delta}$ highlights decreasing adulthood survival of the mutant as larval density increases. (B) Adult eclosion rate of w^{DAH} and $Ptth^{Delta}$ illustrates decreased survival in crowded larval conditions as well as an additional delay in eclosion timing in the *Ptth* mutant. (C,D) Comparison of w^{DAH} and $Ptth^{Delta}$ in uncrowded (40 L1/t) and crowded (500 L1/t) conditions shows (C) a less severe reduction in mass (values by brackets) and a net increase in weight (values within bars) in $Ptth^{Delta}$; in addition, crowded conditions lead to (D) a less severe reduction in ovariole number (values by brackets) and a net increase in ovariole number (values within bars) in the $Ptth^{Delta}$ mutant. (A,C,D) *$P \leq 0.05$, **$P \leq 0.01$, ***$P \leq 0.001$, unpaired *t*-test. Error bars indicate s.e.m.

different delays and CWs observed in response to PTTH loss compared with PG neuron ablation.

DISCUSSION

PTTH signaling is a nexus for coordinating environmental input with adaptive plasticity

A central problem that all organisms face is to adjust their development to variation in environmental conditions. This adaptive phenotypic plasticity impacts life history traits, enabling a single genotype to produce an optimized output in the face of fluctuating conditions in its natural habitat. In both vertebrates and invertebrates, neuroendocrine signaling is thought to be a central component of the mechanism that responds to environmental cues to allow phenotypic plasticity (Denver, 1997; Gotthard and Nylin, 1995; Lessells, 2008), but the molecular circuitry remains ill-defined. In this report, we demonstrate that the insect neuropeptide PTTH is a key brain-derived signal that modulates hormone production to alter developmental timing in response to both nutritional cues and population density. In its absence, larvae spend additional time feeding and growing larger, which, in the face of a time-limited food supply such as rotting fruit, is likely to be detrimental to the long-term survival of these individuals. Indeed, recent studies suggest that, given a choice, *Drosophila* larvae regulate their macronutrient uptake (protein versus carbohydrate) to ratios that result in the shortest developmental time (Rodrigues et al., 2015). Short developmental time results in trade-offs with other life history traits such as body size and ovariole number that are maximized by longer developmental intervals and larger bodies (Rodrigues et al., 2015), as we observed for *Ptth* mutants.

Although we do not yet know all the various inputs that PG neurons integrate, their extensive dendritic arbors (Ghosh et al., 2010; McBrayer et al., 2007) suggest that they are capable of processing a multitude of extrinsic and intrinsic signals. For example, Ilp8 (Dilp8), an imaginal disc damage-induced signal, is received by a set of LGR3-positive neurons that in turn contact PTTH dendrites to reduce PTTH production or release to prolong larval development and thereby facilitate damage repair (Colombani et al., 2015; Garelli et al., 2015; Jaszczak et al., 2016; Vallejo et al., 2015). Likewise, in larval and maturing pupal brains, a subset of central circadian clock neuron terminals are in close proximity to the PG neuron dendritic field, and recent studies have shown that PTTH helps coordinate the activity of the central brain clock with the peripheral clock found in the PG (Selcho et al., 2017). This circuit ensures circadian rhythmicity during pupal development, which both influences the timing of pupal development and the observed rhythmicity of adult eclosion that may aid in reproductive success (Kouser et al., 2013). PTTH signaling has also been shown to enhance larval light avoidance at

Development (2018) 145, dev159699. doi:10.1242/dev.159699

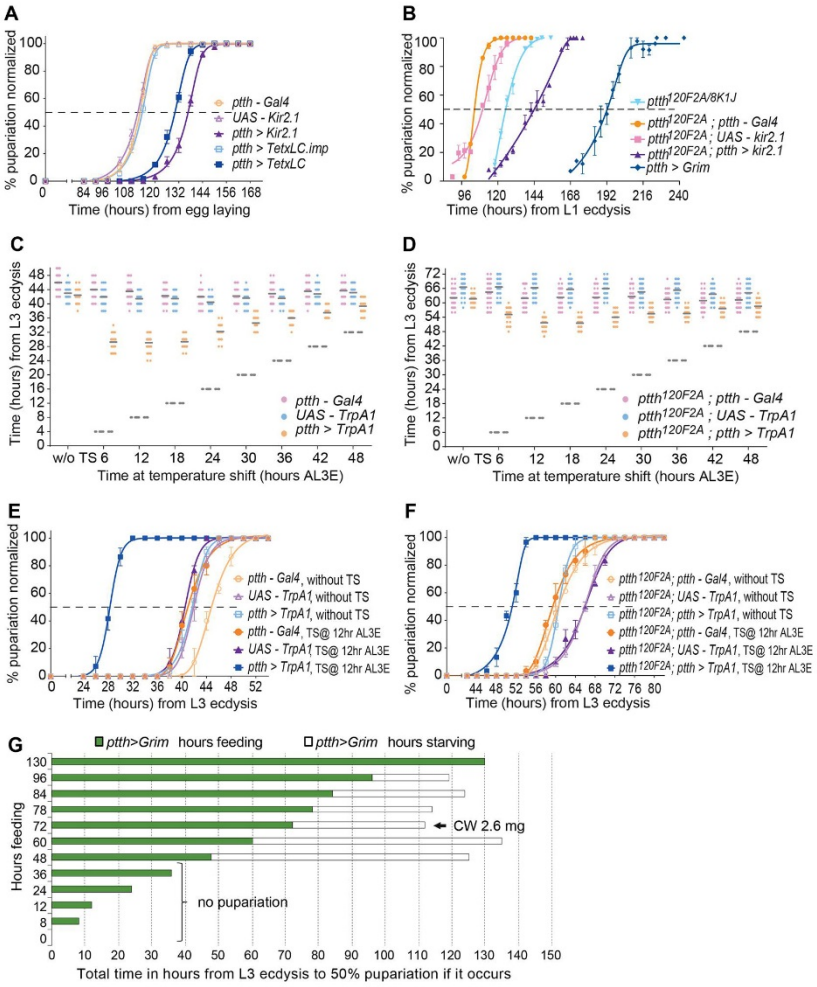

Fig. 7. Electrical manipulation in PG neurons suggests additional ecdysteroidogenic inputs. (A) Inactivation of electrical activity in PG neurons by TetxLC or Kir2.1 results in a timing delay (purple and dark blue) that relies on active toxin (light blue; imp is inactive). Yellow and lilac curves are transgene controls. (B) Inactivation of electrical activity in the PG neurons further delays timing in the *Ptth* mutant background (compare light blue and purple). However, the additive delay is not as great as that associated with PG neuron ablation (dark blue). Yellow and pink curves are transgene controls. (C,D) Temperature shifts at 6 h intervals (dashed lines) and plot of pupariation after L3 ecdysis (AL3E). TrpA1 activation (yellow) is best at 12 h (timing curves shown in E and F). Transgene controls are in pink and light blue. (E,F) Developmental timing curves illustrate acceleration in the 50% pupation time when the TrpA1 calcium channel is activated by temperature shift (TS) in PG neurons (dark blue) in both wild-type and *Ptth* mutant backgrounds. The control without TS is light blue. Yellow, lilac, orange and purple curves are transgene controls. (A,B,E,F) Error bars indicate s.e.m. (G) The CW checkpoint of *Ptth>grim* is about 1.3-fold and 2-fold those of $Ptth^{120F2A}$ and w^{1118} and occurs 52 and 64 h later, respectively. The green bars denote the time spent feeding (value displayed on *y*-axis), while the white bars show the time between switching to starving conditions and achieving 90% pupariation. *n*=10 feeding larvae per time point.

the time of pupation via an E-independent mechanism (Yamanaka et al., 2013a). This process ensures pupation in dark environments, which is likely to aid in pupal survival by reducing dehydration and predation. These examples suggest that the PG neurons, and PTTH signaling in particular, facilitate coordination of developmental processes with environmental conditions to maximize species fitness.

PTTH signaling, critical weight determination and E production kinetics

In holometabolous insects, feeding during the larval stages is especially important for their developmental program since they must accumulate sufficient energy reserves to fuel metamorphosis during the non-feeding pupal stage. As a consequence, various nutritional checkpoints such as CW and MVW have evolved to

ensure that larvae do not enter metamorphosis before sufficient fuel has been stored. Two studies have put forward different mechanisms for determining CW. In the first, the process of larval molting is proposed to produce a transient starvation state leading to nuclear accumulation of a FoxO-USP complex that inhibits E production until sufficient feeding relieves this constraint and CW is achieved (Koyama et al., 2014). In the second paradigm, nutrient-dependent TOR signaling in the PG is thought to regulate endocycle entry, and DNA copy number is found to correlate with attainment of CW (Ohhara et al., 2017). Our examination of *Ptth* mutants clearly demonstrates that PTTH signaling also contributes to setting the CW checkpoint. All three processes share a common feature in that they affect the rate of basal E production, providing support for the notion that CW represents the attainment of a minimal threshold level of E that enables nutrient-independent completion of larval development and commencement of metamorphosis (Rewitz et al., 2013). It is interesting that the low basal E titer caused by *Ptth* loss does not influence larval growth rate, whereas lower basal levels of E produced by other methods have been reported to enhance larval growth rate (Boulan et al., 2013; Colombani et al., 2005; Moeller et al., 2017). We are presently investigating the mechanism responsible for these differences.

Whether and how these three molecular mechanisms intersect remains to be determined, but it is interesting to note that in our present study we demonstrated a role for PTTH in regulating nuclear size. Thus, PTTH signaling might modulate E production in conjunction with TOR by determining the number of DNA templates available for transcription of E biosynthetic enzymes. Alternatively, PTTH might act more directly to influence transcriptional control of E biosynthetic components. Numerous transcription factors, including EcR, Mld, Usp, FoxO, Br, Ftz-f1, HR4, Vvl and Ouija board (Danielsen et al., 2014; Komura-Kawa et al., 2015; Koyama et al., 2014; Moeller et al., 2013; Ou et al., 2011; Parvy et al., 2005) have been implicated in transcriptional regulation of one or more E biosynthetic enzymes, although none has been shown to be a direct target of Rolled (Erk) phosphorylation, the major downstream mediator of PTTH signaling. One factor of particular interest, however, is the nuclear receptor HR4, since it has been shown that knockdown of its expression in the PG accelerates development, while overexpression retards development (Ou et al., 2011). Furthermore, during the first half of the third instar stage, HR4 cycles in and out of the nucleus with a periodicity that depends on Ras/Erk signaling. The proposed mechanism posits that HR4 negatively regulates one or more E biosynthetic genes, including *Cyp6t3*, and that periodic PTTH signals enable the production of transient small E pulses, each of which might represent passage through a specific developmental checkpoint that controls timing of metamorphosis (Ou et al., 2011; Rewitz and O'Connor, 2011; Rewitz et al., 2013). Although this mechanism is an attractive possibility, we find no rescue of developmental timing when certain biosynthetic enzyme genes, including *Cyp6t3*, are individually overexpressed. These observations indicate that either there is an as yet unidentified PTTH-regulated rate-limiting component, or that it is the combined reduction in several enzymes that results in slower E production. Lastly, in Lepidoptera, PTTH has been shown to stimulate translation as well as transcription and this might also come into play when considering how a slow rise in E titer is produced (Keightley et al., 1990; Kulesza et al., 1994; Rybczynski and Gilbert, 1995).

Autonomy versus non-autonomy of PTTH signaling

One of the more unexpected findings of this study is that *Drosophila* PTTH appears to act autonomously for regulating E biosynthesis within the PG, whereas a previous study demonstrated that PTTH in the hemolymph acts non-autonomously, and in a Torso-dependent manner, to regulate larval light avoidance (Yamanaka et al., 2013b). In addition, a recent study showed that Torso expression in the fat body is required for proper insulin signaling and body size control although the ligand involved was not identified (Jun et al., 2016). Since PTTH reaches the PG through the circulatory system in Lepidoptera, it is unlikely that there is an intrinsic functional need to regulate E biosynthesis through direct innervation of the PG, and indeed we found that overexpression of PTTH in the fat body was able to rescue the developmental delay and body size phenotypes of *Ptth* null mutants (data not shown). This apparent dichotomy with respect to autonomous and non-autonomous requirements in different tissues might be explained by the unusual biophysical features of Torso, which binds PTTH asymmetrically resulting in anti-cooperativity (Jenni et al., 2015). Thus, receptor levels determine the nature of the signal output: high receptor levels stimulate a transient burst of enhanced signal, whereas low receptor levels produce a low amplitude, sustained signal. In addition, high receptor levels may facilitate intermolecular disulfide bond formation between Torso monomers within the transmembrane domain and thereby stabilize a preformed dimeric receptor that is primed for activation by ligand binding (Konogami et al., 2016). Perhaps innervation of the gland by PG neurons facilitates clustering of receptors at the synapses, stimulating production of preformed receptor dimers near the PTTH release sites and resulting in a high-level signal in the PG cells that is necessary for rapid induction of E biosynthetic enzymes. By contrast, the non-autonomous effect of PTTH on Bolwig's organ and class IV multidendritic neurons might result from low receptor concentrations leading to the sustained low-level signal needed to modulate light avoidance. It is interesting to note in this regard that we cannot detect endogenous Torso protein by immunolocalization in Bolwig's organ or class IV multidendritic neurons, but can readily detect it in PG cells, consistent with the idea that receptor levels may influence the type of signal produced by PTTH in different tissues.

An alternative possibility is that two synergistic signals, one of which is localized in the PG, are required to produce rapid induction of E biosynthetic gene transcription in the PG, but two signals are not required for light avoidance. We provide evidence that at least one other signal from the PG neurons is essential for proper timing of E production. Local loss of this signal in cells lacking a varicosity could be sufficient to prevent high-level induction of E biosynthetic enzymes in those cells, while release of PTTH from remaining varicosities could provide sufficient systemic levels of PTTH to stimulate light avoidance. It is interesting to note with respect to the two-signal model that, in a tissue culture assay system, Torso activation can be stimulated by the synergistic interaction of Trunk, a second Torso ligand involved in the specification of terminal embryonic cell fates, and Tsl, the product of the *torso-like* locus (Amarnath et al., 2017).

Additional timing signals produced by PG neurons

Although the data presented here provide strong evidence that PTTH is a key environmentally responsive developmental timing signal in *Drosophila*, our manipulation of PG neuron activity, coupled with previously reported ablation studies (Ghosh et al., 2010; McBrayer et al., 2007), clearly suggest the presence of at least one additional timing factor, the release of which is activity dependent. Whether this factor also signals through Torso or another receptor is unresolved, but it is interesting to note that spätzle-like proteins show some structural features common to both PTTH and Trunk, the two known Torso ligands (Casanova et al., 1995). The presence of multiple timing signals is perhaps not

Development (2018) 145, dev159699. doi:10.1242/dev.159699

surprising since redundancy is likely to provide both robustness to the circuit and flexibility for output responses. Recent characterization of *Ptth* mutants in *Bombyx* also showed alterations in developmental timing during larval stages (Uchibori-Asano et al., 2017). However, there was much more variability in the timing delay phenotype, as well as significantly enhanced lethality, compared with what we observe in *Drosophila*, perhaps indicating that alternative signals are either not present or less effective in compensating for *Ptth* loss in *Bombyx*.

MATERIALS AND METHODS

TALEN-directed mutagenesis

Plasmids TAL248NN and TAL249NN (in the pT3TS-delta152, +63 backbone) were digested with *Ecl*136II, and 1 µg was transcribed using the T3 mMessage mMachine Kit (Ambion). The 5′-capped mRNAs were phenol-chloroform extracted and precipitated with isopropanol. These left and right *Ptth* TALEN monomers were dissolved in 30 µl 0.1× PBS (DEPC treated) and mixed to make a 30 µl solution with each mRNA at a final concentration of 400 µg/ml in 0.1× PBS. An aliquot was injected into w^{1118} embryos (Duke Injection Services) and individual G0 adults were crossed to balancer line sna^{Sco}/CyO* (BDSC #3198). Once larva were observed in the vial, the G0 fly was removed and frozen at −80°C for subsequent single-fly DNA extraction with squishing buffer (Gloor et al., 1993). Genomic DNA from 75 fertile G0 flies was analyzed by PCR with primers PTTH TAL 01F and PTTH TAL 03R (Table S1) incorporating the LightCycler 480 High Resolution Melting Master (Roche) and using the Tm calling program. Five mosaic G0 lines were selected based on an altered Tm peak: either wider, displaying a shoulder, or the presence of two Tm peaks. Ten to fifteen individual balanced F1 males from the mosaic candidates were backcrossed to w*;sna^{Sco}/Cyo* females and then self-crossed to obtain homozygous stocks. These homozygous stocks were again analyzed by Tm calling and the region of interest sequenced. Subsequent analyses used w^{1118} as the control to the $Ptth^{120F2A}$ and $Ptth^{8K1J}$ mutants since that was the line originally injected and so should adequately serve as a control.

Two distinct lesions were found at the targeted *Ptth* site, and no additional changes were observed in these lines when the complete gene was sequenced. The lesions identified comprise: (1) a 7 bp deletion (ΔCGTTTGC between nucleotides 465 and 471 of the PTTH-RF coding sequence) in line $Ptth^{120F2A}$; and (2) a 6 bp deletion (ΔATGCCG between nucleotides 461 and 466 of the PTTH-RF coding sequence) in line $Ptth^{8K1J}$. The $Ptth^{120F2A}$ allele generated a frameshift distal to N154 of PTTH-PR that continued out of frame for 24 amino acids before reaching a stop codon. This mutation removed much of the predicted mature ligand portion of PTTH. The 6 bp deletion found in line $Ptth^{8K1J}$ leads to a deletion of N154 and A155 and a V156I substitution (Fig. 1A). A third allele, $Ptth^{8M9A}$, which deleted 5 bp (ΔCGTTT) between nucleotides 465 and 469 of the PTTH-RF coding sequence, was not used in this work.

Accelerated homologous recombination mutagenesis

To generate the $Ptth^{Delta}$ mutant, the accelerated homologous recombination technique was used as described (Baena-Lopez et al., 2013). Two homology arms were amplified from genomic DNA using the primers listed in Table S1, which incorporate *Not*I or *Bgl*II restriction sites for cloning. The resulting PCR products were digested and cloned into pTV-Cherry vector (2.7 kb corresponding to the 5′ arm with *Not*I and 2.3 kb for the 3′ arm with *Bgl*II). This *Ptth* targeting vector, containing the appropriate homology arms, was introduced at random genomic locations by P-element-mediated transformation (BestGene). Transformants (not necessarily mapped or homozygosed) were crossed to *hs-FLP, hs-I-SceI* flies (BDSC #25679) and the resulting larvae were heat shocked at 48 h and 72 h after egg laying for 1 h at 37°C. Approximately 200 adult females with mottled red eyes (indicating the presence of the targeting vector and the transgene carrying hs-FLP and hs-I-SceI) were crossed to *ubiquitin-Gal4[3×P3-GFP]* males and the progeny screened for the presence of red eyes. The *ubiquitin-Gal4[3×P3-GFP]* transgene was subsequently removed by selecting against the presence of GFP in the ocelli. Red-eyed flies resulting from these crosses were subjected to PCR with primers PTTH forward and reverse (Table S1). One line was confirmed to be a *Ptth* null homologous recombinant, referred to herein as $Ptth^{Delta}$. Sequencing results confirmed a deletion of 604 bp in the $Ptth^{Delta}$ allele that included the putative ATG and signal peptide (Fig. 1A).

The $Ptth^{Delta}$ allele was backcrossed into the w^{DAH} standardized genetic background for at least ten generations before any experimental procedures. Thus, we used w^{DAH} as the correct background control for $Ptth^{Delta}$.

Molecular biology and production of transgenic lines

D. melanogaster release 6 (FlyBase Consortium) was used to define the DNA, RNA and amino acid coordinates of *Ptth*. Three start sites are identified in FlyBase, and we used the cDNA identified as G.

The genomic fragment of HA-tagged PTTH from pMBO2318 (McBrayer et al., 2007) was excised as a *Not*I-*Eco*RI fragment and placed in a *pattB* vector (pattB-QF-sv40, Addgene #24367) which was digested with *Not*I and *Eco*RI in order to drop out the QF fragment. This plasmid, pMBO2604, was inserted into the *attP2* site of $y^1\ w^{67c23};\ P\{CaryP\}attP2$ (BDSC #8622) by injection (GenetiVision) and *phiC31* integration. The transformant line was designated *Ptth* WT-*attP2-2A3*. The *spok>Gal4* line was made by inserting a 1.4 kb upstream fragment of *spok* (Komura-Kawa et al., 2015) into the Pelican-Gal4 vector (from M.B.O.'s lab.). Transgenic line *spok-Gal4* 1L3 was derived after injection into w^{1118}.

Fly stocks, stock building and food

Animals were reared at 25°C on a variation of standard cornmeal food (CMF, BDSC), in which brewer's yeast was substituted for baker's yeast and Tegosept was added for mold control. Live baker's yeast granules were shaken liberally onto the surface. Some timing experiments were performed on 'normal' fly food, which contains per liter: 17 g inactivated yeast powder, 83 g corn flour, 10 g agar and 4.6 g Nipagin; for 'rich' or 'poor' food, the amount of inactivated yeast powder was adjusted to 34 g/l or 5 g/l, respectively.

The following fly stocks were used: *P0206-Gal4* (Colombani et al., 2005), *UAS-spok 4A2* (Komura-Kawa et al., 2015), *UAS-dib 20A2* (*Not*I-*Asp*718I *dib* cDNA in pUAST), *UAS-nvd* (Yoshiyama et al., 2006), *spok-Gal4 1L3* and *UAS-Cyp6t3* (Ou et al., 2011), *fb-Gal4* (Tom Neufeld, University of Minnesota, USA), *UAS-Ptth IIA 96L3* (McBrayer et al., 2007), $gt^{E1};UAS\text{-}GFP;Feb^{211}\text{-}Gal4,\ UAS\text{-}mCD8\text{-}GFP$ (Siegmund and Korge, 2001), *Ptth-Gal4 45A3, 117bA3* (McBrayer et al., 2007), *Ptth-Gal4 45A3, 117bA3; UAS-grim* (McBrayer et al., 2007), *UAS-TrpA1/TM6B, Tb* (BDSC #26264), *UAS-Kir2.1* on the 3rd chromosome (BDSC #6595), *UAS-TetxLC* on the 3rd chromosome (BDSC #28997), *UAS-TetxLC.IMP* on the 3rd chomosome (BDSC #28841), *UAS-dORKΔC* on the 3rd chromosome (BDSC #6586), *NP0394-Gal4* [*Drosophila* Genetic Resource Center (DGRC) Kyoto, Japan #103604], *UAS-Ptth-RNAi* (Vienna *Drosophila* Resource Center (VDRC) #102043], $UAS\text{-}torso\text{-}RNAi_{GD}$ (VDRC #36280), *UAS-Synaptobrevin-GFP* (BDSC #60677) and *Ay-Gal4 (act-FRT-stop-FRT-Gal4)* (BDSC #3953). Recombinant or combination stocks were made using standard genetic methods.

Developmental timing curves

All developmental timing experiments were performed at 25°C in 12 h light/dark cycle conditions. One- to four-hour time collections of embryos laid on apple juice plus yeast paste plates were aged for 20 h, at which point freshly ecdysing L1 larvae were transferred to vials. Each vial contained 30, 40, 150, 350 or 500 L1 larvae. The time and date of pupariation were scored every 1-5 h during the light cycle and the time in hours from L1 ecdysis to puparium formation was determined using the time duration calculator (www.timeanddate.com). Data from four vials were compiled and ordered by progressive pupariation time and cumulative percentage pupariation and subsequently analyzed in GraphPad Prism using non-linear regression curve fit or in Microsoft Excel.

Measurements of pupal volume and adult mass

Male and female pupae were photographed and measured with ImageJ. Pupal length was measured along the medial line between anterior and posterior, not including the anterior and posterior spiracles. Pupal width was measured along the axial line. Pupal volume was determined using the formula for a prolate spheroid: $(\pi/6)W^2\times L$, where W is width and L is

length. Sexed adults were weighed in groups of three to five flies or individually using a Mettler Toledo XP26 microbalance.

Immunohistochemistry of larval tissues

Tissues dissected from larvae in 1× PBS (137 mM NaCl, 2.7 mM KCl, 4.3 mM Na_2HPO_4, 1.47 mM KH_2PO_4, pH 8) at the indicated hours after egg deposition were fixed in 4% formaldehyde (Sigma) in PBS for 20 min at room temperature, washed in PBS containing 0.1% Triton X-100 (PBT), blocked for 2 h in PBT containing 10% FBS (PBS-TF), and incubated overnight with primary antibodies at 4°C. The next day, tissues were washed, blocked in PBS-TF, and incubated with secondary antibodies for 2 h at room temperature. After washing, tissues were mounted in Vectashield containing DAPI (Vector Labs) for staining of DNA. Fluorescence images were acquired using a Leica SP5 DS (20× and 40× objectives) and processed using Adobe Photoshop CS5 or ImageJ.

Antibodies

Primary antibodies were anti-PTTH (guinea pig, 1:200; P.L.), anti-NC82 (mouse hybridoma, 1:50; DSHB), anti-Dib [rabbit, 1:500; Parvy et al. (2005)] and anti-GFP (rabbit polyclonal, 1:500; Abcam). Secondary antibodies were Alexa Fluor 555 goat anti-guinea pig, Alexa Fluor 488 sheep anti-rabbit, AlexaFluor 488 donkey anti-rabbit (1:500; Abcam) and Cy3 sheep anti-mouse (1:200; Jackson ImmunoResearch).

Wing disc analyses: growth rate and nuclear size

Four-hour egg collections were performed on agar plates, and after 20 h L1 larvae were collected and reared at 40 animals per tube at 25°C. Larvae that ecdysed from L2 to L3 over a 2 h period were transferred onto new food plates and allowed to feed until they reached the appropriate age. After immunohistochemistry of larval tissues, the image of wing discs was acquired using a Leica SP5 DS, and the disc and nucleus area were measured using ImageJ.

Wing size measurement

L1 larvae were collected 24 h after egg deposition (4 h egg collections) and reared at 40 animals per tube at 25°C. Adult flies of the appropriate genotype were collected and stored in ethanol and mounted in a Euparal solution (ROTH). Images of dissected wings were acquired using a Leica MZ16 FA fluorescence stereomicroscope and DFC 490 digital camera. Wing areas were measured using ImageJ.

Adult ovariole number

Newly eclosed flies were maintained in vials on standard food until the time of dissection (3-4 days after eclosion). Ovaries were dissected in cold PBS, and ovarioles were teased apart and counted under a dissecting microscope.

Determination of critical weight

A variation of published methods (McBrayer et al., 2007; Mirth et al., 2005) was used. Larvae were raised at 25°C in continuous light conditions. Newly ecdysed L1 larvae, as described above, were transferred at intervals to CMF in 35 mm diameter plates and aged for 48 h. Freshly ecdysed L3 larvae were transferred to a new CMF plate at 1 h intervals at a density of less than 30 L3 larvae per plate, and timing initiated. Every 2 h starting at L3 ecdysis (T0) and continuing until 24 h for w^{1118} and 48 h for $Ptth^{120F2A}$, ten feeding larvae were removed, individually weighed and placed in starvation medium [1.5% Bacto Agar (BD Diagnostics) in water]. Puparium formation was quantitated and timed, as well as eclosion rates. The critical period was defined as the number of hours after starvation when ≥90% of the larvae pupariated and did so without a delay. The CW was the average weight of those ten larvae at the critical time.

Rescue by 20-hydroxyecdysone feeding

Thirty freshly ecdysed $Ptth^{120F2A}$ L3 larvae, grown at 25°C under 12 h light/dark conditions, were washed with water and transferred to a small CMF plate for additional aging. After 20 h, larvae were washed and transferred to a vial supplemented with either 20-hydroxyecdysone (Cayman Chemical; dissolved in 95% ethanol, final concentration 0.2 mg/ml) or 95% ethanol (same volume as 20-HE). The control w^{1118} larvae were directly transferred to vials upon L3 ecdysis. Once seeded with L3 larvae, the vials were returned to 25°C under 12 h light/dark and monitored, as well as timed, for pupariation.

PG neuron innervation studies

To show that PTTH is the trophic signal to the PG, females of genotype gl^{E1}/*FM, act-GFP;* $Ptth^{120F2A}$*/CyO, act-GFP* were crossed to $Ptth^{120F2A}$*; Feb*^{211}*-Gal4, UAS-mCD8-GFP* males. CNS plus RG complexes from GFP-negative wandering larvae were dissected, fixed and mounted. About 25% of animals had asymmetric innervation. For the same purpose, females of the variegated driver *NP0394-Gal4* were crossed to *UAS-Ptth-RNAi* and the offspring larvae were grown on food containing per liter: 8.5 g inactivated yeast powder, 83 g corn flour, 10 g agar and 4.6 g Nipagin. CNS plus RG complexes were dissected, fixed and stained with anti-PTTH antibody. About 15% of animals had asymmetric *Ptth* silencing.

Torso RNAi Flp-out clones

Mitotic clones marked by GFP were generated using *hsFLP; Act>CD2>Gal4, UAS-nGFP* in combination with *UAS-torso-RNAi*. Clonal induction was performed for 5 min at 37°C in the second instar.

PG neuron activation by TrpA1

Larvae of the indicated genotypes were first synchronized at L2/L3 molting, and then vials of 25-30 larvae were further reared at 25°C. Vials were transferred to 29°C at progressive times to activate the TrpA1-expressing neurons. Pupariation was monitored by counting the number of pupae at consecutive time points.

Raising L3 larvae for timed sample collections

Timed samples were raised at 25°C under continuous light. Forty newly ecdysed L1 larvae, precisely timed on apple juice collection plates, were transferred at 1 h intervals to 35 mm diameter plates containing CMF with surface granules of live baker's yeast. Larvae continued to develop for ~48 h and were then monitored for morphological features characteristic of ecdysis to the third instar stage. These freshly ecdysed L3 larvae were transferred to a fresh food plate, and timing of L3 age in hours commenced. For qRT-PCR, larvae of defined ages were removed from the food, washed in DEPC-treated water, homogenized in Trizol (Invitrogen), and stored at −80°C. For E titers, larvae of defined ages were removed from the food, washed twice in water, dried on a Kimwipe, weighed in bulk for biological replicates, and stored at −80°C.

qRT-PCR

Total RNA was purified from Trizol, transcript RNA was isolated using the RNeasy Mini Kit (Qiagen), and reverse transcribed with the SuperScript III First-Strand Synthesis Kit (Invitrogen). qRT-PCR reactions used LightCycler 480 SYBR Green I Master Mix on a LightCycler 480 instrument (Roche). Primers are listed in Table S1. All reactions were performed in duplicate. Expression (arbitrary units) was determined relative to *RpL23* using the formula $(2^{-\Delta Cp})\times 100{,}000$ (or a factor that gives an expression value of 10-500 arbitrary units). The average of four biological replicates ±s.e.m. was plotted.

Ecdysone titers

Biological replicates of 4-15 larvae were homogenized twice in methanol and cleared by centrifugation to give a final combined volume of ~360 µl. Duplicate 100 µl samples were dried and resuspended overnight in 50 µl EIA buffer (Cayman Chemical). Cayman Chemical reagents for 20-HE ELISA were used as per manufacturer's recommendation with two changes: in some experiments, the E antibody L2-B (kind gift of Jean-Paul Delbecque, Aquitaine Institute for Cognitive and Integrative Neuroscience, Bordeaux, France) was substituted for the Cayman antiserum, and in other cases where there was a low E titer because of small sample size, the 20-HE AChE tracer was diluted up to 1:5 in the reaction. The standard curve was determined using GraphPad Prism software, non-linear regression curve fit, asymmetric sigmoidal, 5PL, X is log (conc). Per animal, E titers were adjusted for the volume used in the assay.

Acknowledgements
We thank the Bloomington *Drosophila* Stock Center (BDSC) for numerous *Drosophila* lines and Aidan Peterson and Derya Deveci for comments on the manuscript; Colby Starker, Michelle Christian and Dan Voytas for help in designing and making TALENs for the *Ptth* null mutant production; Anna Petryk and Michael Jarcho for producing UAST-*sad*, *phm* and *dib* constructs; and Thomas Phil for technical support.

Competing interests
The authors declare no competing or financial interests.

Author contributions
Conceptualization: M.S., F.A.M., P.L., M.B.O., N.M.R.; Methodology: M.S., P.L., M.B.O., N.M.R.; Formal analysis: M.S., N.M.R.; Investigation: M.S., X.P., F.A.M., A.C.G., N.M.R.; Writing - original draft: M.B.O., N.M.R.; Writing - review & editing: M.S., P.L., M.B.O., N.M.R.; Visualization: M.S., X.P., F.A.M., N.M.R.; Supervision: P.L., M.B.O., N.M.R.; Project administration: M.S., N.M.R.; Funding acquisition: P.L., M.B.O.

Funding
This work was supported by Institut National de la Santé et de la Recherche Médicale (INSERM), Centre National de la Recherche Scientifique (CNRS), Fondation ARC pour la Recherche sur le Cancer grant PGA120150202355 and European Research Council Advanced Grant 268813 to P.L. and N.M.R.; and National Institutes of Health grant R35-GM118029 to M.B.O. F.A.M. is a recipient of Ramon y Cajal Contract RyC-2014-14961 from the Ministerio de Economía y Competitividad and supported by BFU2014-54346-JIN. Deposited in PMC for release after 12 months.

Supplementary information
Supplementary information available online at
http://dev.biologists.org/lookup/doi/10.1242/dev.159699.supplemental

References

Amarnath, S., Stevens, L. M. and Stein, D. S. (2017). Reconstitution of Torso signaling in cultured cells suggests a role for both Trunk and Torso-like in receptor activation. *Development* **144**, 677-686.
Baena-Lopez, L. A., Alexandre, C., Mitchell, A., Pasakarnis, L. and Vincent, J.-P. (2013). Accelerated homologous recombination and subsequent genome modification in *Drosophila*. *Development* **140**, 4818-4825.
Barker, J. S. F. and Podger, R. N. (1970). Interspecific competition between *Drosophila melanogaster* and *Drosophila simulans*: effects of larval density on viability, developmental period and adult body weight. *Ecology* **51**, 170-189.
Bergland, A. O., Genissel, A., Nuzhdin, S. V. and Tatar, M. (2008). Quantitative trait loci affecting phenotypic plasticity and the allometric relationship of ovariole number and thorax length in *Drosophila melanogaster*. *Genetics* **180**, 567-582.
Boulan, L., Martín, D. and Milán, M. (2013). bantam miRNA promotes systemic growth by connecting insulin signaling and ecdysone production. *Curr. Biol.* **23**, 473-478.
Bubli, O. A., Imasheva, A. G. and Loeschcke, V. (1998). Selection for knockdown resistance to heat in *Drosophila Melanogaster* at high and low larval densities. *Evolution* **52**, 619-625.
Caldwell, P. E., Walkiewicz, M. and Stern, M. (2005). Ras activity in the *Drosophila* prothoracic gland regulates body size and developmental rate via ecdysone release. *Curr. Biol.* **15**, 1785-1795.
Casanova, J., Furriols, M., McCormick, C. A. and Struhl, G. (1995). Similarities between trunk and spatzle, putative extracellular ligands specifying body pattern in *Drosophila*. *Genes Dev.* **9**, 2539-2544.
Chippindale, A. K., Leroi, A. M., Kim, S. B. and Rose, M. R. (1993). Phenotypic plasticity and selection in *Drosophila* life-history evolution. 1. Nutrition and the cost of reproduction. *J. Evol. Biol.* **6**, 171-193.
Colombani, J., Bianchini, L., Layalle, S., Pondeville, E., Dauphin-Villemant, C., Antoniewski, C., Carre, C., Noselli, S. and Leopold, P. (2005). Antagonistic actions of ecdysone and insulins determine final size in *Drosophila*. *Science* **310**, 667-670.
Colombani, J., Andersen, D. S., Boulan, L., Boone, E., Romero, N., Virolle, V., Texada, M. and Léopold, P. (2015). *Drosophila* Lgr3 couples organ growth with maturation and ensures developmental stability. *Curr. Biol.* **25**, 2723-2729.
Danielsen, E. T., Moeller, M. E. and Rewitz, K. F. (2013). Nutrient signaling and developmental timing of maturation. *Curr. Top. Dev. Biol.* **105**, 37-67.
Danielsen, E. T., Moeller, M. E., Dorry, E., Komura-Kawa, T., Fujimoto, Y., Troelsen, J. T., Herder, R., O'Connor, M. B., Niwa, R. and Rewitz, K. F. (2014). Transcriptional control of steroid biosynthesis genes in the *Drosophila* prothoracic gland by ventral veins lacking and knirps. *PLoS Genet.* **10**, e1004343.
David, J. R. (1970). Le numbre d'ovarioles chez la avec la fecondite et valeur adaptive. *Arch. Zool. Exp. Genet.* **111**, 357-370.
Deng, H. and Kerppola, T. K. (2013). Regulation of *Drosophila* metamorphosis by xenobiotic response regulators. *PLoS Genet.* **9**, e1003263.
Denver, R. J. (1997). Environmental stress as a developmental cue: corticotropin-releasing hormone is a proximate mediator of adaptive phenotypic plasticity in amphibian metamorphosis. *Horm. Behav.* **31**, 169-179.
Di Cara, F. and King-Jones, K. (2013). How clocks and hormones act in concert to control the timing of insect development. *Curr. Top. Dev. Biol.* **105**, 1-36.
Garelli, A., Heredia, F., Casimiro, A. P., Macedo, A., Nunes, C., Garcez, M., Dias, A. R., Volonte, Y. A., Uhlmann, T., Caparros, E. et al. (2015). Dilp8 requires the neuronal relaxin receptor Lgr3 to couple growth to developmental timing. *Nat. Commun.* **6**, 8732.
Ghosh, A., McBrayer, Z. and O'Connor, M. B. (2010). The *Drosophila* gap gene giant regulates ecdysone production through specification of the PTTH-producing neurons. *Dev. Biol.* **347**, 271-278.
Gibbens, Y. Y., Warren, J. T., Gilbert, L. I. and O'Connor, M. B. (2011). Neuroendocrine regulation of *Drosophila* metamorphosis requires TGFbeta/Activin signaling. *Development* **138**, 2693-2703.
Gloor, G. B., Preston, C. R., Johnson-Schlitz, D. M., Nassif, N. A., Phillis, R. W., Benz, W. K., Robertson, H. M. and Engels, W. R. (1993). Type I repressors of P element mobility. *Genetics* **135**, 81-95.
Gokhale, R. H., Hayashi, T., Mirque, C. D. and Shingleton, A. W. (2016). Intra-organ growth coordination in *Drosophila* is mediated by systemic ecdysone signaling. *Dev. Biol.* **418**, 135-145.
Gotthard, K. and Nylin, S. (1995). Adaptive plasticity and plasticity as an adaptation: a selective review of plasticity in animal morphology and life-history. *Oikos* **74**, 3-17.
Hackney, J. F., Zolali-Meybodi, O. and Cherbas, P. (2012). Tissue damage disrupts developmental progression and ecdysteroid biosynthesis in *Drosophila*. *PLoS ONE* **7**, e49105.
Hamada, F. N., Rosenzweig, M., Kang, K., Pulver, S. R., Ghezzi, A., Jegla, T. J. and Garrity, P. A. (2008). An internal thermal sensor controlling temperature preference in *Drosophila*. *Nature* **454**, 217-220.
Herboso, L., Oliveira, M. M., Talamillo, A., Perez, C., Gonzalez, M., Martin, D., Sutherland, J. D., Shingleton, A. W., Mirth, C. K. and Barrio, R. (2015). Ecdysone promotes growth of imaginal discs through the regulation of Thor in *D. melanogaster*. *Sci. Rep.* **5**, 12383.
Hock, T., Cottrill, T., Keegan, J. and Garza, D. (2000). The E23 early gene of *Drosophila* encodes an ecdysone-inducible ATP-binding cassette transporter capable of repressing ecdysone-mediated gene activation. *Proc. Natl. Acad. Sci. USA* **97**, 9519-9524.
Hodge, J. J. (2009). Ion channels to inactivate neurons in *Drosophila*. *Front. Mol. Neurosci.* **2**, 13.
Horvath, B. and Kalinka, A. T. (2016). Effects of larval crowding on quantitative variation for development time and viability in *Drosophila melanogaster*. *Ecol. Evol.* **6**, 8460-8473.
Jaszczak, J. S., Wolpe, J. B., Bhandari, R., Jaszczak, R. G. and Halme, A. (2016). Growth coordination during *Drosophila melanogaster* imaginal disc regeneration is mediated by signaling through the relaxin receptor Lgr3 in the prothoracic gland. *Genetics* **204**, 703-709.
Jenni, S., Goyal, Y., von Grotthuss, M., Shvartsman, S. Y. and Klein, D. E. (2015). Structural basis of neurohormone perception by the receptor tyrosine kinase Torso. *Mol. Cell* **60**, 941-952.
Joshi, A., Knight, C. D. and Mueller, L. D. (1996a). Genetics of larval urea tolerance in *Drosophila melanogaster*. *Heredity* **77**, 33-39.
Joshi, A., Shiotsugu, J. and Mueller, L. D. (1996b). Phenotypic enhancement of longevity by environmental urea in *Drosophila melanogaster*. *Exp. Gerontol.* **31**, 533-544.
Jun, J. W., Han, G., Yun, H. M., Lee, G. J. and Hyun, S. (2016). Torso, a *Drosophila* receptor tyrosine kinase, plays a novel role in the larval fat body in regulating insulin signaling and body growth. *J. Comp. Physiol. B* **186**, 701-709.
Kataoka, H., Nagasawa, H., Isogai, A., Ishizaki, H. and Suzuki, A. (1991). Prothoracicotropic hormone of the silkworm, Bombyx mori: amino acid sequence and dimeric structure. *Agric. Biol. Chem.* **55**, 73-86.
Kawakami, A., Kataoka, H., Oka, T., Mizoguchi, A., Kimura-Kawakami, M., Adachi, T., Iwami, M., Nagasawa, H., Suzuki, A. and Ishizaki, H. (1990). Molecular cloning of the Bombyx mori prothoracicotropic hormone. *Science* **247**, 1333-1335.
Keightley, D. A., Lou, K. J. and Smith, W. A. (1990). Involvement of translation and transcription in insect steroidogenesis. *Mol. Cell. Endocrinol.* **74**, 229-237.
Kolss, M., Vijendravarma, R. K., Schwaller, G. and Kawecki, T. J. (2009). Life-history consequences of adaptation to larval nutritional stress in *Drosophila*. *Evolution* **63**, 2389-2401.
Komura-Kawa, T., Hirota, K., Shimada-Niwa, Y., Yamauchi, R., Shimell, M., Shinoda, T., Fukamizu, A., O'Connor, M. B. and Niwa, R. (2015). The *Drosophila* zinc finger transcription factor Ouija board controls ecdysteroid biosynthesis through specific regulation of spookier. *PLoS Genet.* **11**, e1005712.
Konogami, T., Yang, Y., Ogihara, M. H., Hikiba, J., Kataoka, H. and Saito, K. (2016). Ligand-dependent responses of the silkworm prothoracicotropic hormone receptor, Torso, are maintained by unusual intermolecular disulfide bridges in the transmembrane region. *Sci. Rep.* **6**, 22437.

Kopec, S. (1922). Studies on the necessity of the brain for the inception of insect metamorphosis. *Biol. Bull.* **42**, 323-342.
Kouser, S., Palaksha, S. and Shakunthala, V. (2013). Study on fitness of *Drosophila melanogaster* in different light regimes. *Biol. Rhythm. Res.* **45**, 293-300.
Koyama, T., Rodrigues, M. A., Athanasiadis, A., Shingleton, A. W. and Mirth, C. K. (2014). Nutritional control of body size through FoxO-Ultraspiracle mediated ecdysone biosynthesis. *Elife* **3**, e03091.
Kulesza, P., Lee, C.-Y. and Watson, R. D. (1994). Protein synthesis and ecdysteroidogenesis in prothoracic glands of the tobacco hornworm (Manduca sexta): stimulation by big prothoracicotropic hormone. *Gen. Comp. Endocrinol.* **93**, 448-458.
Lafont, R., Dauphin-Villemant, C. and Warren, J. T. (2005). Ecdysteroid chemistry and biochemistry. In *Comprehensive Molecular Insect Sciences* (ed. L. I. Gilbert, K. Iatrou and S. Gill), pp. 125-195. Oxford: Elsevier.
Lavalle, S., Arquier, N. and Léopold, P. (2008). The Tor pathway couples nutrition and developmental timing in *Drosophila*. *Dev. Cell* **15**, 568-577.
Lessells, C. M. (2008). Neuroendocrine control of life histories: what do we need to know to understand the evolution of phenotypic plasticity? *Philos. Trans. R. Soc. Lond. B Biol. Sci.* **363**, 1589-1598.
Mast, J. D., De Moraes, C. M., Alborn, H. T., Lavis, L. D. and Stern, D. L. (2014). Evolved differences in larval social behavior mediated by novel pheromones. *Elife* **3**, e04205.
May, C. M., Doroszuk, A. and Zwaan, B. J. (2015). The effect of developmental nutrition on life span and fecundity depends on the adult reproductive environment in *Drosophila melanogaster*. *Ecol. Evol.* **5**, 1156-1168.
McBrayer, Z., Ono, H., Shimell, M., Parvy, J.-P., Beckstead, R. B., Warren, J. T., Thummel, C. S., Dauphin-Villemant, C., Gilbert, L. I. and O'Connor, M. B. (2007). Prothoracicotropic hormone regulates developmental timing and body size in *Drosophila*. *Dev. Cell* **13**, 857-871.
Mendes, C. C. and Mirth, C. K. (2016). Stage-specific plasticity in ovary size is regulated by insulin/insulin-like growth factor and ecdysone signaling in *Drosophila*. *Genetics* **202**, 703-719.
Miller, R. S. and Thomas, J. L. (1958). The effects of larval crowding and body size on the longevity of adult *Drosophila melanogaster*. *Ecology* **39**, 118-125.
Mirth, C. K. and Riddiford, L. M. (2007). Size assessment and growth control: how adult size is determined in insects. *BioEssays* **29**, 344-355.
Mirth, C. K. and Shingleton, A. W. (2012). Integrating body and organ size in *Drosophila*: recent advances and outstanding problems. *Front. Endocrinol.* **3**, 49.
Mirth, C., Truman, J. W. and Riddiford, L. M. (2005). The role of the prothoracic gland in determining critical weight for metamorphosis in *Drosophila melanogaster*. *Curr. Biol.* **15**, 1796-1807.
Moeller, M. E., Danielsen, E. T., Herder, R., O'Connor, M. B. and Rewitz, K. F. (2013). Dynamic feedback circuits function as a switch for shaping a maturation-inducing steroid pulse in *Drosophila*. *Development* **140**, 4730-4739.
Moeller, M. E., Nagy, S., Gerlach, S. U., Soegaard, K. C., Danielsen, E. T., Texada, M. J. and Rewitz, K. F. (2017). Warts signaling controls organ and body growth through regulation of ecdysone. *Curr. Biol.* **27**, 1652-1659.e4.
Nijhout, H. F., Riddiford, L. M., Mirth, C., Shingleton, A. W., Suzuki, Y. and Callier, V. (2014). The developmental control of size in insects. *Wiley Interdiscip. Rev. Dev. Biol.* **3**, 113-134.
Niwa, R., Sakudoh, T., Namiki, T., Saida, K., Fujimoto, Y. and Kataoka, H. (2005). The ecdysteroidogenic P450 Cyp302a1/disembodied from the silkworm, Bombyx mori, is transcriptionally regulated by prothoracicotropic hormone. *Insect Mol. Biol.* **14**, 563-571.
Niwa, R., Namiki, T., Ito, K., Shimada-Niwa, Y., Kiuchi, M., Kawaoka, S., Kayukawa, T., Banno, Y., Fujimoto, Y., Shigenobu, S. et al. (2010). Non-molting glossy/shroud encodes a short-chain dehydrogenase/reductase that functions in the 'Black Box' of the ecdysteroid biosynthesis pathway. *Development* **137**, 1991-1999.
Noguti, T., Adachi-Yamada, T., Katagiri, T., Kawakami, A., Iwami, M., Ishibashi, J., Kataoka, H., Suzuki, A., G[illegible], M. and Ishizaki, H. (1995). Insect prothoracicotropic hormone: a new member of the vertebrate growth factor superfamily. *FEBS Lett.* **376**, 251-256.
Ohhara, Y., Kobayashi, S. and Yamanaka, N. (2017). Nutrient-dependent endocycling in steroidogenic tissue dictates timing of metamorphosis in *Drosophila melanogaster*. *PLoS Genet.* **13**, e1006583.
Ou, Q., Magico, A. and King-Jones, K. (2011). Nuclear receptor DHR4 controls the timing of steroid hormone pulses during *Drosophila* development. *PLoS Biol.* **9**, e1001160.
Parker, N. F. and Shingleton, A. W. (2011). The coordination of growth among *Drosophila* organs in response to localized growth-perturbation. *Dev. Biol.* **357**, 318-325.
Parvy, J.-P., Blais, C., Bernard, F., Warren, J. T., Petryk, A., Gilbert, L. I., O'Connor, M., B. and Dauphin-Villemant, C. (2005). A role for betaFTZ-F1 in regulating ecdysteroid titers during post-embryonic development in *Drosophila melanogaster*. *Dev. Biol.* **282**, 84-94.
Popoff, M. R. and Poulain, B. (2010). Bacterial toxins and the nervous system: neurotoxins and multipotential toxins interacting with neuronal cells. *Toxins* **2**, 683-737.
Prout, T. and Mcchesney, F. (1985). Competition among immatures affects their adult fertility: population dynamics. *Am. Nat.* **126**, 521-558.
Rewitz, K. F. and O'Connor, M. B. (2011). Timing is everything: PTTH mediated DHR4 nucleocytoplasmic trafficking sets the tempo of *Drosophila* steroid production. *Front. Endocrinol.* **2**, 108.
Rewitz, K. F., Yamanaka, N., Gilbert, L. I. and O'Connor, M. B. (2009). The insect neuropeptide PTTH activates receptor tyrosine kinase torso to initiate metamorphosis. *Science* **326**, 1403-1405.
Rewitz, K. F., Yamanaka, N. and O'Connor, M. B. (2013). Developmental checkpoints and feedback circuits time insect maturation. *Curr. Top. Dev. Biol.* **103**, 1-33.
Rodrigues, M. A., Martins, N. E., Balancé, L. F., Broom, L. N., Dias, A. J. S., Fernandes, A. S. D., Rodrigues, F., Sucena, E. and Mirth, C. K. (2015). *Drosophila melanogaster* larvae make nutritional choices that minimize developmental time. *J. Insect Physiol.* **81**, 69-80.
Rybczynski, R. and Gilbert, L. I. (1995). Prothoracicotropic hormone elicits a rapid, developmentally specific synthesis of beta tubulin in an insect endocrine gland. *Dev. Biol.* **169**, 15-28.
Schering, J. F., Davis, D. G., Ranashinghe, A. and Teeare, C. A. (1984). Effects of larval crowding on life history parameters in *Drosophila melanogaster*. *Exp. Gerontol.* **77**, 329-332.
Selcho, M., Millán, C., Palacios-Muñoz, A., Ruf, F., Ubillo, L., Chen, J., Bergmann, G., Ito, C., Silva, V., Wegener, C. et al. (2017). Central and peripheral clocks are coupled by a neuropeptide pathway in *Drosophila*. *Nat. Commun.* **8**, 15563.
Shimada-Niwa, Y. and Niwa, R. (2014). Serotonergic neurons respond to nutrients and regulate the timing of steroid hormone biosynthesis in *Drosophila*. *Nat. Commun.* **5**, 5778.
Shingleton, A. W., Frankino, W. A., Flatt, T., Nijhout, H. F. and Emlen, D. J. (2007). Size and shape: the developmental regulation of static allometry in insects. *BioEssays* **29**, 536-548.
Siegmund, T. and Korge, G. (2001). Innervation of the ring gland of *Drosophila melanogaster*. *J. Comp. Neurol.* **431**, 481-491.
Stieper, B. C., Kupershtok, M., Driscoll, M. V. and Shingleton, A. W. (2008). Imaginal discs regulate developmental timing in *Drosophila melanogaster*. *Dev. Biol.* **321**, 18-26.
Tennessen, J. M. and Thummel, C. S. (2011). Coordinating growth and maturation – insights from *Drosophila*. *Curr. Biol.* **21**, R750-R757.
Uchibori-Asano, M., Kayukawa, T., Sezutsu, H., Shinoda, T. and Daimon, T. (2017). Severe developmental timing defects in the prothoracicotropic hormone (PTTH)-deficient silkworm, Bombyx mori. *Insect Biochem. Mol. Biol.* **87**, 14-25.
Vallejo, D. M., Juarez-Carreño, S., Bolivar, J., Morante, J. and Dominguez, M. (2015). A brain circuit that synchronizes growth and maturation revealed through Dilp8 binding to Lgr3. *Science* **350**, aac6767.
Walkiewicz, M. A. and Stern, M. (2009). Increased insulin/insulin growth factor signaling advances the onset of metamorphosis in *Drosophila*. *PLoS ONE* **4**, e5072.
Warren, J. T., Yerushalmi, Y., Shimell, M. J., O'Connor, M. B., Restifo, L. L. and Gilbert, L. I. (2006). Discrete pulses of molting hormone, 20-hydroxyecdysone, during late larval development of *Drosophila melanogaster*: correlations with changes in gene activity. *Dev. Dyn.* **235**, 315-326.
Williams, C. M. (1952). Physiology of insect diapause. IV. The brain and prothoracic glands as an endocrine system in the Cecropia Silkworm. *Biol. Bull.* **103**, 120-138.
Yamanaka, N., Rewitz, K. F. and O'Connor, M. B. (2013a). Ecdysone control of developmental transitions: lessons from *Drosophila* research. *Annu. Rev. Entomol.* **58**, 497-516.
Yamanaka, N., Romero, N. M., Martin, F. A., Rewitz, K. F., Sun, M., O'Connor, M. B. and Leopold, P. (2013b). Neuroendocrine control of *Drosophila* larval light preference. *Science* **341**, 1113-1116.
Yamanaka, N., Marqués, G. and O'Connor, M. B. (2015). Vesicle-mediated steroid hormone secretion in *Drosophila melanogaster*. *Cell* **163**, 907-919.
Yoshiyama, T., Namiki, T., Mita, K., Kataoka, H. and Niwa, R. (2006). Neverland is an evolutionally conserved Rieske-domain protein that is essential for ecdysone synthesis and insect growth. *Development* **133**, 2565-2574.

APPENDIX II. Dpp signaling regulates developmental response to nutrient restriction in *Drosophila*.

Linda Setiawan, **Xueyang Pan**, Alexis L Woods, Michael B O'Connor, Iswar K Hariharan. 2018. The BMP2/4 ortholog Dpp can function as an inter-organ signal that regulates developmental timing. *Life Science Alliance*. 1: e201800216.

Decapentaplegic (Dpp), a *Drosophila* homolog of mammalian BMP2/4, functions in a series of developmental events (review, see (Upadhyay et al., 2017)). In the study described in this appendix, Setiawan et al. demonstrated that Dpp signaling plays an important role in developmental timing control through inter-organ communication between imaginal discs and the PG. In early L3 stage, imaginal disc derived Dpp are released from the disc and subsequently signal to the PG systemically to suppress ecdysone biosynthesis in the PG. As larva grows, more Dpp molecules are trapped within the discs which results in a decrease of circulating Dpp concentration. In this way, the systemic Dpp signaling reflects the growth status of the imaginal discs and coordinates developmental timing with peripheral tissue growth (Setiawan et al., 2018).

In this study, we firstly found that constitutively high level of systemic Dpp signaling resulted in delayed developmental transition of the animal (Setiawan et al., 2018, Figure 2). Then we sought to test whether suppression of the signaling caused any developmental timing change. It turned out that suppression of the signaling did not accelerate development but abrogated the critical weight checkpoint which controls the larval response to nutrient restriction (Setiawan et al., 2018, Figure 5). I set up the crosses and carried out the critical weight estimation assay. The results showed that knocking down of Mad, the key downstream signaling molecule of the Dpp signaling, cause precocious pupariation of undersized larvae during starvation, indicating a failure of body weight sensing in the animals (Setiawan et al., 2018, Figure 5F-5L). These data

demonstrate that the Dpp signaling is required for body weight sensing and the determination of the nutritional checkpoint.

A full reprint of the article is included in Appendix II.

Published Online: 19 November, 2018 | Supp Info: http://doi.org/10.26508/lsa.201800216
Downloaded from life-science-alliance.org on 19 June, 2019

Research Article

TRANSPARENT PROCESS OPEN ACCESS Life Science Alliance

The BMP2/4 ortholog Dpp can function as an inter-organ signal that regulates developmental timing

Linda Setiawan[1], Xueyang Pan[2], Alexis L Woods[1], Michael B O'Connor[2], Iswar K Hariharan[1]

Developmental transitions are often triggered by a neuroendocrine axis and can be contingent upon multiple organs achieving sufficient growth and maturation. How the neurodendocrine axis senses the size and maturity of peripheral organs is not known. In *Drosophila* larvae, metamorphosis is triggered by a sharp increase in the level of the steroid hormone ecdysone, secreted by the prothoracic gland (PG). Here, we show that the BMP2/4 ortholog Dpp can function as a systemic signal to regulate developmental timing. Dpp from peripheral tissues, mostly imaginal discs, can reach the PG and inhibit ecdysone biosynthesis. As the discs grow, reduced Dpp signaling in the PG is observed, consistent with the possibility that Dpp functions in a checkpoint mechanism that prevents metamorphosis when growth is insufficient. Indeed, upon starvation early in the third larval instar, reducing Dpp signaling in the PG abrogates the critical-weight checkpoint which normally prevents pupariation under these conditions. We suggest that increased local trapping of morphogen within tissues as they grow would reduce circulating levels and hence provide a systemic readout of their growth status.

DOI 10.26508/lsa.201800216 | Received 15 October 2018 | Revised 6 November 2018 | Accepted 7 November 2018 | Published online 19 November 2018

Introduction

Organismal development is often orchestrated by a neuroendocrine axis, such as the hypothalamic–pituitary axis in mammals. Mechanisms likely exist by which the growth and maturation of peripheral organs are monitored by the neuroendocrine axis before important developmental transitions. In most cases, these mechanisms remain undefined. The onset of metamorphosis in *Drosophila* is a dramatic developmental transition which lends itself to genetic analysis (reviewed by Yamanaka et al [2013], Boulan et al [2015]). The larva is capable of feeding and hence acquiring additional nutrients for growth until it achieves its final size. In contrast, the pupa is essentially a closed system where any new growth and tissue remodeling can only occur either by mobilizing stored nutrients or by the breakdown of larval tissues. The mechanisms by which *Drosophila* larvae assess their growth and maturity before committing to metamorphosis are of considerable interest because they might suggest principles that govern the relationship between growth and developmental timing in diverse organisms.

The endocrine gland that regulates the timing of metamorphosis in *Drosophila* is the ring gland (Fig 1A), which is composed of three main parts (King et al, 1966). The prothoracic gland (PG) secretes the steroid hormone ecdysone, the corpus allatum (CA) secretes juvenile hormone (JH), and the corpora cardiaca (CC) are neurosecretory cells that secrete adipokinetic hormone (AKH) (discussed in Christesen et al [2017]). During the third larval instar, entry into metamorphosis is characterized by a decline in JH levels and a steep increase in the level of ecdysone. In *Drosophila* at least, changes in JH levels do not seem to have a major effect on the timing of pupariation, whereas ecdysone levels seem crucial (Riddiford et al, 2010; Boulan et al, 2015). In the PG, multiple cytochrome P450 enzymes, encoded by the Halloween genes, convert cholesterol to ecdysone (Petryk et al, 2003; Gilbert, 2004; Warren et al, 2004; Ono et al, 2006). Larval molts and the onset of pupariation are each preceded by distinct peaks of circulating ecdysone secreted by the PG. The PG is innervated by two neurons in each brain lobe; the release of the peptide, prothoracicotropic hormone (PTTH), by these neurons stimulates ecdysone production by the PG via the PTTH receptor Torso (Rewitz et al, 2009) and the Ras/MAPK signaling pathway (Caldwell et al, 2005). In *Drosophila* and in other insects such as *Manduca*, production of PTTH seems to be set in motion by achievement of a critical size or some correlate thereof (reviewed in Nijhout et al [2014], Boulan et al [2015]) and is dependent on circadian rhythms (Di Cara & King-Jones, 2016). Critical weight (CW) is defined as the minimum larval weight after which starvation no longer delays metamorphosis (Beadle et al, 1938; Mirth et al, 2005; Stieper et al, 2008). Indeed, once larvae are above CW (estimated to be approximately 0.8 mg in *Drosophila*), a mild acceleration to metamorphosis is often observed following starvation (Stieper et al, 2008). A related parameter is the minimum viable weight (MVW), which is operationally defined as the minimal weight required for 50% of larvae to survive to a particular developmental stage when starved (Mirth et al, 2005). The minimal viable weights needed for pupariation (MVW(P)) and eclosion (MVW

[1]Department of Molecular and Cell Biology, University of California, Berkeley, CA, USA [2]Department of Genetics, Cell Biology, and Development, University of Minnesota, Minneapolis, MN, USA

Correspondence: ikh@berkeley.edu

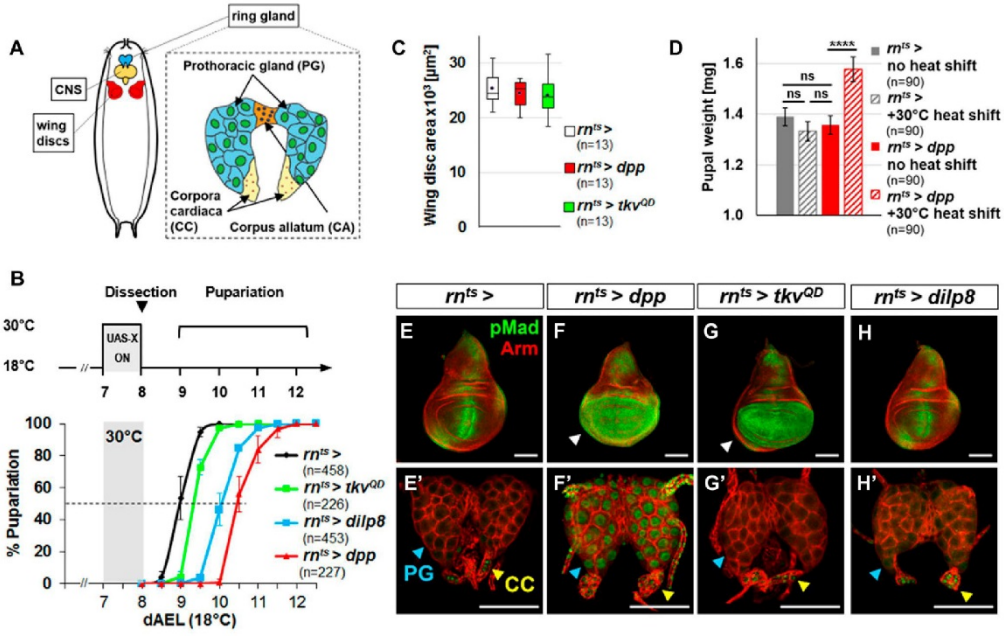

Figure 1. Expression of Dpp in peripheral tissues induces Dpp signaling in the PG and delays pupariation.
(A) Schematic of the larval ring gland. **(B)** Pupariation delay after a 24 h pulse of expression 7 d AEL induced by heat shift to 30°C: rn^{ts}>*dpp* 36.5 ± 3.5 h; rn^{ts}>tkv^{QD} 9.5 ± 3.0 h and rn^{ts}>*dilp8* 26.0 ± 3.7 h. **(C)** Areas of wing discs dissected after 24 h of expression. **(D)** Pupal weights without heat shift: rn^{ts}> 1.39 ± 0.04 mg; rn^{ts}>*dpp* 1.36 ± 0.04 mg. Pupal weights after 24 h of expression: rn^{ts}> 1.33 ± 0.04 mg; rn^{ts}>*dpp* 1.58 ± 0.05 mg. **(E–H)** Wing discs (E–H) and ring glands **(E′–H′)** dissected after 24 h pulse of expression. Nuclear pMad is observed in the PG (blue arrowhead) in rn^{ts}>*dpp*, and in all genotypes in the CC (yellow arrowhead) and not in the CA. Data information: Error bars indicate standard deviations. ns, not significant; ***P < 0.001; ****P < 0.0001. Scale bars = 100 μm.

(E)) in *Drosophila* are approximately 0.68 mg and 0.98 mg, respectively (Stieper et al, 2008). The mechanism by which the size or weight of the *Drosophila* larva can impede or permit progression to the pupal stage is not known.

A major promoter of larval growth is the insulin signaling pathway. In parallel to its effects on other larval tissues, insulin receptor (InR)–mediated signaling in PG cells promotes ecdysone release (Colombani et al, 2005; Mirth et al, 2005). InR signaling may be necessary for the pulses of ecdysone production that occur during larval development and the large increase in ecdysone that drives the onset of metamorphosis. InR signaling promotes ecdysone production, in significant part, by cytoplasmic retention of the transcription factor FOXO (Koyama et al, 2014) and inhibition of the synthesis or action of the microRNA *bantam* in the cells of the PG (Boulan et al, 2013). This requirement of InR signaling for metamorphosis to occur appears necessary only before the attainment of CW. After that point, a reduction in InR activity no longer delays the timing of pupariation (Shingleton et al, 2005). This is consistent with a scenario where nutrient availability and the consequent growth need to reach a threshold value to drive this developmental transition. Conversely, under conditions of starvation, circulating Hedgehog made by enterocytes delays metamorphosis by inhibiting ecdysone production by the PG (Rodenfels et al, 2014). Thus, the availability of food and its consequences can impact developmental timing in multiple ways. In addition, the Activin pathway also promotes the competence of the PG to respond to insulin and PTTH (Gibbens et al, 2011). Thus, multiple inputs seem capable of influencing developmental timing via a variety of diffusible signals that reach the PG. Within the PG, there is clearly crosstalk between these different pathways in ways that are not yet fully understood.

The growth status of imaginal discs, the larval primordia of adult structures such as wings and eyes, can also influence developmental timing. Although the complete absence of imaginal discs does not result in a change in developmental timing, growth abnormalities in imaginal discs can delay pupariation (reviewed in Jaszczak et al [2016]). Damaged or overgrown imaginal discs secrete the insulin/relaxin family member Dilp8 (Colombani et al, 2012; Garelli et al, 2012), which binds to receptors in the nervous system and PG (Colombani et al, 2015; Garelli et al, 2015; Vallejo et al, 2015; Jaszczak et al, 2016) and inhibits ecdysone production. Imaginal discs that grow slowly, as occurs in *Minute* mutants, also delay pupariation (Stieper et al, 2008; Parker & Shingleton, 2011). It is unclear whether this happens because of the growth status of discs or because disruptions in cell physiology elicited by *Minute* mutations activate a cellular stress response (Lee et al, 2018). A key unanswered question is whether

there is a mechanism that operates under normal physiological conditions to coordinate imaginal disc growth and maturation with entry into metamorphosis.

Here, we show that the morphogen Dpp, the *Drosophila* BMP2/4 ortholog, which has been studied extensively for its role in regulating growth and patterning within tissues, can also diffuse between tissues, such as between imaginal discs and the PG. Dpp signaling in the PG can negatively regulate ecdysone production, and moreover decreases as larvae approach metamorphosis. Our results suggest a role for Dpp as an inter-organ signal in the larva that regulates the timing of metamorphosis and has a role in the CW checkpoint.

Results

Dpp expressed in peripheral tissues can delay pupariation

The BMP2/4 ortholog, Dpp, functions as a morphogen to regulate growth and patterning within many tissues including imaginal discs (Hamaratoglu et al, 2014). We examined the effects of temporarily increasing *dpp* expression during the early third larval instar (L3) using *rn-Gal4* and a temperature-sensitive repressor, $Gal80^{ts}$ (hereafter rn^{ts}>*dpp*) (Fig 1B). *rn-Gal4* is expressed in wing discs and also some other tissues as assessed by the G-trace method (Evans et al, 2009) (Fig S1A). Under the conditions of this experiment, rn^{ts}>*dpp* did not increase wing disc size (Fig 1C) or adult wing size (not shown) but markedly delayed pupariation (Fig 1B) resulting in larger pupae, likely because of an extended growth phase (Fig 1D). Surprisingly, an activated form of the Dpp receptor Thickveins (Tkv^{QD}) (Nellen et al, 1996), (rn^{ts}>tkv^{QD}), which functions in cells autonomously and also does not affect disc size, elicited only a modest delay (Fig 1B and C). Consistent with the known ability of Dpp to spread within tissues, expression of *dpp*, but not tkv^{QD}, increased Dpp signaling beyond the wing pouch in the wing disc, as assessed by increased nuclear phosphorylated Mad (pMad) (Fig 1E–G, arrowheads in Fig 1F and G).

Because of the dramatic effects on pupariation timing caused by a relatively brief increase in *dpp* expression, we wondered whether Dpp could have effects on the ring gland. We therefore examined ring glands in these larvae for alterations in Dpp signaling. Within the ring gland, we observed increased levels of nuclear pMad in the PG with rn^{ts}>*dpp* but not rn^{ts}>tkv^{QD} (Fig 1E′–G′). Nuclear pMad was observed in the CC in all genotypes examined (Fig 1E′–G′). Because *rn-Gal4* is not expressed in the ring gland (Fig S1A), these observations suggest that Dpp might be reaching the ring gland from another location. One possibility is the central nervous system (CNS) because the ring gland is known to be innervated and because *rn-Gal4* is also expressed in the CNS (Fig S1A). However, when neuronal expression of *rn-Gal4* was prevented using *elav-Gal80*, there was no alleviation of the delayed pupariation, nuclear localization of pMad in the PG, or increased pupal size (Fig S1B–I). Thus, the Dpp that reaches the PG in these experiments is likely produced by more distant nonneuronal cells. Indeed, we found that when *dpp* was overexpressed in a variety of peripheral tissues using different driver lines, pupariation was always delayed suggesting that Dpp can reach the PG from a variety of locations in the larva (Fig S2A–G).

The insulin/relaxin-family member Dilp8 is produced by imaginal discs in response to injury, cell death, or various types of overgrowth. Although we did not observe disc overgrowth under the conditions of our experiment (Fig 1C), it is nevertheless possible that the presence of inappropriate amounts of Dpp could have promoted Dilp8 production, raising the possibility that Dpp delayed pupariation indirectly via Dilp8 production. rn^{ts}>*dpp* or rn^{ts}>tkv^{QD} caused little cell death and only a modest level of *dilp8* expression (Fig S3A–F). Moreover, rn^{ts}>*dpp* delayed pupariation even more than rn^{ts}>*dilp8* (Fig 1B) suggesting that *dpp* does not function upstream of *dilp8*. Conversely, rn^{ts}>*dilp8* did not affect nuclear pMad in the wing disc or PG (Fig 1H and H′) indicating that Dilp8 does not activate Dpp signaling. Most importantly, rn^{ts}>*dpp* delayed pupariation in a *dilp8* mutant implying that Dpp can function independently of *dilp8* (Fig S3G). Taken together, these observations suggest that Dpp and Dilp8 induce delays in pupariation by separate pathways.

If Dpp reaching the ring gland is the cause of the delayed pupariation, then activating Dpp signaling autonomously in the ring gland should also delay pupariation. To test this hypothesis, we expressed tkv^{QD} using the ring gland driver *P0206-Gal4* (Colombani et al, 2005) and found that it delayed pupariation and increased pupal mass (Fig 2A–C). When we examined each component of the ring gland separately, pupariation was delayed using *phm-Gal4*, a PG-specific driver (Ono et al, 2006), but not using the *Aug21-Gal4* driver which is expressed in the CA (Adam et al, 2003) or the *AKH-Gal4* driver which is expressed in the CC (Fig 2D and E) (Lee & Park, 2004). All of these observations, taken together, point to the possibility that Dpp can reach the PG from peripheral tissues and that increased Dpp signaling in the PG can delay pupariation.

Dpp expressed in peripheral tissues can reach the PG

To test more directly whether Dpp expressed in peripheral tissues could reach the PG, we used the *GFP-dpp* transgene that encodes a form of Dpp tagged with GFP which can activate Dpp signaling. When *GFP-dpp* (Entchev et al, 2000) was expressed using *rn-Gal4* (rn^{ts}>*GFP-dpp*), both GFP and nuclear pMad were detected in the PG but not in the immediately adjacent CA (Fig 3A and B) suggesting that its accumulation in the PG and the activation of the signaling pathway is dependent on binding to specific receptors. A different GFP-tagged secreted protein, atrial natriuretic factor (ANF-GFP) (Rao et al, 2001), expressed under the same conditions, was not detected in the PG (Fig 3C and D). Consistent with the possibility that Dpp can circulate in the hemolymph, a processed form of GFP-Dpp was detected in the hemolymph of rn^{ts}>*GFP-dpp* larvae (Fig 3E).

To determine whether Dpp can diffuse from discs to the PG in the absence of other tissues, we co-cultured rn^{ts}>*GFP-dpp* discs with wild type ring glands Fig 3F and G). Nuclear pMad was observed in the PG portion of those ring glands indicating that Dpp can diffuse from discs to the PG ex vivo. Nuclear pMad was not observed in the PG portion of ring glands cultured alone. Addition of hemolymph from rn^{ts}>*dpp* larvae was sufficient to elicit pMad nuclear localization (Fig 3H) indicating the presence of functional Dpp in the hemolymph of those larvae. Thus, Dpp can diffuse from discs to the hemolymph and from the hemolymph to the PG.

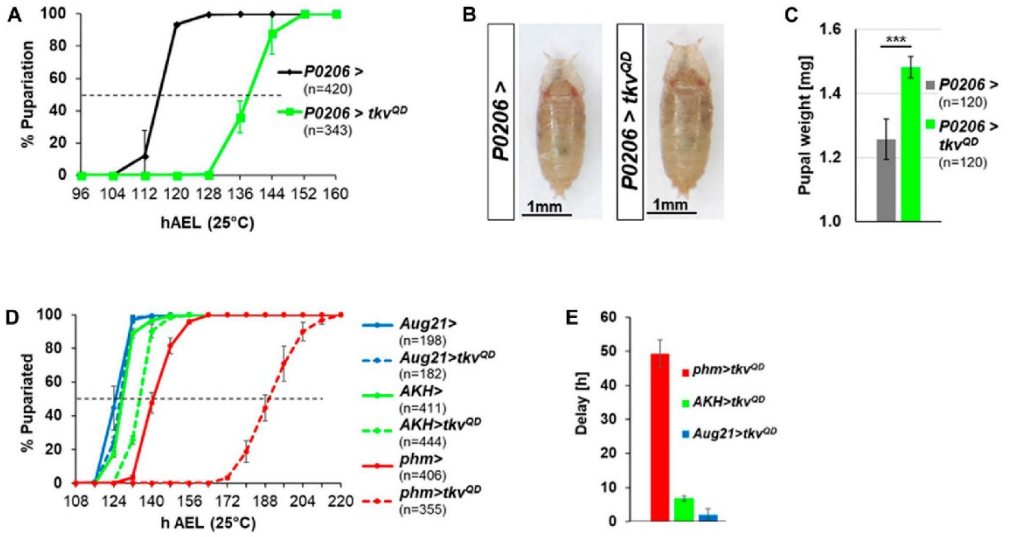

Figure 2. Cell-autonomous Dpp signaling in the PG delays pupariation and increases organismal size.
(A) *P0206>tkv*^{QD} has a 22.2 ± 2.1 h developmental delay. **(B)** Representative pupae of *P0206>* and *P0206>tkv*^{QD}. **(C)** Pupal weights are *P0206* > 1.26 ± 0.06 mg; *P0206>tkv*^{QD} 1.48 ± 0.03 mg. **(D)** Effect of expressing *tkv*^{QD} in different parts of the ring gland on pupariation timing. *phm-Gal4* drives expression in the PG; *AKH-Gal4* is expressed in the CC; *Aug21-Gal4* is expressed in the CA. Mean pupariation times are: *phm* > 140.3 ± 1.5 h; *phm>tkv*^{QD} 189.7 ± 2.5 h; *Aug21* > 124.3 ± 1.5 h; *Aug21>tkv*^{QD} 126.3 ± 0.6 h; *AKH* > 127.8 ± 0.3 h; and *AKH>tkv*^{QD} 134.7 ± 0.6 h. **(E)** Pupariation delays are shown in (D), normalized to the corresponding *Gal4* driver line alone: *phm>tkv*^{QD} 49.3 ± 4.0 h; *Aug21>tkv*^{QD} 2.0 ± 1.7 h; *AKH>tkv*^{QD} 6.8 ± 0.8 h. Data information: Error bars indicate standard deviations. ***$P < 0.001$. Scale bars = 1 mm.

If the Dpp receptor Tkv is indeed expressed in cells of the PG, then inactivating it in those cells should block the ability of Dpp in the hemolymph to activate the signaling pathway. To examine this possibility, we constitutively expressed *GFP-dpp* in discs using the lexOp-GAD system using *ap-GAD* and *lexOp-EGFP::dpp* (Fig 3I–M). Concurrently, we expressed *UAS-tkv*^{RNAi} in cells of the PG using *phm-Gal4*. Expression of *tkv*^{RNAi} in the PG-blocked Dpp signaling as assessed by the absence of nuclear pMAD staining. Thus, Tkv is necessary in cells of the PG to mediate the response of Dpp secreted by disc cells.

Dpp signaling in the PG is developmentally regulated

Our experiments thus far indicate that Dpp expressed at increased levels in a variety of tissues including discs can diffuse to the PG and activate the signaling pathway via Tkv. What could be the physiological function of a pathway where Dpp from peripheral tissues acts on the PG to delay development? One possibility is that like Dilp8, Dpp is released from tissues such as imaginal discs under conditions of damage or overgrowth. To address this possibility, we induced apoptosis in discs either by targeted expression of the pro-apoptotic gene *eiger* (*egr*) or *reaper* (*rpr*) or with X-ray irradiation of larvae (Fig S4A–C and E–G). In all cases, we observed increased Dilp8 production in imaginal discs, but no increase in nuclear pMad in the PG. This was also the case with overgrown discs in *discs large* (*dlg*) hemizygotes (Woods & Bryant, 1991) (Fig S4D and H). Thus, Dpp signaling is not activated in the PG in response to tissue damage or overgrowth and is therefore unlikely to function in a mechanism that slows development under those conditions.

To address a role for Dpp signaling in the PG during normal development, we extended our analysis to include ring glands at earlier time points during the final larval stage (L3) by visualizing nuclear pMad (Fig 4A–C) and two reporters, *dad-RFP* (Wartlick et al, 2011) (Fig 4D–I) and *brk-GFP* (Dunipace et al, 2013) (Fig 4D–F and J–L). *dad-RFP* expression increases with Dpp signaling, whereas *brk-GFP* expression increases as Dpp signaling decreases. In contrast to the PG in late L3 (120 h after egg lay [AEL]), we observed strong nuclear pMad in the PG in early L3 (72 h AEL). As larvae progress through L3, the levels of nuclear pMad and expression of *dad-RFP* decrease, whereas *brk-GFP* expression increases. Together, these observations indicate that Dpp signaling progressively decreases during the course of L3 in the PG. By comparison, Dpp signaling was consistently high in the CC (Fig 4A–C) and consistently low in the CA (Fig 4J–L). When Dpp signaling was reduced in the CC by overexpression of *dad*, pMad staining was reduced as well (Fig S5), indicating that it was unlikely to be a result of the anti-pMad antibody binding to another epitope. To our knowledge, the role of Dpp signaling in the CC is not known.

Dpp signaling in the PG inhibits expression of ecdysone biosynthesis enzymes

The biosynthesis of ecdysone from cholesterol requires a number of enzymes encoded by genes known as the Halloween genes. In the

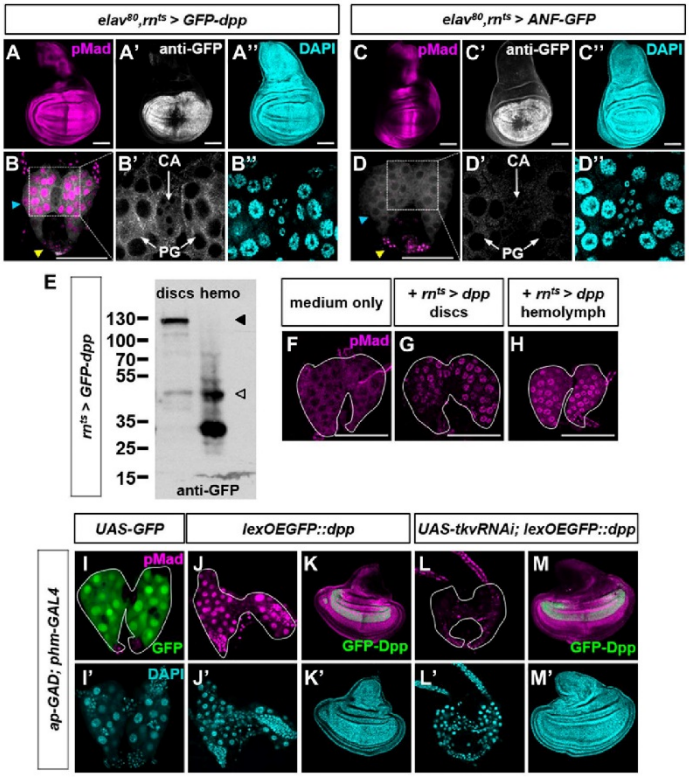

Figure 3. Dpp can diffuse from peripheral tissues via the hemolymph to the PG and activate signaling via the Tkv receptor.
(A, B) *elav-Gal80 rn^{ts}>GFP-dpp* wing disc **(A, A″)** and ring gland **(B, B″)**. Note GFP in PG but not CA **(B′)**. The blue arrowhead indicates PG and the yellow arrowhead indicates CC. **(C, D)** *elav-Gal80 rn^{ts}>ANF-GFP* wing disc **(C–C″)** and ring gland **(D–D″)**. **(E)** Western blot of *rn^{ts}>GFP-dpp* discs and hemolymph. Predicted unprocessed (filled arrowhead) and processed (unfilled arrowhead) forms. **(F–H)** Ex vivo cultured wild-type ring glands co-cultured with wing discs (G) and hemolymph (H) from *rn^{ts}>dpp* larvae. **(I–M)** Constitutive and simultaneous expression of *ap-GAD* in the dorsal wing disc and *phm-Gal4* in the PG. **(I, I′)** *UAS-GFP* confirms expression in the PG. *lexOEGFP::dpp* induces pMad activation in the PG **(J)** and local pMad and overgrowth in the wing disc **(K)**. However, no pMad activation occurs in the PG during simultaneous Tkv knockdown **(L)** despite the same local pMad and overgrowth in the wing disc **(M)** where Tkv is not knocked down. Data information: Scale bars = 100 μm.

wild-type PG, the levels of these enzymes increase toward the end of L3 as Dpp signaling decreases. Their up-regulation is known to occur, in significant part, at the level of transcription. To examine the consequence of changes in Dpp signaling in the PG, we examined the expression of several ecdysone biosynthesis enzymes (Ou & King-Jones, 2013) in FLP-out clones with altered Dpp signaling (Fig 5A). In early L3, when Dpp signaling is high, reducing Dpp signaling by overexpressing *dad* (Tsuneizumi et al, 1997) increased expression of Disembodied (Dib) (Fig 5B) or, to a lesser extent, Shadow (Sad) (Fig S6A) when compared with adjacent wild-type cells. In late L3, when cells in the PG have lower levels of Dpp signaling, augmenting Dpp signaling with activated Tkv reduced expression of Dib (Fig 5C), Shadow (Sad), Spookier (Spok), and Phantom (Phm) (Fig S6B–D). Thus, Dpp signaling in the PG negatively regulates the expression of multiple ecdysone biosynthesis enzymes. As a consequence, when Dpp signaling decreases in late L3, this would be expected to alleviate the repression of Halloween genes and allow an increase in ecdysone biosynthesis and hence entry into metamorphosis.

These findings suggest that the mechanism by which artificially increasing Dpp signaling in the PG delays pupariation is, at least in part, by reducing the levels of enzymes required for ecdysone biosynthesis. If so, then providing exogenous ecdysone might overcome this limitation. Feeding larvae the active form of ecdysone, 20-Hydroxyecdysone (20E) reduced the delay in pupariation caused by increased Dpp signaling in the PG (Fig 5D) and also reduced the delay-induced increase in pupal mass (Fig 5E).

Reducing Dpp signaling in the PG has minor effects under fed conditions but abrogates the critical-weight checkpoint under conditions of starvation

Because reducing Dpp signaling in the PG in early L3 increased expression of at least a subset of Halloween genes (Figs 5B and S6A), it could potentially also result in early pupariation. We have previously shown that expression of *UAS-tkv^{RNAi}* in the PG using *phm-Gal4* can prevent the increase in Dpp signaling elicited by overexpression of Dpp in discs (Fig 3L). Thus, at endogenous levels of Dpp expression, *phm>tkv^{RNAi}* larvae would be expected to have reduced levels of Dpp signaling in the PG. We tested different *tkv^{RNAi}* and *Mad^{RNAi}* lines, a dominant-negative form of *tkv* (*tkv^{D95K}*), or *dad* expressed using *phm-Gal4* (Fig S7A–C). In all cases, the larvae developed normally through all three instars, and we did not

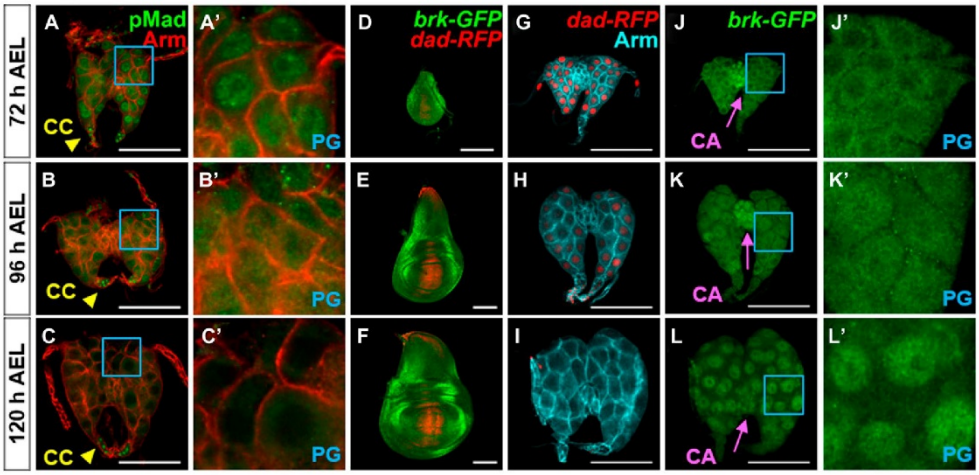

Figure 4. Dpp signaling in the PG decreases during L3.
(A–C) Ring glands at 72, 96, and 120 h ALL at 25°C. **(A′–C′)** Blue boxed region showing PG cells at higher magnification. **(D–F)** Wing discs expressing *dad-RFP* and *brk-GFP*. **(G–I)** Ring glands expressing *dad-RFP*. **(J–L)** Same ring glands as in (G–I) expressing *brk-GFP*. **(J′–L′)** Blue boxed regions showing PG cells at higher magnification. Data information: Scale bars = 100 μm.

observe a robust and reproducible acceleration of pupariation or a reduction in pupal size that would be expected to be a consequence of premature pupariation. A subset of the lines tested elicited a modest (2–3 h) acceleration. However, given the variability of genetic backgrounds and the comparatively slow developmental timing of the *phm-Gal4* driver line on its own (Fig 2D and legend), it is difficult to evaluate the relevance of these small effects. Reducing the availability of Dpp ligand by dpp^{RNAi} expression using *dpp-Gal4* also did not induce precocious pupariation (Fig S7D). Overexpression of *brinker* (*brk*) in the PG, which would be expected to repress many Dpp target genes, arrested larvae in L2, yet caused wandering (prepupal) behavior (Fig S7E–Q). Although this observation is difficult to interpret, it is similar to the precocious metamorphosis observed with increased Activin signaling (Gibbens et al, 2011). Although we do not currently understand the mechanism underlying this L2 arrest, it may further illustrate how the Dpp and Activin signaling pathways act in opposite ways. Another possibility for this L2 arrest is that the overexpression of *brk* at this early stage may simply be toxic to the PG. Because of the small size of the ring gland at this early stage, we were unable to dissect and examine the PG for cell death. Taken together, our experiments do not provide convincing evidence that reducing Dpp signaling in the PG can accelerate the onset of pupariation and therefore suggest that reducing Dpp signaling in the PG may, in itself, be insufficient to trigger the onset of metamorphosis. However, because maintaining elevated levels of Dpp signaling in the PG delays pupariation, a reduction in Dpp signaling in late L3 is necessary, in combination with other signals, for timely metamorphosis.

Although disruption of Dpp signaling in the PG did not elicit a robust effect on developmental timing under fed conditions, we wondered if it had a role in mediating the CW or MVW checkpoints, both of which in *Drosophila* occur approximately 8 h after L3 ecdysis (AL3E). When larvae were starved beginning at 2 h AL3E, larvae carrying either the *phm-Gal4* or $UAS\text{-}Mad^{RNAi}$ transgene did not pupariate and instead arrested development as larvae (Fig 5F, G, and K). When the larvae were transferred to starvation conditions beginning at 4 h or 6 h AL3E, a pupariation delay was observed. When starvation was initiated after the 8 h AL3E, no delay in developmental timing was observed. This is consistent with the time when CW is reached. Strikingly, when $phm{>}Mad^{RNAi}$ larvae were moved to starvation conditions at 2 h AL3E, 72% were able to form pupae (Fig 5H) which were much smaller than $phm{>}Mad^{RNAi}$ pupae obtained under fed conditions (Fig 5L). An even greater percentage of larvae pupariated when starvation was commenced at 4 h or 6 h AL3E (Fig 5I). When starvation was commenced at 8 h AL3E, no developmental delay was observed in all genotypes. Most of the small $phm{>}Mad^{RNAi}$ pupae generated when starvation was commenced at 0–6 h AL3E did not develop to viable adults (Fig 5J). The small, subviable pupae observed under these conditions are similar to those observed when ecdysone is fed to larvae shortly after the L2/L3 ecdysis (Koyama et al, 2014). Thus, although reducing the level of Dpp signaling in the PG has only subtle effects when food is abundant, under conditions of starvation, it appears to abrogate a mechanism that functions to prevent larvae that have grown insufficiently from proceeding to pupariation.

Dpp signaling in the PG in early L3 requires Dpp expression in imaginal discs

To help identify the source of Dpp that reaches the PG, we expressed $UAS\text{-}dpp^{RNAi}$ using Gal4 drivers and examined pMad levels in the PG at 72 h AEL when nuclear pMad is normally

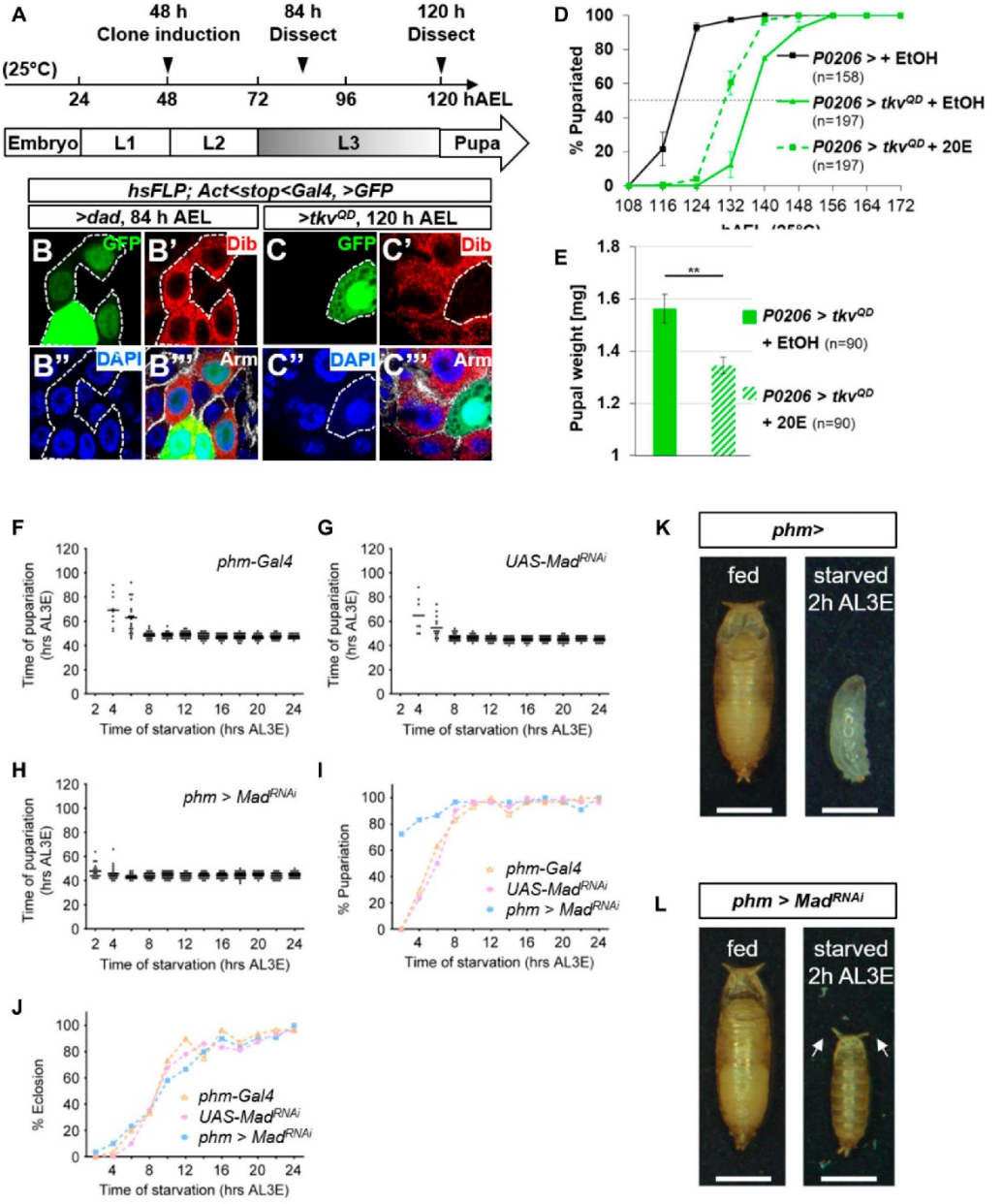

Figure 5. Dpp signaling in early L3 represses ecdysone biosynthesis enzymes and prevents precocious pupariation during starvation.
(A) Schematic of heat-shock clone induction experiments. Cultures were maintained at 25°C. FLP-out clones (*act<stop<Gal4*) were induced 48 h AFL. FLP-out clones in the PG show uneven expression of *UAS-GFP* possibly because of asynchrony of or variability in the number of endocycles between the individual polyploid cells of the PG. **(B, C)**

observed. The *dpp-Gal4* driver is expressed only in a subset of cells that express Dpp. Nevertheless, in *dpp-Gal4, UAS-dpp^{RNAi}* larvae, the level of nuclear pMad in the PG is greatly reduced (Fig 6A and B). Thus, the Dpp that reaches the PG must be produced by cells with current or past expression of *dpp-Gal4*. In addition, the ability of *dpp-Gal4, UAS-dpp^{RNAi}* to reduce pMad levels in the PG indicates that the pathway is indeed mostly being activated by Dpp and not by other ligands capable of activating the same signaling pathway such as Gbb (Haerry et al, 1998).

We used G-TRACE (Evans et al, 2009) to identify both current (RFP) and previous (GFP) expression of *dpp-Gal4* (Fig 6C–H). Expression was strongest in in imaginal discs (Figs 6C and Fig S8A–C), the salivary glands (Fig 6D), and some portions of the CNS (Fig 6E). Expression was not observed in the ring gland (Fig 6F), gut (Fig 6G), fat body (Fig 6H), or lymph gland (Fig S8D). Others have reported expression of a *dpp-Gal4* transgene in scattered cells in the gut of late L3 larvae (Denton et al, 2018) and therefore lower levels of expression may escape detection by this method. A previous study (Huang et al, 2011) reported the expression of a *dpp-lacZ* reporter in the CA of the ring gland. In that same study, *dpp* expression in the ring gland, measured using quantitative RT-PCR from total RNA prepared from ring glands, was reported to increase in late L3, peaking in wandering L3 larvae. We took advantage of stocks constructed recently where gene editing has been used to tag endogenous Dpp with an HA-tag (Bosch et al, 2017). Using anti-HA antibody, we detected Dpp in the stripe of Dpp producing cells in the wing disc and in cells of the CC even in late L3 ring glands (when no pMad is observed in the PG), but no expression in the PG or CA (Fig 6I and J). Furthermore, we could not detect expression of a *lacZ* reporter of *dpp* in the CA using three *different dpp-lacZ* lines obtained from the Bloomington *Drosophila* Stock Center (data not shown). Moreover, when we expressed *UAS-GFP-dpp* in the CC using the *AKH-Gal4* driver, we did not observe any pMad in the PG (Fig 6K and L) indicating that Dpp is unlikely to reach the PG from the CC. Expression of *UAS-GFP-dpp* in the CA using *Aug21-Gal4* resulted in pMad being observed only in PG cells immediately adjacent to the CA; uniform nuclear pMad throughout the PG was not observed (Fig 6M and N). These observations indicate that other portions of the ring gland are unlikely to produce the Dpp that reaches the PG. Importantly, because *dpp-Gal4* is not expressed in the ring gland and *dpp-Gal4, UAS-dpp^{RNAi}* can reduce pMad in the PG in early L3 larvae, the Dpp must mostly originate in tissues other than the ring gland.

In the CNS, *dpp-Gal4* is expressed in the optic lobes and parts of the ventral nerve cord (Fig 6E) and the PTTH-expressing neurons which innervate the PG (Fig S8E and E′). When using *dpp-Gal4* and *UAS-tdTom*, tdTom fluorescence can be visualized in the cell bodies of the PTTH neurons and the axonal branches that innervate the PG (Fig S8F) that show punctate staining with anti-PTTH (Fig S8F′). In the presence of *elav-Gal80*, these branches still show staining with anti-PTTH, but no longer have tdTom fluorescence (Fig S8G and G′) confirming the neuronal characteristics of these cells. However, expression of *GFP-dpp* in PTTH-producing neurons does not reach the PG nor is nuclear pMad observed in PG cells when *GFP-dpp* is expressed using *ptth-Gal4* (Fig S8H–K). In addition, expression of *dpp^{RNAi}* either using *elav-Gal4* (which is expressed in most neurons) (Fig S8L, M, and P) or *ptth-Gal4* does not reduce pMad expression in the PG (Fig S8N and O), indicating that the Dpp is unlikely to be from the PTTH neurons or other neurons.

Other than the CNS, *dpp-Gal4* is expressed in the salivary glands (Fig 6D) and in the imaginal discs (Figs 6C and S8A–C). However, *dpp* itself is not expressed in the salivary glands either in embryos (St Johnston & Gelbart, 1987) or in wandering L3 larvae (Brown et al, 2014). Taken together, these experiments suggest that the Dpp that reaches the PG is mostly from the imaginal discs. In support of this possibility is recent work that shows that Dpp is secreted basolaterally in imaginal discs, that it can reach the basement membrane, and, at least under conditions of overexpression, can reach distant pericardial cells (Harmansa et al, 2017; Ma et al, 2017). Our experiments, however, cannot exclude the possibility that Dpp is secreted into the hemolymph in a stage-dependent manner by a small population of cells that has escaped detection using our methods.

Interaction of Dpp signaling with pathways that regulate ecdysone production in the PG

Several signaling pathways have been shown to regulate ecdysone production by the PG, most notably the insulin-PI3K pathway (Colombani et al, 2005; Mirth et al, 2005), the Ras-MAPK pathway (Caldwell et al, 2005), the *bantam* microRNA (Boulan et al, 2013) and the Activin pathway (Gibbens et al, 2011). Each of these pathways can be manipulated to delay pupariation. To test whether these pathways delay pupariation by increasing Dpp signaling in the PG, we examined late L3 ring glands where either the insulin-PI3K, Ras, or Activin pathways were inhibited or where *ban* was overexpressed for alterations in pMad levels. None of these manipulations caused an increase in pMad in the PG indicating that these pathways do not delay pupariation by augmenting Dpp signaling (Fig 7A–F).

We then tested whether Dpp signaling could function upstream of any of these pathways. Signaling via the insulin-PI3K pathway results in the phosphorylation and cytoplasmic retention of the FOXO transcription factor. Activation of Dpp signaling in the PG resulted in increased levels of nuclear FOXO indicating that Dpp

FLP-out clones induced 48 h ALL, ring glands dissected 84 h ALL or 120 h ALL, examined for Disembodied (Dib) expression. **(B–B″)** GFP-expressing cells expressing the Dpp signal inhibitor Dad have enhanced Dib expression. **(C–C″)** GFP-expressing cells expressing the Dpp signal activator *UAS-tkv^{QD}* have lower Dib expression. **(D, E)** Effect of feeding 20-hydroxyecdysone (20E) to *P0206>tkv^{QD}* larvae. Mean pupariation times: *P0206>* +LtOH 119.0 ± 0.5 h; *P0206>tkv^{QD}* + LtOH 136.8 ± 0.3 h; *P0206>tkv^{QD}* 128.8 ± 2.9 h (D) and pupal weight (E). **(F–H)** Pupariation times of larvae that were initially raised on food and then starved beginning at different 2 h-interval time points after L3 ecdysis. Both *phm-Gal4* (F) and *UAS-Mad^{RNAi}* (G) larvae are not viable when starvation begins at 2 h AL3E and pupariate only after a delay when starved beginning at 4 h AL3E (median pupariation time is 68 h AL3E for *phm-Gal4* and 56 h AL3E for *UAS-Mad^{RNAi}*) or 6 h AL3E (median pupariation time is 62 h AL3E for *phm-Gal4* and 52 h AL3E for *UAS-Mad^{RNAi}*). Beginning at 8 h AL3E, starvation no longer induces a pupariation delay and the median pupariation times are between 47.5 h and 50 h AL3E for *phm-Gal4* and between 44 h and 46 h AL3E for *UAS-Mad^{RNAi}*; *phm>Mad^{RNAi}* (H) larvae are viable and able to pupariate when starvation begins at 2 h AL3E. At this and all following starvation time points, there is no delay and median pupariation times are between 44 h and 48 h AL3E (n = 28–32 for each time point). **(I)** Percentages of larval populations that pupariate (n = 28–32 for each time point). **(J)** Percentages of adult eclosion (n = 28–32 for each time point). **(K)** *phm-Gal4* larvae pupariate as wandering L3 larvae when continuously raised on food and do not pupariate when starved at 2 h AL3E. **(L)** *phm>Mad^{RNAi}* larvae pupariate as wandering L3 larvae when continuously raised on food and 72% of larvae form small early L3 pupae with everted spiracles (arrows) when starved at 2 h AL3E. Data information: $^{**}P < 0.01$. Scale bars are 1 mm.

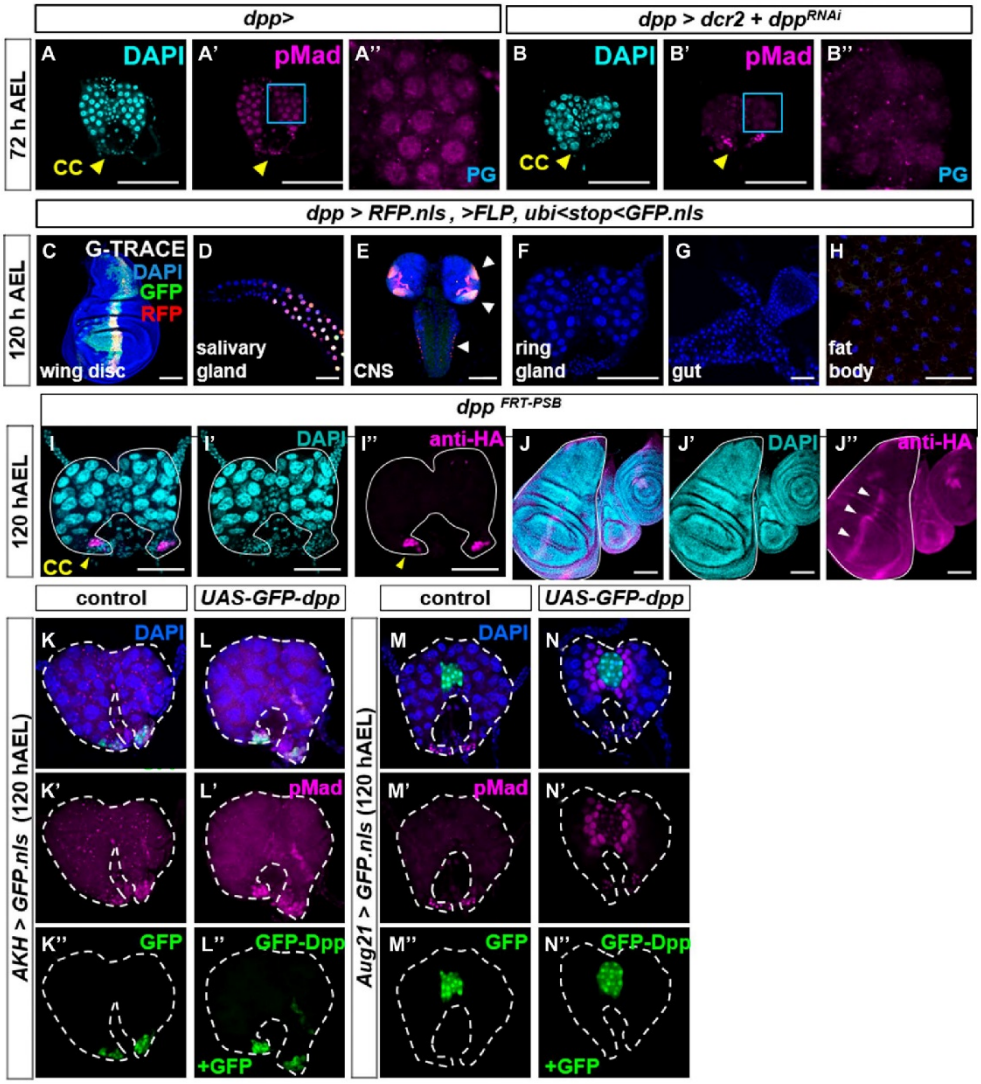

Figure 6. The PG receives Dpp from *dpp-Gal4* expressing cells and not from the CA or CC.
(A, B) Effect of *dpp-Gal4, UAS-dpp*^{RNAi} in ring glands dissected at 72 h AEL. Nuclear pMad is detected in PG cells of control *dpp-Gal4* **(A–A″)** but not in PG cells of *dpp-Gal4, UAS-dcr2, ± UAS-dpp*^{RNAi} **(B–B″)**. **(C–H)** *dpp-Gal4* expression analyzed using G-TRACE. Current (RFP) or prior (GFP) expression. **(I, J)** Expression of HA-tagged Dpp protein expressed by the allele *dpp*$^{FRT-PSB}$. HA-tagged Dpp is expressed in CC cells, indicated by yellow arrowhead (I) and in the anterior stripe of wing discs, indicated by white arrowheads (J). **(K, L)** Ring glands in which *UAS-GFP* **(K–K″)** or *UAS-GFP + UAS-GFP-dpp* **(L–L″)** is overexpressed in CC cells. **(M, N)** Ring glands in which *UAS-GFP* **(M–M″)** or *UAS-GFP + UAS-GFP-dpp* **(N–N″)** is overexpressed in CA cells.

signaling can act antagonistically to the insulin-PI3K pathway in regulating FOXO localization (Fig 7G–I). It has been shown that nuclear FOXO acts indirectly to increase the level of the *ban* microRNA (Boulan et al, 2013). Consistent with this observation, expression of *UAS-tkv*^{QD} in the PG increases *ban* levels as assessed by reduced expression of the *ban* sensor (Fig 7J). The antagonism

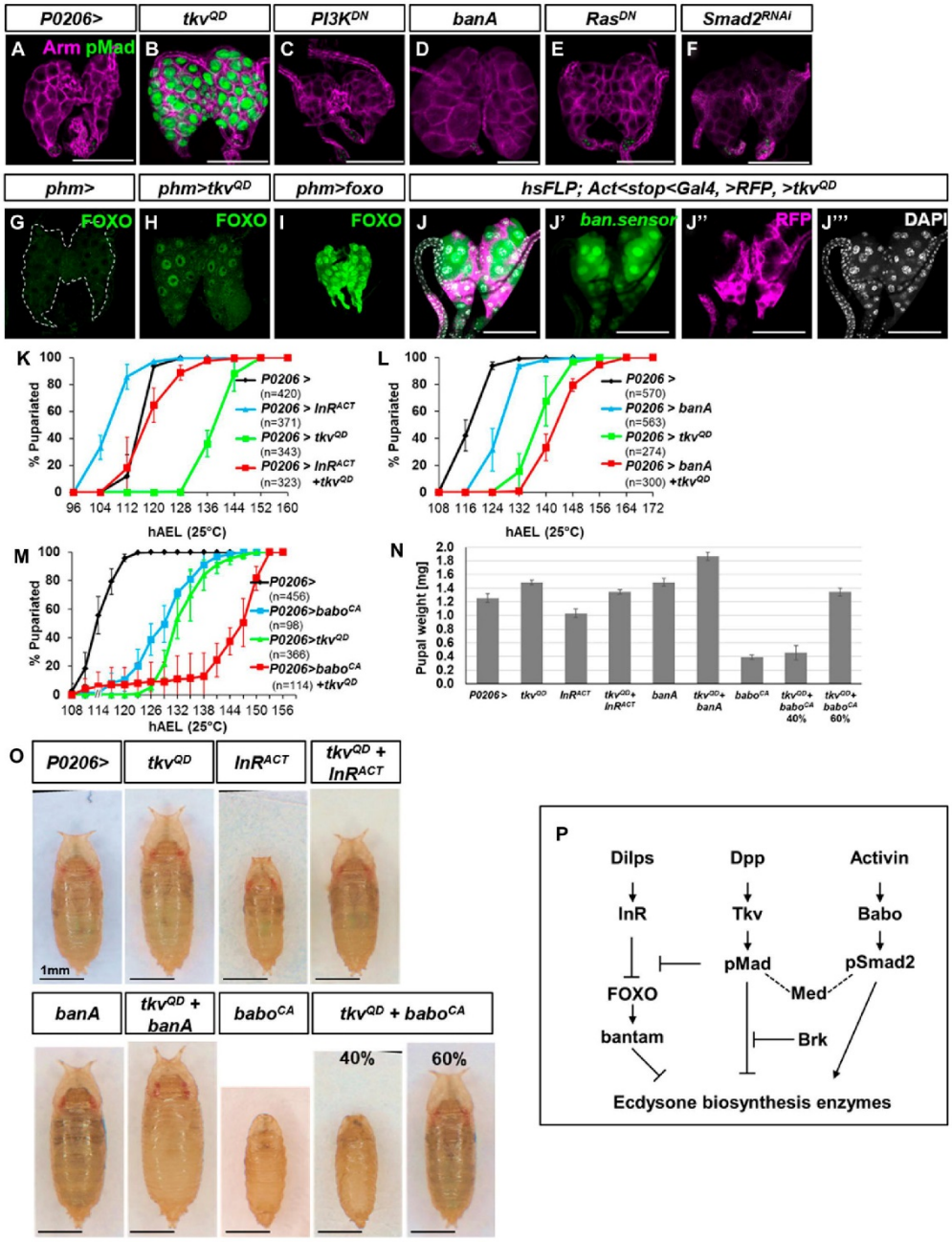
P0206>
tkvQD
PI3KDN
banA
RasDN
Smad2RNAi
A Arm pMad
B
C
D
E
F
phm>
phm>tkvQD
phm>foxo
hsFLP; Act<stop<Gal4, >RFP, >tkvQD
G FOXO
H FOXO
I FOXO
J
J' ban.sensor
J'' RFP
J''' DAPI
K
% Pupariated
P0206 > (n=420)
P0206 > InRACT (n=371)
P0206 > tkvQD (n=343)
P0206 > InRACT +tkvQD (n=323)
hAEL (25°C)
L
P0206 > (n=570)
P0206 > banA (n=563)
P0206 > tkvQD (n=274)
P0206 > banA +tkvQD (n=300)
M
P0206> (n=456)
P0206>baboCA (n=98)
P0206>tkvQD (n=366)
P0206>baboCA +tkvQD (n=114)
N
Pupal weight [mg]
O
P0206>
tkvQD
InRACT
tkvQD + InRACT
1mm
banA
tkvQD + banA
baboCA
tkvQD + baboCA
40%
60%
P
Dilps
Dpp
Activin
InR
Tkv
Babo
pMad
pSmad2
Med
FOXO
bantam
Brk
Ecdysone biosynthesis enzymes

between the insulin-PI3K and Dpp pathways in the PG is also evident from their opposite effects, when activated, on the timing of pupariation and pupal size (Fig 7K, N, and O). In contrast, both increasing Dpp signaling and *ban* overexpression delay pupariation (Fig 7L, N, and O). Because increased Dpp signaling elicits a much greater pupariation delay than *ban* overexpression, and because simultaneous activation of both pathways causes a greater delay than activation of either alone, it is likely that each also has effects on the timing of pupariation that are independent of the other.

The Activin pathway appears to function antagonistically to the Dpp pathway in the regulation of imaginal disc growth (Peterson & O'Connor, 2013) although the mechanism by which the two pathways interact has not been elucidated. The interaction of these two pathways in the PG also seems complicated. Although the expression of an activated form of the Activin receptor Baboon ($Babo^{CA}$) elicits a similar delay to the expression of an activated form the Dpp receptor Tkv (Fig 7M), the appearance of the pupae is quite different. Activation of Tkv in the PG cells results in an extended L3 stage and larger pupae. However, with $Babo^{CA}$, larvae have an extended L2 stage before pupariating stage precociously and giving rise to smaller pupae (Fig 7N and O) that fail to evert their spiracles (Gibbens et al, 2011). This spiracle eversion phenotype is observed in other mutants where ecdysone levels are high as occurs in *ban* mutants consistent with antagonistic effects of these two pathways on ecdysone biosynthesis (Boulan et al, 2013). Concurrent activation of both pathways results in an even stronger delay in pupariation. However, when the pupae are examined, they seem to fall into two groups—approximately 60% of the pupae resemble Tkv^{QD}-expressing pupae, whereas 40% resemble $Babo^{CA}$-expressing pupae. Thus, as in the wing disc (Peterson & O'Connor, 2013), there does not seem to be a simple mechanism which accounts for the interaction between these pathways. The interactions of Dpp signaling with pathways previously implicated in regulating ecdysone production by the PG are summarized in Fig 7P.

Discussion

The morphogen Dpp has mostly been studied for its roles in regulating growth and patterning within tissues where a subset of cells secrete Dpp and the remaining cells respond to Dpp. Here, we provide evidence that Dpp expressed in a variety of tissues can reach distant tissues via the hemolymph and impact the physiology of those tissues. Although we have focused on the effects in the PG, it is possible, even likely, that circulating Dpp can have effects on many tissues and can therefore also function like a hormone.

Dpp as an inter-organ signal

How could Dpp secreted by discs reach the hemolymph? Although it has been reported previously that Dpp is secreted from the disc proper epithelium into the lumenal space enclosed by the peripodial epithelium (Gibson et al, 2002), recent work using nanobodies that can detect GFP-tagged Dpp proteins suggests that Dpp is mostly secreted basolaterally and that it can be detected within the extracellular matrix of the basement membrane (Harmansa et al, 2017). Although our experiments show the presence of overexpressed, tagged versions of Dpp in the hemolymph, the detection of native Dpp has been challenging in the study of *Drosophila* morphogens and has only been accomplished by few (Panganiban et al, 1990; Akiyama & Gibson, 2015). We could not detect physiological levels of Dpp in the hemolymph, either using antibodies to detect native Dpp or anti-HA antibodies to detect endogenously tagged Dpp, mainly because of the limited volume of hemolymph that can be extracted manually while avoiding clotting and because of the high background produced on Western blots. Notably, others have detected Dpp that is overexpressed in discs in pericardial cells which filter the hemolymph (Ma et al, 2017). Based on these recent findings, it would be expected that a small fraction of Dpp expressed in discs at endogenous levels would indeed reach the hemolymph.

Figure 7. Dpp signaling acts upstream of *bantam* and FOXO to regulate ecdysone synthesis.
(A–F) Ring glands dissected at 120 h AEL. pMad is not activated by other pathways known to inhibit ecdysone synthesis. (A) *P0206>*; (B) $P0206>tkv^{QD}$; (C) $P0206>PI3K^{DN}$; (D) *P0206>banA*; (E) $P0206>Ras^{DN}$; (F) $P0206>Smad2^{RNAi}$. Other than $P0206>tkv^{QD}$, none of these transgenes that have each been reported to cause a delay in pupariation, cause nuclear pMad accumulation in the PG, indicating that these pathways do not activate Dpp signaling in the PG. **(G–I)** FOXO protein visualized in ring glands using anti-FOXO antibody. FOXO is cytoplasmic in *phm>* ring glands (G) and nuclear in *phm>FOXO* ring glands (I). However, in 20% of $phm>tkv^{QD}$ ring glands, we observed nuclear FOXO (H). The reason for the incomplete penetrance of this phenomenon is unclear. A similar frequency of nuclear FOXO was observed when using two different transgenes that encode activated *tkv* and also when using the *P0206-Gal4* instead of *phm-Gal4*. Thus, Dpp signaling could impact the insulin pathway upstream of FOXO. **(J)** Ring glands with FLP-out clones expressing $UAS\text{-}tkv^{QD}$ and RFP. Reduced *ban* sensor expression (green in **J, J'**) indicates increased *ban* expression. **(K–O)** Activation of different signaling pathways in the ring gland using *P0206-Gal4*. *phm-Gal4* was not used because that driver line itself has a developmental delay. **(K)** Interaction of Dpp signaling with the insulin pathway in the PG. $UAS\text{-}tkv^{QD}$ delays pupariation. Expression of an activated form of the insulin receptor ($UAS\text{-}InR^{ACT}$) accelerates pupariation. With concurrent expression of both transgenes, pupariation timing is similar to that of the *P0206-Gal4* driver alone. Pupariation times were *P0206* > 115.8 ± 0.3 h; $P0206>tkv^{QD}$ 140.7 ± 7.2 h; $P0206>InR^{ACT}$ 106.3 ± 1.3 h; and $P0206>tkv^{QD} + InR^{ACT}$ 117.0.7 ± 3.0 h. Similarly, $P0206> InR^{ACT}$ pupae are small, $P0206>tkv^{QD}$ pupae are large, and $P0206> InR^{ACT} + tkv^{QD}$ pupae are similar in size or weight to *P0206>* pupae (N, O). **(L)** Interaction of Dpp signaling with *ban*. *UAS-banA* also delays pupariation. Pupariation times were *P0206* > 117.0 ± 1.0 h; $P0206>tkv^{QD}$ 138.0 ± 2.6 h; *P0206>banA* 125.7 ± 1.5 h; and $P0206>tkv^{QD} + banA$ 143.0 ± 1.7 h. Thus, co-expression of $UAS\text{-}tkv^{QD}$ and *UAS-banA* delays pupariation more than either transgene alone. Because the delay elicited by *UAS-banA* overexpression is less than that obtained with $UAS\text{-}tkv^{QD}$, it is unlikely that tkv^{QD} delays pupariation exclusively by increasing *ban* expression. Similarly, the increase in pupal size or weight obtained with co-expression of $UAS\text{-}tkv^{QD}$ and *UAS-ban* is greater than the effect obtained with either transgene alone (N, O). Note that even though the pupariation delay obtained with *UAS-banA* is less than that obtained with $UAS\text{-}tkv^{QD}$, the effects on pupal size are similar suggesting that *UAS-banA* is more effective than $UAS\text{-}tkv^{QD}$ in increasing growth rate. **(M)** Interaction of Dpp signaling with Activin signaling. Pupariation times were *P0206* > 114.5 ± 1.3 h; $P0206>tkv^{QD}$ 129.2 ± 1.5 h; $P0206>babo^{CA}$ 133.5 ± 3.1 h; and $P0206>tkv^{QD} + babo^{CA}$ 148.0 ± 3.0 h. Expression of a constitutively active form of the Activin receptor ($UAS\text{-}babo^{CA}$) delayed development. However, the larvae appeared delayed in L2, generating small pupae as has been described previously. With co-expression of tkv^{QD} and $babo^{CA}$, 40% of the pupae resembled $P0206>babo^{CA}$ pupae in appearance and the remaining 60% resembled pupae that had gone through the L3 stage. The delay in pupariation was close to being additive of the delays caused by either $P0206>tkv^{QD}$ or $P0206>babo^{CA}$ alone. **(N)** Pupal weights of all of the conditions shown in panels (A–C). Summary of tests of statistical significance of pairwise comparisons of pupal weight measurements is in Table 1. **(O)** Images of pupae of all the conditions shown in panels (K–M). **(P)** Model for interaction of Dpp pathway with the InR/FOXO/*bantam* and β-Activin pathways.
Data information: Scale bars = 100 μm, except in (O) where they are 1 mm.

Our experiments also demonstrate that the Dpp receptor Tkv is expressed on cells of the PG and that it is capable of responding to circulating Dpp. We have shown that the overexpression of *dpp* using *ap-LexGAD* induces pMad activation in the PG and that this effect can be suppressed by expressing tkv^{RNAi} in the cells of the PG. Taken together, our experiments demonstrate that Dpp is capable of functioning as an inter-organ signal.

Dpp signaling in the PG regulates ecdysone production

By manipulating Dpp signaling in subsets of cells in the PG using genetic mosaics, we have shown that Dpp signaling negatively regulates ecdysone production, at least in part, by regulating the levels of enzymes required for ecdysone biosynthesis. The InR signaling pathway has also been shown to regulate the levels of these same enzymes, and this action of InR signaling seems to occur by down-regulating levels of the *bantam* microRNA. Because increasing Dpp signaling can result in increased nuclear localization of FOXO and an increase in *ban* activity, Dpp signaling must modulate InR signaling upstream of FOXO. Our observations do not preclude additional levels of crosstalk. The Activin pathway has been shown to function antagonistically to Dpp signaling in regulating disc growth by an uncharacterized mechanism (Peterson & O'Connor, 2013). A similar antagonism between the two pathways also appears to function in the PG. It can be speculated that this antagonism may occur at the level of Medea, a co-Smad that can associate with either pMad or pSmad2 to activate either the Dpp or Activin pathway downstream. If the initial activation of one of these pathways then inhibits the activation of the other, this could explain why we sometimes observe a developmental delay (Dpp) or a developmental arrest (Activin) under conditions where we activate both pathways simultaneously in the ring gland. A better mechanistic understanding of the interaction of these pathways could explain how inputs from different tissues are integrated in the PG to regulate ecdysone production. In addition, in butterflies, a TGF-β ligand and a Dpp-type ligand have both been shown to regulate JH by the CA (Ishimaru et al, 2016). Thus far, we have not observed binding of Dpp-GFP to the CA (Fig 3B); other ligands could potentially have similar functions in *Drosophila*.

Antagonizing Mad function in the PG abrogates the critical-weight checkpoint

Although reducing Dpp signaling in well-fed larvae had modest effects on developmental timing, expression of a $UAS\text{-}Mad^{RNAi}$ transgene in the PG abrogated the critical-weight checkpoint. When these larvae were starved shortly after the L2/L3 ecdysis, rather than arresting as larvae, they proceeded to generate small pupae that did not develop into viable adults likely because they had not accumulated enough stored nutrients to sustain metamorphosis. A possible explanation is that starvation might normally delay the decline in Dpp signaling in the PG which, based on our findings, would be expected to delay pupariation. By antagonizing Dpp signaling in the PG, the mechanism that would normally delay pupariation would be subverted and allow larvae to proceed to pupariation even if they have not grown sufficiently.

Why does Dpp signaling decrease in the PG during L3?

Our data show that under normal physiological conditions, Dpp signaling in the PG decreases as Halloween gene expression increases. This is consistent with the observation that Dpp signaling negatively regulates ecdysone production. As larvae mature, reduced Dpp signaling in the PG would be expected to allow ecdysone biosynthesis and thereby promote the onset of metamorphosis. This finding, however, seems at odds with the observation that Dpp levels, at least in wing discs, increase as discs grow during L3 (Wartlick et al, 2011). If Dpp from discs can pass freely through the basement membrane into the hemolymph (Harmansa et al, 2017; Ma et al, 2017), then as larvae mature, the hemolymph concentration of Dpp would be predicted to rise. It is therefore surprising that Dpp signaling in the PG decreases concurrently. One possibility is that the circulating levels of Dpp do indeed rise and the PG becomes less sensitive to Dpp, perhaps by down-regulating Dpp receptors or other signaling components. However, pulses of Dpp in late L3 using rn^{ts}>*dpp* elicit strong reporter responses in the PG arguing against this possibility (data not shown). Although we are unable to reliably measure circulating physiological levels of native Dpp at different time points in L3, our data are most consistent with the possibility that circulating levels of Dpp do indeed decrease with time.

How could circulating Dpp levels decrease during L3? We present a speculative model (Fig 8) that might become directly testable as methods for detecting low levels of circulating Dpp improve. Although Dpp levels in discs increase during L3 (Wartlick et al, 2011), disc growth results in a disproportionate increase in the number of cells that do not produce Dpp, yet can bind Dpp, thus expanding the "morphogen sink". In addition, extracellular matrix proteins secreted by the fat body continue to be deposited on the basement membrane throughout L3 (Pastor-Pareja & Xu, 2011) and may lead to decreased permeability. For either or both of these reasons, as discs grow, more Dpp might be retained within the discs and less allowed to escape into the hemolymph and reach the PG (model in Fig 8). Indeed, reduced escape from discs could contribute to the observed increase in Dpp levels in discs as larvae progress through L3. As discs grow significantly during L3, organismal growth also leads to a dramatic size increase of the larval body, which has an open circulatory system as opposed to a vascular system. Therefore, it is possible that an increasing ratio of hemolymph to circulating Dpp is effectively causing a dilution of the ligand titer that correlates with growth. If indeed Dpp levels drop as a result of some or all of these reasons, then it provides a mechanism whereby the growth and maturation of the larva can influence the timing of pupariation.

Although a reduction in Dpp signaling in the PG seems necessary for the timely onset of metamorphosis, reducing Dpp signaling in the PG in well-fed larvae is insufficient to trigger entry into metamorphosis. This suggests that the timing of metamorphosis is primarily dictated by other signals such as the secretion of PTTH or by multiple signaling pathways working together. However, our finding that Dpp signaling seems necessary for the critical-weight checkpoint supports the notion that a decline in circulating Dpp levels might be a signal that indicates that sufficient tissue growth or maturation has occurred to generate a viable adult following metamorphosis. Several vertebrate BMP proteins have also been detected in the circulation (for example van Baardewijk et al [2013])

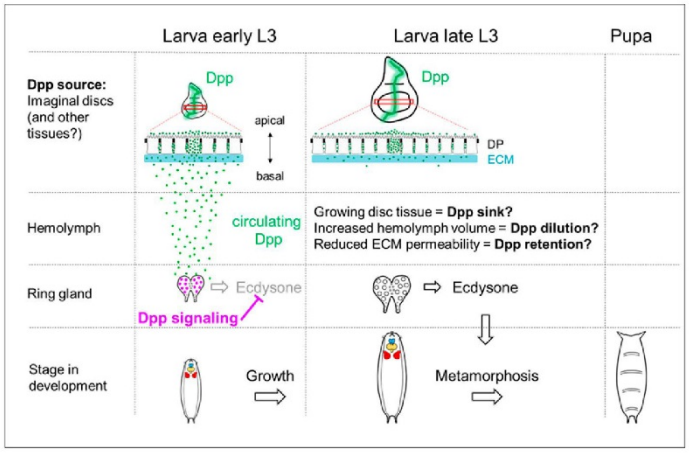

Figure 8. Model of how Dpp from imaginal discs might regulate developmental timing.
As the third instar larva matures, a large increase in imaginal disc size occurs while Dpp is continuously expressed in the imaginal disc. Surprisingly, the PG displays pMad activation early in L3 and its likely source is from the imaginal discs. pMad activity in the PG decreases and is absent late in L3. Because pMad inhibits ecdysone synthesis, a reduction in Dpp signaling in late L3 is necessary to produce sufficient ecdysone required for the timely onset of metamorphosis. This reduction of Dpp signaling may be due to growing disc tissue representing a sink that is outgrowing the source of Dpp, thereby retaining Dpp in discs at an increasing rate; or, an increase in hemolymph volume may outpace the secretion of Dpp, leading to a decreased concentration of circulating ligand that is no longer sufficient to activate pMad. It is also possible that continuous secretion of collagen from the fat body renders the ECM increasingly impermeable during L3, which would reduce the amount of Dpp that can be secreted from the disc.

and it will be of interest to know whether those proteins also have roles in regulating developmental timing.

Materials and Methods

Drosophila strains and husbandry

Animals were raised on standard medium as used by the Bloomington *Drosophila* Stock Center. Fly stocks used were w^{1118} as wild-type control for all experiments, *Oregon-R*, *rn-Gal4,tub-Gal80^{ts}/TM6B-Gal80*, *rn-Gal4,tub-Gal80^{ts};UAS-egr/TM6B-Gal80*, and *rn-Gal4,tub-Gal80^{ts};UAS-rpr/TM6B-Gal80* (Smith-Bolton et al, 2009), *UAS-dpp/TM6B* (Haerry et al, 1998), *UAS-tkv^{Q253D}/TM6B* (Nellen et al, 1996), *dad-nRFP/CyO* (Wartlick et al, 2011), *UAS-GFP-Dpp* (Entchev et al, 2000), *UAS-dilp8::3xFLAG* (Garelli et al, 2012), *dpp-LG*, and *lexOEGFP::dpp/TM6B* (Yagi et al, 2010), *UAS-bantamA* and *bantam.sensor* (Brennecke et al, 2003), *P0206-Gal4*, *phm-Gal4*, and *ptth-Gal4* (from Lynn Riddiford), *UAS-tkv^{D95K}UAS-dad* and *UAS-brk* (from Christine Rushlow), *UAS-babo^{CA}* (from Michael O'Connor), *elav-Gal80* (Yang et al, 2009) (from Lily Yeh Jan and Yuh-Nung Jan), *dlg$^{40-2}$* (from David Bilder), and *dpp$^{FRT-PSB}$* (Bosch et al, 2017) (from Jean-Paul Vincent). Stocks that were obtained from the Bloomington *Drosophila* Stock Center: *dpp-lacZ* (#8404, #8411, #8412) *UAS-InR^{ACT}* (#8263), *dpp-Gal4/TM6B* (#1553), *UAS-dpp* (#1486), *UAS-tkv^{CA}* (#36537), *brk-GFP.FPTB* (#38629), *dilp8^{MI00727}* (#33079), *Aug21-Gal4* (#30137), *AKH-Gal4* (#25684), *UAS-dcr2* (#24650), *UAS-dpp^{RNAi}* (#25782), *r4-Gal4* (#33832), *UAS-preproANF-EMD* (#7001), *G-TRACE-3* (#28281), *UAS-GFP.nls* (#4775, #4776), *UAS-Mad^{RNAi}* (#31315, 43183), *UAS-tkv^{RNAi}* (#35653, #40937), *AbdB-Gal4* (#55848), *UAS-tdTom* (#36328), *UAS-tdGFP* (#35836), and *ap-GAD* (#54268). *UAS-Med^{RNAi}* (#19688) was from the Vienna Drosophila Resource Center (VDRC).

Immunohistochemistry and microscopy

Larvae were dissected in PBS, fixed 20 min in 4% PFA, permeabilized with 0.1% Triton X-100, and blocked with 10% normal goat serum. Primary antibodies used are: rabbit anti-Smad3 (phospho S423 + S425) (#52903, 1:500; Abcam), rabbit anti-Sad (1:250), rabbit anti-Phm (1:250), rabbit anti-Dib (1:250) and guinea pig anti-Spok (1:1000) (gifts from Michael O'Connor), rabbit anti-PTth (1:100) (gift from Pierre Léopold), mouse anti-Armadillo N2 7A1 (Riggleman et al, 1990) (DSHB, 1:100), mouse anti-Dlg 4F3 (Parnas et al, 2001) (DHSB, 1:100), rabbit anti-GFP (#TP401, 1:500; Torrey Pines Biolabs), mouse anti-GFP (AB290, 1:500; Abcam), rabbit anti-cleaved DCP-1 (Asp216, 1:250; Cell Signaling Technology), and rabbit anti-FOXO (1:1000) (gift from Michael Thomas Marr) (Puig et al, 2003). Secondary antibodies used are: goat anti-mouse 555 (#A32727; Invitrogen), goat anti-mouse 647 (#A32728; Invitrogen), goat anti-rabbit 555 (#A32732; Invitrogen), goat anti-rabbit 647 (#A32733; Invitrogen), goat anti-guinea pig 555 (#A-21435; Invitrogen) (all, 1:500), as well as phalloidin-TRITC (#P1951, 1:500; Sigma-Aldrich) and DAPI (#D1306, 1:500; Invitrogen). Samples were mounted in SlowFade Gold (#S36937; Invitrogen) and imaged on a Zeiss 700 LSM confocal microscope.

Developmental timing assay and *rn^{ts}>* temperature shift experiments

Fertilized eggs were collected on grape juice plates for 4 h. L1 stage larvae were transferred onto standard Bloomington food supplemented with yeast paste at a density of 50 animals per vial. For constitutive expression without the presence of a temperature-sensitive *Gal80*, animals were raised consistently at 25°C and pupal counts were taken every 8 h. Three independent experiments were conducted for each condition. *rn^{ts}>* animals were raised at 18°C until day 7 (early third instar), then transferred to 30°C for a 24 h temperature shift and subsequently returned to 18°C. Pupal counts were taken every 12 h. Three independent experiments were conducted for each condition. In the graphs, error bars show standard deviations between the experiments and n stands for the total number of pupae that were counted.

Table 1. Statistical analysis of pupal weight of each genotype versus every other genotype in Fig 7N.

Tukey's multiple comparisons test	*P* Value
P0206> versus *P0206>tkv^{QD}*	0.0001 to 0.001
P0206> versus *P0206>InR^{ACT}*	0.0001 to 0.001
P0206> versus *P0206>InR^{ACT}+tkv^{QD}*	≥0.05
P0206> versus *P0206>babo^{CA}*	<0.0001
P0206> versus *P0206>babo^{CA}+tkv^{QD}* 40%	<0.0001
P0206> versus *P0206>babo^{CA}+tkv^{QD}* 60%	≥0.05
P0206> versus *P0206>banA*	0.0001 to 0.001
P0206> versus *P0206>banA+tkv^{QD}*	<0.0001
P0206>tkv^{QD} versus *P0206>InR^{ACT}*	<0.0001
P0206>tkv^{QD} versus *P0206>*InR^{ACT}+tkv^{QD}	≥0.05
P0206>tkv^{QD} versus *P0206>*babo^{CA}	<0.0001
P0206>tkv^{QD} versus *P0206>*babo^{CA}+tkv^{QD} 40%	<0.0001
P0206>tkv^{QD} versus *P0206>*babo^{CA}+tkv^{QD} 60%	≥0.05
P0206>tkv^{QD} versus *P0206>banA*	≥0.05
P0206>tkv^{QD} versus *P0206>banA+tkv^{QD}*	<0.0001
P0206>InR^{ACT} versus *P0206>InR^{ACT}+tkv^{QD}*	<0.0001
P0206>InR^{ACT} versus *P0206>babo^{CA}*	<0.0001
P0206>InR^{ACT} versus *P0206>*babo^{CA}+tkv^{QD} 40%	<0.0001
P0206>InR^{ACT} versus *P0206>*babo^{CA}+tkv^{QD} 60%	<0.0001
P0206>InR^{ACT} versus *P0206>*banA	<0.0001
P0206>InR^{ACT} versus *P0206>*banA+tkv^{QD}	<0.0001
P0206>InR^{ACT}+tkv^{QD} versus *P0206>babo^{CA}*	<0.0001
P0206>InR^{ACT}+tkv^{QD} versus *P0206>babo^{CA}+tkv^{QD}* 40%	<0.0001
P0206>InR^{ACT}+tkv^{QD} versus *P0206>babo^{CA}+tkv^{QD}* 60%	≥0.05
P0206>InR^{ACT}+tkv^{QD} versus *P0206>banA*	≥0.05
P0206>InR^{ACT}+tkv^{QD} versus *P0206>banA+tkv^{QD}*	<0.0001
P0206>babo^{CA} versus *P0206>babo^{CA}+tkv^{QD}* 40%	≥0.05
P0206>babo^{CA} versus *P0206>*babo^{CA}+tkv^{QD} 60%	<0.0001
P0206>babo^{CA} versus *P0206>banA*	<0.0001
P0206>babo^{CA} versus *P0206>banA+tkv^{QD}*	<0.0001
P0206>babo^{CA}+tkv^{QD} 40% versus *P0206>babo^{CA}+tkv^{QD}* 60%	<0.0001
P0206>babo^{CA}+tkv^{QD} 40% versus *P0206>banA*	<0.0001
P0206>babo^{CA}+tkv^{QD} 40% versus *P0206>banA+tkv^{QD}*	<0.0001
P0206>babo^{CA}+tkv^{QD} 60% versus *P0206>banA*	≥0.05
P0206>babo^{CA}+tkv^{QD} 60% versus *P0206>banA+tkv^{QD}*	<0.0001
P0206>banA versus *P0206>banA+tkv^{QD}*	<0.0001

Quantification of wing discs and pupal weight

Pupae from developmental timing assays collected at the pharate adult stage were cleaned with 70% ethanol, dried, and weighed in groups of 30 in three or four independent experiments. In the graphs, error bars show standard deviations between experimental groups and n stands for the total number of pupae that were weighed. GraphPad Prism 6 was used to determine statistical significance between groups by one-way ANOVA using Tukey's or Dunnett's test. Pupae were placed on double-sided adhesive tape for imaging using a Leica transmitted light microscope (TL RCI). Adobe Photoshop was used to quantify the area of imaginal disc confocal images dissected from larvae from developmental timing assays.

Western blotting

Wing imaginal discs were dissected in chilled PBS supplemented with protease inhibitor (#1169/498001; Roche) and directly transferred into Laemmli sample buffer, then boiled for 10 min. Hemolymph was extracted by bleeding larvae into chilled PBS supplemented with protease inhibitor on a cold aluminum block using a fine tungsten needle to puncture the cuticle, then transferred into Laemmli sample buffer and boiled for 10 min. Samples were run on 10% Mini-Protean TGX gels (Bio-Rad) and transferred to nitrocellulose membrane (Bio-Rad). The primary antibody used was rabbit anti-GFP (#TP401, 1:1,000; Torrey Pines Biolabs). Protein bands were detected with secondary antibody HRP anti-rabbit (#sc-2030, 1:2,500; Santa Cruz Biotechnology), and Western Lightning Plus-ECL (#NEL103001EA; PerkinElmer).

Ex vivo organ culture

20 brain-ring gland complexes were dissected from wandering third instar Oregon R larvae in Schneider's medium (#21720024; Gibco) by pulling mouth hooks from which salivary glands, lymph glands, and fat body were removed. Complexes were subsequently co-cultured for 3 h with either wing imaginal discs or hemolymph from rn^{ts}>*dpp* larvae larvae in Schneider's medium supplemented with 10% FBS (#26140087; Invitrogen) and penicillin-streptomycin at 1:100 of a 5,000 U/ml stock (#15070063; Gibco).

Irradiation

Density controlled third instar larvae were placed on shallow food plates and irradiated with 45 Gy in an X-ray cabinet (Faxitron), followed by dissection after 12 h.

Heat-shock clone induction

Flies with *UAS* transgenes were crossed to *ywhsFlp;;Act≫Gal4, UAS-GFP* and raised at 25°C. Larvae were staged and density controlled as described for developmental timing assay, then heat shocked in a 37°C water bath for 5 min at 24 or 48 h AEL before returning to 25°C until dissection.

Ecdysone feeding

L1 stage larvae were transferred onto standard Bloomington food supplemented with yeast paste at a density of 50 animals per vial. 1 mg 20-hydroxyecdysone (Sigma-Aldrich) in ethanol (100 μl of a 10 mg/ml solution) was added to the surface of each food vial.

Developmental staging and starvation assay

Before egg collection, flies were transferred to a constant light environment for at least 2 d and all subsequent treatments were carried out under constant light to avoid possible influences from diuranal cycles. Eggs were collected on apple juice plates with yeast paste for 4 h and early L1 larvae were transferred to standard laboratory fly food with yeast paste after hatching. After larvae developed to the late L2 stage, newly molted L3 larvae were picked out every 2 h and transferred to new fly food without yeast paste. For the starvation assay, L3 larvae were cultured for the appropriate time and then transferred to 1% agar for starvation. Larvae were then monitored every 2 h until they pupariated or died.

Supplementary Information

Supplementary Information is available at https://doi.org/10.26508/lsa.201800216.

Acknowledgements

We thank many colleagues in the fly community for constructive suggestions; María Domínguez, Marcos González-Gaitán, Pierre Léopold, Michael O'Connor, Lynn Riddiford, Chris Rushlow, Michael Thomas Marr, Hilary Ashe, Jean-Paul Vincent, Markus Affolter, and Konrad Basler for fly stocks and antibodies; the Bloomington, VDRC and TRiP stock centers; Octavio Bejarano, Jane Thomas, and Lupita Hernandez for technical assistance; and Jo Downes Bairzin, David Bilder, Robin Harris, Nipam Patel, Taryn Sumabat, and Melanie Worley for comments on the manuscript. IK Hariharan was funded by National Institutes of Health (NIH) grant R35GM122490 and an American Cancer Society Research Professor Award (RP-16-238-06-COUN). MB O'Connor was funded by NIH grant R35GM118029.

Author Contributions

IK Hariharan: conceptualization, supervision, funding acquisition, and writing—original draft, project administration, review and editing.
L Setiawan: conceptualization, formal analysis, investigation, visualization, methodology, and writing—original draft, review, and editing.
AL Woods: data curation and investigation.
MB O'Connor: conceptualization, supervision, and writing—review and editing.
X Pan: conceptualization, investigation, visualization, and writing—review and editing.
All data with the exception of Fig 5F–L were generated by L Setiawan with assistance from AL Woods. Data in Fig 5F–L were generated by X Pan.

Conflict of Interest Statement

The authors declare no conflicts of interest.

References

Adam G, Perrimon N, Noselli S (2003) The retinoic-like juvenile hormone controls the looping of left-right asymmetric organs in Drosophila. *Development* 130: 2397–2406. doi:10.1242/dev.00460

Akiyama T, Gibson MC (2015) Decapentaplegic and growth control in the developing Drosophila wing. *Nature* 527: 375–378. doi:10.1038/nature15730

Beadle G, Tatum E, Clancy C (1938) Food level in relation to rate of development and eye pigmentation in Drosophila melanogaster. *Biol Bull Mar Biol Lab Woods Hole* 75: 447–462. doi:10.2307/1537573

Bosch PS, Ziukaite R, Alexandre C, Basler K, Vincent JP (2017) Dpp controls growth and patterning in Drosophila wing precursors through distinct modes of action. *eLife* 6. doi:10.7554/elife.22546

Boulan L, Martin D, Milan M (2013) Bantam miRNA promotes systemic growth by connecting insulin signaling and ecdysone production. *Curr Biol* 23: 473–478. doi:10.1016/j.cub.2013.01.072

Boulan L, Milan M, Leopold P (2015) The systemic control of growth. *Cold Spring Harb Perspect Biol* 7: a019117. doi:10.1101/cshperspect.a019117

Brennecke J, Hipfner DR, Stark A, Russell RB, Cohen SM (2003) Bantam encodes a developmentally regulated microRNA that controls cell proliferation and regulates the proapoptotic gene hid in Drosophila. *Cell* 113: 25–36. doi:10.1016/s0092-8674(03)00231-9

Brown JB, Boley N, Eisman R, May GE, Stoiber MH, Duff MO, Booth BW, Wen J, Park S, Suzuki AM, et al (2014) Diversity and dynamics of the Drosophila transcriptome. *Nature* 512: 393–399. doi:10.1038/nature12962

Caldwell PE, Walkiewicz M, Stern M (2005) Ras activity in the Drosophila prothoracic gland regulates body size and developmental rate via ecdysone release. *Curr Biol* 15: 1785–1795. doi:10.1016/j.cub.2005.09.011

Christesen D, Yang YT, Somers J, Robin C, Sztal T, Batterham P, Perry T (2017) Transcriptome analysis of Drosophila melanogaster third instar larval ring glands points to novel functions and uncovers a cytochrome p450 required for development. *G3 (Bethesda)* 7: 467–479. doi:10.1534/g3.116.037333

Colombani J, Andersen DS, Boulan L, Boone E, Romero N, Virolle V, Texada M, Leopold P (2015) Drosophila Lgr3 couples organ growth with maturation and ensures developmental stability. *Curr Biol* 25: 2723–2729. doi:10.1016/j.cub.2015.09.020

Colombani J, Andersen DS, Leopold P (2012) Secreted peptide Dilp8 coordinates Drosophila tissue growth with developmental timing. *Science* 336: 582–585. doi:10.1126/science.1216689

Colombani J, Bianchini L, Layalle S, Pondeville E, Dauphin-Villemant C, Antoniewski C, Carre C, Noselli S, Leopold P (2005) Antagonistic actions of ecdysone and insulins determine final size in Drosophila. *Science* 310: 667–670. doi:10.1126/science.1119432

Denton D, Xu T, Dayan S, Nicolson S, Kumar S (2018) Dpp regulates autophagy-dependent midgut removal and signals to block ecdysone production. *Cell Death Differ* [Epub ahead of print]. doi:10.1038/s41418-018-0154-z

Di Cara F, King-Jones K (2016) The circadian clock is a key driver of steroid hormone production in Drosophila. *Curr Biol* 26: 2469–2477. doi:10.1016/j.cub.2016.07.004

Dunipace L, Saunders A, Ashe HL, Stathopoulos A (2013) Autoregulatory feedback controls sequential action of cis-regulatory modules at the brinker locus. *Dev Cell* 26: 536–543. doi:10.1016/j.devcel.2013.08.010

Entchev EV, Schwabedissen A, Gonzalez-Gaitan M (2000) Gradient formation of the TGF-beta homolog Dpp. *Cell* 103: 981–991. doi:10.1016/s0092-8674(00)00200-2

Evans CJ, Olson JM, Ngo KT, Kim E, Lee NE, Kuoy E, Patananan AN, Sitz D, Tran P, Do MT, et al (2009) G-TRACE: Rapid Gal4-based cell lineage analysis in Drosophila. *Nat Methods* 6: 603–605. doi:10.1038/nmeth.1356

Garelli A, Gontijo AM, Miguela V, Caparros E, Dominguez M (2012) Imaginal discs secrete insulin-like peptide 8 to mediate plasticity of growth and maturation. *Science* 336: 579–582. doi:10.1126/science.1216735

Garelli A, Heredia F, Casimiro AP, Macedo A, Nunes C, Garcez M, Dias AR, Volonte YA, Uhlmann T, Caparros E, et al (2015) Dilp8 requires the neuronal relaxin receptor Lgr3 to couple growth to developmental timing. *Nat Commun* 6: 8732. doi:10.1038/ncomms9732

Gibbens YY, Warren JT, Gilbert LI, O'Connor MB (2011) Neuroendocrine regulation of Drosophila metamorphosis requires TGFbeta/Activin signaling. *Development* 138: 2693–2703. doi:10.1242/dev.063412

Gibson MC, Lehman DA, Schubiger G (2002) Lumenal transmission of decapentaplegic in Drosophila imaginal discs. *Dev Cell* 3: 451–460. doi:10.1016/s1534-5807(02)00264-2

Gilbert LI (2004) Halloween genes encode P450 enzymes that mediate steroid hormone biosynthesis in Drosophila melanogaster. *Mol Cell Endocrinol* 215: 1–10. doi:10.1016/j.mce.2003.11.003

Haerry TE, Khalsa O, O'Connor MB, Wharton KA (1998) Synergistic signaling by two BMP ligands through the SAX and TKV receptors controls wing growth and patterning in Drosophila. *Development* 125: 3977–3987.

Hamaratoglu F, Affolter M, Pyrowolakis G (2014) Dpp/BMP signaling in flies: From molecules to biology. *Semin Cell Dev Biol* 32: 128–136. doi:10.1016/j.semcdb.2014.04.036

Harmansa S, Alborelli I, Bieli D, Caussinus E, Affolter M (2017) A nanobody-based toolset to investigate the role of protein localization and dispersal in Drosophila. *eLife* 6. doi:10.7554/elife.22549

Huang J, Tian L, Peng C, Abdou M, Wen D, Wang Y, Li S, Wang J (2011) DPP-mediated TGFbeta signaling regulates juvenile hormone biosynthesis by activating the expression of juvenile hormone acid methyltransferase. *Development* 138: 2283–2291. doi:10.1242/dev.057687

Ishimaru Y, Tomonari S, Matsuoka Y, Watanabe T, Miyawaki K, Bando T, Tomioka K, Ohuchi H, Noji S, Mito T (2016) TGF-beta signaling in insects regulates metamorphosis via juvenile hormone biosynthesis. *Proc Natl Acad Sci U S A* 113: 5634–5639. doi:10.1073/pnas.1600612113

Jaszczak JS, Halme A (2016) Arrested development: Coordinating regeneration with development and growth in Drosophila melanogaster. *Curr Opin Genet Dev* 40: 87–94. doi:10.1016/j.gde.2016.06.008

Jaszczak JS, Wolpe JB, Bhandari R, Jaszczak RG, Halme A (2016) Growth coordination during Drosophila melanogaster imaginal disc regeneration is mediated by signaling through the relaxin receptor Lgr3 in the prothoracic gland. *Genetics* 204: 703–709. doi:10.1534/genetics.116.193706

King RC, Aggarwal SK, Bodenstein D (1966) The comparative submicroscopic morphology of the ring gland of Drosophila melanogaster during the second and third larval instars. *Z Zellforsch Mikrosk Anat* 73: 272–285. doi:10.1007/bf00334868

Koyama T, Rodrigues MA, Athanasiadis A, Shingleton AW, Mirth CK (2014) Nutritional control of body size through FoxO-Ultraspiracle mediated ecdysone biosynthesis. *eLife* 3. doi:10.7554/elife.03091

Lee CH, Kiparaki M, Blanco J, Folgado V, Ji Z, Kumar A, Rimesso G, Baker NE (2018) A regulatory response to ribosomal protein mutations controls translation, growth, and cell competition. *Dev Cell* 46: 456–469 e4. doi:10.1016/j.devcel.2018.07.003

Lee G, Park JH (2004) Hemolymph sugar homeostasis and starvation-induced hyperactivity affected by genetic manipulations of the adipokinetic hormone-encoding gene in Drosophila melanogaster. *Genetics* 167: 311–323. doi:10.1534/genetics.167.1.311

Ma M, Cao X, Dai J, Pastor-Pareja JC (2017) Basement membrane manipulation in Drosophila wing discs affects dpp retention but not growth mechanoregulation. *Dev Cell* 42: 97–106 e4. doi:10.1016/j.devcel.2017.06.004

Mirth C, Truman JW, Riddiford LM (2005) The role of the prothoracic gland in determining critical weight for metamorphosis in Drosophila melanogaster. *Curr Biol* 15: 1796–1807. doi:10.1016/j.cub.2005.09.017

Nellen D, Burke R, Struhl G, Basler K (1996) Direct and long-range action of a DPP morphogen gradient. *Cell* 85: 357–368. doi:10.1016/s0092-8674(00)81114-9

Nijhout HF, Riddiford LM, Mirth C, Shingleton AW, Suzuki Y, Callier V (2014) The developmental control of size in insects. *Wiley Interdiscip Rev Dev Biol* 3: 113–134. doi:10.1002/wdev.124

Ono H, Rewitz KF, Shinoda T, Iloyama K, Petryk A, Rybczynski R, Jarcho M, Warren JT, Marques G, Shimell MJ, et al (2006) Spook and Spookier code for stage-specific components of the ecdysone biosynthetic pathway in Diptera. *Dev Biol* 298: 555–570. doi:10.1016/j.ydbio.2006.07.023

Ou Q, King-Jones K (2013) What goes up must come down: Transcription factors have their say in making ecdysone pulses. *Curr Top Dev Biol* 103: 35–71. doi:10.1016/b978-0-12-385979-2.00002-2

Panganiban GE, Rashka KE, Neitzel MD, Hoffmann FM (1990) Biochemical characterization of the Drosophila dpp protein, a member of the transforming growth factor beta family of growth factors. *Mol Cell Biol* 10: 2669–2677. doi:10.1128/mcb.10.6.2669

Parker NF, Shingleton AW (2011) The coordination of growth among Drosophila organs in response to localized growth-perturbation. *Dev Biol* 357: 318–325. doi:10.1016/j.ydbio.2011.07.002

Parnas D, Haghighi AP, Fetter RD, Kim SW, Goodman CS (2001) Regulation of postsynaptic structure and protein localization by the Rho-type guanine nucleotide exchange factor dPix. *Neuron* 32: 415–424. doi:10.1016/s0896-6273(01)00485-8

Pastor-Pareja JC, Xu T (2011) Shaping cells and organs in Drosophila by opposing roles of fat body-secreted Collagen IV and perlecan. *Dev Cell* 21: 245–256. doi:10.1016/j.devcel.2011.06.026

Peterson AJ, O'Connor MB (2013) Activin receptor inhibition by Smad2 regulates Drosophila wing disc patterning through BMP-response elements. *Development* 140: 649–659. doi:10.1242/dev.085605

Petryk A, Warren JT, Marques G, Jarcho MP, Gilbert LI, Kahler J, Parvy JP, Li Y, Dauphin-Villemant C, O'Connor MB (2003) Shade is the Drosophila P450 enzyme that mediates the hydroxylation of ecdysone to the steroid insect molting hormone 20-hydroxyecdysone. *Proc Natl Acad Sci U S A* 100: 13773–13778. doi:10.1073/pnas.2336088100

Puig O, Marr MT, Ruhf ML, Tjian R (2003) Control of cell number by Drosophila FOXO: Downstream and feedback regulation of the insulin receptor pathway. *Genes Dev* 17: 2006–2020. doi:10.1101/gad.1098703

Rao S, Lang C, Levitan ES, Deitcher DL (2001) Visualization of neuropeptide expression, transport, and exocytosis in Drosophila melanogaster. *J Neurobiol* 49: 159–172. doi:10.1002/neu.1072

Rewitz KF, Yamanaka N, Gilbert LI, O'Connor MB (2009) The insect neuropeptide PTTH activates receptor tyrosine kinase torso to initiate metamorphosis. *Science* 326: 1403–1405. doi:10.1126/science.1176450

Riddiford LM, Truman JW, Mirth CK, Shen YC (2010) A role for juvenile hormone in the prepupal development of Drosophila melanogaster. *Development* 137: 1117–1126. doi:10.1242/dev.037218

Riggleman B, Schedl P, Wieschaus E (1990) Spatial expression of the Drosophila segment polarity gene armadillo is posttranscriptionally regulated by wingless. *Cell* 63: 549–560. doi:10.1016/0092-8674(90)90451-j

Rodenfels J, Lavrynenko O, Ayciriex S, Sampaio JL, Carvalho M, Shevchenko A, Eaton S (2014) Production of systemically circulating Hedgehog by the intestine couples nutrition to growth and development. *Genes Dev* 28: 2636–2651. doi:10.1101/gad.249763.114

Shingleton AW, Das J, Vinicius L, Stern DL (2005) The temporal requirements for insulin signaling during development in Drosophila. *PLoS Biol* 3: e289. doi:10.1371/journal.pbio.0030289

Smith-Bolton RK, Worley MI, Kanda H, Hariharan IK (2009) Regenerative growth in Drosophila imaginal discs is regulated by Wingless and Myc. *Dev Cell* 16: 797–809. doi:10.1016/j.devcel.2009.04.015

St Johnston RD, Gelbart WM (1987) Decapentaplegic transcripts are localized along the dorsal-ventral axis of the Drosophila embryo. *EMBO J* 6: 2785–2791. doi:10.1002/j.1460-2075.1987.tb02574.x

Stieper BC, Kupershtok M, Driscoll MV, Shingleton AW (2008) Imaginal discs regulate developmental timing in Drosophila melanogaster. *Dev Biol* 321: 18–26. doi:10.1016/j.ydbio.2008.05.556

Tsuneizumi K, Nakayama T, Kamoshida Y, Kornberg TB, Christian JL, Tabata T (1997) Daughters against dpp modulates dpp organizing activity in Drosophila wing development. *Nature* 389: 627–631. doi:10.1038/39362

Vallejo DM, Juarez-Carreno S, Bolivar J, Morante J, Dominguez M (2015) A brain circuit that synchronizes growth and maturation revealed through Dilp8 binding to Lgr3. *Science* 350: aac6767. doi:10.1126/science.aac6767

van Baardewijk LJ, van der Ende J, Lissenberg-Thunnissen S, Romijn LM, Hawinkels LJ, Sier CF, Schipper IB (2013) Circulating bone morphogenetic protein levels and delayed fracture healing. *Int Orthop* 37: 523–527. doi:10.1007/s00264-012-1750-z

Warren JT, Petryk A, Marques G, Parvy JP, Shinoda T, Itoyama K, Kobayashi J, Jarcho M, Li Y, O'Connor MB, et al (2004) Phantom encodes the 25-hydroxylase of Drosophila melanogaster and Bombyx mori: A P450 enzyme critical in ecdysone biosynthesis. *Insect Biochem Mol Biol* 34: 991–1010. doi:10.1016/j.ibmb.2004.06.009

Wartlick O, Mumcu P, Kicheva A, Bittig T, Seum C, Julicher F, Gonzalez-Gaitan M (2011) Dynamics of Dpp signaling and proliferation control. *Science* 331: 1154–1159. doi:10.1126/science.1200037

Woods DF, Bryant PJ (1991) The discs-large tumor suppressor gene of Drosophila encodes a guanylate kinase homolog localized at septate junctions. *Cell* 66: 451–464. doi:10.1016/0092-8674(81)90009-x

Yagi R, Mayer F, Basler K (2010) Refined LexA transactivators and their use in combination with the Drosophila Gal4 system. *Proc Natl Acad Sci U S A* 107: 16166–16171. doi:10.1073/pnas.1005957107

Yamanaka N, Rewitz KF, O'Connor MB (2013) Ecdysone control of developmental transitions: Lessons from Drosophila research. *Annu Rev Entomol* 58: 497–516. doi:10.1146/annurev-ento-120811-153608

Yang CH, Rumpf S, Xiang Y, Gordon MD, Song W, Jan LY, Jan YN (2009) Control of the postmating behavioral switch in Drosophila females by internal sensory neurons. *Neuron* 61: 519–526. doi:10.1016/j.neuron.2008.12.021